MODELING SIZE-RESOLVED PARTICLE NUMBER EMISSIONS FROM ADVANCED TECHNOLOGY AND ALTERNATIVE FUELED VEHICLES IN REAL-OPERATING CONDITIONS

A Dissertation

Presented to the Faculty of the Graduate School

of Cornell University

In Partial Fulfillment of the Requirements for the Degree of

Doctor of Philosophy

by

Darrell Bruce Sonntag

February 2010

MODELING SIZE-RESOLVED PARTICLE NUMBER EMISSIONS FROM ADVANCED TECHNOLOGY AND ALTERNATIVE FUELED VEHICLES IN REAL-OPERATING CONDITIONS

Darrell Bruce Sonntag, Ph. D.

Cornell University 2010

Two particle number emission datasets were analyzed in detail. The first data set contained particle number emissions from four transit buses, including two hybrid diesel-electric buses, under a variety of driving conditions and technological/fuel treatments including: diesel oxidation catalysts, diesel particle filters and ultra-low sulfur diesel fuel. A linear mixed model was used to control for multiple sources of variability in real-world particle measurements, and identified significant factors influencing particle number emissions. Subsequently, link-level particle number emission models were developed for the DOC-equipped conventional buses, using different sets of available predictive data. Principle component analysis was used to reduce the variability of engine parameters to three interpretable parameters: percent engine load, engine speed and exhaust temperature.

Time-resolved particle emissions from the diesel transit buses were evaluated in detail to understand the relationship of particle emissions, operating modes, and the relationship among multiple pollutants. Particle number and mass emissions are generally well-correlated during real-world behavior, however number are emissions are more influenced by the storage and subsequent release of particles evident during high engine speeds, while particle mass emission are more consistent with fuel events. Acceleration events on a stop-and-go urban route caused the maximum particle

emission rates at resolved spatial scales, while over large spatial scales the highest emission rates occurred on the freeway. The concept of emission modes was introduced to understand the variability of gaseous and particle pollution during transient operation of the transit bus. Six repeatable emission modes were identified as being capable of explaining more than 75% of the total variability in emissions.

Functional data analysis was introduced to analyze particle size distributions collected on a flex-fuel vehicle. A non-parametric smoothing technique can optimally smooth particle size distribution data without imposing prior distributional assumptions. The relationship among particle concentrations, operation conditions, and fuel type was estimated as a function of particle size using a functional linear model. Future paths of research are identified which take into account the smoothness of particle-size distributions. In summary, this dissertation contributes data, understanding, and quantitative concepts and methods to advance both research and practice-oriented particle emission models.

BIOGRAPHICAL SKETCH

Darrell Sonntag graduated with a BS in Civil Engineering from Brigham Young University in 2005. His experience living in the dense cities of Italy, as well as a love of the outdoors encouraged him to study the interplay of civil infrastructure and the environment for both his undergraduate and graduate studies.

At Cornell his studies have been interdisciplinary, with a concentration in transportation systems, and minors in both applied statistics and atmospheric science. His coursework has branched into other areas including operations research and economics. His researched has focused on the air quality impacts of transportation, with an emphasis on transportation emission models. He has presented research on several aspects of transportation emissions, including the impacts of EPA emission model, modeling particle emissions from diesel transit buses, and conducting on-board emission measurement studies. Darrell received his MS in Civil and Environmental Engineering in 2008, and his PhD will officially be conferred February 2010.

To my parents

For teaching me to run towards my dreams

To Amy

For running with me

ACKNOWLEDGMENTS

I gratefully acknowledge my advisor, Dr. H. Oliver Gao, for guiding my research and investing tremendous effort in my education and development. I feel honored to be his first PhD student, and know there will be many to follow after me. I also acknowledge the guidance of my minor advisors Dr. Giles Hooker and Dr. K. Max Zhang, for guiding both my studies and dissertation. I acknowledge Dr. Britt Holmén for allowing me to collaborate in analyzing the Connecticut Transit data and Dr. Eric Jackson for assistance with data processing and geographical information systems. I would also like to thank the research assistants who assisted me in collecting emissions data: Deepthi Swamy, Kyle Miller, Viktor Koltko, and Dr. Jon Symonds for instructing us to conduct on-board emission studies. Further, I acknowledge the useful insights provided by members of Dr. Gao's research group, including Timon Stasko, Dr. Yiannis Kamarianakis, and Dr. Yilin Liu, in providing advice on emission studies and statistical methods.

This research was sponsored by the Federal Highway Administration through the Eisenhower Graduate Fellowship Program, the New York Metropolitan Transportation Council and University Transportation Research Council through the September 11th Program Fellowship Program, the New York State Energy Research Development Authority through the Environmental Monitoring, Evaluation, and Protection PhD Fellowship Program, the Joint Highway Research Advisory Council of the University of Connecticut, and the Connecticut Department of Transportation through Projects 03-8 and 05-9.

Most importantly, I acknowledge the many hours my wife, Amy, spent editing and formatting the dissertation. Only with her sacrifice and endless encouragement was I able to accomplish this work.

TABLE OF CONTENTS

LIST OF FIGURES

Chapter 2

Chapter 3

Chapter 4

Chapter 5

Chapter 6

Chapter 7

LIST OF TABLES

Chapter 3

Chapter 4

Chapter 5

Chapter 6

Chapter 7

LIST OF ABBREVIATIONS

Air fuel ratio (AFR)

Akaike information criterion (AIC)

Bayes information criterion (BIC)

Carbon dioxide (CO2)

Carbon monoxide (CO)

Clean Air Act (CAA)

Compressed natural gas (CNG)

Continuously regenerating trap (CRT)

Conventional diesel (CD)

Cubic centimeters (cc)

Cumulative particle concentration (N)

Diesel oxidation catalysts (DOCs)

Diesel particle filters (DPFs)

Differential Mobility Spectrometer (DMS)

Electrical Low-Pressure Impactor (ELPI)

Elemental carbon (EC)

Engine computer unit (ECU)

Engine Exhaust Particle Sizer (EEPS)

Error sum of squares (SSE)

Exhaust gas recirculation (EGR)

Functional data analysis (FDA)

Functional principle component analysis (fPCA)

Geographical Information System (GIS)

High occupancy vehicle (HOV)

Hybrid diesel-electric (HDE)

Hydrocarbons (HC)

Kilometers (km)

Maximum likelihood estimation (MLE)

Micrometers (μm) (meters × 10^{-6})

Miles per hour (mph)

Nanometers (nm) (meters × 10^{-9})

National Ambient Air Quality Standards (NAAQS)

Nitrogen oxides (NOx)

Particle diameter (Dp)

Particulate matter (PM)

Particulate matter mass with particle diameters < 2.5 μm ($PM_{2.5}$)

Particulate matter mass with particle diameters < 10 μm (PM_{10})

Particle measurement procedure (PMP)

Particle number (PN)

Parts per million (ppm)

Portable emission measurement systems (PEMS)

Principle Component Analysis (PCA)

Relative humidity (RH)

Rotations per minute (RPM)

Scanning Mobility Particle Sizer (SMPS)

Selective catalytic reduction (SCR)

State implementation plans (SIPs)

Ultra-low sulfur diesel fuel (ULSD)

US Environmental Protection Agency (EPA)

Vehicle specific power (VSP)

CHAPTER 1

INTRODUCTION

Background

The development of vehicle emission models capable of estimating size-resolved particle emissions has been identified as a research priority. The particle number concentrations of vehicle exhaust are dominated by ultrafine particles (smaller than 100 nanometers) which pose a serious threat to public health, especially in near-roadway environments where particle number concentrations are many times above background levels.

Several challenges prevent the modeling of size-resolved particle emissions from vehicle sources.

1. Limited data is available on the dynamic behavior of particle number emissions during transient real-world vehicle operation. Most particle number emissions studies evaluate vehicles in steady-state or average driving conditions. Previous transient particle emission studies were conducted in the laboratory on chassis dynamometers that cannot fully replicate real-world emissions.
2. The understanding of factors influencing ultrafine particle emissions and techniques for accurately measuring such particles is still evolving. Size-resolved particle number emissions are highly variable and are sensitive to many factors including vehicle operation mode, fuel type, exhaust aftertreatments, atmospheric conditions, sampling systems and sampling conditions. Comparing measurement results between individual tests and studies is difficult because slight differences in sampling conditions can have enormous effects on ultrafine particle formation.
3. Analyzing particle emissions collected in real-world driving conditions poses serious challenges, where influential factors such as engine loads and ambient

conditions are constantly changing. The latest commercial particle measurement instruments can measure size-resolved particle concentrations at high temporal resolutions (up to 10 samples/sec). Measurements from a thirty minute vehicle test can easily record more than half a million size-resolved particle number concentrations. The large amount of data coupled with its significant variability, demand novel analysis concepts and statistical applications to reach meaningful and accurate conclusions.

Research Objectives

The dissertation objective is to advance research in modeling size-resolved particle emissions from important transportation sources. This dissertation focused on addressing each of these challenges to facilitate size-resolved particle number emission modeling, by:

1. Collecting and/or processing emissions data from two on-road particle number emission studies. The first study was collected by Holmen et al. (2005) from four Connecticut Transit buses, including two hybrid-diesel electric buses. Particle number emissions were measured in real-driving conditions using an on-board sampling system. Data was also collected by the author from a light-duty flex-fuel vehicle, which was equipped with an on-board particle sampling system, and operating in real-operating conditions on conventional gasoline and an ethanol-gasoline blend (E85).
2. Analysis of the particle emission data was anticipated to improve knowledge of particle emissions processes. The study set out to identify the operational, technological, environmental, and experimental factors that influence particle number emissions in real-world driving conditions. The study sought to reduce the complex relationships among diesel transit bus particle emissions and operating parameters to produce meaningful relationships. To better understand relationships among co-pollutants, the variability of transient particle number emissions was compared to

particle mass and gaseous emissions. The range of particles influenced by ethanol fuel and vehicle operation was investigated from the flex-fuel vehicle exhaust.

3. Novel analysis concepts and statistical applications were introduced that facilitated meaningful conclusions. These analysis concepts and statistical models may assist transportation policy and planning decisions, in regard to important decisions including:

- Evaluate the benefits of advanced technologies, such as hybrid electric-diesel buses, on particle emissions (Chapter 2)
- Predict the anticipated particle number emissions from transit buses according to roadway type and driving conditions (Chapter 3)
- Assign transit buses to bus routes to limit particle exposure of the urban population (Chapter 4)
- Assess multi-pollutant exhaust aftertreatments operation in real-world conditions (Chapter 5)
- Determine the particle emission effects of alternative fuels on the size-distribution of particle emissions (Chapter 6)

In summary, this dissertation was anticipated to contribute data, understanding, and quantitative concepts and methods to advance both research and practice-oriented size-resolved particle emission models

Dissertation Organization

Chapter 1-2 presents a literature review on vehicle-source particle numbers emissions, including health effects, particle size distributions, chemical characteristics, and factors influencing particle emission rates from vehicles. A review is also given of the transportation/air quality regulations pertaining to particulate matter emissions, and the state-of-practice for modeling particulate matter emissions. Chapter 2 presents an analysis of the factors influencing particle emissions from diesel and hybrid diesel-

electric transit buses. Chapter 3 develops a particle emissions model from the diesel buses that estimates particle number emissions at the link-level of a transportation network. Chapter 4 presents an in-depth analysis of the factors influencing particle emissions at resolved temporal and spatial scales. Specifically, particle number emissions are compared with particle mass emissions to provided added insight into the complexity of particle emissions. Chapter 5 develops the concept of emissions modes, which are used to analyze the complex relationship of gaseous and particle vehicle emissions. Chapter 6 presents the application of functional data analysis to model particle size distributions from a light-duty flex-fuel vehicle. Functional data analysis is used to account for the relationship between particle size and particle concentration, while analyzing the variability and important factors influencing particle emissions. Chapter 7 places the contributions of the dissertation into a broader context, and outlines future paths of research discovered by this study.

CHAPTER 2

LITERATURE REVIEW

Health impacts of vehicle-source particulate matter

Particulate matter is one of the six criteria pollutants monitored by the Environmental Protection Agency under the Clean Air Act. Unlike other criteria pollutants, particulate matter (PM) is not defined by a specific chemical compound or element, but comprises all the liquid droplets and solid particles suspended in the atmosphere (US EPA, 2002; US EPA, 2004). Particulate matter emissions from motor vehicles are a major health risk throughout the world. Particulate matter has been associated with many harmful health effects, including heart disease, lung cancer, asthma, and increased rate of mortality (US EPA, 2007; Brunekreef and Holgate 2002). The US Environmental Protection Agency (EPA) regulates ambient concentrations of particulate matter pollution through PM_{10} and $PM_{2.5}$ measurements, which measure the mass concentration of coarse particles (particles between 10 and 2.5 um) and fine particles (diameter < 2.5 um).

According to the most recent estimates of the EPA, more than 67 million US citizens live in areas that do not reach the National Ambient Air Quality Standards (NAAQS) for fine $PM_{2.5}$ (US EPA, 2005) (particulate matter with aerodynamic diameter < 2.5 μm, are also referred to as fine particles). The EPA has determined that there is sufficient evidence to link the following health effects with PM pollution: increased mortality rates for people with heart and lung disease, development of lung cancer and other respiratory and cardiovascular diseases, and increased respiratory symptoms for children, elderly, and people with existing respiratory conditions such as asthma (US EPA, 2007). Particulate matter pollution places a heavy burden on the environment. The deposition of particulate matter containing acid, metals and

nutrients disturbs both terrestrial and aquatic ecosystems. Further, particulate matter causes aesthetic damage by producing haze and reducing visibility not only in urban areas but also otherwise pristine wilderness areas (National Research Council, 2004).

The size of particles is an important indicator of the health effects of particulate pollution. The EPA first adopted the $PM_{2.5}$ standard in 1997 to better measure fine particles, because "fine particles have been more clearly linked to the most serious health effects" (US EPA, 2002). While fine particles have shown increasing health effects, the coarse particle fractions, measured as the mass of particles between $PM_{2.5}$ and $PM_{10-2.5}$, have also shown positive effects on cardiovascular and respiratory diseases (US EPA, 2004). Coarse particles and fine particles are believed to have distinct health effects due to the differences in particle composition and deposition location within the respiratory system. However, not all studies have not been able to distinguish health effects from $PM_{2.5}$ and PM_{10} (Brunerkreef and Holgate, 2002).

Ultrafine particles, classified by having a diameters less than 100 nm, have been proposed as an effective health measure of particulate matter (Brunekreef and Holgate, 2002), yet contribute very little mass to $PM_{2.5}$ or PM_{10} measurements. Particles have been found to be increasingly toxic at smaller sizes (Lighty et al., 2000). Ultrafine particles have a larger biological effect than the equal amount of mass distributed among larger particles (Lighty et al., 2000). Ultrafine particles can efficiently deposit toxic pollutants in the lungs due to their abundant number concentration, ability to penetrate deep within the lung, large surface area to mass ratio, and high deposition fraction (Brunerkreef and Holgate, 2002; Chalupa et al., 2004). Roadside ultrafine particles have been shown to contain higher air toxics per unit mass than fine particles (Sioutas et al., 2005).

Ultrafine particles dominate the total number of particles from both light-duty gasoline and heavy-duty diesel vehicle emissions (Morawska et al., 2008; Kittelson 1998). The concentration of ultrafine particles on or next to major roadways can be 25 times larger than background levels in urban areas (Zhu et al., 2002), whereas other indicators of particulate matter, such as $PM_{2.5}$ show only a slight increase on roadways (McCarthy et al., 2006). Due to the highly elevated concentrations of ultrafine particles near emission sources, evidence suggests that ultrafine particles may be a causal factor in observed higher mortality rates for persons living near major roadways (Brunekreef and Holgate, 2002). Significantly higher rates of asthma have also been reported for children living near roadways with heavy truck traffic (American Lung Association, 2007).

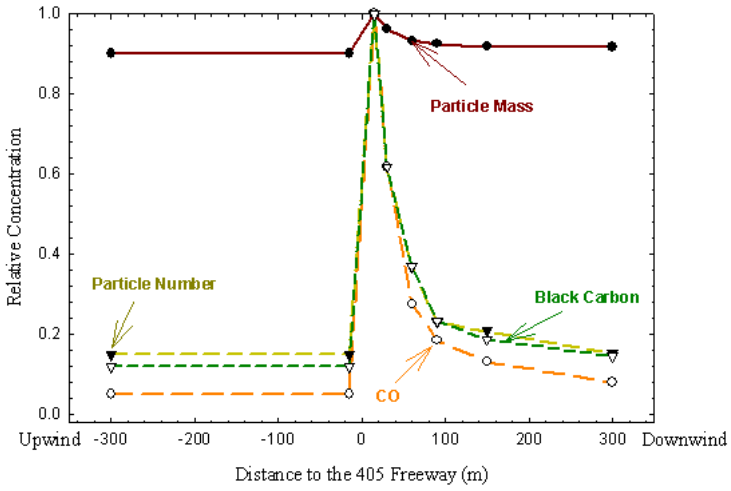

Figure 2.1. Particle number, particle mass, carbon monoxide and black carbon concentrations near 405 Freeway in Southern California. Reprinted with permission. Zhu et al. (2002).

Environmental justice concerns are raised because minority and low-income populations are more likely to live in urban areas with high levels of motor vehicle traffic (National Research Council, 2004). In light of this evidence, there is still an unresolved debate about the relative health impacts of ultrafine and fine particles (Brunekreef and Holgate, 2002). While useful information about the exhaust aerosol

can be quantified through current metrics such as $PM_{2.5}$, a more complete picture of the health effects can be presented by measuring the ultrafine number concentration or better yet, the entire particle-size distribution. Indeed, additional ambient data on the size distribution of particulate matter is needed to better distinguish health effects due to each size fraction (Wichmann and Peters, 2000).

Characterization of Particulate Matter from Motor Vehicles

Vehicle particles can be distinguished by multiple factors including: their composition, density, and origin. Particle size largely determines the dominant forces acting on the particle, (e.g. diffusion, gravity, particle drag,) from which important properties can be calculated, such as the atmospheric residence time and deposition efficiency within the respiratory system. Thus, particle-size is an important indicator of the emission source, behavior and residence time in the atmosphere, and thus health effects.

Particulate matter emissions are commonly evaluated using three metrics: number concentration, surface area concentration and mass concentration. Particle concentrations are plotted against particle size to yield particle-size distribution graphs. Typically, particle diameters are plotted in the log-scale, and particle concentrations are plotted as the change of the cumulative concentration over the change in the log-transformed particle size, expressed as

$$\frac{dC}{d\log D_p}.$$

(Sienfield and Pandis, 2006, Chapter 8). More details on the mathematical expressions of particle size-distributions are given in the article size-distribution measurement section.

Figure 2 illustrates characteristics of particle size distributions from diesel exhaust according to number, surface and mass-based concentrations. The particle-size

distributions from vehicle exhaust may have one of the three illustrated modes: nuclei, accumulation and coarse. Figure 2 displays the particle deposition efficiency within the lung based on particle size. As shown, the nuclei or nucleation mode dominates the particle number distribution. The majority of the mass and surface area of particles is contributed by particles within the accumulation mode. The coarse mode has a very small particle number concentration, but may be present when representing the mass concentration. The presence of each mode is dependent on multiple factors and the size range capabilities of the particle measurement instrument.

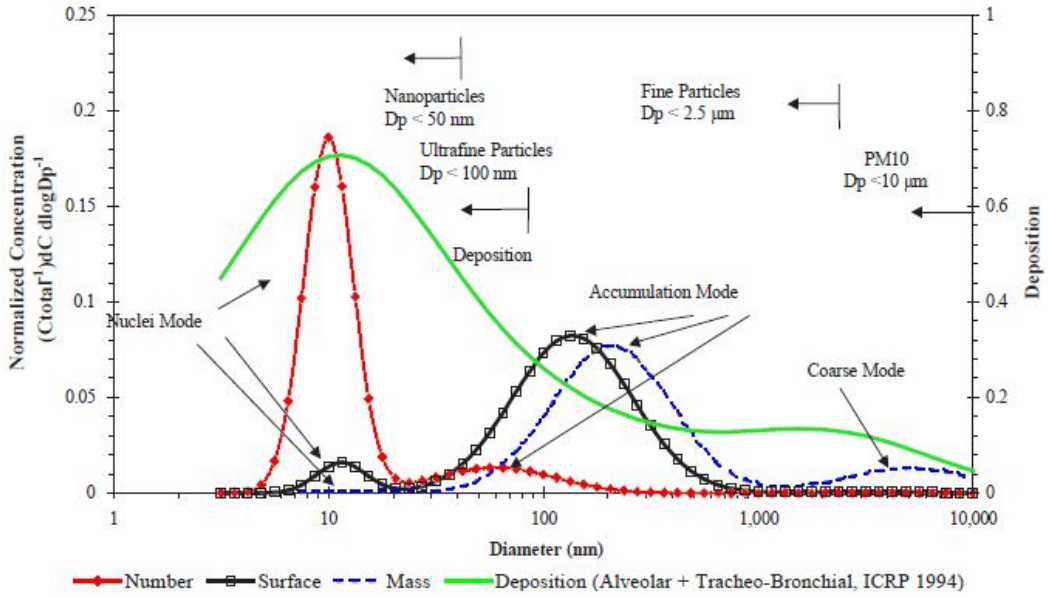

Figure 2.2. Typical Diesel Particle Size-Distribution. Reprinted with permission. Kittelson et al. (2004).

Nucleation Mode. The nuclei or nucleation mode refers to ultrafine particles (typically smaller than 50 nm) that form from gas-phase precursors of semi-volatile organic compounds and sulfates (Lighty et al., 2000; Kittelson, 1998; Kittleson et al., 2004; Kittelson et al., 2006a; Rönkkö et al., 2006). Nuclei mode particles are formed from the condensation and nucleation of volatile species upon dilution and cooling of the exhaust, and their formation is highly dependent on dilution conditions (Sienfield and Pandis, 2006; Burtscher, 2005). In many cases, the nuclei mode composes over

90% of the total particle number of diesel exhaust, while in other cases it may be nonexistent (Kittelson, 1998; Burtscher, 2005; Lighty et al., 2000). The nucleation mode particles are composed of semi-volatile organics, sulfates, and in certain conditions can be composed of solid particles such as metallic ash (Kittelson et al., 2006a). Regardless, due to the small size of the particles, the nuclei mode only constitutes a minor fraction of the total particulate mass from diesel engines (Kittleson et al., 2004). The nuclei mode particles have a short residence time in the atmosphere due to coagulation with larger particles (Sienfield and Pandis, 2006, p. 60).

Accumulation Mode. Accumulation mode particles are composed of a solid core composed of elemental carbon (also referred to as graphitic carbon, black carbon, and soot) and organic material (Sienfield and Pandis, 2006; Morawska et al., 2008; Kittelson, 1998; Robert et al., 2007). Elemental carbon (EC) is formed in combustion and subsequently emitted as solid particles. Organic matter can be directly emitted as a solid material, or can be vaporized and form secondary particles after combustion (Sienfield and Pandis, 2006). Semi-volatile organics, sulfates and other trace compounds absorb and condense on the solid particles that form the accumulation mode (Morawska et al., 2008). Because the accumulation mode of diesel vehicles is composed primarily of solid carbonaceous particles, the accumulation mode is less dependent on dilution conditions, and more repeatable measurements can be obtained in both laboratory and on-road tests (Kittelson et al., 2006a).

The chemical composition of the accumulation mode is substantially different between spark-ignition gasoline engines and compression-ignition diesel engines. Gasoline accumulation mode particles are almost completely composed of organic compounds, while the diesel accumulation mode particles contain a significant amount of both elemental carbon and organic carbon (Kleeman et al., 2000).

Coarse Mode. Coarse mode particles can be present in vehicle exhaust from re-entrained particles that have accumulated in the engine or exhaust system (Kittelson, 1998). Road-side coarse mode particles can be generated by tire wear and mechanically re-entrained road dust (Sienfield and Pandis, 2006, p. 373). Coarse mode concentrations occur at very low number concentrations compared to accumulation particles within tail-pipe exhaust. One study reported coarse mode concentrations of ~1 particle/cm^3 while accumulation particles were from 10^4-10^5 particles/cm^3. However, one 5-μm diameter particle has the same mass as one hundred thousand 100-nm diameter particles (Lighty et al., 2000). Convert mass size distributions from a particle counts over a wide range of particle sizes, can be prone to error, because a few artificial counts of large diameter particles can greatly influence the derived mass distributions (Maricq, 2007).

Influential factors on vehicle-source particle number size distributions and concentrations

The formation of particulate matter emissions within the engine, the effectiveness of particle control devices, and subsequent evolution of the aerosol in the atmosphere is a complex and much researched topic. Many studies have been conducted to examine the factors that influence particle number size distributions and concentrations from vehicle exhaust.

Particle emissions are influenced by many factors including: engine type, engine design, engine operation, fuel and oil parameters, exhaust aftertreatment, sampling system and sampling conditions (Kittelson et al., 2006a; Rönkkö et al., 2006). A review is given for many of the most common and influential factors influencing particle number size distributions. Comparisons between studies must be conducted with care due to differences in each of these factors.

Engine Type. Diesel compression ignition engines and gasoline spark ignition engines constitute the majority of motor vehicles in the U.S. The difference between diesel and gasoline engine classes is the largest distinguishing factor between particle size distributions from on-road vehicle emissions. Advanced technologies that have limited use, such as gasoline direct injection vehicles, will not be discussed in detail.

Conventional diesel vehicles produce much higher particle concentrations than gasoline particle emissions, for both ultrafine and fine particles. Diesel vehicles emit 20 times more PM mass than gasoline vehicle per unit of fuel burned (Maricq, 2007). In California alone, heavy-duty vehicles are estimated to make up only 2% of the vehicle fleet, but contribute to over 65% of mobile-source mass-weighted particulate matter emissions (Yanowitz et al., 2000). While gasoline vehicles have smaller particle emission rates, their large proportion to the on-road fleet make them important contributors as well. In the Denver metropolitan area, gasoline vehicles were estimated to contribute 60% of the total carbon $PM_{2.5}$ concentrations (Kittelson et al., 2006b). Diesel vehicles also contribute disproportionately to high particle number concentrations observed near major roadways. The particle number emission rates for heavy-duty diesel vehicles are one to two orders of magnitude higher than gasoline-fueled passenger cars. (Morawska et al., 2008). Keogh et al. (2009) estimated that the heavy-duty vehicle fleet comprises 6% of the total vehicle kilometers traveled, but contributes over 50% of the particle number emissions in South-East Queensland, Australia.

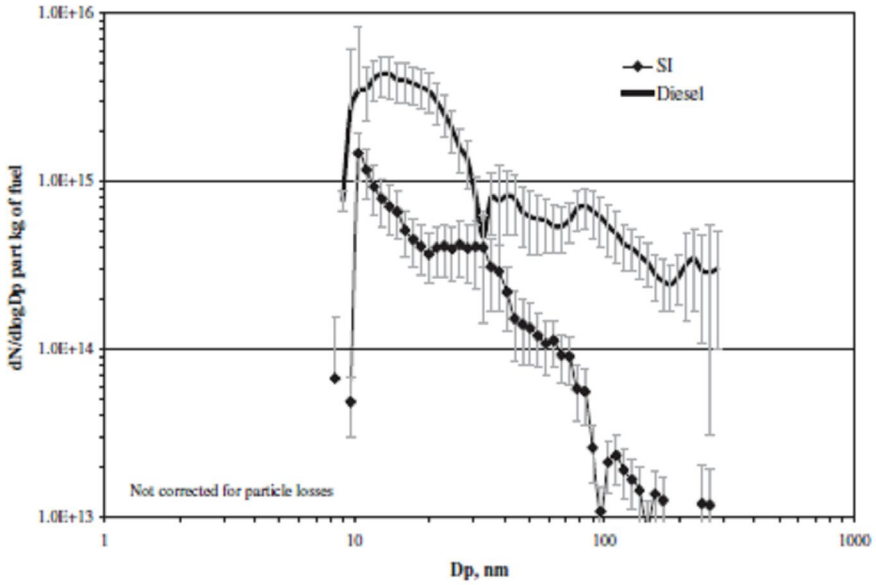

Figure 2.3. Comparison of particle size distribution measured according to a diesel engine and a spark-ignition gasoline vehicle. The particle size distributions were measured by a following vehicle on an urban highway. Units are particle concentrations per kg of fuel. Reprinted with permission. Kittelson et al. (2006b).

Figure 3 displays the particle size distribution (plotted on the log-scale) measured for diesel and gasoline vehicles from on-road measurements. Figure 3 illustrates that particle concentrations and size distributions between diesel and gasoline vehicles differ dramatically. The large differences in particle size distributions evident in Figure 3 have been corroborated from multiple studies. Diesel vehicles measured in true ambient conditions have large nucleation modes that have very high particle number concentrations. In the on-road measurement studies of diesel vehicles a large nucleation mode was measured within the exhaust plume under all (Kittelson et al., 2006a) or most driving operating conditions (Rönkkö et al., 2006). However, the nucleation mode was largely variable, in the study by Kittelson et al. (2006a), the nucleation mode contained between 37% and 89% of the total particles measured between 7.5 and 300 nm. Kittelson et al. (2004) discovered that when sampling on-road ambient concentrations, the particle size distribution had a significantly larger nucleation mode in the presence of a diesel vehicle.

The accumulation mode is one of the distinguishing characteristics of diesel exhaust, with a consistent peak around 60-100 nm for the particle number size distribution, and with a consistent standard deviation (Burtscher, 2005; Shi et al., 2000). Dilution conditions have little influence on the accumulation mode particles, and the accumulation mode is observed in almost all conventional diesel emissions studies. In fact, the diesel accumulation mode is found to have a similar log-normal shape, with a peak between 60-100 nm (number-weighted), and between 100-180 (mass weighted) and a consistent standard deviation (Burtscher, 2005; Shi et al., 2000; Robert et al., 2007). Because the accumulation mode dominates the mass concentrations, the mass size distribution is well parameterized by a single lognormal distribution.

The accumulation particles from gasoline vehicles tend to have smaller particle modes between 40-80 nm (number-weighted), and have more asymmetric distributions (Harris and Maricq, 2001; Maricq et al., 1999). However, Kleeman et al. (2000) found that the mass-weighted accumulation mode for gasoline and diesel vehicles both had peaks around 100 nm. The particle number and mass emission rates of the accumulation mode are much smaller compared to conventional diesel for accumulation mode particles (Maricq et al., 1999). Mass emission rates can be 10-100 times smaller than diesel engines, while number emission rates for accumulation range particles can be 10^4-10^5 times smaller (Harris and Maricq, 2001).

Vehicle Operation. Limited research has been conducted on the effects of transient operating conditions on particle-size distributions. The sample response time for many particle instruments is too long to measure the particle size distributions of emissions due to transient engine and vehicle operating conditions (Maricq et al., 1999). To obtain particle-size distributions using these instruments, measurements are recorded at idle or steady-state operating conditions (constant vehicle speed).

However, these conditions are not representative of real-world conditions (Kittelson et al., 2006a; Robert et al., 2007). The increased use of fast particle sizing instruments such as the TSI EEPS (Liu et al., 2007) and Cambustion DMS500/50 (Lee et al., 2009) will facilitate more studies on the effects of operating mode on particle size distribution.

Diesel Vehicles. The accumulation mode particles are a more repeatable function of the engine operating conditions. Several diesel engine dynamometer studies have confirmed that the concentration of accumulation mode particles has a positive relationship with engine load and engine speed (Kittelson et al., 2006a; Mathis et al. 2005b; Harris and Maricq, 2001; Virtanen et al., 2004). In general, the peak or median diameter of the accumulation mode stays constant at higher engine loads on different driving cycles (Shi et al. 2000; Harris and Maricq, 2001; Kittelson et al., 2006a; Robert et al., 2007; Vaaraslahti et al., 2004), however other researchers have found that the median diameters can increased at high loads (Mathis et al., 2005b). The shape of the accumulation mode can also be responsive to load, with the width increasing at higher loads, on both light-duty and heavy-duty conventional diesel engines (Virtanen et al., 2004).

The nucleation mode of diesel exhaust is very responsive to engine loads. Giechaskiel et al. (2005) conducted both a plume-chasing study and laboratory study on a light-duty diesel vehicle. Vehicle speed and engine load had very little impact on the particle size distribution for the accumulation mode range. In contrast, the nucleation mode was very responsive to vehicle speed and engine loads. At low vehicle speeds (50 km/h) no nucleation mode was present, but consistently appeared at high vehicle speeds (100 km/h) and engine loads.

Large nucleation modes can be present at both high engine loads (Giechaskiel et al., 2005) and low loads (Vaarashlahti et al., 2004). One reason for the similarly

disparate results based on engine load may be due to the composition of the nucleation mode particles. At low engine loads, the nucleation mode is composed primarily of hydrocarbons and non-volatile solid particles such as metallic ash (Rönkkö et al., 2006; Kittelson et al., 2006a). While at high engine loads and exhaust temperatures, the nucleation mode is dominated by sulfates, which are formed in the catalytic converter at high exhaust temperatures. Additionally, the nucleation mode is highly dependent on other factors including fuel parameters, exhaust aftertreatment, and meteorological conditions (Rönkkö et al., 2006). In general, accumulation mode particles are more stable and less influenced by operating conditions. However, repeatable observations of nucleation mode particles can be obtained in well-controlled emission studies with realistic dilution conditions (Giechaskiel et al., 2005; Kittelson et al., 2006a).

Gasoline vehicles. Gasoline particles emissions are more responsive to operating conditions than diesel engines. Gasoline cars have much lower particle emission rate than diesel vehicles, but at full-throttle accelerations, the particle emissions from gasoline vehicle can be similar to those of diesel vehicles under the same conditions (Kittelson et al., 2006b). Particle concentrations across the entire measured spectrum (8-283 nm) are shown to be affected by acceleration events. However, the particle size distributions of individual vehicles differ greatly, with some particle size distributions being dominated by a nucleation mode, while in other cases the nucleation mode is absent (Kittelson et al., 2006b).

The effect of operating conditions on nucleation mode particles for both diesel and gasoline vehicles is complicated by the storage and release of particles. During transient conditions, nucleation mode particles can deposit in the engine and exhaust system and be subsequently released during high exhaust temperatures and exhaust

flow achieved at high loads (Kittelson et al., 2006a; Kittelson et al., 2006b; Mathis et al., 2005a).

Exhaust Aftertreatments. Both diesel oxidation catalysts (DOCs) and diesel particle filters (DPFs) are identified as verified technologies by the EPA to reduce particulate matter emissions (US EPA, 2009c). DOCs can reduce PM mass emission rates by roughly 20%, while particle filters can reduce PM by over 90%. However, the impact on the particle number size distribution is more complex.

Diesel Oxidation Catalysts. Catalysts are standard features on light-duty gasoline vehicles, and the previous discussion on gasoline particle emissions, assumes that gasoline vehicle are equipped with functioning catalysts. On the other hand, many in-use diesel vehicles do not have catalysts, and diesel oxidation catalysts (DOCs) are a common emissions reduction retrofit for the in-use diesel fleet. However, the impact on the particle number size distribution is not well quantified. Kittelson et al. (2006a) predicted that diesel catalysts should reduce hydrocarbons in the emissions while favoring the formation of sulfates. Particle number emissions may be lower due to the presence of a DOC, especially at low loads where the nucleation mode is comprised mainly of hydrocarbons (Rönkkö et al., 2006), but at high loads and high engine temperatures the diesel oxidation catalyst likely contributes to a large nucleation mode. Rönkkö et al. (2006) tested a 2002 model year European diesel bus equipped with a DOC, and found that the nucleation mode was highly sensitive to engine torque, which is attributed to the high fuel rate and exhaust temperature, which promotes the oxidation of SO_2 to SO_3, and the subsequent formation of sulfate particles. The shape of the nucleation mode is influenced by engine torque with the geometric median diameter increasing at higher torque levels. Luders et al. (1997) demonstrated that diesel oxidation catalysts can increase the number of nanoparticles for diesel passenger cars and heavy-duty diesel engines under certain driving

conditions. The effect of diesel oxidation catalysts on particle size distributions is complex and dependent on multiple factors, including operating conditions. More research needs to be conducted to better understand their effects on size-resolved particle emissions (Morawska et al., 2008).

Diesel Particle Filters. The introduction of ultra-low sulfur diesel fuel in the US has permitted the use of diesel particle filters which significantly reduce diesel emissions in all 2007 or later heavy-duty vehicles. However, diesel engines are notably durable, and routinely record over 1 million miles, so retrofitting the current 11 million diesel engines that do not meet 2007 emission standards can have a major impact on air quality (US EPA 2009d).

Diesel particle filters (also referred as particle traps) are highly efficient at removing solid particles (>90%), while volatile particle precursors can still form a substantial nucleation mode after the aerosol passes through the filter (Burtscher, 2005; Morawska et al., 2008). By providing a catalytic environment and removing the accumulation mode particles, catalyst equipped particle filters favor conditions for the nucleation of sulfate particles (Biswas et al. 2008; Burtscher, 2005; Morawaksa et al, 2008). This phenomenon has been observed from testing of an Engelhard DPX filter (Biswas et al. 2008), which is analyzed in Chapter 3.

Particle traps can effectively reduce accumulation mode to background concentrations (Vaaraslahti et al., 2004). However, the presence of the nucleation mode is affected by operating conditions. In laboratory testing, Vaaraslahi et al. (2004) found that a nucleation mode was only present during high load conditions. The high nucleation mode is believed to be due to sensitivity of high fuel rates and higher exhaust temperature, which can both increase the number of sulfate particles in the exhaust. More research needs to quantify the toxicity of the nanoparticles formed from diesel particle filters (Morawska et al., 2008).

Diesel Fuel and Lubricating Oil Parameters. The sulfur content of diesel fuel and lubricating oil has been a much researched topic due to the promulgation of new ultra-low sulfur diesel fuel (ULSD) standards (US EPA, 2001). The use of ULSD fuel is required for the operation of diesel particle filters/traps, required for new diesel vehicles to reach tighter mass-based particulate matter standards (Kittelson et al., 2008).

The use of ULSD fuel has been shown to have a significant impact on the particle-size distribution for particles<50 nm (Kittelson et al., 2006a; Ristoviski, 2006). The nucleation mode is composed of sulfuric acid and hydrocarbons that reach super saturation as the exhaust cools after leaving the engine. Reducing sulfur in the fuel in general also reduces the concentration of a large number of particles formed in the nucleation mode. However, reducing the sulfur content does not necessarily reduce the nucleation mode emissions in a linear relationship, and reducing the sulfur content may have no effect on reducing the nucleation mode particles under certain engines, exhaust aftertreatments, operation conditions, or sulfur content levels (Kittelson et al., 2006a). Kittelson et al. (2006a) found that for a conventional diesel (no diesel particle trap) at low engine loads, a significant non-volatile nucleation mode formed that was not comprised of sulfates. In other instances, a large accumulation mode may absorb the sulfates, thus preventing a large nucleation mode to form from high sulfur diesel fuel.

Kittelson et al. (2008) evaluated the particle size distributions from a diesel vehicle with a continuously regenerating trap (CRT) at different sulfur levels in the fuel and lubricating oil. Most diesel particle filters have catalysts that convert sulfur in the fuel and oil into sulfates. Because the particle trap removes the accumulation mode particles, the sulfates have a higher propensity to nucleate forming a large nucleation mode (Kittelson et al., 2008). The particle size distribution is thus a large function of

the use of a diesel trap and the sulfur content of the fuel. For tests on a diesel vehicle with a CRT, the particle number size distribution was dominated by a large nucleation mode, and low concentration of particles above 50 nanometers. At larger sulfur levels the nucleation mode significantly increased in size. Without a CRT, and at low sulfur fuel and oil levels, the same diesel vehicle showed a broad and flat distribution of particles with no peak of particles in the nucleation mode, but a large amount of accumulation mode particles (Kittelson et al., 2008).

Alternative fuels. Production of alternative fuels increased exponentially during the last five years, as such fuels have been promoted for reducing energy dependency and greenhouse gas emissions. Current ethanol production is replacing roughly 8% of the total gasoline consumed in the US, and biodiesel almost replaces 1% of the total diesel consumed (Coyle, 2007; Tyner, 2008; Davis et al., 2008). However, use of biofuel in motor vehicles is anticipated to continue dramatically within the US. The Energy Independence and Security Act of 2007 mandates production of biofuels annually to reach 36 billion gallons by 2022, which will equal 18% of current transportation fuel consumption (US DOE 2008, National Biodiesel Board 2007).

Ethanol blends have been shown to reduce PM mass (Mulawa et al., 1997) and number (Lee et al., 2009) in light-duty gasoline vehicles. In laboratory testing of a spark ignition flex-fuel vehicle, Lee et al. (2009) showed that an E10 ethanol blend impacted the particle size distribution, with an observed decrease in accumulation mode particles (50-150 nanometers), while only a slight decrease for particles < 50 nanometers. However the effect across the entire particle-size range was not fully quantified and results will likely differ in real-driving conditions.

Studies evaluating biodiesel on heavy-duty engines typically show a significant reduction in PM mass emissions, but effects on particle number emissions have mixed

results. Ultrafine particles have been shown to both increase and decrease due to biodiesel blends (Lapuerta et al., 2008; McCormick, 2007). More research is needed to assess the effects of biofuels on size-resolved PM number emissions across different blends, temperatures, engine technologies, and driving conditions (McCormick 2007).

Holmen and Ayala (2002) compared a compressed natural gas (CNG) bus to a diesel bus with and without a continuous regenerating trap (CRT). The shape of the particle size distribution for the CNG bus was similar to those observed for the CRT bus, with a high nucleation mode at 10 nm, and very low concentrations for larger particles. The results differed according to dilution and sampling conditions. Real-world studies should be conducted to determine the true effect of operating condition CNG particle size-distributions.

Particle size-distribution measurement

Vehicle exhaust is composed of millions of individual particles that have a continuum of diameters. Because the diameter of each individual particle cannot be measured, the particle size distribution is approximated by measuring particles within discrete size range bins. Improved aerosol measurement technology has facilitated the measurement of size-resolved particle concentrations, including instruments such as the SMPS, ELPI, and DMS500 (see introduction). Examples of the range and resolution of the particle size distribution measurements from several recent studies are particles measuring between 7 and 8,100 nm at 12 size fractions using the ELPI (Holmen et al., 2005), from 12 to 661 nm at 106 size fractions using the SMPS (Beddows et al., 2009) and from 5 and 500 nm at 34 size fractions using the DMS50 (Chapter 7). Although the particle size distribution is measured at a finite number of bins across the particle spectrum, the particle size distribution is best represented by a smooth continuous function.

The particle number size-distribution is mathematically represented as $n_N(\log D_p) = dN/d\log Dp$, where N represents the cumulative particle size distribution measured in particles/cm^3, and D_p is the particle diameter, typically measured by the aerodynamic or electric mobility diameter. When plotting the diameter on the log-scale, $dN/d\log Dp$ is used to represent the particle size distribution, so that the area under the particle size distribution is the total number of particles, represented as the integral:

$$N(\log D_p) = \int_1^{\log(D_p)} n_N(\log D_p) d\log D_p \quad .$$

(Sienfield and Pandis, 2006). To approximate the smooth function $n_N(\log D_p)$, the values of $\Delta N / \Delta \log D_p$ are plotted at the midpoints of each measured size bin and frequently interpolated or a fitted with a probability density function, such as the lognormal distribution.

Analyzing particle-size distributions adds a critical dimension to particulate matter emission studies. Not only is the magnitude of particle-size distribution important, but the shape, or relative proportion of different sized particles is of interest. In several instances within Kittelson et al. (2006a) and Clark et al. (2007), the particle concentration was not calculated due to difficulties in accurately measuring the dilution rate. However, the standardized particle size distribution still yielded important information about the nature of the particles.

Measurement Instruments

Filter measurements have become the standard for mass measurements in the US, with the sampling protocol for diesel exhaust detailed in the Federal Code of Regulations (US EPA, 2001). In filter collections, the particles are removed from the air onto a porous medium or filter (Lee and Mukund, 2001). Improved aerosol measurement technology has facilitated the accurate measurement of ultrafine size-

resolved ultrafine particles, including the ELPI and DMS50 used in this thesis. These particle instruments use one of two derived particle diameters to classify particle number concentrations: 1. Aerodynamic diameter 2. Electrical mobility diameter. Derived particle diameters are used because each particle shape is unique, and cannot be directly measured. The aerodynamic diameter is defined as the diameter of a unit density (ρ^o = 1 gm/cm^3) spherical particle that has the same settling velocity as the actual particle (Sienfield and Pandis, 2006, p.429).

The most widespread instrument used to measure particle number size distributions using the aerodynamic diameter is the Electric Low-Pressure Impactor (ELPI, Dekati Inc.). The ELPI was used to measure the particle number size distribution analyzed in Chapters 3 through 6 of the dissertation, and is reviewed in detail. The ELPI charges particles before they enter a cascade impactor column, similar to the schematic in Figure 4. The inertia of the larger particles will cause them to leave the air stream and impact each impaction plate which induces an electrical current that is recorded by corresponding electrometers (Baltensperger et al., 2001). Each impaction plate or stage is designed to capture particles with a smaller aerodynamic diameter. The ELPI is often used to supplement other particle measurement instruments, due to its ability to measure a wide interval of particles diameters (30 to 10,000 nm) at a high temporal resolution (Maricq et al., 1999; Kinsey, Kittelson et al., 2006a). Comparison of particle size distribution measurements between the ELPI and SMPS have been shown to agree relatively well. Although, the ELPI can systematically overestimate the particle concentrations for the lowest ELPI channel (Maricq et al., 2000)

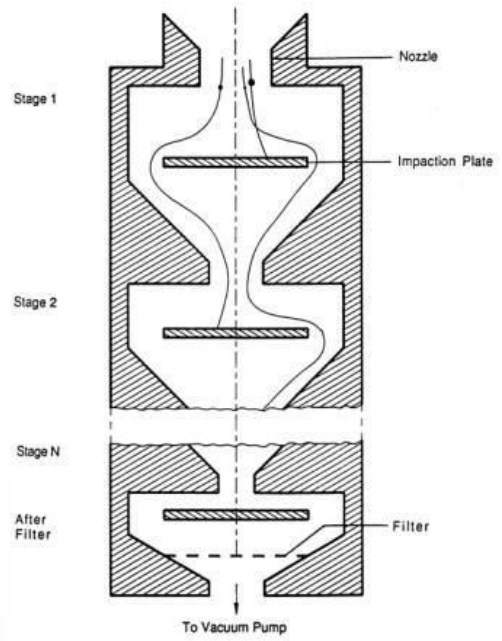

Figure 2.4. Schematic Diagram of Cascade Impactor. Marple et al. (2001).

Several widespread particle instruments classify particles according to electronic mobility diameter, including the Scanning Mobility Particle Sizer (SMPS, TSI inc.), the Engine Exhaust Particle Sizer (EEPS TSI inc.), and the Differential Mobility Spectrometer (DMS500, Cambustion Inc.). The electrical mobility diameter is determined by the velocity of a singly charged particle within a magnetic field.

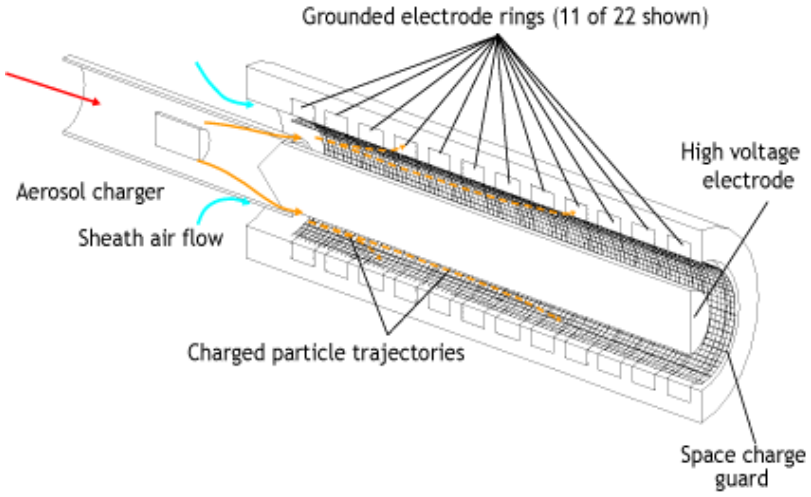

Figure 2.5. DMS500 diagram of classification column. Reprinted with permission. (Cambustion Ltd, 2009).

The SMPS is used in a wide variety of both vehicle exhaust and ambient measurement studies. The SMPS has increased precision at low particle sizes from 2 to 10 nm because it combines both a particle counter with an electrostatic classifier (Morawska et al., 2008) and because it only measures one size range of the entire particle size distribution at a time. As such, the SMPS can be used to measure low concentration ambient particle size-distributions as well as vehicle exhaust measurements. However, the increased precision comes at the expense of high temporal resolution. The SMPS requires several minutes to scan through the entire particle spectrum, therefore limiting its application in measuring transient particle size distributions (Maricq et al., 1999; Kittelson et al., 2006a).

In contrast, the DMS500 and similar instruments are designed to sample entire particle size distributions at a high temporal resolution. The operating principle of the DMS500 is reviewed in detail because the DMS50 (the smaller and mobile version of the DMS500) was used to collect particle number size distributions analyzed in Chapter 7. The classifier column for the DMS500 is displayed in Figure 5 which is used to measure particles between 5 and 500 nm. The particles are charged as they enter the classifier column, and are subsequently repelled by the central electrode in the middle of the column to the perimeter of the classifier column. As the particles impact the outer perimeter of the column, the charge is measured by electrode rings. The impaction location is a function of the aerodynamic drag and the electrical charge the particles receive, which is a function of the particle size. Using known properties of diesel and gasoline particles, including charging efficiency, the DMS500 can calculate a particle size distribution. The advantage of the differential particle sizer, or measurements systems such as the SMPS, is that the entire particle size distribution can be measured at up to 10 samples per second (Cambustion Ltd, 2009).

Meteorological and Artificial Dilution Conditions

The formation of the nucleation mode particles and condensation of the volatile compounds on existing particles is highly dependent on dilution conditions, both in the artificial dilution tunnels for laboratory tests (Abdul-Khalek et al. 1999, Burtscher, 2005), and ambient conditions for vehicle chase studies (Rönkkö et al., 2006; Kittelson et al., 2006a; Giechaskiel et al., 2005).

Several chase studies compared measurements of particle size-distributions from the exhaust plume to laboratory measurements made in artificial dilution conditions (Rönkkö et al., 2006; Kittelson et al., 2006a; Giechaskiel et al., 2005) The dilution ratio is largely a function of the distance between the tail-pipe and following vehicle and the vehicle speed. Dilution ratios in the studies ranged between 200 and 7000:1, with the highest dilution ratio measured at vehicle speeds of 120 km/h (Giechaskiel et al., 2005). The nucleation mode was consistently reported from heavy-duty diesel vehicles (Rönkkö et al., 2006; Kittelson et al., 2006a), and was consistently observed for the light-duty diesel at moderate to high vehicle speeds (Giechaskiel et al., 2005).

While atmospheric conditions have very large dilution ratios, high dilution ratios have been found to suppress nucleation mode formation, in the dilution sampling tunnels. Lower dilution ratios, longer dilution residence times, lower dilution temperature, and high relative humidity create more favorable conditions for nucleation mode formation in sampling dilution tunnels (Abdul-Khalek et al. 1999, Rönkkö et al., 2006, Shi and Harrison, 1999). In the comparison studies, Rönkkö et al. (2006) and Kittelson et al. (2006a) suggest adjusting the dilution ratio and residence time to best replicate on-road particle size distribution measurements. Even still, the nucleation mode particle tended to be underestimated, occasionally by an order of magnitude, in the laboratory (Rönkkö et al., 2006; Kittelson et al., 2006a).

No protocol has been established for measuring nucleation mode particles and measurements can be substantially different based on sampling conditions and the sampling equipment. The European Union has established a particle measurement procedure (PMP) used to establish a particle number based standard. The PMP removes the volatile fraction of the exhaust, which is responsible for the formation of the nucleation mode, in order to maintain repeatable results (Morawska et al., 2008). Ideally, sampling methods should repeatedly measure the true magnitude of nucleation mode particles that exist in the exhaust plume from vehicles driving in real-world conditions, however such measurement methods are still evolving for artificial dilution systems (Rönkkö et al., 2006; Kittelson et al., 2006a).

Cold-starts significantly increase the particles for both gasoline and trap-equipped diesel vehicles (Mathis et al., 2005a). However, in general, the shape of the particle size distribution is insensitive to temperature changes from the cold start. Cold ambient conditions have no observed effect on non-volatile particle size concentrations (Mathis et al., 2005a). But lower dilution air temperatures caused higher particle number concentrations by causing more of the volatile fraction to condense and nucleate (Shi et al., 2000). The negative effect of temperature on nucleation particle number concentrations has also been observed for engine exhaust diluted in the atmosphere (Kittelson et al., 2004; Zhu et al., 2002).

Transformation of ambient particle concentration near roadways

An in-depth discussion of the formation, transformation, and deposition mechanics for particles suspended in the atmosphere is beyond the scope of the introduction. Nonetheless, inferences are often made about the particle size distribution of motor vehicle emissions, from ambient measurements made from tunnels (Gellar et al., 2005), the road-side (Charron and Harrison, 2003; Zhu et al.,

2002) and on-road studies (Kittelson et al., 2004). An overview of the factors influencing the transformation of particles is provided to help interpret findings from ambient measurement studies.

The nucleation mode rapidly decays after the exhaust plume disperses in the near-by roadway environment. Particle number concentrations next to major roadways have been observed ~25 times higher than background levels as little as 300 meters from the roadway (Zhu et al., 2002). In contrast, fine particles accumulate in the atmosphere. Only small differences in mass concentrations (PM2.5) are observed between background concentrations and the roadway.

The nucleation mode can be eliminated by volatilization (enhanced by the Kelvin effect on small particles) and coagulation with larger particles (enhanced by the high diffusion rate for small particles) (Zhu et al., 2002). Under night and winter inversion conditions, the nucleation mode can persist, and grow above 30 nm through vapor condensation (Kerminen et al., 2007).

In the roadside study conducted by Zhu et al. (2002), the particles above 100 nanometers only slightly decreased as the distance increased from the roadway. The particle size distribution shifted from having two dominant modes at 10 and 30 nanometers at the roadside to having a dominant mode at 100 nanometers for measurements taken 300 meters away. The accumulation mode continues to grow as particles coagulate and volatile material condenses on these particles, while the removal mechanisms are slowest for accumulation mode particles (Lighty et al., 2000). In summary, the particle size distribution of vehicle exhaust are in a dynamic state after leaving the tailpipe, and will change based on distance from the roadway, background particle concentrations, and atmospheric conditions.

Transportation Emissions Regulations

Quantitative assessment of the environmental effects of transportation projects and policies is mandated through federal environmental and transportation legislation with the Clean Air Act and the current transportation funding act SAFETEA-LU (Federal Highway Administration, 2006). Vehicle emission models are used to calculate the mobile emission inventories, or the total contribution of transportation emissions in a metropolitan area. Mobile emission inventories are key component of State Implementation Plans (SIPs), which are the key drivers to assure transportation policies and plans are consistent with national air quality goals (Federal Highway Administration, 2006). Substantial resources are placed into modeling transportation emissions in all major metropolitan areas in the United States, because federal transportation funds are contingent on the approval of SIP, in a process known as transportation conformity (Federal Highway Administration, 2006).

Particulate Matter Hot-Spots. Transportation projects that have the potential to cause localized violations of the national air quality standards are required to perform hot-spot analysis (US EPA, 2006). Quantitative hot-spot analysis is conducted by estimating project-level vehicle emissions, and estimating localized and regional air quality using a micro-scale air quality model (McCarthy et al., 2006). Near-source exposure to vehicle-source particulate matter (PM) poses a serious health risk (Brunerkreef and Holgate, 2002; McCarthy et al., 2006). Transportation projects that will have substantial levels of diesel traffic, such as construction of freight depots or freeway expansion projects, are required to perform PM hot-spot analysis for $PM_{2.5}$ and PM_{10} (mass of particles smaller than 2.5 and 10 microns, respectively). Currently, only qualitative project-level analysis is required to assess PM hot-spots due to the limitations of current regulatory vehicle emission models (US EPA, 2006).

The current regulatory emission models used in the United States are MOBILE (US EPA, 2003) and EMFAC (California Air Resources Board, 2007) which estimate vehicle-source emission rates, including $PM_{2.5}$ and PM_{10}. However, neither emission model is able to measure PM emission rates that are sensitive to project-level driving conditions (McCarthy et al., 2006). The EPA is currently developing a new emission model, entitled MOVES, that will model PM emissions according to vehicle operating mode, defined by instantaneous vehicle speed and vehicle specific power. The modal-based emission rates will facilitate quantitative project-level analysis for particulate matter, and will be required for quantitative hot-spot analysis when the EPA finalizes the development of MOVES (US EPA, 2006).

To date, regulatory emission models are based on emissions data obtained from laboratory tests where engines or vehicles are tested with simulated loads and driving conditions using dynamometers. However, emissions data from engine dynamometer test need to be extrapolated to actual vehicle operation using approximate correction factors (Kear and Niemeier, 2006) and even chassis dynamometer tests cannot fully replicate real-world driving conditions (Kittelson et al., 2006a; Robert et al., 2007). To address this issue, MOVES was designed to be able to incorporate emissions data collected from real-world vehicle tests. The draft version of MOVES is currently using PM emission rates for light-duty and heavy-duty vehicles (US EPA 2009a,b) from chassis dynamometer tests. While real-world gaseous emission rates have been incorporated into MOVES (US EPA 2009b), more work is needed to establish reliable and repeatable PM emission rates using portable emission measurement systems (PEMS) in real-world driving conditions (US EPA, 2008).

Particle Number Emission Model

Because particle number emissions are intensely concentrated near emission sources, and are known to have adverse health effects, transportation projects should be evaluated in terms of particle number emissions. The evaluation of potential transportation projects for particle number pollution requires the development of particle number emission models. Researchers and practitioners have recognized the importance of developing ultrafine (McCarthy et al., 2006) and size-resolved particle emission number emission models (Zhang et al., 2005).

Summary of Literature Review

The understanding of vehicle-source emissions is evolving and changing rapidly. Although the causal mechanisms are not fully understood, particle emissions are consistently related to adverse health effects. Particle size plays a key role in the relative toxicity of particles. The ultrafine particles fraction, quantified by total particle number, may be a more effective health measure of particulate matter pollution, than PM2.5 and PM10. Modern particle instruments facilitate rapid and resolved measurements of particle number size distributions.

Motor vehicles are major sources of particle pollution, with diesel engines contributing more than an order of magnitude higher particle number and mass emission rates. The particle number size distribution from conventional diesel vehicles has characteristic modes detecting nucleation and accumulation mode particles. Gasoline vehicles also detect nucleation and accumulation mode particles, with the accumulation mode peak occurring at smaller diameters for gasoline vehicles.

Both gasoline and diesel particle emissions are highly influenced by vehicle operating modes; however the effects on particle concentrations are highly dependent on particle size. Factors such as vehicle aftertreatments and fuel types have significant impacts on particle concentrations, and also influence particles differently according to

size. For example, continuous regenerating traps drastically reduce accumulation mode particles, but can encourage the formation of small nucleation mode particles.

Nucleation mode particles can be difficult to detect in artificial dilution tunnels, but are almost always present in real-world exhaust plumes. The particle size distribution evolves rapidly in the atmosphere, with the nucleation mode decaying significantly short distances from vehicle emission sources.

Current, regulatory emission models are developing capabilities to model PM emissions according to vehicle operating mode. Particle emission factors (particles/km) have been estimated for many traffic sources. Less data are available to examine the effect of transient operating modes on particle number emission rates, as well as the effect of advanced technologies and alternative fuels. The development of emission models capable of estimating size-resolved particle emissions has been identified as a research priority.

REFERENCES

Abdul-Khalek, I. S.; Kittelson, D. B.; Brear, F.; The Influence of Dilution Conditions on Diesel Exhaust Particle Size Distribution Measurment. Presented at 1999 International Congress and Exposition, March 1999, Detroit, Michigan. SAE Technical Paper Series 1999-01-1142 SAE International. 1999.

American Lung Association (ALA): State of the Air 2007. Available at http://www.lungusa.org.

Baltensperger, U.; Weingartner, E.; Burtscher, H.; Dynamic Mass and Surface Area Measurements. In *Aerosol Measurement - Principles, Techniques, and Applications (2nd Edition)*. Baron, P. A.; Willeke, K. John Wiley & Sons: New York, 2001.

Beddows, S. C. D.; Dall'osto, M.; Harrison, R. M. Cluster analysis of rural, urban, and curbside atmospheric particle size data. *Environ. Sci. Technol.*. **2009**, *43* (13), 4694-4700.

Biswas, S.; Hu, S.; Verma, V.; Herner, J. D.; Robertson, W. H.; Ayala, A; Sioutas, C. Physical properties of particulate matter (PM) from late model heavy-duty diesel vehicles operating with advanced PM and NOx emission control technologies. *Atmospheric Environment*. **2008**, *42* (22), 5622-5634.

Brunerkreef, B.; Holgate, S. T. Air pollution and health. *Lancet.* **2002**, *360*, 1233-42.

Burtscher H. Physical characterization of particulate emissions from diesel engines: A review. *Aerosol Science* **2005**, 36, 896-932.

California Air Resources Board. EMFAC2007 version 2.30. Calculating emission inventories for vehicles in California User's Guide. Available at: http://www.arb.ca.gov/msei/onroad/latest_version.htm. Accessed November 2009.

Cambustion Limited Website; DMS500 Principles of Operation. Available at: http://www.cambustion.com/instruments/dms500/principle-operation. Accessed November 2009.

Clark, N. N.; Gautam, M.; Wayne, W. S.; Lyons, D. W.; Thompson, G., Zielinska, B. HEAVY-DUTY Vehicle Chassis Dynamometer Testing for Emissions Inventory, Air Quality Modeling, Source Apportionment and Air Toxics Emissions Inventory August 2007; CRC Report No. E55/59: Desert Research Institute (Subcontractor),: West Virginia University Research Corporation, Department of Mechanical & Aerospace Engineering: Morgantown, WV, 2007.

Charron, A.; Harrison, R. M. Primary particle formation from vehicle emissions during exhaust dilution in the roadside atmosphere. *Atmospheric Environment*, **2003**, 37(29), 4109-4119.

Chalupa, D. C.; Morrow, P. E.; Oberdörster, G.; Utell, M. J.; Frampton, M. W. (2004). Ultrafine particle deposition in subjects with asthma. *Environmental Health Perspectives*. **2004**, *112*(8), 879–882.

Coyle, W. The Future of biofuels: A global perspective. *Amber Waves.* **2007**, *5*(5), 24-29.

Davis, S. C.; Diegel, S. W.; Boundy, R. G.; Transportation Energy Data Book. Edition 27; Oak Ridge National Laboratory ORNL-6981: Oak Ridge, TN, 2008.

Federal Highway Administration: Transportation Conformity Reference Guide. Revised March 2006. Retrieved October 23, 2009, Available at http://www.fhwa.dot.gov/environment/conformity/ref_guid/index.htm.

Geller, M. D.; Sardar, S. B.; Phuleria H.; Fine, P. M.; Sioutas, C. Measurements of particle number and mass concentrations and size distributions in a tunnel environment. *Environ. Sci. Technol*. **2005**, *39,* 8653-8663.

Giechaskiel, B.; Ntziachristos, L.; Samaras, Z.; Scheer, V.; Casati, R.; Vogt, R. Formation potential of vehicle exhaust nucleation mode particles on-road and in the laboratory. *Atmospheric Environment*. **2005**, *39* (18), 3191-3198.

Harris, S. J.; Maricq, M. M. Signature size distributions for diesel and gasoline engine exhaust particulate matter. *Journal of Aerosol Science*. **2001**, *32*, 749–764.

Holmén, B. A.; Ayala, A. Ultrafine PM emissions from natural gas, oxidation-catalyst diesel, and particle-trap diesel heavy-duty transit buses. *Environ. Sci. Technol*. **2002**, *36*, 5041-5050

Holmén, B. A.; Chen, Z.; Davila, A. C.; Gao, O. H.; Vikara, D. M. *Particulate Matter Emissions from Hybrid Diesel-Electric and Conventional Diesel Transit Buses: Fuel and Aftertreatment Effects*. JHR 05-304, Project 03-8; Joint Highway Research Advisory Council: Hartford, CT, 2005.

Kear, T., Niemeier, D.A. On-road heavy-duty diesel particulate matter emissions modeled using chassis dynameter data. *Environ. Sci. Technol*. **2006**, *40*, 7828-7833.

Keogh, D. U.; Ferreira, L.; Morawska, L. Development of a particle number and particle mass vehicle emissions inventory for an urban fleet. *Environmental Modeling & Software*. **2009**, *24*, 1323–1331.

Kerminen, V-M.; Pakkanen, T. A.; Makela, T.; Hillamo, R. E.; Sillanpaa, M.; Rönkkö, T.; Virtanen, A.; Keskinen, J.; Pirjola, L.; Hussein, T.; Hameri, K. Development of particle number size distribution near a major road in Helsinki during an episodic inversion situation. *Atmospheric Environment*. **2007**, *41* (8), 1759-1767.

Kinsey, J. S.; Mitchell W. A.; Squier W. C.; Linna, K.; King, F. G.; Logan, R.; Dong, Y.; Thompson G. J.; Clark, N. N. Evaluation of methods for the determination of diesel-generated fine particulate matter: Physical characterization results. *J. of Aerosol Science*. **2006**, *37*, 63-87.

Kittelson, D. B. Engines and nanoparticles: a review. *J. Aerosol Sci*. **1998,** *29*(5-6), 575-588.

Kittleson, D. B.; Watts, W. F.; Johnson, J. P. Nanoparticle emissions on Minnesota highways. *Atmos. Environ*. **2004**, *38*, 9-19.

Kittelson, D. B.; Watts, W.F.; Johnson, J. P. On-road and laboratory evaluation of combustion aerosols—Part1: Summary of diesel engine results. *Aerosol Science*. **2006a**, *37*, 913–930.

Kittelson, D. B.; Watts, W. F.; Johnson, J. P.; Schauer, J. J.; Lawson, D. R. On-road and laboratory evaluation of combustion aerosols—Part 2: Summary of spark ignition engine results. *Aerosol Science*. **2006b**, *37*, 931 – 949.

Kittelson, D. B.; Watts, W. F.; Johnson, J. P.; Thorne, C.; Higham, C.; Payne, M.; Goodier, S.; Warrens, C.; Preston, H.; Zink, U.; Pickles, D.; Goersmann, C.; Twigg, M. V.; Walker, A. P.; Boddy, R. Effect of fuel and lube oil sulfur on the performance of a diesel exhaust gas Continuously Regenerating Trap. *Environmental Science & Technology*. **2008** *42* (24), 9276-9282.

Kittelson, D. B.; Watts, W. F.; Johnson, J. Diesel Aerosol Sampling Methodology; Final Report No CRC-E43; University of Minnesota: Minneapolis, MN, 2002.

Kleeman, M.J.; Schauer, J.J.; Cass, G.R. Size and composition distribution of fine particulate matter emitted from motor vehicles. *Environ. Sci. Technol*. **2000**, *34*, 1132-1142.

Lapuerta M.; Rodríguez-Fernández J.; Agudelo J. R.; Diesel particulate emissions from used cooking oil biodiesel. *Bioresource technology*. **2008**, *99*(4), 731-740.

Lee, K. W.; Mukund, R.; Filter Collection. In *Aerosol Measurement - Principles, Techniques, and Applications (2nd Edition)*. Baron, P. A.; Willeke, K. John Wiley & Sons: New York, 2001.

Lee, H.; Myung, C.; Park, S. Time-resolved particle emission and size distribution characteristics during dynamic engine operation conditions with ethanol-blended fuels. *Fuel*. In Press, Corrected Proof, Available online 27 March 2009.

Lighty, J. S.; Veranth, J. M.; Sarofim, A. F. Combustion aerosols: factors governing their size and compositions and implications to human health. *J. Air & Waste Manage. Assoc*. **2000**, *50*, 1565-1618.

Liu, Z. G.; Ford, D. C.; Vasys, V. N.; Chen, D.; Johnson, T. R. Influence of engine operating conditions on diesel particulate matter emissions in relation to transient and steady-state conditions. *Environ. Sci. Technol*. **2007**, *41* (13), 4593-4599.

Luders, H.; Kruger, M.; Stommel, P.; Luers, B. Role of sampling conditions in particle size distribution measurements. SAE Special Publications 1367, Advances in General Emissions, Warrendale, PA, 1997, 1-8.

Maricq, M. M. Chemical characterization of particulate emissions from diesel engines: A review. *Aerosol Science*. **2007**, *38*, 1079 – 1118.

Maricq, M. M.; Podsiadlik, D. H.; Chase, R. E. Examination of the size-resolved and transient nature of motor vehicle particle emissions. *Environ. Sci. Technol*. **1999**, *33* (10), 1618-1626.

Maricq, M. M.; Podsiadlik D. H.; Chase R. E. Size Distributions of Motor Vehicle Exhaust PM: A Comparison Between ELPI and SMPS Measurements. *Aerosol Sci. Technol*. **2000**, 33, 239-260.

Marple, V. A.; Olson, B. A.; Rubow, K. L.; Inertial, Gravitational, Centrifugal, and Thermal Collection Techniques. In *Aerosol Measurement - Principles, Techniques, and Applications (2nd Edition)*. Baron, P. A.; Willeke, K. John Wiley & Sons: New York, 2001.

Mathis, U.; Mohr, M.; Forss, A. Comprehensive particle characterization of modern gasoline and diesel passenger cars at low ambient temperatures. *Atmos. Environ.* **2005a**, *39*, 107–117.

Mathis, U.; Mohr, M.; Kaegi, R.; Bertola, A.; Boulouchos, K. Influence of diesel engine combustion parameters on primary soot particle diameter. *Environ. Sci. & Technol*. **2005b**, *39* (6), 1887-1892.

McCarthy, M. C.; Eisinger, D. S.; Hafner, H. R.; Chinkin, L. R.; Roberts, P. T.; Black, K. N.; Clark, N. N.; McMurry, P. H.; Winer, A. M. Particulate matter: A strategic vision for transportation-related research. *Environ. Sci. Technol*. **2006**, *40*, 5593–5599.

McCormick, R. L. The impact of biodiesel on pollutant emissions and public health. *Inhalation Toxicology*. **2007**, *19*, 1033-1039.

Morawska, L.; Ristovski, Z.; Jayaratne, E. R.; Keogh, D. U.; Ling, X. Ambient nano and ultrafine particles from motor vehicle emissions: Characteristics, ambient processing and implications on human exposure. *Atmospheric Environment*, **2008**, *42*, 8113-8138.

Mulawa, P. A.; Cadle, S. H.; Knapp, K.; Zweidinger, R.; Snow, R.; Lucas, R.; Goldbach, J. Effect of ambient temperature and E-10 fuel on primary exhaust particulate matter emissions from light duty vehicles. *Environ. Sci. Technol*. **1997**, *31*(5), 1302-1307.

National Biodiesel Board. Overview of H.R.6, Energy Independence and Security Act of 2007. http://www.biodiesel.org/news/RFS/Biodiesel.

National Research Council. *Air Quality Management in the United States*: National Academies Press: Washington, D.C., 2004.

Ristovski, Z. D.; Jayaratne, E. R.; Lim, M.; Ayoko, G. A.; Morawska, L. Influence of diesel fuel sulfur on nanoparticle emissions from city buses. *Environ. Sci. Technol*. **2006**, *40*, 1314-1320.

Robert, M.A.; Jakober, C.A.; Kleeman, M.J. Size and composition distribution of particulate matter: Part 1—Light-duty gasoline vehicles. *J. Air & Waste Manage. Assoc*. **2007a**, *57*, 1414-1428.

Robert, M. A.; Kleeman, M. J.; Jakober, C. A. Size and composition distributions of particulate matter emissions: Part 2—Heavy-duty diesel vehicles. *J. Air & Waste Manage.* Assoc. **2007b**, *57*, 1429–1438.

Rönkkö, T.; Virtanen, A.; Vaaraslahti, K.; Keskinen, J.; Pirjola, L.; Lappi, M. Effect of dilution conditions and driving parameters on nucleation mode particles in diesel exhaust: Laboratory and on-road study. *Atmospheric Environment*. **2006**, *40* (16), 2893-2901.

Shi, J. P.; Mark, D.; Harrison, R. M. Characterization of particles from a current technology heavy-duty diesel engine. *Environ. Sci. Technol*. **2000**, *34*, 748-755.

Shi, J. P.; Harrison, R. M. Investigation of ultrafine particle formation during diesel exhaust dilution. *Environ. Sci. Technol*. **1999**, *33*, 3730-3736.

Sienfield, J. H.; Pandis S. N.; Atmospheric Chemistry and Physics: From Air Pollution to Climate Change; John Wiley & Sons, Inc.: Hoboken, New Jersey, 2006.

Sonntag, D.B.; Gao, H. O.; Holmén, B. A. Variability of particle number emissions from diesel and hybrid diesel-electric buses in real driving conditions. *Environ. Sci. Technol*. **2008,** *42,* 5637-5643.

Tyner, W. E. The US ethanol and biofuels boom: Its origins, current status, and future prospects. *BioScience*. **2008**, *58*(7), 646-653.

U.S. Environmental Protection Agency. Control of air pollution from new motor vehicles: Heavy-duty engine and vehicle standards and highway diesel fuel sulfur control requirements; Final Rule. 40 CFR Parts 69, 80, and 86. *Fed. Regist*. **2001,** *66,* 5001–5193.

U.S. Environmental Protection Agency. *Latest Findings on National Air Quality-2001 Status and Trends*. Publication EPA 454/K-02-001. U.S. EPA, September 2002.

US Environmental Protection Agency. User's Guide to MOBILE6.1 and MOBILE6.2. Publication EPA420-R-03-010. US EPA, 2003.

U.S. Environmental Protection Agency. *Air Quality Criteria for Particulate Matter,* Vol. 2. Publication EPA/600/P-99/002bF. U.S. EPA, October 2004.

U.S. Environmental Protection Agency. PM2.5 and PM10 hot-Spot analyses in project-level transportation conformity determinations for the new PM2.5 and existing PM10 national ambient air quality standards; Final Rule. 40 CFR Part 93. *Fed. Regist*. **2006**, *71*, 12468–12511.

US Environmental Protection Agency. Fact Sheet Final Revisions to the National Ambient Air Quality Standards for Particle Pollution. U.S. EPA. Accessed Oct. 22, 2007. Available at http://www.epa.gov/oar/particlepollution/pdfs/20060921_factsheet.pdf.

U.S. Environmental Protection Agency. *Determination of PEMS Measurement Allowances for Gaseous Emissions Regulated Under the Heavy-Duty Diesel Engine*

In-Use Testing Program: Revised Final Report; EPA420-R-08-005: Prepared for EPA by Southwest Research Institute, 2008.

U.S. Environmental Protection Agency. *Latest Findings on National Air Quality-2006 Status and Trends*; EPA-454/R-07-007: U.S. EPA, 2008.

U.S. Environmental Protection Agency. *Development of Emission Rates for Light-Duty Vehicles in the Motor Vehicle Emissions Simulator (Draft MOVES2009): Draft Report*. EPA-420-P-09-002. U.S. EPA, 2009a.

U.S. Environmental Protection Agency. *Development of Emission Rates for Heavy-Duty Vehicles in the Motor Vehicle Emissions Simulator (Draft MOVES2009): Draft Report*. EPA-420-P-09-005. U.S. EPA, 2009b.

US EPA. Diesel Retrofit Technology Verification Website; http://www.epa.gov/oms/retrofit/verif-list.htm. 2009c.

US EPA. National Clean Diesel Campaign Website; http://www.epa.gov/otaq/diesel/index.htm. 2009d.

EPA Office of Transportation and Air Quality: EPA Will Propose Historic Greenhouse Gas Emissions Standards for Light-Duty Vehicles. EPA-420-F-09-028. Available at http://epa.gov/otaq/climate/regulations/420f09028.htm. Accessed July 21, 2009.

Vaaraslahti, K.; Virtanen, A.; Ristimäki, J.; Keskinen, J. Nucleation mode formation in heavy-duty diesel exhaust with and without a particulate filter. *Environ. Sci. Technol*. **2004**, *38* (18), 4884-4890.

Virtanen, A. K. K.; Ristimäki, J. M.; Vaaraslahti, K. M.; Keskinen, J. Effect of engine load on diesel soot particles. *Environ. Sci. Technol*. **2004**, *38* (9), 2551-2556.

Wichmann, H. E.; Peters, A.; Epidemiological evidence of the effects of ultrafine particle exposure. In *Ultrafine Particles in the Atmosphere*; Brown, L. M., Collings, N., Harrison, R. M., Maynard, A.D., Maynard, R.L., Eds.; Imperial College Press: London, 2000.

Yanowitz, J.; Mccormick, R. L.; Graboski, M. S. In-use emissions from heavy duty diesel vehicles. *Environ. Sci. & Technol.* **2000**, *34* (5), 729-740.

Zhang K. M.; Wexler, A. S.; Niemeier, D. A.; Zhu Y. F.; Hinds, W. C.; Sioutas, C. Evolution of particle number distributions near roadways Part III: Traffic analysis and on-road size resolved particulate emission factors. *Atmospheric Environment*. **2005**, *39*(22), 4155-4166.

Zhu, Y.; Hinds, W.; Kim, S.; Sioutas, C. Concentration and size distribution of ultrafine particles near a major highway. *J. Air Waste Manage. Assoc*. **2002**, *52*, 1032–1042.

CHAPTER 3

VARIABILITY OF PARTICLE NUMBER EMISSIONS FROM DIESEL AND HYBRID DIESEL-ELECTRIC BUSES IN REAL DRIVING CONDITIONS[1]

Abstract

A linear mixed model was developed to quantify the variability of particle number emissions from transit buses tested in real-world driving conditions. Two conventional diesel buses and two hybrid diesel-electric buses were tested throughout 2004 under different aftertreatments, fuels, drivers, and bus routes. The mixed model controlled for the confounding influence of factors inherent to on-board testing. Statistical tests showed that particle number emissions varied significantly according to the aftertreatment, bus route, driver, bus type, and daily temperature, with only minor variability attributable to differences between the fuel types. The daily setup and operation of the sampling equipment (Electrical Low Pressure Impactor) and mini-dilution system contributed to 30-84% of the total random variability of particle measurements among tests with the diesel oxidation catalysts. By controlling for the sampling day variability, the model better defined the differences in particle emissions among bus routes. In contrast, the low particle number emissions measured with the diesel particle filters (decreased by over 99%) did not vary according to operating conditions or bus type, but did vary substantially with ambient temperature.

Introduction

Health studies have associated increased risk of mortality to persons living close to major roads, proposing that ultrafine particles may be one of the causal links

---

[1]Sonntag, D.B., H. O. Gao, and B. A. Holmén. Variability of particle number emissions from diesel and hybrid diesel-electric buses in real driving conditions. *Environ. Sci. & Technol*. **2008,** 42, 5637-5643.

(Finkelstein et al., 2004; Brunekreef and Holgate, 2002). Motor vehicles are typically the largest source of ultrafine and fine particles, which dominate the number distribution of particulate matter (PM) emissions (Kittelson et al., 2004), in urban areas (Hitchins et al., 2000). More over, roadside and on-road studies assert that ultrafine particle *number* concentrations can be 10~25 times greater on or next to major freeways than in background areas (Zhu et al., 2002), whereas PM *mass* concentrations are only slightly elevated near busy roads (McCarthy et al., 2006).

To provide added insight to the health impact of motor vehicle exhaust, substantial research has been conducted to evaluate particle number emissions from gasoline and diesel vehicles, in both laboratory tests (Zervas et al, 2004; Mathis et al., 2005) and roadway tests (Kittelson et al., 2004; Jamriska et al, 2004). However, the factors that influence vehicular particle number emissions are hard to establish and quantify because variability observed in particle number emission tests can make it difficult to distinguish between true emission processes and random artifacts of the data. Analysis and understanding of emissions variability is a critical first step for quantifying particle number emissions according to traffic, environmental, and road network conditions.

This work explained the variability of bus particle number emissions by analyzing particle number data collected from an on-board transit bus study that evaluated two types of buses (conventional diesel and hybrid diesel-electric buses) tested under different fuels, aftertreatments, routes, drivers, and ambient environmental conditions. On-board testing permitted the vehicles to be subject to real-world variations in driving behavior, road grade, traffic and weather conditions that cannot be simulated in the laboratory. However, controlling for multiple variability sources poses a special challenge to on-board measurements. Even in laboratory testing, where the driving cycle and ambient conditions are strictly

controlled, the between-test variability can be substantial (Zervas et al, 2004). In on-board testing many factors that affect particle emissions vary simultaneously, making their respective effects difficult to distinguish from one another. Because each of the confounding factors could not be controlled experimentally, this study adopted a statistical mixed model, which controlled for the confounding influence of each factor, to characterize the variability of measured bus particle number emissions associated with the experimental factors.

Experimental error has two components: variation and bias. This study focused on a systematic treatment of variability. The systematic bias of particle measurements due to sampling equipment (Maricq et al., 2000) or dilution systems (Kittelson et al., 2004) is beyond the scope of this study.

Particle Number Emissions Data

In 2005, Holmén *et al.* (2005) completed a study testing PM emissions differences between two conventional diesel (CD) and two hybrid diesel-electric (HDE) buses in the Connecticut Transit bus fleet. The CD buses were equipped with 2002 Detroit Diesel Series 40 engines, while the HDE buses were equipped with 2003 Cummins ISL 280 diesel engines with an electric drive parallel hybrid GM Allison E^p transmission. Both bus types had 40-foot New Flyer chassis, with engines certified to meet EPA PM emission standards. The two buses within each group were identical in make and model year with comparable odometer readings (Holmén et al., 2005).

The buses were subject to on-board testing under three fuel/aftertreatment configurations throughout 2004. The buses ran on No. 1 Diesel fuel in Phase I (15 days, January-April) and ultra-low sulfur diesel (ULSD) during Phase II (9 days, July-September). The buses had diesel oxidation catalysts (DOCs) in phases I+II. In Phase III (9 days, Oct-Nov) the buses were run on ULSD fuel and outfitted with diesel particle filters (DPFs). No. 1 Diesel fuel had a sulfur content between 230~320 ppm,

and the ULSD had a sulfur content between 8~51 ppm which exceeds the EPA's current 15 ppm sulfur standard for ULSD. In phase III the CD buses were equipped with Engelhard DPX diesel particulate filters, and the HDE buses were equipped with Johnson-Matthey CRT diesel particulate filters. A single bus driver was used in all testing days from April until the end of the year. However, two primary bus drivers were used during Phase I, with a third bus driver used on January 23rd (Holmén et al., 2005).

The buses were tested on three routes in Hartford, CT: Enfield, Farmington, and Avon. Enfield is a freeway commuting route, 16.4 miles in length. The Farmington route runs 5.2 miles through downtown Hartford, with stop-and-go driving conditions due to intersections and simulated bus stops. The Avon route travels 8.2 miles up and down Talcott Mountain, with sections exceeding 8% grade on both sides of the mountain. For purposes of this analysis, uphill and downhill sections of Avon were considered as separate routes. After an initial warm-up run on each testing day, the bus routes were typically tested in both outbound and inbound runs[2]. Several days and runs were removed from the analysis due to equipment failure or other errors that caused unrepresentative measurements. Even so, each bus was successfully tested for at least two full days under each fuel/aftertreatment. Table 3.1 summarizes the average vehicle speed and engine load recorded using VANSCO engine computer unit (ECU) scan tool for each route according to bus type. The two bus types operated similarly on the four routes with exception of the Farmington Route, where the HDE bus operated at a noticeably lower percent engine load.

[2] Inbound and outbound runs are not exact replicates due to changes in factors such as traffic and road grade. This between-run variability for the same route is accounted for by the random "run" factor in the mixed model in Table 2.

Table 3.1. Vehicle Parameters by Routes for both Bus Technologies

	Conventional Diesel Bus			Hybrid Diesel-Electric Bus		
Vehicle Speed (km/h)	**Average**	**Std Dev**	**(Min/Max)**	**Average**	**Std Dev**	**(Min/Max)**
Avon Down	59.1	4.6	(43.3/71.5)	59.7	4.7	(44.3/70.5)
Avon Up	55.3	3.3	(45.9/65.6)	55.1	3.4	(46.9/63.9)
Enfield	95.5	1.9	(89.5/100.9)	96.1	2.6	(81.8/101.1)
Farmington	16.2	0.9	(11.8/18.4)	17.2	0.9	(14.0/20.7)
% Engine Load						
Avon Down	11%	7.5	(3%/36%)	9%	6.8	(1%/31%)
Avon Up	92%	11.1	(53%/100%)	93%	4.9	(78%/96%)
Enfield	74%	6.6	(61%/86%)	73%	5.2	(61%/81%)
Farmington	42%	2.8	(37%/47%)	27%	2.3	(22%/31%)

On each sampling day, one of the four buses was outfitted with experimental equipment consisting of a dual constant flow mini-dilution system, sampling instruments and computers, and a small trailer containing a generator to power the auxiliary equipment and an air compressor for the mini-dilution system. A constant exhaust flow was sampled and transferred from the exhaust pipe to a 6-foot long, 1-inch diameter mini-dilution tunnel located within the bus. The exhaust was single-stage ejector diluted with ambient air that passed through condensate traps, silica gel, activated carbon and a high-efficiency particulate air filter to remove water, hydrocarbons and background particles. The dilution ratio was regularly calibrated and did not change significantly between runs on each sampling day, with the average dilution ratio ranging between 23~32 across the experimental days.

The particle number concentration of the diluted exhaust was measured using a Dekati electrical low pressure impactor (ELPI) at a temporal resolution of 1~2 seconds. An estimated 10-second lag occurred between the engine start and initial

ELPI data recording, which accounts for the exhaust residence time in the mini-dilution system. The ELPI was outfitted with an electrical filter stage accessory to extend the lower cut size, yielding 12 size bins measuring particles with aerodynamic diameters between 7 nm and 10 μm. The output measurement of the ELPI is the particle number concentration per cubic centimeter of sampled air (#/cc), with corrections for charger efficiency and small particle losses (Holmén et al., 2005). The unit of analysis for this study is the route-average particle number concentration (i.e., sum over all 12 ELPI size bins) for each test run.

Model Formulation

A linear mixed model was used to account for the sources of variability of the particle number emissions data. The complex variance structure of the data was modeled by representing the effect of each factor as fixed or random, as shown in Table 3.2. Fixed effects represent the mean response of the dependent variable (particle number concentration) according to categorical factors (e.g., routes, bus technologies, fuel types, etc.) or continuous covariates (e.g., temperature), where the levels within each factor (e.g. CD and HDE within the bus technology factor) represent all levels of interest (West et al., 2007).

Random factors are categorical variables that contain only a sample of all possible levels of interest to the analyst. For example, the day random factor contains a sample of potential days that could have been selected for testing. Each level within a random factor is modeled as a random value, drawn from a population of potential effects. Random effects, with a mean zero and variance σ^2, represent the random deviations from the fixed effects (West et al., 2007).

Table 3.2. Linear Mixed Model Structure

Model Structure		Variables	Effect Notation	Interpretation
Level 3	Random Factor:	Bus	bus_i i = 1:4	Two buses of each bus technology
	Fixed Factor:	Technology	$Tech_l$ l=1:2	CD or HDE bus
Level 2	Random Factor:	Day	$day_{j[i]}$ j = 1:6-10 [a]	Days tested with each bus
	Fixed Factors:	Fuel	$Fuel_m$ m=1:2	#1 Diesel or ULSD
		Aftertreatment	$After_n$ n = 1:2	DOC or DOC+DPF
		Driver	$Driver_o$ o = 1:2	Pre-April or post-April drivers
	Covariates :	Temperature	β·Temperature	β=fixed slope for daily temperature change
Level 1	Random Factor:	Run	$e_{k[j,i]}$ k = 1:8 [b]	Runs made each day
	Fixed Factor:	Route	$Route_p$ p = 1:4	Avon Up, Avon Down, Enfield, Farmington

[a]Each bus was tested for 6,7, or 10 days. [b]Typically 8 runs were made each day, exceptions noted in Supporting Information.

Random Effects. By including random factors, the variation of the particle number emissions was distributed to the three levels shown in Table 3.2. The lowest level (level 1) of the model was route-average particle concentration of each bus run, which is the unit of analysis for the study. The effect of each run was considered a random effect or more frequently referred to as the residual error. It represents the within-bus and within-day variability that exists between bus runs, after controlling for all fixed effects.

The random day factor was used to account for the variation between testing runs that occurred on different days. The 33 testing days between January 6 and November 10 provided a wide range of testing conditions in all four seasons of the year. Modeling testing day as a random effect enabled the inference about such variance. Because only one bus was tested each day, the days were clustered within each bus, which was modeled as a random effect at the third level of the data. Even

though the bus sample size was limited, by modeling the random bus effect we were able to account for the variability that occurred between individual buses of the same technology type.

Fixed Effects. At each level of data, fixed effects are used to explain variability that would otherwise be attributed to random effects. At level 1, the route factor accounted for the variability that can be attributed to changes in road and traffic conditions of the bus route. At level 2, multiple fixed factors were added to explain differences between day-to-day testing. Each day, one bus was tested under one fuel, aftertreatment and driver. These factors were anticipated to explain a significant amount of the variation that occurs between days and were included as fixed categorical factors. The daily temperature recorded at the beginning of the testing day was added as a continuous covariate to control for differences in meteorological conditions. The technology factor quantified the difference in particle emissions between the four buses that is explained by the CD and HDE classification.

Interaction Effects. The effect of each factor may interact with other factors. For example, the effect of using the hybrid bus may depend on the bus route. Adding all potential interactions (>20 possible two- and three-way interactions) and retaining all that are statistically significant could cause the model to overfit the data. Overfitting occurs when the fixed effects account for more than their true effects, and explain the random variability of the sample. To avoid model overfitting, only those interactions that made intuitive sense were included, yielding the following model.

$$\begin{aligned}\log_{10}(PNC_{i,j,k}) = {} & \mu + Tech_l + Fuel_m + After_n + Driver_o + Route_p \\ & + Tech \times Fuel_{l,m} + Tech \times After_{l,n} + Tech \times Route_{l,p} \\ & + Driver \times Route_{o,p} + After \times Route_{n,p} \\ & + (After \times \beta_n) \cdot Temperature \\ & + bus_i + day_{j[i]} + e_{k[i,j]}\end{aligned}$$

where $PNC_{i,j,k}$ = average particle number concentration of each bus run, and μ = model intercept. The main fixed effects and the random effects were previously defined in Table 3.2. The interaction effects are represented as the two fixed effects crossed. Tech×Fuel permits the effect of fuel to depend on bus type, Tech×After accounts for the effect of the different aftertreatments installed on different bus types, Driver×Route represents the effect that bus drivers may drive on each route differently, After×β_1 models the effect of DPF that could depend on temperature, and After×Route reflects route effects possibly depending on whether a DPF is used or not.

Model Diagnostics. The linear mixed model assumes that random effects are normally distributed with mean zero and variance associated with each random factor. To comply with the model assumptions of normally distributed errors, first the particle number concentration was transformed by taking the logarithm to control for the large positive skewness of the data. Then a heterogeneous residual structure was estimated, with one variance for the residual errors under the DPF aftertreatment and four under the DOC aftertreatment (one for each route). The model fit significantly increased (*p*-value <0.0001), and the residuals passed the standard normality tests (See Supporting Information). This assured that the large variation of particle number emissions was accurately modeled and the statistical inference tests conducted were sound (West et al., 2007).

Table 3.3. Linear Mixed Model Results for Bus Particle Number Emissions Effects

Random Effects

	Variance of Random Effects			% Total Random Variation		
Group	bus	Day	Residual	Bus	day	Residual
DPF	7E-06	0.013	0.141	0.004%	8%	92%
Avon Down (DOC)	7E-06	0.013	0.030	0.02%	30%	70%
Avon Up (DOC)	7E-06	0.013	0.002	0.05%	84%	16%
Enfield (DOC)	7E-06	0.013	0.010	0.03%	56%	44%
Farmington (DOC)	7E-06	0.013	0.008	0.03%	63%	37%

Fixed Effects [a]

		Estimate	t Value	P > |t|	Relative to baseline
Intercept		5.6842	66.61	0.0002	
Tech	HDE	0.2878	3.51	0.0725	194%
	CD	baseline	.	.	100%
Fuel	#1 D	0.02634	0.32	0.7497	106%
	ULSD	baseline	.	.	100%
Aftertreatment	DOC+DPF	-2.7605	-15.86	<.0001	0.17%
	DOC	baseline	.	.	100%
Driver	Pre-April 1	-0.1823	-2.12	0.0454	66%
	Post-April 1	baseline	.	.	100%
Temperature		-0.0139	-5.32	<.0001	97%
Route	Avon Down	-0.4276	-9.71	<.0001	37%
	Avon Up	0.3376	14.89	<.0001	218%
	Enfield	0.4062	13.48	<.0001	255%
	Farmington	baseline	.	.	100%

[a] The main fixed effects reported are based on a baseline scenario of the CD bus, ULSD fuel, DOC aftertreatment, post-April bus driver, and Farmington route. Because interaction effects are modeled, the main effects will change with a different baseline scenario.

Results

Table 3.3 displays the estimated variances for the random effects and the parameters for the main fixed effects, which are further discussed.

Random Effects. The five residual variances grouped according to the DPF aftertreatment and routes tested with the DOC aftertreatment are shown in Table 3.3. Single variance terms were estimated for the random bus and day effects for all treatment levels. The variance estimates help to quantify the random variability attributable to each factor. For example, the amount of variation explained by the day factor for the DPF runs was:

$$\frac{\sigma_{day}^2}{\sigma_{bus}^2 + \sigma_{day}^2 + \sigma^2} = \frac{0.013}{7 \cdot 10^{-6} + 0.013 + 0.141} = 8\%$$

The estimated variances also reveal the correlation structure of emissions variation (Singer, 1998). For example, within a certain bus, the random effects of each bus run with DPF were correlated with the correlation coefficient:

$$\rho = \frac{\sigma_{day}^2}{\sigma_{day}^2 + \sigma^2} = \frac{0.013}{0.013 + 0.141} = 8\%$$

Because the bus random effect is minimal, total random variability explained by the day effect and the correlation of bus runs within a testing day were roughly equivalent. Similar calculations were performed for other residual groups, which were found to be highly correlated with the day effects, with correlation coefficients ranging from 30-84% depending on the bus route.

Fixed Effects. The fixed effects reported in Table 3.3 are in relation to the baseline case of a CD bus with ULSD fuel and DOC aftertreatment driven on the Farmington route. Because the model estimated the logarithm of particle number concentration, the effects estimated the change in particle concentrations from the baseline in orders of magnitude. For example, the HDE bus effect (0.2878)

corresponds to a $10^{0.2878}$ = 195% increase in particle number concentrations. The temperature effect suggests that the particle emission concentration was reduced by 3% for 1°C increase in ambient temperature. The *p*-values indicate that the effects of aftertreatment, driver, temperature and route were all significant at the 5% level.

Because the main fixed effects depend on the baseline scenario, more general conclusions can be made by evaluating the interaction effects. The interaction effects are demonstrated in Figure 1 by plotting least square means, which are model-based estimates of the mean particle number concentration, according to specified fixed effects. Confidence intervals for the least square means are plotted on the interaction plots and can be used to determine significant differences between the fixed effects. Differences between least square means were also calculated using adjusted *p*-values, which control for the type I error rate when multiple comparisons were made (see Supporting Information) (Littell et al., 2006).

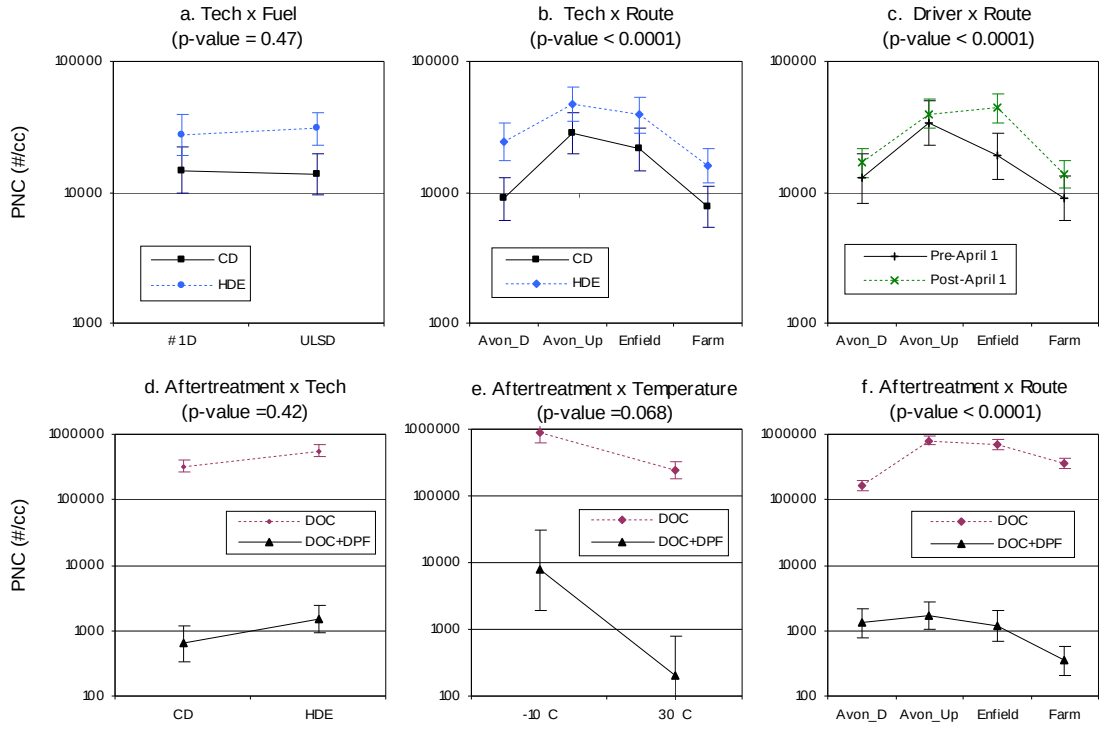

Figure 3.1. Graphical evaluation of the six two-way interactions

The interactions of bus technology with fuel and aftertreatment were not significant (evidenced by the roughly parallel lines in Figures 1a and 1d). Compared to #1 diesel, ULSD did not have a significant effect on particle emissions, regardless of the bus technology type. The DPF had a tremendous effect on particle emissions, reducing the particle number concentrations to <0.3% of the mean concentrations from the DOC aftertreatment for both bus types. The HDE buses had significantly higher particle emissions than the CD buses under the DOC aftertreatment (adjusted *p*-value = 0.0016), but there was only a marginal difference between the bus technologies under the DPF aftertreatment (adjusted *p*-value = 0.10).

The technology and route interaction (Figure 1b) was significant, but the CD buses had consistently lower particle emissions on all routes, including the stop-and-go Farmington route. The Avon-up route was the only route where the CD and HDE buses did not have significantly different particle emissions (adjusted *p*-value = 0.12). The driver and route interaction (Figure 1c) indicates that the driver effect varied across routes, with an important difference between the drivers on the Enfield (freeway) route (adjusted *p*-value <0.0001), and insignificant differences between drivers on the other routes.

The interaction of temperature and aftertreatment (Figure 1e) was illustrated by showing the relative effect of temperature (at two selected levels) under the two aftertreatments: one unit (1 ^{o}C) of increase in ambient temperature decreased the particle emissions by 3% for the DOC–equipped buses and 9% for the DOC+DPF-equipped buses.

The route effects also depended on aftertreatment (Figure 1f). Under the DOC aftertreatment, the route effects were statistically distinguishable from one another. The largest particle concentrations occur on Avon Up, followed by Enfield, Farmington and Avon Down. Under the DPF treatment, the Farmington route had the

lowest particle number emissions, with no significant differences detected among other routes.

Discussion

Extending the linear mixed model results, we discuss the relevant factors that influence particle number emissions variability in on-board testing, including treatments that varied according to the testing schedule, and other sources that could not be controlled experimentally.

Aftertreatment. Particle number measurements varied most significantly according to the aftertreatment, with an over 99% reduction in the mean particle emissions with the DPF. Previous studies have noted similar reductions in particle number emissions due to DPF aftertreatment with diesel engines (Zervas et al., 2004; Mathis et al., 2005; Holmén et al., 2005). The interaction between the aftertreatment and technology factors was insignificant, suggesting that the different DPFs installed on the two types of buses (Engelhard DPX for the CD buses, Johnson-Matthey CRT for the HDE buses) were equally effective in reducing particle emissions.

Because the aftertreatment had such a drastic effect on the particle number concentrations, all subsequent sources of variability will be discussed in relation to whether the bus was operated with or without the DPF. It should also be noted that the particle concentrations measured with the DPF aftertreatment were near the lower detection limits of the ELPI. Caution is necessary when using such data for the establishment of absolute particle emission levels (e.g., emission factors) from DPF-equipped diesel vehicles.

Bus Technology. The differences in the two types of buses were captured through the fixed technology effect. The hybrid technology was anticipated to reduce engine loads and subsequent particle emissions from a comparable conventional diesel bus. However, the CD bus emissions, with the DOC aftertreatment, were statistically

shown to be lower than those from the HDE bus on all the routes tested, including the Farmington stop-and-go route that had lower percent engine loads for the HDE bus. The variation of the particle emissions between the two bus technologies is believed to reflect the engine and fuel system differences.

There were essentially no differences between individual buses of the same technology as estimated by the bus random effects. This assures that no systematic effects occurred due to setting up the dilution and sampling equipment on individual buses, or variations in driving or maintenance histories that would affect the particle emissions. Although the bus random effect was negligible in this study, it is important to be aware that particle emissions may be strongly influenced by intra-vehicle class variation (Jamriska et al., 2004).

Fuel. The fuel effect was examined for the DOC aftertreatment only, because the tests with DPFs ran on ULSD fuel (ULSD is required for DPFs). The particle emissions changed only slightly when switching from #1 diesel to ULSD. As suggested in Holmén et al. (2005), the sulfur content in the lubricating oil may be a more important precursor source for nanoparticles (<50 nm) than the sulfur content in the diesel fuel. An additional explanation may be that the particle size range (7 nm~10 um) of the ELPI was unable to detect an important fraction of nanoparticles below 7 nm (Zhang and Wexler, 2002), or that the artificial dilution conditions suppressed nanoparticles formation (Kittelson et al., 2004). Existing studies have shown mixed results (significant or insignificant differences) for the sulfur content effect of diesel fuel on particle number emissions from relatively newer (e.g., post-2002) diesel buses (Ristovski et al., 2006).

Operating Conditions. The significant variation in particle number emissions among the bus routes tested under the DOC aftertreatment was attributed to the diverse operating conditions. The average particle emissions from each route followed

the same trend as the average engine load (Table 3.1), ascending in the following order: Avon down, Farmington, Enfield, and Avon up.

The variability across testing runs on the same sampling day was the highest for the Avon down route, followed by Enfield, Farmington, and then Avon up. The increase in variation for the Avon down route could be caused by more varied operating conditions between runs (Table 3.1). The variations in operating conditions between runs depend on the travel direction (inbound or outbound), traffic conditions (e.g. April 21st the HOV lane was closed on the southbound Enfield run), driving behavior, and the length of the route tested. The Avon up route had the smallest cross-run variation in particle emissions even though it tended to have more variable operating parameters than the Enfield and Farmington routes. Since Avon down had the smallest engine loads and Avon up experienced the highest, the results from this study tended to suggest that on-board tests were more repeatable at higher engine loads even though previous laboratory particle emission tests were generally less repeatable for high speed, high acceleration driving cycles (Zervas et al., 2004).

By reducing the emitted particle concentration to near background levels, the DPF aftertreatment essentially removed all route differences, except for Farmington, which had significantly lower particle concentrations, particularly for the HDE bus type. The data was inconclusive regarding whether the low particle counts could be attributed to superior performance of the HDE bus in stop-and-go driving conditions, which was clearly not the case for the DOC aftertreatment. In addition, the ELPI measurements were near the lower detection limit for the DPF runs which could have reduced sensitivity, and other confounding sources (e.g. less vibration of the ELPI due to the slower speeds on the Farmington route) existed.

Driving Behavior. The effects of driving behavior on particle emissions were represented with the driver effect. Because only two primary bus drivers were

evaluated in the study their influences on emissions were easier to control, but conclusions regarding multiple driving behaviors was limited. The results indicated that the post-April driver drove more aggressively on the freeway route, which significantly increased the environmental impact of the bus emissions.

Ambient Conditions. The daily temperature was included in the model as a surrogate variable to control for differing ambient conditions that occurred throughout data collection[3]. The model showed that the ambient daily temperature had a significant negative relationship with tailpipe particle number emission measurements. The dilution air in this study was unheated, causing the dilution temperature to depend on the ambient temperature. At lower temperatures, a greater fraction of semi-volatile particle precursors nucleate to create higher particle counts in the 7nm~10um range recorded by the ELPI. A negative association was also observed between temperature and on-road (Kittelson et al., 2004) and roadside (Zhu et al., 2006) PM number concentrations.

Temperature had a larger relative effect under the DPF aftertreatment. A plausible explanation was that the DPF removed a higher fraction of the carbonaceous particles than the more volatile species. The volatile particle precursors were more influenced by the dilution temperature, causing the relative temperature effect to be stronger under the DPF (Holmén and Qu, 2004).

Sampling Equipment. The ELPI sampling equipment was a potential source for both day-to-day and run-to-run variability, as represented by the day and residual effects in the mixed model. At the beginning of each sampling day the ELPI was zeroed while placing a HEPA filter at the sampling inlet, though variation in zeroing

[3] The daily relative humidity (RH) and daily dilution ratio were also tested in the model selection process to examine their effects -- neither was significant as a main effect.

could still occur and the ELPI measurements could drift during testing (Holmén and Qu, 2004). Another potential source of variation (both day and residual) for the on-board testing was vibration of the ELPI. The ELPI was placed on a plywood shock-absorbing module designed to isolate the vibration of bus from the sampling equipment. On certain sampling days (November 16th and 17th) there was excessive vibration on the bus due to a transmission problem on the HDE bus. Because highly inflated counts were observed on these sampling days they were not included in the analysis, yet vibration between runs and days could be an important source of variability for on-board tests.

The lag between combustion emission and subsequent measurement of the ELPI could also contribute to the variation between runs. The temporal lag was estimated to be ~10 seconds using engine starts, although the exhaust residence time is anticipated to vary during operating of the bus due to changes in vehicle speed and exhaust flow rates. A residence time of multiple seconds might not impact the average particle emissions from the longer Farmington and Enfield routes, however it could affect the shorter Avon route-averages.

Dilution System. The day random variation in particle emissions could also be influenced by the setup of the dilution system and changes in the equipment (e.g. fittings and environmental conditions) between testing days that would cause slight differences in the dilution environment (Holmén et al., 2005). In laboratory dilution studies, much of the variability between tests is attributed to the deposition of particles on the surface of the dilution and exhaust system in previous tests, and subsequent release of particles in later runs, particularly at high temperatures and exhaust flow rates (Zervas et al., 2004). This explanation seems consistent with the variation observed in our study, even though our estimated relative variability was the greatest for the runs with the lowest counts (Avon down for the DOC aftertreatment, and the

DPF runs). Avon down had low engine loads, but it immediately followed the Avon up route which could cause the engine to operate at high temperatures. Release of particles during the early portion of these runs, which otherwise had low counts, could greatly impact the variability of mean particle concentrations across test runs.

The increase in relative variation for the DPF aftertreatment (residual error more than 4 times larger under the DPF aftertreatment) has been noted in other studies as well, and could be attributed to volatile particle precursor species absorbing onto carbonaceous particles within the DPF, and desorbing at high speeds or regeneration events (Zervas et al., 2004; Mathis et al., 2005). It must be noted that the increase in variation is in terms of the percentage change in particle concentration, because the absolute range of particle concentrations is much smaller for the DPF configuration.

The particle emissions variability due to the dilution system and sampling equipment was confounded, making it difficult to quantify the relative variation attributed to each source. In addition, such equipment variability (mainly setup variability) was believed and found to be closely correlated with the day of testing as expected. The mixed model was able to account for all these confounded variation sources using the random day factor and apportioned a substantial fraction (30-84% for the DOC) of the total variability to the day effect. This led to a more accurate estimation of the variability in the residual errors, and helped unmask significant differences that occurred among routes for the DOC aftertreatment.

While including the day effect assisted in detecting route effects, the standard errors for the main effects of the technology, fuel, aftertreatment, temperature, and driver factors increased, making differences less significant for these factors with the mixed model formulation. Without the mixed model formulation some of the variability that occurred between sampling days due to the dilution and sampling equipment would be attributed incorrectly to these factors.

Acknowledgments

This research was sponsored in part by the Joint Highway Research Advisory Council of the University of Connecticut and the Connecticut Department of Transportation through Project 05-9.

APPENDIX

The appendix provides detailed testing schedule information, specifications for the two bus technologies, additional route average operating parameters, graphs of average particle concentration for each bus run, model diagnostic tests, fixed effects for interaction parameters, and differences in least-square means.

Table 3A.1. Specifications of Conventional Diesel and Hybrid Diesel-Electric Buses Tested

Specification	Conventional Diesel (CD)	Hybrid Diesel-Electric (HDE)
Engine	2002 Detroit Diesel Series 40E	2003 Cummins ISL 280
# cylinders, displacement (L)	6 cyl., 8.7 L	6 cyl., 8.9 L
Transmission	Allison B400R Automatic	Allison EP 40
Rated Power @ 2000 RPM, bhp (kW)	280 (205)	289 (205)
Peak Torque, lb-ft (N-m)	900 (1166)	900 (1220)
Combustion/Fuel System	Direct Injection	Electronic Timing Control
Exhaust Aftertreatment	Phase I – II: single-brick DOC; Phase III: Englehard DPX	Phase I-II: dual-brick DOC Phase III: Johnson-Matthew CRT DPF
Electric motors	N/A	Two Concentric AC Induction Motors
Battery	N/A	Sealed Nickel-Metal Hydride
Bus mileage prior to testing, mi	78,400 (201) 67,000 (202)	29,600 (H301) 28,800 (H302)
Weight, kg	13,086 (empty)	13,318 (empty)

Table 3A.2. Engine Speed by Routes for both Bus Technologies [a]

	Conventional			Hybrid Diesel-Electric		
Engine Speed (rpm)	Average	St. Dev	(Min/Max)	Average	St. Dev	(Min/Max)
Avon Down	1340	72	(1182/1471)	1454	145	(1236/1762)
Avon Up	1591	67	(1473/1689)	1841	61	(1722/1975)
Enfield	1963	57	(1868/2048)	1873	83	(1734/2039)
Farmington	1055	26	(978/1089)	993	20	(961/1048)

[a] Route parameters are recorded second-by-second using a Vansco USB Data Link Adapter on all 4 buses from April 16 onward. 9 pre-April testing days are not included, and 1 Enfield run from Nov. 9 is missing. [b] The listed values are averages, standard deviations, minimums and maximums of averages. The second-by-second data is averaged for each route, and then the average, minimum, and maximum across all test runs were calculated.

Table 3A.3. Summary of Testing Days Used in Statistical Analysis

	CD Bus 1	CD Bus 2	HDE Bus1	HDE Bus 2
Phase I				
Fuel: No. 1 Diesel	23-Jan	11-Feb	6-Jan	27-Feb
Aftertreatment: DOC	30-Jan	13-Feb [a]	21-Jan	30-Apr
Ambient Temperature Range:	23-Apr	18-Feb [b]	16-Apr	
(-9.4 to 22.8 °C)		28-Apr	21-Apr	
		26-May		
		27-May		
Phase II				
Fuel: ULSD	6-Aug	20-Sep	29-Jul	25-Aug
Aftertreatment: DOC	10-Aug	21-Sep	3-Aug	26-Aug
Ambient Temperature Range: (18.2 to 29.4 °C)			4-Aug	
Phase III				
Fuel: ULSD	20-Oct	9-Nov	12-Oct [c]	2-Nov
Aftertreatment: DOC+DPF	25-Oct	10-Nov	13-Oct	3-Nov
Ambient Temperature Range: (0.6 to 18.9 °C)			15-Oct	

[a] Missing Avon Inbound and Farmington Inbound runs. [b] Each inbound and outbound run was made twice (16 runs) [c] Missing Enfield runs

Details on Experimental Data

Table 3A.3 contains the testing schedule, bus number, fuel/aftertreatment configuration. Figures 3A.1 through 3A.6 graphically display the average particle number concentration as recorded on each bus run for each day of testing.

On February 18th, two complete runs were made, providing an additional set of replications (2 inbound and 2 outbound runs for each route). On two days of the study, issues arose that prevented all of the routes to be recorded, or caused the recorded data to be unrepresentative of true conditions. On February 13th, the air compressor used with the dilution system failed before the Avon Inbound and Farmington Inbound routes could be measured. On October 12th all of the routes except the Enfield route were measured. The remaining data that was correctly recorded for these days was included in the statistical analysis.

Several testing days were not included in the statistical analysis due to issues with the sampling equipment that yielded unrepresentative measurements of the true particle number concentration. On May 28th and June 2nd the desiccant became saturated from rain, this erroneously affected the formation of particles on all routes. On November 16th and 17th there was excessive vibration on the HDE buses, which caused the ELPI to yield erroneously high counts to be recorded for these two days, except for the Farmington route, which may have been because the bus was operating at lower speeds. More complete information on the testing setup and schedule is available in Holmen et al. (2005)

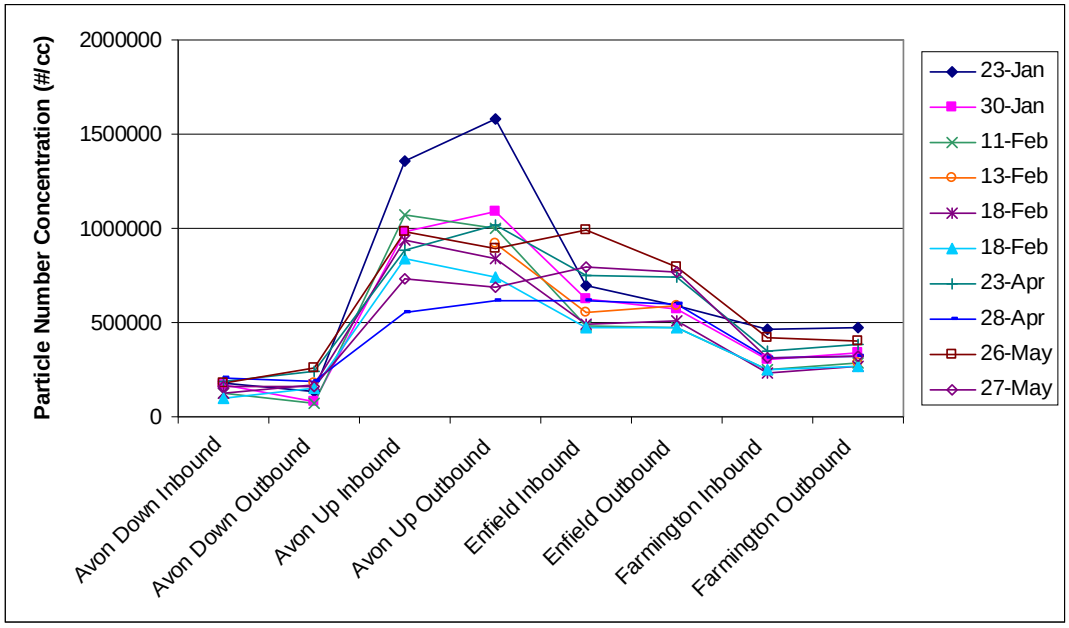

Figure 3A.1. Particle Number Concentrations according to Route and Testing Day for Conventional Diesel Buses on No. 1 Diesel Fuel

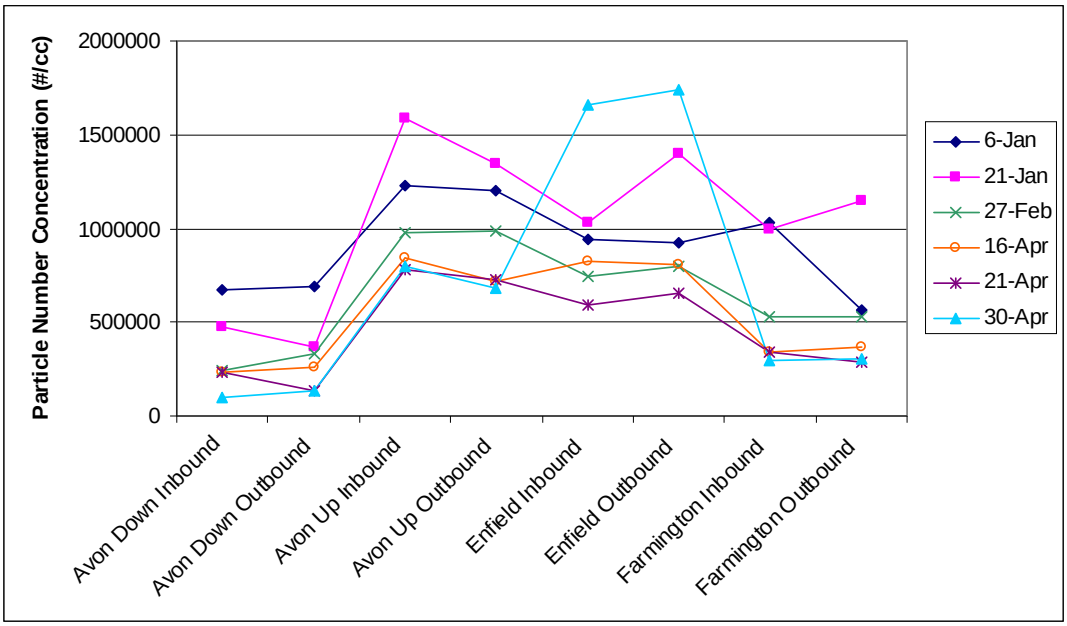

Figure 3A.2. Particle Number Concentrations according to Route and Testing Day for Hybrid Diesel-Electric Buses on No. 1 Diesel Fuel

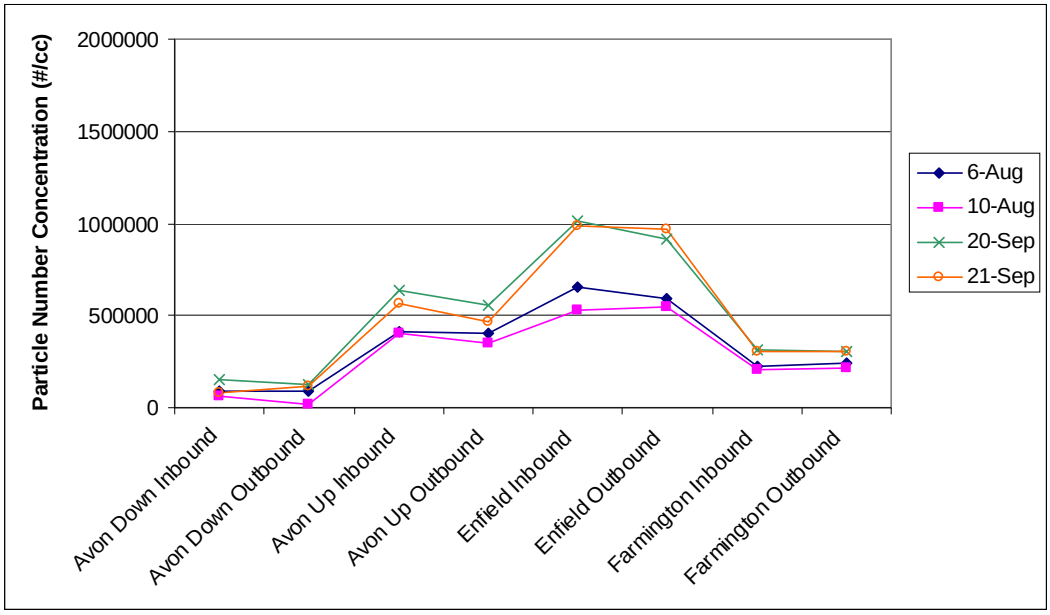

Figure 3A.3. Particle Number Concentrations according to Route and Testing Day for Conventional Diesel Buses on ULSD fuel

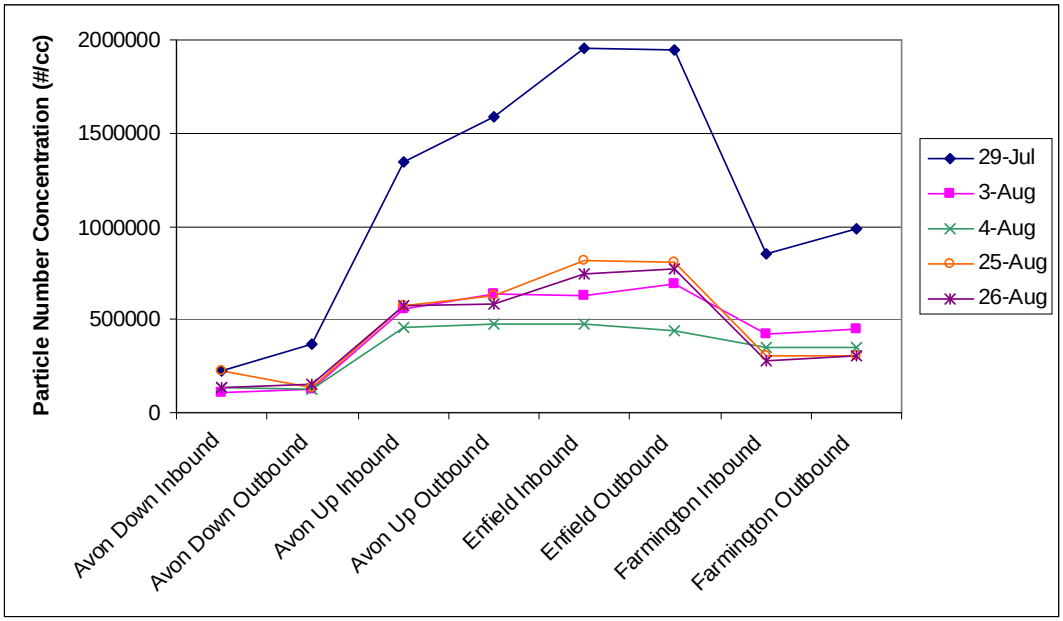

Figure 3A.4. Particle Number Concentrations according to Route and Testing Day for Hybrid Diesel-Electric Buses on ULSD fuel

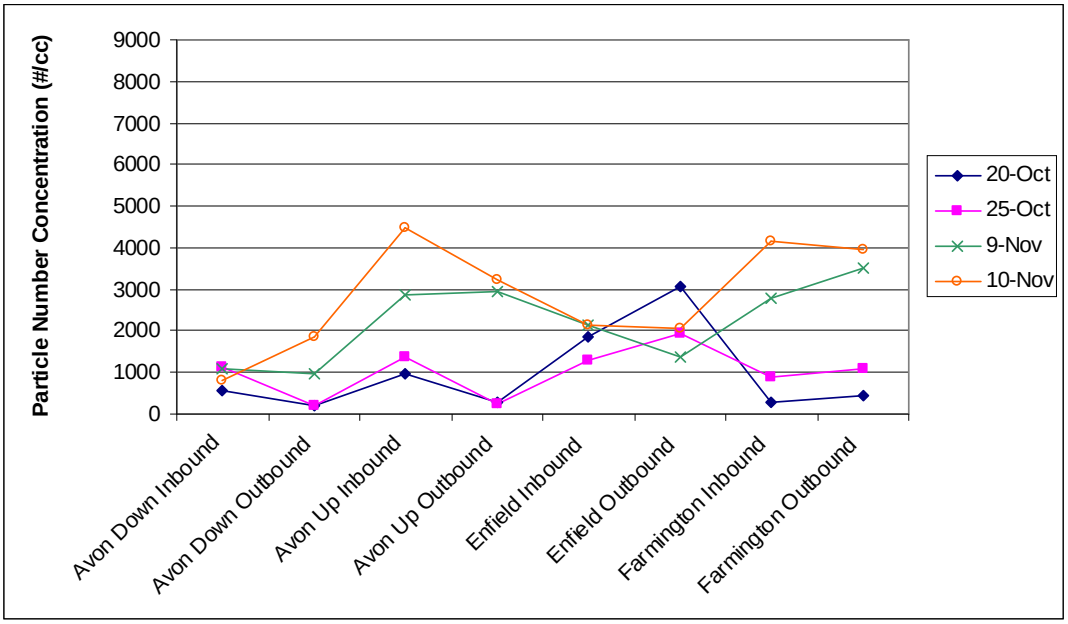

Figure 3A.5. Particle Number Concentrations according to Route and Testing Day for Conventional Diesel Buses on ULSD with Diesel Particulate Filters

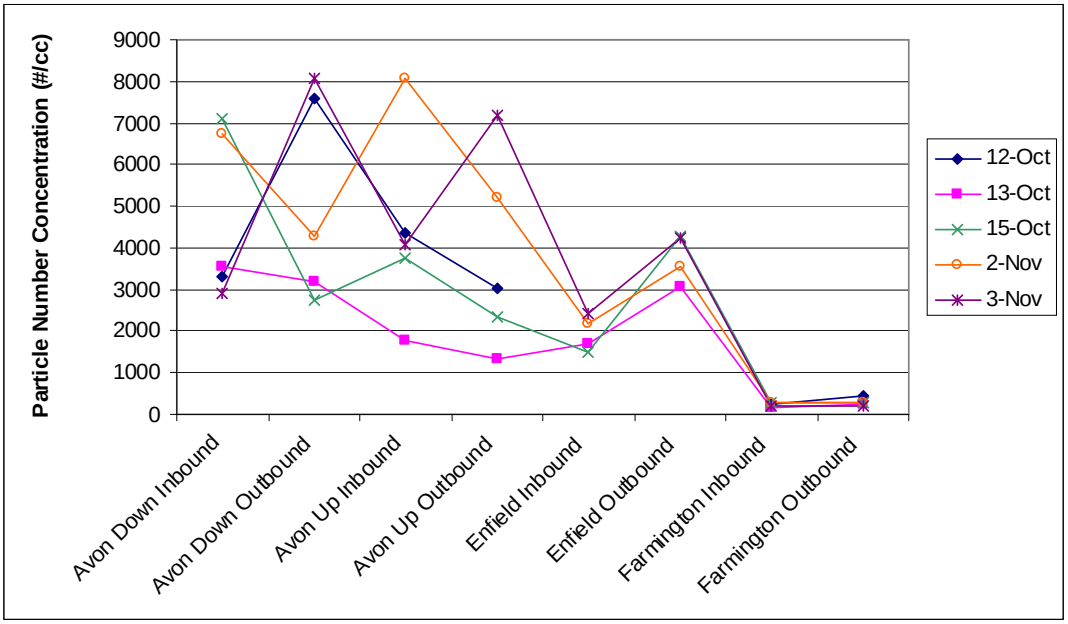

Figure 3A.6. Particle Number Concentrations according to Route and Testing Day for Hybrid Diesel-Electric Buses on ULSD with Diesel Particulate Filters

Model Diagnostic Tests

The statistics for the model fit with homogeneous residuals are shown in Table 3A.4. In Figure 3A.7, the conditional studentized residuals from the full interaction model are plotted alongside the predicted emissions. The conditional studentized residuals account for both the random and fixed effects, and are corrected by their estimated standard error (Maricq et al., 2000). The predicted values are clearly divided into two groups; the lower values correspond to the particle number emissions recorded from buses outfitted with the DPF. These have a noticeably higher variation than for the concentrations without DPFs. This property violates the model assumption that the residuals errors are independent and identically distributed.

Table 3A.4. Homogeneous Residual Model Fit Statistics

-2 Res Log Likelihood	6.8
AIC (smaller is better)	12.8
AICC (smaller is better)	12.9
BIC (smaller is better)	6.8

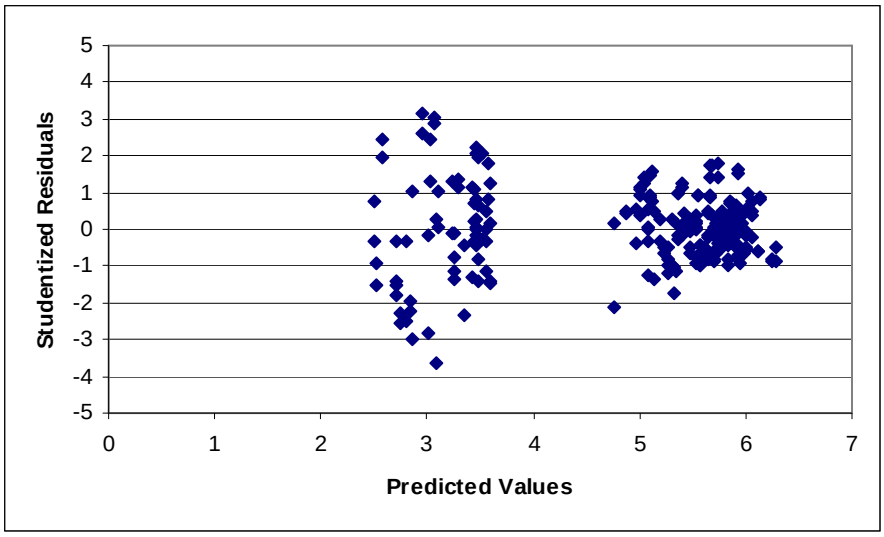

Figure 3A.7. Residuals from Homogeneous Residual Variance

To assure that the residuals are independent and identically distributed, we first implemented an alternative model that estimates a separate residual variance for the buses with and without DPFs (heterogeneous residual structure). The likelihood and other fit statistics are shown in Table 3A.5, which shows an increase in fit for all of the criteria. A likelihood ratio test determined that the heterogeneous residual model provides a significant increase in the goodness-of-fit (p-value <0.0001). Figure 3A.8 plots the studentized residuals from the alternative model that estimated separate residual variances for the DOC and DOC+DPF treatments. By implementing a heterogeneous residual structure the studentized residuals have more comparable variances.

The studentized residuals are useful for detecting outliers. Figure 3A.8 contains several residuals that are at least 3 standard errors from the mean, with one

value almost 5 standard errors from the mean values. The experimental information was reviewed from these days to see if there were experimental errors that would warrant their removing from the analysis. No evidence was found that would suggest that the data points were unrepresentative of the testing measurements.

Table 3A.5. Heterogeneous Residual Model Fit Statistics (Residuals Grouped according to DPF and DOC treatments)

-2 Res Log Likelihood	-124.7
AIC (smaller is better)	-116.7
AICC (smaller is better)	-116.5
BIC (smaller is better)	-124.7

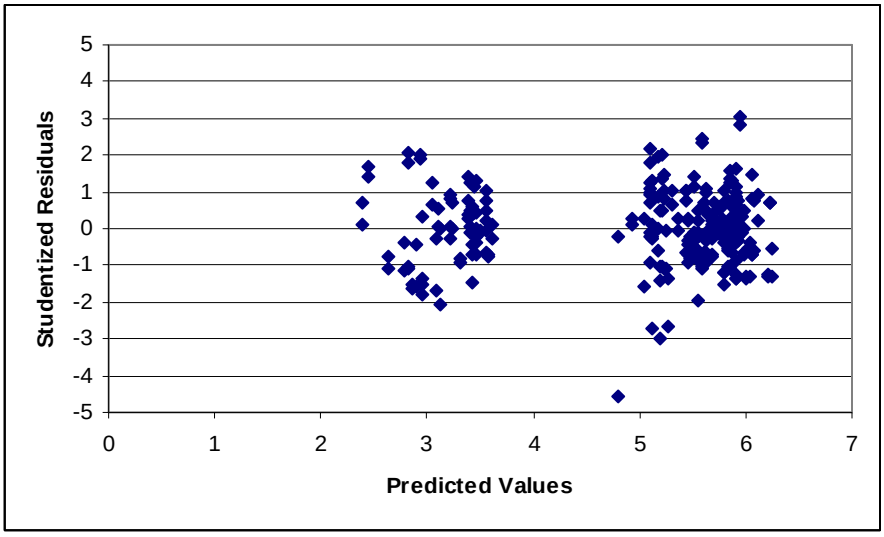

Figure 3A.8. Residuals from Heterogeneous Residual Variances Grouped According to DOC and DPF treatments

Next, we implemented a third model that estimated separate variance for the DPF treatment, as well as separate variances for each route under the DOC treatment (total of 5 residual variance terms). The fit statistics of the model were all improved as shown in Table 3A.6. A likelihood ratio test determined that the third model provided a significant increase in fit (p-value <0.0001) over the previous model. All studentized residuals were within 3 standard errors as shown in Figure 3A.9. Standard normality tests were used to test if the residuals pass the normality assumptions in Table 3A.7 through 3A.11. All of the statistics are insignificant, meaning that the null hypothesis of normally distributed errors was not rejected for each residual group. By implementing the current heterogeneous residual structure, the large variability of the data was able to be modeled accurately without having to remove influential outliers.

Table 3A.6. Heterogeneous Residual Model Fit Statistics (Residuals Grouped according to DPF and each route with DOC treatment)

-2 Res Log Likelihood	-171.0
AIC (smaller is better)	-157.0
AICC (smaller is better)	-156.5
BIC (smaller is better)	-171.0

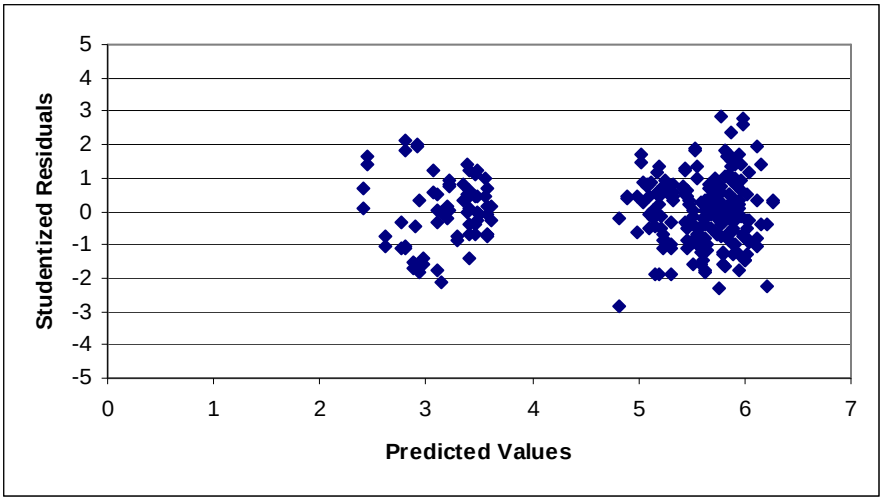

Figure 3A.9. Residuals from Heterogeneous Residual Variances Grouped According to DOC and DPF, an Each Route with the DOC Treatment

Table 3A.7. Normality Tests for Residuals from Avon Down + DOC treatment

Test	Statistic		p Value	
Shapiro-Wilk	W	0.973963	Pr < W	0.3455
Kolmogorov-Smirnov	D	0.096256	Pr > D	>0.1500
Cramer-von Mises	W-Sq	0.062684	Pr > W-Sq	>0.2500
Anderson-Darling	A-Sq	0.389508	Pr > A-Sq	>0.2500

Table 3A.8. Normality Tests for residuals from Avon Up + DOC treatment

Test	Statistic		p Value	
Shapiro-Wilk	W	0.98518	Pr < W	0.7890
Kolmogorov-Smirnov	D	0.058678	Pr > D	>0.1500
Cramer-von Mises	W-Sq	0.018977	Pr > W-Sq	>0.2500
Anderson-Darling	A-Sq	0.174784	Pr > A-Sq	>0.2500

Table 3A.9. Normality Tests for residuals from Enfield + DOC treatment

Test	Statistic		p Value	
Shapiro-Wilk	W	0.964446	Pr < W	0.1365
Kolmogorov-Smirnov	D	0.09405	Pr > D	>0.1500
Cramer-von Mises	W-Sq	0.054703	Pr > W-Sq	>0.2500
Anderson-Darling	A-Sq	0.416065	Pr > A-Sq	>0.2500

Table 3A.10. Normality Tests for residuals from Farmington + DOC treatment

Test	Statistic		p Value	
Shapiro-Wilk	W	0.979072	Pr < W	0.5270
Kolmogorov-Smirnov	D	0.059585	Pr > D	>0.1500
Cramer-von Mises	W-Sq	0.026199	Pr > W-Sq	>0.2500
Anderson-Darling	A-Sq	0.219712	Pr > A-Sq	>0.2500

Table 3A.11. Normality Tests for residuals from DPF treatment

Test	Statistic		p Value	
Shapiro-Wilk	W	0.986493	Pr < W	0.6560
Kolmogorov-Smirnov	D	0.047477	Pr > D	>0.1500
Cramer-von Mises	W-Sq	0.021333	Pr > W-Sq	>0.2500
Anderson-Darling	A-Sq	0.181594	Pr > A-Sq	>0.2500

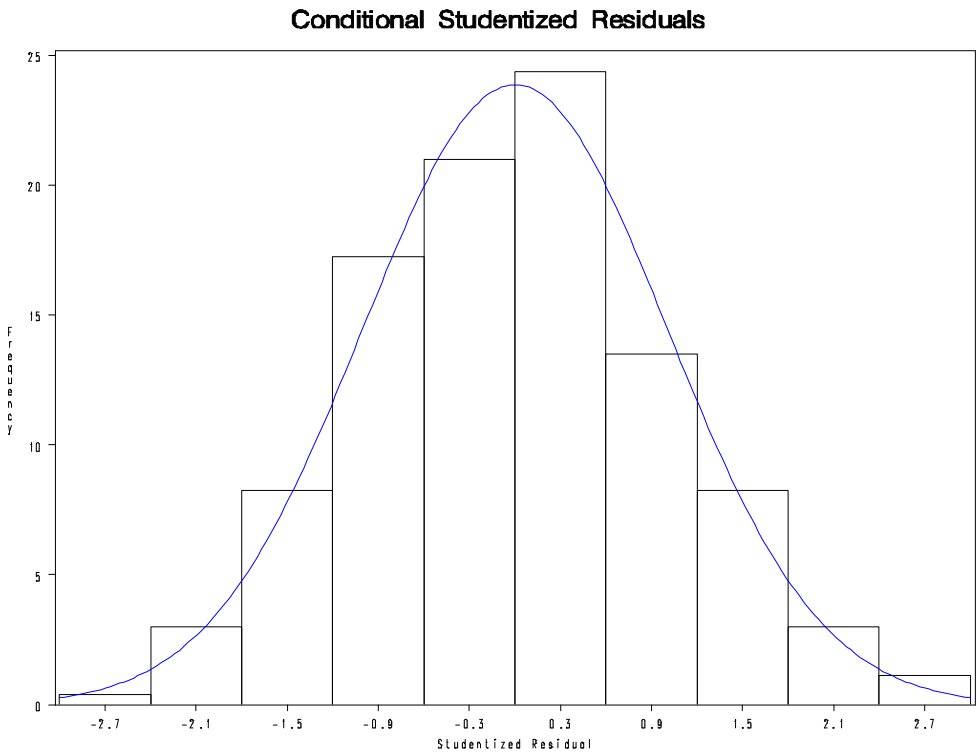

Figure 3A.10. Histogram of Conditional Studentized Residuals with Heterogeneous Residuals Variances for the DPF Treatment, and each route under the DOC treatment.

Table 3A.12. Type 3 Tests of Fixed Effects.

Effect	Num DF	Den DF	F Value	Pr > F
Tech	1	2	13.93	0.0649
Fuel	1	22	0.03	0.8555
Aftertreatment	1	22	180.53	<.0001
Driver	1	22	4.89	0.0378
Temperature	1	222	14.48	0.0002
Route	3	222	27.77	<.0001
Tech*Fuel	1	22	0.54	0.4706
Tech*Aftertreatment	1	22	0.67	0.4225
Tech*Route	3	222	9.42	<.0001
Route*Driver	3	222	27.27	<.0001
Temperature*Aftertreatment	1	222	3.37	0.0677
Route*Aftertreatment	3	222	17.55	<.0001

Table 3A.13 Fixed Effect Parameters (Including Interaction Effects) according to baseline case of: CD bus, ULSD fuel, DOC aftertreatment, Post-April Driver, and Farmington Route. Interactions with zero effect are not included.

Effect			Estimate	Standard Error	DF	t Value	Pr > |t|
Intercept			5.6842	0.08533	2	66.61	0.0002
Tech	HDE		0.2878	0.08205	2	3.51	0.0725
Tech	CD		0	.	.	.	.
Fuel	#1 D		0.02634	0.08156	22	0.32	0.7497
Fuel	ULSD		0	.	.	.	.
Aftertreatment	DOC+DPF		-2.7605	0.1740	22	-15.86	<.0001
Aftertreatment	DOC		0	.	.	.	.
Driver	Pre-April 1		-0.1823	0.08592	22	-2.12	0.0454
Driver	Post-April 1		0	.	.	.	.
Temperature			-0.01390	0.002614	222	-5.32	<.0001
Route	Avon_down		-0.4276	0.04405	222	-9.71	<.0001
Route	Avon_up		0.3376	0.02267	222	14.89	<.0001
Route	Enfield		0.4062	0.03014	222	13.48	<.0001
Route	Farmington		0	.	.	.	.
Tech*Fuel	#1 D	HDE	-0.07592	0.1034	22	-0.73	0.4706
Tech*Aftertreatment	DOC+DPF	HDE	0.1379	0.1687	22	0.82	0.4225
Tech*Route	Avon_down	HDE	0.1139	0.05493	222	2.07	0.0392
Tech*Route	Avon_up	HDE	-0.1054	0.02864	222	-3.68	0.0003
Tech*Route	Enfield	HDE	-0.05744	0.03792	222	-1.51	0.1313
Route*Driver	Avon_down	Pre-April 1	0.06316	0.05903	222	1.07	0.2858
Route*Driver	Avon_up	Pre-April 1	0.1116	0.03014	222	3.70	0.0003
Route*Driver	Enfield	Pre-April 1	-0.1833	0.03982	222	-4.60	<.0001
Temperature*After	DOC+DPF		-0.02595	0.01414	222	-1.84	0.0677
Route*Aftertreatment	Avon_down	DOC+DPF	0.9180	0.1299	222	7.07	<.0001
Route*Aftertreatment	Avon_up	DOC+DPF	0.3514	0.1264	222	2.78	0.0059
Route*Aftertreatment	Enfield	DOC+DPF	0.2520	0.1317	222	1.91	0.0570

Differences in Least Square means
The simulation method within SAS® is used to compute the adjusted *p*-values.

Table 3A.14. Differences of Tech×Fuel Least Square Means

Effect	Tech	Fuel	_Tech	_Fuel	Estimate	StdErr	DF	tValue	Adjp
Tech*Fuel	HDE	#1 D	HDE	ULSD	-0.04958	0.08156	22	-0.61	0.9271
Tech*Fuel	CD	#1 D	CD	ULSD	0.02634	0.08156	22	0.32	0.9874
Tech*Fuel	HDE	#1 D	CD	#1 D	0.2686	0.1083	22	2.48	0.0212
Tech*Fuel	HDE	ULSD	CD	ULSD	0.3446	0.08437	22	4.08	0.0005

Table 3A.15. Differences of Tech×Aftertreatment Least Square Means

Effect	Tech	After	_Tech	_After	Estimate	StdErr	DF	tValue	Adjp
Tech*After	HDE	DOC+DPF	HDE	DOC	-2.5699	0.1036	22	-24.81	<.0001
Tech*After	CD	DOC+DPF	CD	DOC	-2.7078	0.1340	22	-20.21	<.0001
Tech*After	HDE	DOC+DPF	CD	DOC+DPF	0.3755	0.1574	22	2.39	0.0261
Tech*After	HDE	DOC	CD	DOC	0.2376	0.05428	22	4.38	0.0002

Table 3A.16. Differences of Tech×Route Least Square Means

Effect	Tech	Route	_Tech	_Route	Estimate	StdErr	DF	tValue	Adjp
Tech*Route	HDE	Avon_down	HDE	Avon_up	-0.2867	0.07196	222	-3.98	0.0018
Tech*Route	HDE	Avon_down	HDE	Enfield	-0.2062	0.07611	222	-2.71	0.0900
Tech*Route	HDE	Avon_down	HDE	Farmington	0.1769	0.07332	222	2.41	0.1747
Tech*Route	HDE	Avon_up	HDE	Enfield	0.08053	0.06862	222	1.17	0.8758
Tech*Route	HDE	Avon_up	HDE	Farmington	0.4636	0.06564	222	7.06	<.0001
Tech*Route	HDE	Enfield	HDE	Farmington	0.3831	0.07010	222	5.47	<.0001
Tech*Route	CD	Avon_down	CD	Avon_up	-0.5060	0.07028	222	-7.20	<.0001
Tech*Route	CD	Avon_down	CD	Enfield	-0.3775	0.07354	222	-5.13	<.0001
Tech*Route	CD	Avon_down	CD	Farmington	0.06302	0.07142	222	0.88	0.9627
Tech*Route	CD	Avon_up	CD	Enfield	0.1285	0.06751	222	1.90	0.4357
Tech*Route	CD	Avon_up	CD	Farmington	0.5690	0.06507	222	8.75	<.0001
Tech*Route	CD	Enfield	CD	Farmington	0.4406	0.06869	222	6.41	<.0001
Tech*Route	HDE	Avon_down	CD	Avon_down	0.4328	0.09243	222	4.68	0.0001
Tech*Route	HDE	Avon_up	CD	Avon_up	0.2134	0.08303	222	2.57	0.1254
Tech*Route	HDE	Enfield	CD	Enfield	0.2614	0.08582	222	3.05	0.0388
Tech*Route	HDE	Farmington	CD	Farmington	0.3188	0.08491	222	3.75	0.0034

Table 3A.17. Differences of Route×Driver Least Square Means

Effect	Route	Driver	_Route	_Driver	Estimate	StdErr	DF	tValue	Adjp
Route*Driver	Avon_down	Pre-April 1	Avon_down	Post-April 1	-0.1191	0.09738	222	-1.22	0.8539
Route*Driver	Avon_up	Pre-April 1	Avon_up	Post-April 1	-0.07073	0.08310	222	-0.85	0.9695
Route*Driver	Enfield	Pre-April 1	Enfield	Post-April 1	-0.3656	0.08680	222	-4.21	<.0001
Route*Driver	Farmington	Pre-April 1	Farmington	Post-April 1	-0.1823	0.08592	222	-2.12	0.3129
Route*Driver	Avon_down	Pre-April 1	Avon_up	Pre-April 1	-0.4206	0.07837	222	-5.37	<.0001
Route*Driver	Avon_down	Pre-April 1	Enfield	Pre-April 1	-0.1686	0.08321	222	-2.03	0.3684
Route*Driver	Avon_down	Pre-April 1	Farmington	Pre-April 1	0.1516	0.08057	222	1.88	0.4593
Route*Driver	Avon_down	Post-April 1	Avon_up	Post-April 1	-0.3722	0.06463	222	-5.76	<.0001
Route*Driver	Avon_down	Post-April 1	Enfield	Post-April 1	-0.4151	0.06720	222	-6.18	<.0001
Route*Driver	Avon_down	Post-April 1	Farmington	Post-April 1	0.08840	0.06495	222	1.36	0.7848
Route*Driver	Avon_up	Pre-April 1	Enfield	Pre-April 1	0.2520	0.07083	222	3.56	0.0084
Route*Driver	Avon_up	Pre-April 1	Farmington	Pre-April 1	0.5721	0.06775	222	8.44	<.0001
Route*Driver	Avon_up	Post-April 1	Enfield	Post-April 1	-0.04293	0.06554	222	-0.66	0.9924
Route*Driver	Avon_up	Post-April 1	Farmington	Post-April 1	0.4606	0.06322	222	7.28	<.0001
Route*Driver	Enfield	Pre-April 1	Farmington	Pre-April 1	0.3202	0.07327	222	4.37	0.0002
Route*Driver	Enfield	Post-April 1	Farmington	Post-April 1	0.5035	0.06585	222	7.65	<.0001

Table 3A.18. Differences of Route×Aftertreatment Least Square Means

Effect	Route	After	_Route	_After	Estimate	StdErr	DF	tValue	Adjp
Route*After	Avon_down	DOC+DPF	Avon_up	DOC+DPF	-0.1130	0.1281	222	-0.88	0.9833
Route*After	Avon_down	DOC+DPF	Enfield	DOC+DPF	0.04119	0.1331	222	0.31	1.0000
Route*After	Avon_down	DOC+DPF	Farmington	DOC+DPF	0.5790	0.1286	222	4.50	<.0001
Route*After	Avon_down	DOC	Avon_up	DOC	-0.6797	0.02743	222	-24.78	<.0001
Route*After	Avon_down	DOC	Enfield	DOC	-0.6249	0.03036	222	-20.58	<.0001
Route*After	Avon_down	DOC	Farmington	DOC	-0.3390	0.02952	222	-11.49	<.0001
Route*After	Avon_up	DOC+DPF	Enfield	DOC+DPF	0.1542	0.1307	222	1.18	0.9173
Route*After	Avon_up	DOC+DPF	Farmington	DOC+DPF	0.6920	0.1261	222	5.49	<.0001
Route*After	Avon_up	DOC	Enfield	DOC	0.05481	0.01666	222	3.29	0.0180
Route*After	Avon_up	DOC	Farmington	DOC	0.3406	0.01507	222	22.60	<.0001
Route*After	Enfield	DOC+DPF	Farmington	DOC+DPF	0.5378	0.1311	222	4.10	0.0014
Route*After	Enfield	DOC	Farmington	DOC	0.2858	0.01991	222	14.36	<.0001
Route*After	Avon_down	DOC+DPF	Avon_down	DOC	-2.1012	0.1177	222	-17.85	<.0001
Route*After	Avon_up	DOC+DPF	Avon_up	DOC	-2.6678	0.1139	222	-23.41	<.0001
Route*After	Enfield	DOC+DPF	Enfield	DOC	-2.7672	0.1202	222	-23.03	<.0001
Route*After	Farmington	DOC+DPF	Farmington	DOC	-3.0192	0.1147	222	-26.33	<.0001

Table 3A.19. Type 3 Tests of Fixed Effects for Model that does not include Bus and Day Random Effects (Compare with Table 3A.12)

Effect	Num DF	Den DF	F Value	Pr > F
Tech	1	246	29.79	<.0001
Fuel	1	246	0.08	0.7821
Aftertreatment	1	246	294.12	<.0001
Driver	1	246	7.02	0.0086
Temperature	1	246	23.02	<.0001
Route	3	246	26.88	<.0001
Tech*Fuel	1	246	0.39	0.5306
Tech*Aftertreatment	1	246	2.22	0.1376
Tech*Route	3	246	4.29	0.0057
Route*Driver	3	246	10.00	<.0001
Temperature*Aftertreatment	1	246	7.54	0.0065
Route*Aftertreatment	3	246	17.65	<.0001

REFERENCES

Brunekreef, B.; Holgate, S. T. Air Pollution and Health. *Lancet.* **2002**, 360, 233-42.

Finkelstein, M. M.; Jerrett, M.; Sears, M. R. Traffic Air Pollution and Mortality Rate Advancement Periods. *Am. J. Epidemiol.* **2004**, 160, 173-177.

Hitchins, J.; Morawska, L.; Wolff, R.; Gilbert, D. Concentrations of Submicrometer Particles from Vehicle Emissions Near a Major Road. *Atmos. Environ.* **2000**, 34, 51-59.

Holmén, B. A.; Chen, Z.; Davila, A. C.; Gao, O. H.; Vikara, D. M. *Particulate Matter Emissions from Hybrid Diesel-Electric and Conventional Diesel Transit Buses: Fuel and Aftertreatment Effects*. JHR 05-304, Project 03-8. Joint Highway Research Advisory Council, 2005.

Holmén, B. A.; Qu, Y. Uncertainty in Particle Number Modal Analysis during Transient Operation of Compressed Natural Gas, Diesel, and Trap-Equipped Diesel Transit Buses. *Environ. Sci. Technol.* **2004**, 38, 2413-2423.

Jamriska, M.; Morawska, L.; Thomas, S.; He, C. Diesel Bus Emissions Measured in a Tunnel Study. *Environ. Sci. Technol.* **2004**, 38, 6701-6709.

Kittleson, D.B.; Watts, W. F.; Johnson, J. P. Nanoparticle emissions on Minnesota highways. *Atmos. Environ.* **2004**, 38, 9-19.

Littell, R. C.; Milliken, G. A.; Stroup, W. W.; Wolfinger, R. D.; Schabenberger, O. *SAS® for Mixed Models, Second Edition*; SAS Institue: Cary, NC, 2006.

Maricq, M. M.; Podsiadlik D. H.; Chase R. E. Size Distributions of Motor Vehicle Exhaust PM: A Comparison Between ELPI and SMPS Measurements. *Aerosol Sci. Technol.* **2000**, 33, 239-260.

Mathis, U.; Mohr, M.; Forss, A. Comprehensive particle characterization of modern gasoline and diesel passenger cars at low ambient temperatures. *Atmos. Environ.* **2005**, 39, 107-117.

McCarthy, M.C.; Eisinger, D.S.; Hafner, H.R.; Chinkin, L.R.; Roberts, P.T.; Black, K.N.; Clark, N.N.; McMurry, P.H.; and Winer, A.M. Particulate Matter: a strategic vision for transportation-related research. *Environ. Sci. & Technol.* **2006**, 40, 5593-5599.

Ristovski, Z. D.; Jayaratne, E. R.; Lim, M.; Ayoko, G. A.; Morawska, L. Influence of Diesel Fuel Sulfur on Nanoparticle Emissions from City Buses. *Environ. Sci. Technol*. **2006**, 40, 1314-1320.

Singer, J. D. Using SAS PROC MIXED to Fit Multilevel Models, Hierarchical Models, and Individual Growth Models. *J. Educ. Behav. Stat.* **1998**, 24(4), 323-355.

West, B. T; Welch, K. B.; Galecki, A. T. *Linear Mixed Models*; Chapman & Hall/CRC: Boca Raton, FL, 2007.

Zervas, E.; Dorlhène, P.; Daviau, R.; Dionnet, B. Repeatability of fine particle measurement of diesel and gasoline vehicles exhaust gas. SAE Technical Paper Series 2004-01-1983.

Zhang, K.M.; Wexler, A.S. A hypothesis for growth of fresh atmospheric nuclei. *J. Geophys. Res.* **2002**, 107(D21), 4577.

Zhu, Y.; Hinds, W.; Kim, S.; Sioutas, C. Concentration and Size Distribution of Ultrafine Particles Near a Major Highway. *J. Air Waste Manag. Assoc.* **2002**, 52, 1032-1042.

Zhu, Y.; Kuhn, T.; Mayo, P.; Hinds, C.W. Comparison of Daytime and Nighttime Concentration Profiles and Size Distributions of Ultrafine Particles near a Major Highway. *Environ. Sci. Technol.* **2006**, 40, 2531-2536.

CHAPTER 4

DEVELOPING LINK-BASED PARTICLE NUMBER EMISSION MODELS FOR DIESEL TRANSIT BUSES USING ENGINE AND VEHICLE PARAMETERS[1]

Abstract

To better assess health impacts from diesel transportation sources, particle number emissions can be modeled on a road network using traffic operating parameters. In this work, real-time particle number emissions rates from two diesel transit buses were aggregated to the roadway link level and modeled using engine parameters and then vehicle parameters. Modern statistical methods were used to identify appropriate predictor variables in the presence of multicollinearity, and controlled for correlated emission measurements made on the same day and testing route. Factor analysis helped to reduce the number of potential engine parameters to three predictor variables (engine load, engine speed, and exhaust temperature). The three engine parameters were incorporated into a linear mixed model that was shown to explain the variation attributable to link-characteristics. Vehicle specific power and speed were identified as two surrogate vehicle travel variables that can be used in the absence of engine parameters, although with a loss in predictive power compared to the engine parameter model. If vehicle speed is the only operating input available, including road grades in the model can significantly improve particle number emission estimates even for links with mild grade (<0.5%). Although the data used in the analyses are specific to the bus model tested, the modeling approach can be applied to modeling emissions from other vehicle models with different engine types, exhaust systems, and engine retrofit technologies.

[1] Sonntag, D. B., H. O. Gao. Developing link-based particle number emission models for diesel transit buses using engine and vehicle parameters. *Transportation Research Part D*. **2009**, 14, 240-248.

Introduction

Particle number is a useful indicator for the presence of ultrafine particles (particles <100 nm) which make up the majority of the total particle number emissions of diesel exhaust (Kittelson, 1998). Ultrafine particles may be one of the most serious health threats from diesel exhaust due to their ability to diffuse deep within the lungs and enter the bloodstream (Brunekreef and Holgate, 2002). Additionally, ultrafine particles are believed to be one of the explaining factors for the observed increase in premature death in residences near major roadways (Brunekreef and Holgate, 2002; Finkelstein, 2004). The concentration of ultrafine particles on or next to major roadways can be 25 times larger than background levels in urban areas (Zhu et al., 2002), whereas other indicators of particulate matter, such as $PM_{2.5}$ (mass of particles with aerodynamic diameters < 2.5 μm) show only slight increase on roadways (McCarthy et al., 2006). Heavy-duty diesel trucks and buses are responsible for a disproportionately large share of on-road particle number emissions, with particle number emission rates one to two orders of magnitude higher than gasoline passenger vehicles (Morawska et al., 2008).

Air quality analyses rely on accurate estimates of mobile-source emissions inventories from transportation networks. Emission inventories are calculated by combining emission rates from mobile emission models and traffic activity data. In the US, regulatory air quality studies use the Environmental Protection Agency's MOBILE and the California Air Resources Board's EMFAC models, which output link-based and trip-based emission rates, respectively (Bai et al., 2007). These models adjust the emission rates based on ambient conditions, vehicle characteristics, fuel properties, and average speed. Link-level traffic volume and average speed are obtained from traffic studies, simulation models, and transportation demand models. In the US Environmental Protection Agency's upcoming mobile emissions model,

MOVES, link-level emission rates can be estimated from resolved vehicle activity data: instantaneous speed and vehicle specific power (Koupal et al., 2005). To date, no efforts have been taken to develop rates for particle number emissions in these models.

The objective of this paper is to identify methods for modeling link-level particle number emissions from diesel transit buses according to traffic operating parameters. The data used in the current study was collected as part of a broader study evaluating transit bus emissions from two conventional and two hybrid diesel-electric buses performed by Holmén et al. (2005). Previous analysis showed that particle number emissions from the diesel transit buses varied significantly on different routes when operating on diesel oxidation catalysts (DOCs), but did not vary significantly when the buses were operated with diesel particulate filters (Sonntag et al., 2008). Because hybrid diesel-electric buses are customarily equipped with diesel particulate filters, only the conventional DOC-equipped diesel buses were analyzed in this study.

As of 2006, over 80% of transit buses in the US were conventional diesel (American Public Transportation Association, 2007). DOCs are one of the most economical and proven diesel retrofits, and have been installed on more than 1.5 million new heavy-duty vehicles in the US since 1994 (Manufacturers of Emission Controls Association, 2006). Thus, DOC-equipped buses are anticipated to make a significant fraction of transit bus fleet in the US for the next twenty to thirty years, and longer in developing nations, making it important to understand and develop effective modeling techniques for particle emissions from this vehicle-class. Although the numerical results are specific to the two diesel buses in the study, the key observations and methods are anticipated to be applicable to diesel-source particle emissions that vary significantly according to traffic conditions.

Experimental Data

The diesel transit buses evaluated in the current work are two 2002 Connecticut Transit buses equipped with direct injection, turbocharged Detroit Diesel Series 40 Series engines, without exhaust gas recirculation or diesel particulate filters. Particle number emissions were recorded on-board the diesel transit buses on three bus routes in Hartford (CT), USA: Enfield (freeway route), Farmington (stop-and-go urban route), and Avon (rural mountainous route). On each day, one bus was tested on each route twice (once in each direction). The data selected for analysis includes 8 days of testing ranging from 23 April to 21 September, 2004.

To measure particle number emissions, a sample of the tailpipe exhaust was diluted in a mini-dilution tunnel and measured by an Electrical Low Pressure Impactor (ELPI) located on-board the bus. The ELPI measured particle number counts with 12 size cuts for a particle size range between 7 nm and 10 μm. The particle counts across each size cut were summed to determine the total particle number emissions at a temporal resolution of 1~2 seconds. The total exhaust flow rate was measured at the end of the tail-pipe using a pitot tube from a Horiba OBS-1000 gas-emission analyzer at a temporal resolution of one-second intervals. The diesel engine was turned off after each test route, and the Horiba pitot tube was re-zeroed to prevent instrument drift (Holmén et al. 2005). Notwithstanding, slight variations in the equipment setup may have influenced measurements and the artificial dilution system may have suppressed particle formation (Kittelson et al., 2004).

To calculate the particle number emission rate, the data from the Horiba and ELPI instruments was time-aligned to account for the lag between the engine events, emissions, and exhaust measurements. Then the particle number emission rate (in particles/second) was calculated by multiplying the particle number concentration of sampled exhaust by the total exhaust flow rate and dilution ratio.

A data link adapter connected to the network port of the diesel buses recorded instantaneous engine operation data and vehicle speed. The Horiba OBS-1000 included exhaust sensors that recorded other engine parameters such as exhaust flow rate, exhaust temperature, fuel rate, and air fuel ratio. A global positioning system unit on the Horiba OBS-1000 was used to spatially locate the bus on the defined bus routes and roadway links. Accurate roadway grade was measured every 10 meters along the testing routes from an Automatic Road Analyzer Photologging van and was spatially merged to the emissions dataset using ArcGIS. Further information on the measurement equipment and bus specifications is detailed in the comprehensive report by Holmén et al. (2005).

In this work, the three routes were divided into links to correspond to roadway links in a road network defined by a transportation demand model or traffic simulation model. In this analysis, the roadway links were defined between major intersections, different road types, and different roadway conditions. On the urban Farmington route, the links were defined between intersections where the bus typically stopped on each run. The freeway links were defined between on and off-ramps. On the rural Avon route, the links were defined between major intersections and between the uphill and downhill section of the route to elucidate the emissions variability due to grade differences. The Enfield route contained 32 links (16 outbound and 16 inbound), the Farmington Route contains 31 links (15 outbound and 16 inbound) and the Avon route contains 20 Links (9 outbound, 11 inbound), yielding 83 links in total. The routes were tested on 8 testing days, yielding a data set of 661 replications (3 replications were removed due to data collection problems). A summary of the links within each route is given in Table 4.1.

Figure 4.1 displays a map of a one-directional run of the three routes on the Hartford roadway network with the link-level particle number emission rates

(averaged across all eight days) shaded according to magnitude. The particles/km were also plotted (Figure 4.2) to illustrate that although the particles/second emission rates are generally much lower on the urban and rural routes, their emissions exposure (particles/distance) is comparable to the freeway route. The particles/second was the unit of analysis in this study, however for use in air quality studies, the particles/second emission rates can be converted to particles/km by using the average link-speed.

Table 4.1. Summary Statistics of Roadway Links

Route	Link Type	Number of Links	Ave. travel time, m:ss	Ave. speed, km/hr (mph)	Average percent idling, %	Average length, km (miles)	Min and Max grade, %
Enfield	Divided Highway	26	1:09	97.5 (60.6)	0%	1.9 (1.2)	-2.3/1.0
	On-Ramp	2	1:55	41.0 (25.4)	2%	0.9 (0.5)	-1.0/0.0
	Off-Ramp	2	0:44	33.1 (20.6)	12%	0.4 (0.3)	-0.7/0.0
	Urban Arterial	2	2:19	23.4 (14.6)	22%	1.0 (0.6)	-0.5/0.4
Farming-ton	Urban Arterial	31	1:38	17.8 (11.1)	30%	0.5 (0.3)	-3.2/2.9
Avon	Rural Arterial	12	2:13	45.4 (28.2)	9%	1.7 (1.1)	-6.7/6.2
	Urban Arterial	8	1:42	26.8 (16.6)	25%	0.7 (0.4)	-3.2/1.4

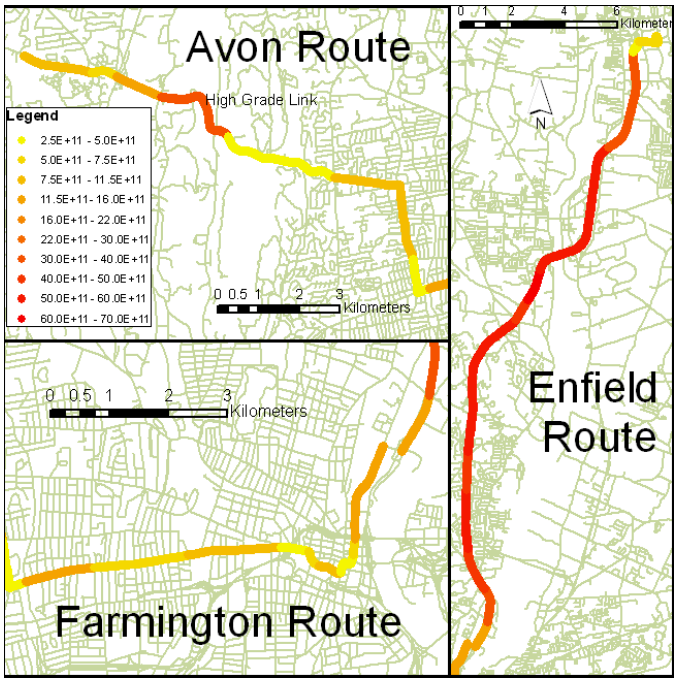

Figure 4.1. Time-based Link Average Particle Number Emission Rates (particles/second)

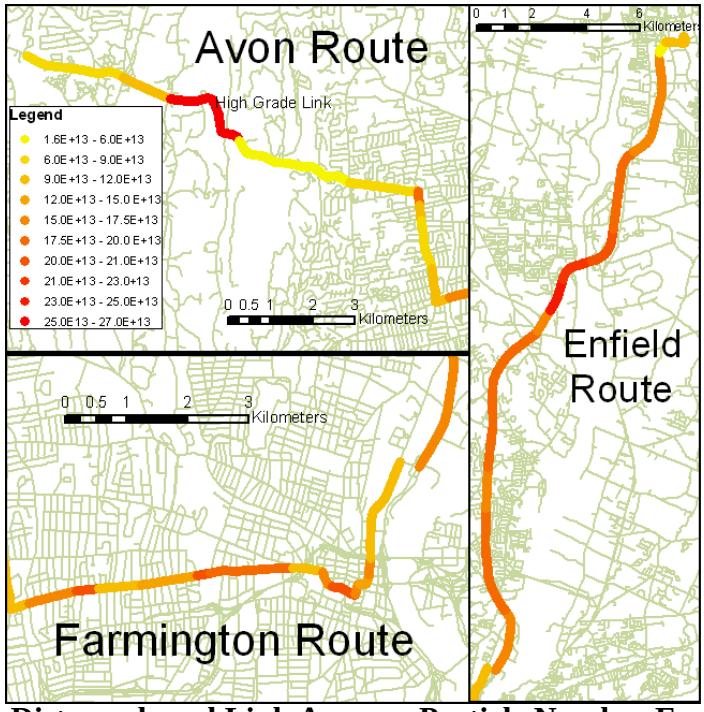

Figure 4.2. Distance-based Link Average Particle Number Emission Rate (particles/km)

Modeling Approach

Link-level particle number emission rates were statistically modeled by taking a two-step approach: 1) using engine operating parameters and 2) using vehicle travel parameters. The authors hypothesized that engine parameters are better predictors of particle emissions than vehicle parameters, and that a robust vehicle parameter model could be built using information gained from engine parameter-based modeling. Additionally, by using the two-step approach, the efficiency of modeling particle number emissions using only vehicle parameters could be evaluated.

In contrast to a physical model which could be used to understand the underlying processes of particle formation, the statistical models used the correlation with operating parameters to predict emissions to a reasonable degree. In reality, particle formation within an engine is a highly non-linear and complex process that depends on a whole array of inputs, engine design, operation, temperature, fuel and oil type specific to the engine and exhaust system. The current analysis sought to approximate this relationship with linear regression models, which could be easily extended to different vehicle/engine types and applied in cases where a limited number of traffic operation parameters are available for emission estimation.

The engine operating parameters recorded from the tests include: boost pressure, injection pressure, coolant temperature, exhaust temperature, exhaust pressure, fuel consumption, exhaust flow rate, air fuel ratio, percent engine load, engine speed, and oil temperature. The vehicle operating parameters are all functions of the second-by-second speed and location of the vehicle that could potentially be available to emission modelers. The vehicle travel parameters considered include: speed, acceleration, grade, percent idling, acceleration events from idling, velocity × acceleration, and vehicle specific power. Velocity ×acceleration was computed because it has been used previously to predict diesel transit bus particulate mass

emissions (Clark et al. 2003). Vehicle specific power (VSP) is a surrogate estimate of engine load based on instantaneous speed, vehicle weight, road grade, and load coefficients. VSP was calculated using the equation for buses in EPA's MOVES model: $VSP = (0.064)v + (0.000265)v^3 + a \times v + g \times \sin\theta \times v$, where v = velocity (m/s), a = acceleration (m/s^2), g = acceleration due to gravity, sin θ = fractional road grade (Beardsley et al. 2004). The link-aggregates (e.g., averages) of the listed parameters were used to model link-level particle number emission rates.

Modeling Particle Number Emission Rates using Engine Parameters

Model Development. Identifying the most important engine parameters to model particle number emissions was challenging because the emissions effect of each engine parameter is highly dependent on the state of other engine parameters. For example, by increasing the injection pressure of a heavy-duty diesel engine while holding the engine load constant, researchers determined that the soot particle concentration reduced substantially (Mathis et al., 2005). However, in general particle number concentrations will increase with injection pressure, due to a subsequent increase in fuel rate, as shown in engine dynamometer tests (Kweon et al., 2002). Other operation parameters identified in the literature that influence particle number emissions from heavy-duty diesel engines include the air fuel ratio (Kittelson, 1998), injection timing, combustion temperature (Kweon et al., 2002), and engine speed (Shi et al., 2000).

All engine parameters that were not listed in the literature as being important or related to important factors were removed from the analysis, leaving boost pressure, injection pressure, air fuel ratio, fuel rate, exhaust flow, exhaust temperature, percent engine load and engine speed. Because these covariates are highly correlated with one another (e.g. multicollinear), if all the variables were used to predict emissions in a statistical model, the model coefficients would be unstable and it would be difficult to

determine which parameters are the most valuable in predicting emissions. Therefore, factor analysis was performed to reduce the engine parameters to a smaller set of uncorrelated factors using principle component analysis[2].

Figure 4.3 displays a Scree plot, which shows the Eigenvalues of the principle components, and the associated cumulative variation explained by each principle component. Because the seven variables were all highly related, one principle component (or factor) explained more than 92% of the total variation of the seven variables. The Scree plot "elbows" off around two or three components, with two principle components explaining more then 97% of the total variation and three components explaining over 99%.

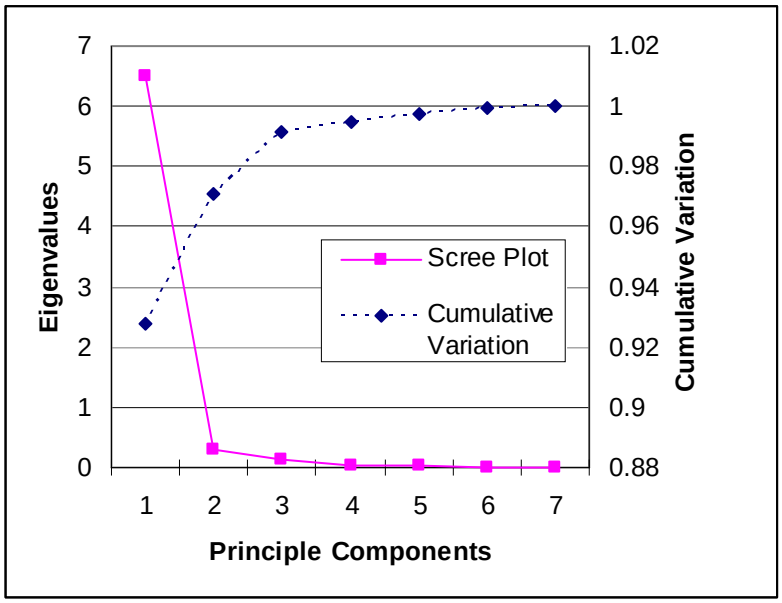

Figure 4.3. Scree Plot from Principle Component Analysis of Engine Parameters

Factor patterns can be used to interpret the contribution of each original variable to the resulting factors. The factor patterns include the standardized regression coefficients between the original variables and the resulting factors. As shown in Table 4.2, when only one factor is selected, boost pressure or fuel rate best

[2] The air fuel ratio, although identified as important for emissions, is uniquely determined from the exhaust flow rate and fuel rate and was not included in the factor analysis.

summarized the combined variability of the seven engine parameters, although all the variables are highly correlated with Factor 1.

Table 4.2. Factor Analyses of Engine Operation Parameters

	One Factor Pattern	Two Factor Pattern		Three Factor Pattern		
	Factor 1	Factor 1	Factor 2	Factor 1	Factor 2	Factor 3
Percent Variance Explained:	92.8%	51.8%	45.3%	41.0%	39.9%	18.1%
Factor Pattern:						
Boost pressure	0.99	0.74	0.66	0.63	0.67	0.38
Injection pressure	0.98	0.63	0.76	0.74	0.58	0.31
Exhaust temperature	0.93	0.77	0.54	0.46	0.52	0.71
Exhaust flow	0.98	0.81	0.57	0.55	0.74	0.38
Fuel rate	0.99	0.67	0.74	0.71	0.59	0.38
Percent Engine Load	0.92	0.41	0.91	0.88	0.34	0.33
Engine Speed	0.94	0.90	0.40	0.38	0.85	0.36

Next, two-factor and three-factor analyses was performed, which explained 97.1% and 99.1% of total variation, respectively. The factors were orthogonally rotated using the VARIMAX procedure in SAS to simplify the factor structure which resulted in more interpretable factors (UTASS, 1995). From the two-factor analysis, there appears to be an underlying factor strongly correlated to engine speed (as well as exhaust flow and boost pressure which are dependent on engine speed), and a factor highly correlated with engine load (as well as fuel rate and injection pressure, which determines the engine load). In the three-factor analysis, the engine load/fuel rate factor (Factor 1) and the engine speed/air flow factor (Factor 2) are also apparent, along with an exhaust temperature factor which is more independent of the other variables. The dominant two-factor split has theoretical underpinnings as the air fuel ratio is an important indicator of the engine operating state (Kittelson, 1998)

Linear mixed models for link-level particle number emission rates were then estimated using the engine parameters identified as key components in factor analyses. The rationale for adopting linear mixed models is because of their capability of controlling for the potential correlation among particle number emission rates

measured within the same route on the same day. Multiple candidate models were evaluated using the following model formulation:

$$\log_{10}(PNR_{i,j,k}) = \mu + \beta \cdot Categorial\ Variables + \beta \cdot Engine\ Parameters + \beta \cdot Ambient\ temperature + day_i + route_{j[i]} + e_{k[i,j]}$$

where $PNR_{i,j,k}$ is the particle number emission rate (#/second) on a certain testing day (i=1:8), testing route (j=1:6), and link (k=1:16). The ambient temperature was included to control for the effect of ambient conditions on particle emissions. The $\log_{10}$-transformation of the dependent variable was conducted to better satisfy the normality assumption of the residual errors, $e \sim N(0, \sigma^2_{residual})$. The effects of testing days and routes were modeled as random effects (since the days and routes were randomly chosen from large populations) with distributions: $day \sim N(0, \sigma^2_{day})$ and $route \sim N(0, \sigma^2_{route})$. Such a model structure implies that the log-transformed particle number emission rates for different road links are correlated by $\rho = \frac{\sigma^2_{day}}{\sigma^2_{day} + \sigma^2_{route} + \sigma^2_{residual}}$ on the same testing day, and correlated by $\rho = \frac{\sigma^2_{route}}{\sigma^2_{route} + \sigma^2_{residual}}$ for the same testing route.

First a reference model (Model 1) was estimated. The model contains a categorical variable "link" that represents the different roadway links, ambient temperature, and the random day and route factors. Next several candidate models, as shown in Table 4.3, were estimated that included the engine parameters selected from the factor analysis. Maximum likelihood estimation (MLE) was used to fit each model and obtain estimates of the -2 log likelihood, Akaike information criterion (AIC), and the Bayes information criterion (BIC). For these fit statistics, a small

number (or more negative) means a better model fit. The likelihood ratio R^2 was also calculated to improve interpretation[3].

For the reference model, 94.8% of the variation of the log-transformed emission rate was explained without using any engine information. This model included indicator variables for the 83 different links to quantify the amount of variation occurring between different links. The engine parameter models were compared to the reference model to evaluate their explanatory power of the particle number emission rates across road links.

Model 2 used fuel rate, which was selected from the one factor analysis to predict link-level particle number emission rates. Model 3 also included the categorical variable "road type" (divided highway, on-ramp, off-ramp, urban arterial, and rural arterial) that significantly improved the fit of the model. Road type is subsequently included in the rest of the models. Model 4 substituted fuel rate with engine load and engine speed, which were selected from the two factor analysis. Model 5 used the engine covariates identified from the three factor analysis: engine load, engine speed, and exhaust temperature. The fit statistics indicated progressive improvement in these models and all of the independent variables are highly significant. Since engine load and engine speed could be seen as a surrogate representation of the air fuel ratio, the air fuel ratio was evaluated directly as an independent variable in model 6, but only to yield an inferior fit to the data. This suggests that the overall magnitude of the fuel rate and air flow is important for the total particle number emission rate. Model 7 was constructed to investigate if an

[3] The log likelihood R^2 should be interpreted as the percentage of the variability explained by a model in the log-transformed particle number emission rates. In general, the log-transformation is a variation reduction technique, so the R^2 will be higher for a model with a log-transformed dependent variable. For example, a simple linear model (without random effects) similar to model 1, but fitted to the untransformed emission rates, had an R^2 of 0.85. The log-transformation was used in this analysis to better satisfy the assumptions of the linear model in order to conduct accurate statistical inference.

interaction term between engine load and engine speed further improves the model fit. Finally Model 8 included the $\log_{10}$-transformed engine covariates.

Table 4.3. Particle Number Emission Models Using Engine Parameters

Candidate Models			Fit Statistics			
Model #	Categorical Variables	Engine Parameters	-2 log likelihood	AIC	BIC	log likelihood R^2
1	Links		-1153.5	-979.5	-972.6	94.8%
2		fuel rate	-475.1	-463.1	-462.6	85.5%
3	road type	fuel rate	-667.4	-647.4	-646.6	89.2%
4	road type	engine load, engine speed	-983.1	-961.1	-960.2	93.3%
5	road type	engine load, engine speed, exhaust temperature	-1065.0	-1041.0	-1040.0	94.1%
6	road type	air fuel ratio, exhaust temperature	-524.8	-502.8	-501.9	86.6%
7	road type	engine load, engine speed, exhaust temp, engine load ×engine speed	-1387.1	-1361.1	-1360.1	96.4%
8	road type	log(engine load), log(engine speed), log(exhaust temp)	-1433.9	-1409.9	-1408.9	96.6%

Model Results. Model 8 was selected as the final engine parameter model, which had better fit statistics than all the other candidate models in Table 4.3. The log likelihood R^2 of model 8 is larger than that of model 1, indicating that Model 8 is able to explain a portion of the within-link variability associated with engine operating conditions in addition to the cross-link variability explained in the reference Model 1. In other words, the final model sufficiently explains the variability of link-level particle number emissions due to link-characteristics as well as a portion of the variability due to different driving conditions on the same link. Based on the log likelihood R^2, model 8 explains 35% of the within-link variability that was unexplained by model 1.

Table 4.4. Estimates of the Final Engine Parameter Model

Random Effects	Estimate	Proportion of Total Random Variability		
σ^2_{date}	0.0047	40%		
σ^2_{route}	0.0012	10%		
$\sigma^2_{residual}$	0.0059	50%		
Fixed Effects	**Estimate**	**Standard Error**	**t Value**	**Pr > |t|**
Intercept	1.97	0.24	8.3	<.0001
log(engine speed)	3.24	0.08	39.2	<.0001
log(engine load)	0.93	0.02	41.8	<.0001
log(exhaust temperature)	-0.59	0.08	-7.0	<.0001
Ambient temperature	-0.004	0.002	-2.5	0.014
Divided Highway	-0.14	0.02	-6.5	<.0001
Off-Ramp	-0.25	0.02	-10.5	<.0001
On-Ramp	-0.07	0.02	-2.9	0.004
Rural Arterial	-0.07	0.01	-6.0	<.0001
Urban Arterial	baseline			

Estimates of the fixed effects (of engine operating parameters) and the random effects (as variance of day and route effects) from model 8 are shown in Table 4.4. The t-values show that engine speed and engine load are the most important variables in the model, and both are positively associated with the particle number emission rates. The effects of exhaust temperature and ambient temperature are negative, which could correspond to increase in condensation and nucleation of volatile pre-cursors under cooler temperatures (Kittelson et al., 2004). The effects of road type were estimated using the urban arterial as the baseline. As shown in the model results, the random effects of testing routes and dates were important sources of variability in link-level particle number emission rates, which were correlated by 17% within the same route and by 40% on the same day. A likelihood ratio test (*p*-value <0.0001) showed that the inclusion of these random effects in the model improved the model fit significantly.

Particle mass emission rates for diesel transit buses have been found to be a strong function of acceleration or fuel rate transients (Hofeldt and Chen, 1996). Kear and Neimeier (2006) extended these results by modeling heavy-duty diesel particle mass using a property termed "intensity", which is calculated by summing the product of all positive occurrences of horsepower and acceleration along the driving cycle. Yanowitz et al. (2002) used "severity", which is defined as the sum of all positive changes in horsepower over a driving cycle, to model heavy-duty diesel PM mass emission rates. In this study, comparative models for particle number emission rates were also estimated using intensity and severity. The resulting models had poor fit statistics, suggesting that link-level particle number emissions for the evaluated diesel transit buses are better related to the link average engine conditions such as average engine speed and engine load.

Modeling Particle Number Emission Rates Using Vehicle Travel Parameters

Model Development. For the development of particle number emission models using vehicle travel parameters, the engine operating parameters used in the previous section (engine load and engine speed) were replaced with the corresponding surrogate vehicle parameters. Correlations between the recorded vehicle travel parameters and engine load and engine speed were subsequently calculated. Vehicle specific power (VSP) was found to be highly correlated with engine load (ρ=0.96), and vehicle speed with engine speed (ρ=0.98). These two vehicle travel variables, VSP and vehicle speed, were hence selected for further analysis.

The same linear mixed model framework was used to estimate the predictive power of vehicle parameters:

$$\log_{10}(PNR_{i,j,k}) = \mu + \beta \cdot Categorial\ Variables + \beta \cdot Vehicle\ Parameters + \beta \cdot Ambient\ temperature + day_i + route_{j[i]} + e_{k[i,j]}$$

Candidate models are reported in Table 4.5, along with corresponding fit statistics. Again, models were compared to a reference model (Model A), which includes indicator variables to represent the average emissions on each of the 83 links. In Model B, the link categorical variables were substituted with the VSP and vehicle speed, and road type was added in Model C. Next Models D and E tested the interaction between VSP and speed and the log transformation of the selected vehicle covariates, respectively.

Table 4.5. Particle Number Emission Models Using Vehicle Travel Parameters

Candidate Models			Fit Statistics			
	Categorical Variables	Vehicle Parameters	-2 Log Likelihood	AIC	BIC	Log likelihood R^2
A	Links		-1153.5	-979.5	-972.6	94.8%
B		vehicle speed, VSP	-760.3	-746.3	-745.7	90.6%
C	road type	vehicle speed, VSP	-854.3	-832.3	-831.4	91.8%
D	road type	vehicle speed, VSP, vehicle speed × VSP	-1003.8	-979.8	-978.8	93.5%
E	**road type**	**log(vehicle speed), log(VSP+10)**	**-1010.2**	**-988.2**	**-987.3**	**93.6%**
F	road type	log(vehicle speed)	-364.9	-344.6	-344.1	82.9%
G	road type	log(vehicle speed), log(grade)	-947.2	-925.2	-924.3	92.9%

Model Results. The fit statistics indicate that Model E provides the best fit to the data among the evaluated vehicle parameter models, and was selected as the final vehicle parameter model. Nevertheless, in terms of explanatory power Model E predicts a smaller proportion of the variability in particle number emissions when compared to the engine parameter model and the reference link-categorical model (Model A). This supports the initial hypothesis that engine parameters better predict emissions than vehicle parameters, and means that the vehicle parameter model was not able to explain all the variation in link-level emissions due to link characteristics.

But for practical applications, Model E explains the variation in log-transformed emissions quite well (93.6%).

The estimated parameters for Model E are shown in Table 4.6. The fixed effects of vehicle speed and VSP are both positive, with ambient temperature having a negative effect that is statistically similar to the ambient temperature effect in the engine parameter model. The road type effects are statistically different than the previous model, and appear to be dependent on other variables used in the model. The loss of fit caused by using vehicle parameters instead of engine parameters increased the residual variance, while the variance estimates for the random date and route factors were relatively unchanged.

Table 4.6. Estimates of the Final Vehicle Parameter Model

Random Effects	Estimate	Proportion of Total Random Variability		
σ^2_{date}	0.0051	27%		
σ^2_{route}	0.0023	12%		
$\sigma^2_{residual}$	0.0114	61%		
Fixed Effects	**Estimate**	**Standard Error**	**t Value**	**Pr > |t|**
Intercept	10.05	0.070	143.1	<.0001
log(vehicle speed)	0.58	0.028	20.9	<.0001
log(VSP+10)	1.27	0.038	33.7	<.0001
Ambient temperature	-0.004	0.002	-2.2	0.0268
Divided Highway	0.15	0.026	5.8	<.0001
Off-Ramp	-0.23	0.032	-7.1	<.0001
On-Ramp	0.04	0.031	1.3	0.2058
Rural Arterial	-0.06	0.018	-3.3	0.0011
Urban Arterial	baseline			

In the study link-level vehicle specific power was estimated using second-by-second speed, acceleration, and grade data. This resolution of data would typically be unavailable to transportation modelers of a large road network, who may only have average speed estimates on each link. Model F (Table 4.5) was estimated using road

type and vehicle speed as predictor variables. A significant amount of explanatory power of the model was lost, but the model still explained 82.9% of the total variability in particle number emission rates. By including the average grade of each link, Model G is almost able to explain all of the variability in the best vehicle parameter model with a log likelihood R^2 of 92.9%. To test if the grade was only significant on links with large grades, Model G was refit to the dataset that only included links with moderate or no grade (average grade between -0.5% an 0.5%), and grade remained highly significant (*p*-value = 0.0016).

Conclusions

The analysis demonstrated that the evaluated diesel transit buses' particle number emissions are a strong function of operating parameters at the link-level. Engine speed and engine load are two of the most effective variables for modeling particle number emissions. These measures provided significantly better fit than descriptors of acceleration transients previously used to model particle mass emissions from other heavy-duty vehicles. Among vehicle travel parameters, vehicle specific power and vehicle speed were useful surrogates for engine load and engine speed. If only the average link speed is available to estimate emissions, including grade can significantly improve particle number predictions, even for road networks with mild grade. Both the engine and vehicle parameter model were quite effective at estimating the variability between different links. To better estimate the variability of particle number emissions within links for hot-spot analysis, modal emission models can be developed in future studies.

Acknowledgments

We are grateful for the insights given by Dr. Nigel N. Clark and Dr. Britt A. Holmén on particle emissions and diesel engine operation, statistical advice from Dr. Giles Hooker, and GIS assistance from Dr. Eric D. Jackson. This research was sponsored in part by the FHWA Eisenhower Fellowship Program, the Joint Highway Research Advisory Council of the University of Connecticut, and the Connecticut Department of Transportation through Project 05-9.

REFERENCES

American Public Transportation Association. Public Transportation Fact Book: 58th Edition; APTA: Washington, DC, 2007.

Bai, S.; Chiu, Y.; Nimeier, D. A. A comparative analysis of using trip-based versus link-based traffic data for regional mobile source emissions estimation. *Atmos. Environ.* **2007**, *41*, 7512-7523.

Beardsley, M.; Brzezinski, D.; Gianelli, B.; Koupal, J.; Srivastava, S. MOVES2004 Highway Vehicle Population and Activity Data. US EPA. Washington DC. 2004.

Brunerkreef, B.; Holgate, S. T. Air pollution and health. *Lancet.* **2002**, *360*, 1233-42.

Clark, N. N.; Gajendran, P.; Kern, J. M.. A predictive tool for emissions from heavy-duty diesel vehicles. *Environ. Sci. Technol.* **2003,** *37*, 7-15.

Finkelstein, M. M.; Jerrett, M.; Sears, M.R. Traffic air pollution and mortality rate advancement periods. *Am. J. Epidemiol*. **2004,** *160*, 173-177.

Holmén, B. A.; Chen, Z.; Davila, A. C.; Gao, O. H.; Vikara, D. M. *Particulate Matter Emissions from Hybrid Diesel-Electric and Conventional Diesel Transit Buses: Fuel and Aftertreatment Effects*. JHR 05-304, Project 03-8; Joint Highway Research Advisory Council: Hartford, CT, 2005.

Hofeldt, D. L.; Chen G. Transient particulate emissions from diesel buses during the central business district cycle. SAE Technical Paper Series 960251, 1996, 125-138.

Kear, T.; Niemeier, D. A.; On-road heavy-duty diesel particulate matter emissions modeled using chassis dynameter data. *Environ. Sci. Technol*. **2006,** *40,* 7828-7833.

Kittelson, D.B.; Watts, W.F.; Johnson, J.P. Nanoparticle emissions on Minnesota highways. *Atmos. Environ*. **2004**, *38,* 9-19.

Kittelson, D. B. Engines and nanoparticles: a review. *J. Aerosol Sci*. **1998,** *29*(5-6), 575-588.

Koupal, J.; Landman, L.; Nam, E.; Warila J.; Scarbro, C.; Glover, E.; Giannelli, R. MOVES 2004 Energy and Emission Inputs. US EPA. Washington D.C., 2005.

Kweon, C.; Foster, D. E.; Schauer, J. J.; Okada, S. Detailed chemical composition and particle size assessment of diesel engine exhaust. SAE Technical Papers 2002-01-2670, 2002.

Mathis, U.; Mohr, M.; Kaegi, R. Influence of diesel engine combustion parameters on primary soot particle diameter. *Environ. Sci. Technol*. **2005**, *39,* 1887-1892.

Manufacturer of Emission Controls Association. *Retrofitting Emission Controls on Diesel-Powered Vehicles*: Washington, DC, 2006.

McCarthy, M. C.; Eisinger, D. S.; Hafner, H. R.; Chinkin, L. R.; Roberts, P. T.; Black, K. N.; Clark, N. N.; McMurry, P. H.; Winer, A. M. Particulate matter: a strategic vision for transportation-related research. *Environ. Sci. Technol*. **2006**, *40,* 5593-5599.

Morawska, L.; Ristovski, Z.; Jayaratne, E. R.; Keogh, D. U.; Ling, X. Ambient nano and ultrafine particles from motor vehicle emissions: Characteristics, ambient processing and implications on human exposure. *Atmospheric Environment*, **2008**, *42,* 8113-8138.

Shi, J. P.; Mark, D.; Harrison, R. M. Characterization of particles from a current technology heavy-duty diesel engine. *Environ. Sci. Technol*. **2000**, *34*, 748-755.

Sonntag, D. B; Gao H. O; Holmén, B. A. Variability of particle number emissions from diesel and hybrid diesel-electric buses in real driving conditions. *Environ. Sci. Technol*. **2008,** *42,* 5637-5643.

University of Texas at Austin Statistical Services. 1995. Factor Analysis Using SAS PROC FACTOR. Copyright 1995-1997, ACITS, The University of Texas at Austin, viewed 3 July 2008, <http://www.utexas.edu/cc/docs/stat53.html>

Yanowitz, J.; Graboski, M. S.; McCormick, R. L. Prediction of in-use emissions of heavy-duty diesel vehicles from engine testing. *Environ. Sci. Technol*. **2002**, *36,* 270-275.

Zhu, Y.; Kuhn, T.; Mayo, P.; Hinds, C. W. Comparison of daytime and nighttime concentration profiles and size distributions of ultrafine particles near a major highway. *Environ. Sci. Technol*. **2006**, *40*, 2531-2536.

CHAPTER 5

COMPARISON OF PARTICLE NUMBER AND MASS EMISSIONS FROM A DIESEL TRANSIT BUS ACROSS TEMPORAL AND SPATIAL SCALES[1]

Abstract

Two common metrics of particle pollution measure the total number of particles (particle number) and the total mass of the particles (particle mass). This work analyzes particle number and mass emission rates measured from the exhaust of a 2002 diesel transit bus in real-driving conditions using on on-board mini-dilution system. The number concentrations were measured using the Electrical Low Pressure Impactor (ELPI) across a particle range of 7 to 10,060 nm, with 93% of the total particle number concentration measured below 95 nm. Mass emission rates were derived from the number counts using the bottom stages of the ELPI (7 to 387 nm) and were verified to be consistent with concurrent gravimetric filter measurements made on-board the bus. The behavior of the number and mass emission rates are examined at resolved temporal and spatial scales across three facility types: an urban arterial, a rural arterial and a divided freeway. The time-based particle emission rates are highest on the freeway, but at select 50-meter segments the distance-based particle emission rates (i.e., "hot-spots" for exposure assessment) occur at intersections when the bus accelerates from a stop. Generally, the number and mass emissions are highly correlated both temporally and spatially. Some deviations do occur because particle mass emissions are highly elevated during sustained fueling events, such as traveling on high grades and sustained accelerations, while particle number emissions are more sensitive to fuel and engine speed fluctuations. The observations are validated using statistical models across two

[1] Darrell B. Sonntag, H. Oliver Gao, and Britt A. Holmén

days of testing. The results should be used with qualification, as the sampling system did not fully measure the nucleation mode concentrations which contain the majority of the particle numbers in diesel exhaust. The size distribution data are consistent with heavy-duty vehicle emission sampled from artificial dilution tunnels. However, much higher nucleation mode concentrations were detected from studies that 1. Sampled particles directly from the exhaust plume, and 2. Accurately measured particles with diameters smaller than 7 nm.

Introduction

Single metrics are used to represent the entire distribution of particulate matter (PM) emitted from vehicle exhaust. Two common metrics evaluate the total number of particles (particle number) and the total mass of the particles (particle mass). For diesel exhaust from conventional heavy-duty vehicles, ultrafine particles (<100 nm) dominate the total number emissions, but contribute little to the total mass of the diesel particles (Kittelson et al., 2004). Fine particles (< 2.5 um) from heavy-duty diesel vehicles contain the majority of mass, with the peak in particle mass distribution occurring between 100 and 180 nm for heavy-duty diesel vehicles (Robert et al., 2007).

Both metrics are useful from a health perspective, however the relative importance of each are not readily understood. Currently all U.S. ambient regulations, tail-pipe emission standards, and regulatory emission models quantify PM according to mass-based metrics (McCarthy et al., 2006). The number of diesel particles has been proposed as a more effective health measurement of PM emissions because ultrafine particles have the ability to diffuse deep within the lungs and absorb into the bloodstream (Brunekreef and Holgate, 2002) and can contain higher air toxics per unit mass than fine particles (Sioutas et al. 2005).

The spatial distribution of ambient particle concentrations differs significantly depending on the particle size. Near major roadways, particle number concentrations

can be more than ~25 times higher than background levels, while mass-based metrics such as $PM_{2.5}$ are only slightly elevated (Zhu et al., 2002). These spatial differences have caused researchers to suggest that ultrafine particles may play a key role in the increased risk of mortality and children asthma observed near major roadways (Brunekreef and Holgate, 2002; American Lung Association, 2007). To better understand the relative health effects of ultrafine particles and fine particles, more data is needed on their spatial distribution in urban areas (Wichmann and Peters, 2000).

Number and mass-based particle emission measurements from different heavy-duty diesel vehicles do not necessarily correlate (Kittelson, 1998). Limited work has been done that examines the correlation of vehicle-specific number and mass emission rates during vehicle operation. Stationary roadside measurements of total particle number concentrations (> 7 nm) and particle volumes (18 to 300 nm) which is often a surrogate for particle mass) have shown positive correlation through the day due to changing traffic conditions (Imhof et al., 2005). Aerosol transformations that occur after particles exit the tailpipe, as well as background particle concentrations, lead to substantially different temporal distributions of PM1 or PM10 at the same sampling location (Imhof et al., 2005). While the majority of the temporal and spatial differences in the distribution of mass and number measurements are most likely due to post-emission processes, it is worthwhile to examine the variation of particle mass and number emissions due to changing vehicle operating conditions.

This work examined particle number and mass emissions measured from the tailpipe of a diesel transit bus traveling through a real-world road network. By measuring emissions using on-board artificial dilution conditions, the study is somewhat of a cross between a stationary dynamometer study and an on-road ambient measurement study. Stationary dynamometer studies are vital for establishing relationships between vehicle operation and particle emissions in controlled

environments (Robert et al. 2007, Kittelson et al., 2006a). Two aspects make on-board emissions data unique from dynamometer studies, 1. Emissions are spatially allocated in the road network, and 2. Real-world driving conditions are sampled that cannot be fully replicated on a chassis or engine dynamometer (Kittelson et al., 2006a, Robert et al., 2007).

Vehicle chase and road-side measurements are vital for quantifying the nature of particles that people are exposed to on and near roadways. Two aspects set this study apart from ambient studies. 1. By measuring the emissions of one vehicle using an artificial dilution system, the study side-steps the confounding effects of other vehicle emissions, background concentrations, and transformation processes that can change dramatically on different days. 2. Continuous high-resolution data can be collected from the bus under all driving conditions, as compared to chase-studies that collect intermittent data over average driving conditions.

The objective of this study is to understand the behavior of particle mass and number emissions from a diesel transit bus across time and space in a real-transportation network. The particle number emission rates from the evaluated bus have been analyzed previously (Vikara and Holmen, 2006, chapter 2 and 3, Jackson and Holmen, 2009). However, temporally and spatially-resolved mass-emission rates were not previously computed or analyzed. This study specifically compares the effect of operating modes and road network conditions on particle number and mass emissions.

Experimental

The analyzed emissions data was collected by Holmén et al. (2005) on four Connecticut Transit buses in 2004. In this work, data from one bus collected over a two-day period was analyzed in detail. The 2002 model year transit bus was equipped with a direct injection, turbocharged Detroit Diesel Series 40 engine, with a diesel

oxidation catalyst (DOC). The bus was tested on September 20th and 21st under multiple driving conditions common to bus routes in the Hartford, CT area, including a high-speed divided freeway, stop-and-go urban arterial, and rural arterial with sections of high-grade (Table 5.1). The daily test was conducted along three routes, each of which was tested with an out-bound and an in-bound run. After each route was tested (typically 18-30 minutes), a Teflon-coated glass fiber filter was removed and subsequently post-weighted to calculate the particle mass concentration.

The PM size distribution of the diesel exhaust was measured on-board the bus using a TSI, Inc. Scanning Mobility Particle Sizer (SMPS) and a Dekati, Ltd. Electrical Low Pressure Impactor (ELPI) connected to a partial flow, single-stage mini-dilution system. The exhaust sample flow was divided into two parallel mini-diluters, from the first mini-diluter, the SMPS and ELPI measured the particle-size concentration, and from the second mini-diluter the gravimetric filter collected the particle mass emissions.

The ELPI measures real-time particle number concentration using 12 size cuts according to aerodynamic diameter between 30 nm and 10,000 nm. The ELPI was equipped with the electrical filter stage which extends the measurable range of particles down to 7 nm. The SMPS was operating on size-selective mode, and cannot measure the entire particle size distribution at a high temporal resolution, whereas the ELPI particle number measured the particle number concentrations the 12 impactor stages every 1~2 seconds. The SMPS and ELPI measurements from the study were previously shown to coincide (Holmén et al., 2005). The purpose of this work was focused on the effect of transient vehicle behavior on particle emissions, so only the real-time ELPI measurements were analyzed in this study.

The on-board instrumentation included a Horiba OBS-1000 gas emission analyzer, which measured fuel rate, gaseous emissions (NOx, CO_2, CO, HC), and the exhaust flow rate using a calibrated pitot tube. The exhaust flow rate was corrected for

negative and unreasonably low readings by assuming a minimum exhaust flow of 1300 L/min (See Supporting Information). A global positioning system unit on the Horiba OBS-1000 was used to spatially locate the bus on the defined bus routes, for which accurate grade data was available. A data link adapter connected to the network port of the diesel bus recorded instantaneous engine operation data. Further information on the measurement equipment, bus specifications, and experimental design is detailed in the report by Holmén et al. (2005).

Time-based Particle Emission Rates. The size-distributed particle number measurements from the ELPI and the exhaust flow measurements from the Horiba were time aligned with the engine operation parameters to account for the residence and transport time of emissions in the exhaust and dilution system. A constant lag was applied that maximized the cross-correlation between the ELPI, Horiba and engine parameters. Once all the data was synchronized to the engine data, the particle number emissions rate was calculated by multiplying the particle number concentration, total exhaust flow rate (Q_T) and dilution ratio (DR) for the runs on September 20th and 21st:

$$Particle\ Number\ Emission\ Rate\left(\frac{\#}{\sec}\right) = Particle\ Number\ Concentration \times Q_T \times DR$$

The average dilution ratio was 31 and 29 for September 20th and 21st, respectively.

Time-resolved mass emission rates were calculated using the ELPI measurements. Only particle counts on the electrical filter stage and lower five stages of the ELPI were used (diameters < 387 nm), assuming unit-density spherical particles with diameters equal to the geometric mean of the respective impactor stages, as done previously by Kinsey et al. (2006). The large diameter particle readings from the upper stages were excluded because positive artifacts on the upper stages can greatly affect mass concentration estimates (Maricq et al., 2006).

The ELPI-derived mass concentrations were compared to the route-level filter mass measurements. For the 12 test runs conducted on September 20th and 21st, the

ELPI-derived PM mass concentrations were 14% larger than the route-level, filter-based PM mass concentrations and were positively correlated with a R^2 =95%. The lower-stage measurements of the ELPI therefore appear to be a usable surrogate of the total PM mass emissions, and suggest that the accumulation mode measured by the ELPI (56.4- 387 nm) contained the majority of the particle mass. A time-resolved PM mass emission rate was subsequently computed from the ELPI-derived mass concentrations using the exhaust flow rate and dilution ratio as was done in equation (1). Table 5.1 displays the mean particle number and mass emission rates according to facility types and operating modes.

Distance-based Particle Emission Rates. Air quality models require spatially allocated emission factors along a roadway or a grid (Zhang et al., 2005). Distance-based emission rates (emissions per kilometer), are used to spatially allocate emissions and are important for estimating pollution exposure from emissions for persons on or near the road network. Average distance-based emission rates were calculated by dividing the average time-based emission rates for each operating mode by the average speed, yielding emissions per kilometer in Table 5.1. Idling emission rates cannot be expressed or calculated in per-distance terms, although the emissions from idling are included in the mean emission rates at the facility type level. Table 5.1 is discussed in more detail in the exploratory analysis.

Table 5.1. Summary of Particle Emission Rates for September 20th NE Runs analyzed by Road Type and Operating Mode.

	Descriptive Statistics, Time-based means					Time-based emission rates		Distance-based emission rates		R^2 between number and mass emissions (time-based)
Roadtype/ Opertating Mode	Time, sec	Speed, kph	Accel, kph/s	Grade, %	Fuel, g/s	Number, 10^{12} particles/s	Mass, mg/s	Number, 10^{12} particles/km	Mass, mg/km	
Urban Arterial	**2362**	**19**	**0.0**	**-0.4**	**1.5**	**0.9**	**0.11**	**172**	**20**	**0.81**
Acceleration	801	23.8	1.9	-0.5	3.2	1.9	0.22	295	33	
Deceleration	690	20.8	-2.2	-0.6	0.5	0.3	0.03	52	5	
Idle	629	0.0	0.0	-0.2	0.4	0.2	0.05	NA	NA	
Cruise	242	50.3	0.0	-0.3	2.0	1.2	0.09	89	7	
Rural Arterial	**736**	**49**	**0.0**	**-0.2**	**3.1**	**1.7**	**0.26**	**123**	**19**	**0.62**
Acceleration	63	26	2.6	-1.9	4.1	2.9	0.37	406	51	
Deceleration	61	20	-2.7	-1.3	0.2	0.1	0.01	9	2	
Idle	31	0	0.0	0.6	0.3	0.2	0.04	NA	NA	
Uphill Cruise	203	53	0.0	5.6	7.3	3.7	0.70	253	48	
Downhill cruise	266	61	0.2	-4.1	1.1	0.6	0.05	36	3	
Level cruise	112	58	-0.4	-0.1	1.8	1.2	0.10	71	6	
Divided Freeway	**932**	**95**	**0.02**	**0.0**	**6.8**	**7.0**	**1.00**	**268**	**38**	**0.54**
On Ramp	32	56	1.9	NA	7.4	3.8	0.74	243	47	
Off Ramp	33	49	-0.9	-0.7	1.3	0.5	0.06	37	4	
Acceleration	25	90	1.3	-1.1	8.6	6.2	0.90	248	36	
Deceleration	41	90	-1.9	0.4	2.4	2.6	0.27	105	11	
Cruise	801	98	0.0	0.0	7.2	7.7	1.09	282	40	
Overall	**4030**	**42.2**	**0.01**	**-0.3**	**3.0**	**2.5**	**0.34**	**211**	**29**	**0.80**

Exploratory Analysis

Across the entire dataset, the particle number and mass metrics are well correlated across time (R^2 =.80 from Table 5.1), due in part to the overall variability between high and low load vehicle operation. Within given roadway types or operating modes, such as on the divided freeway, the linear correlation is considerably less. To better understand the behavior of each metric on each roadway type, the particle emission rates were evaluated in detail for 3-minute periods from each of the three dominant facilities (Figures 1, 2, and 3). Each 3-minute period was chosen such that it demonstrated the unique driving conditions of each facility. During the urban arterial, the three minute segment included a section of roadway where the bus stopped four times within 800 meters. The 3-minute section for the rural arterial included an

extensive high-grade section with the grade averaging 6.2% for over 2.2 kilometers, with the maximum grade exceeding 9%. On the selected freeway segment, the bus traveled 5.4 kilometers at an average speed of 102 km/hr. Time-series profiles of the time-based particle measurements, and two engine covariates, fuel rate and engine speed, were plotted for each dominant roadway type (Figure 5.1,5.2 and 5.3).

Distance-based PM emission rates were aggregated in terms of number and micrograms per kilometer for every 50, 100, and 200 meter segment for the urban arterial, rural arterial and divided freeway, respectively. By spatially aggregating, the idling emissions were accounted for in each interval, and the particle exposure of the bus can be better interpreted using Geographical Information System (GIS) plots. The GIS plots (Figure 5.1-3, 5.2-3, and 5.3-3) provide a "bird's eye view" of the distance-based emissions rates plotted spatially along the testing route for the same 3-minute period analyzed in the time-series plots. Each segment is color coded according to the percentile of emission rates compared to the entire testing route, with the numerical values for each percentile provided in the supporting documents (Table 5.A5). Different levels of spatial aggregations were used (50, 100, and 200 meters) to maximize the spatial resolution, while assuring that each 50, 100 or 200 meter segment contained at least one particle measurement. The particle number emission rates are plotted in parallel above the particle mass emission rates. A corresponding GIS plot (panel 4) provides information on two roadway covariates, the average grade of each segment, and the average speed of the bus.

In Figures 1 through 3, the particle number size-distributions are plotted for the observations that occurred during select episodes. The episodes are defined over 100, 200, or 400 meter intervals according to roadway type. The episodes were chosen at locations along the road network that may potentially be PM "hot-spots" due to relatively high particle number and/or mass emissions. Spline smoothing was used to

approximate smooth particle size distributions from the ELPI discrete measurements. Mass-weighted size-distributions are included in the supporting information (Figure 5.A8). Key observations about the emission rates are noted on the figures, while comparisons and discussions are included in the text.

Urban Arterial. On the urban arterial, the number and mass emission rates spike as the bus accelerates. Due to the low speed and relative high emission rates during acceleration, large distance-based emission rates occurred near the bus stops and intersections as is evident from Table 5.1 and Figure 5.1-2. By only examining the GIS plot, it may seem reasonable that the elevated emission rates at the intersections could also be due to idling, where the bus was emitting particles but not traveling any distance. Each of the 50-meter segments that captured the 41 stops along the bus route was further evaluated by operating mode (Table 5.A4). The majority of emissions occurred due to acceleration (82.0% of the total particle number emissions and 68.1% of the total particle mass emissions), with the rest split between idling and deceleration. The median idling time was 9 seconds and the median acceleration time was 8 seconds. For the bus to have contributed an equal amount of emissions during idling as accelerating during a typical 50 meter segment, the bus would have to idle for more than 45 seconds (for particle mass) and almost 2 minutes (for particle number). Unless the buses were to idle for an extended stop, particle exposure can be mainly attributed to acceleration events on the stop-and-go arterials.

Rural Uphill. On the uphill accent on the rural arterial, the bus emitted elevated, but relatively stable particle numbers. The mass emissions were highly responsive to the fuel rate and engine speeds, producing variable and very high mass emission rates. The shape of the particle-size distribution varied drastically within the uphill accent (Figure 5.2-5 and 2-6), permitting the number emissions to stay relatively constant, while the mass emissions varied considerably (Figure 5.2-1). For the rural

Figure 5.1. Detailed particle number and mass emission rates for a three-minute segment of the urban arterial. Figure 5.1-1: Time-series plot of particle number and mass emission rates. Figure 5.1-2: Time-series plot of fuel rate and engine speed. Figure 5.1-3: GIS plots of distance-based emission rates for every 50 meter segment. Figure 5.1-4: Average grade and speed over 50 meter segments. Figures 1-5 and Figure 5.1-6: Particle number size-distribution concentrations measured for two 100-meter segments (Episodes A and B).

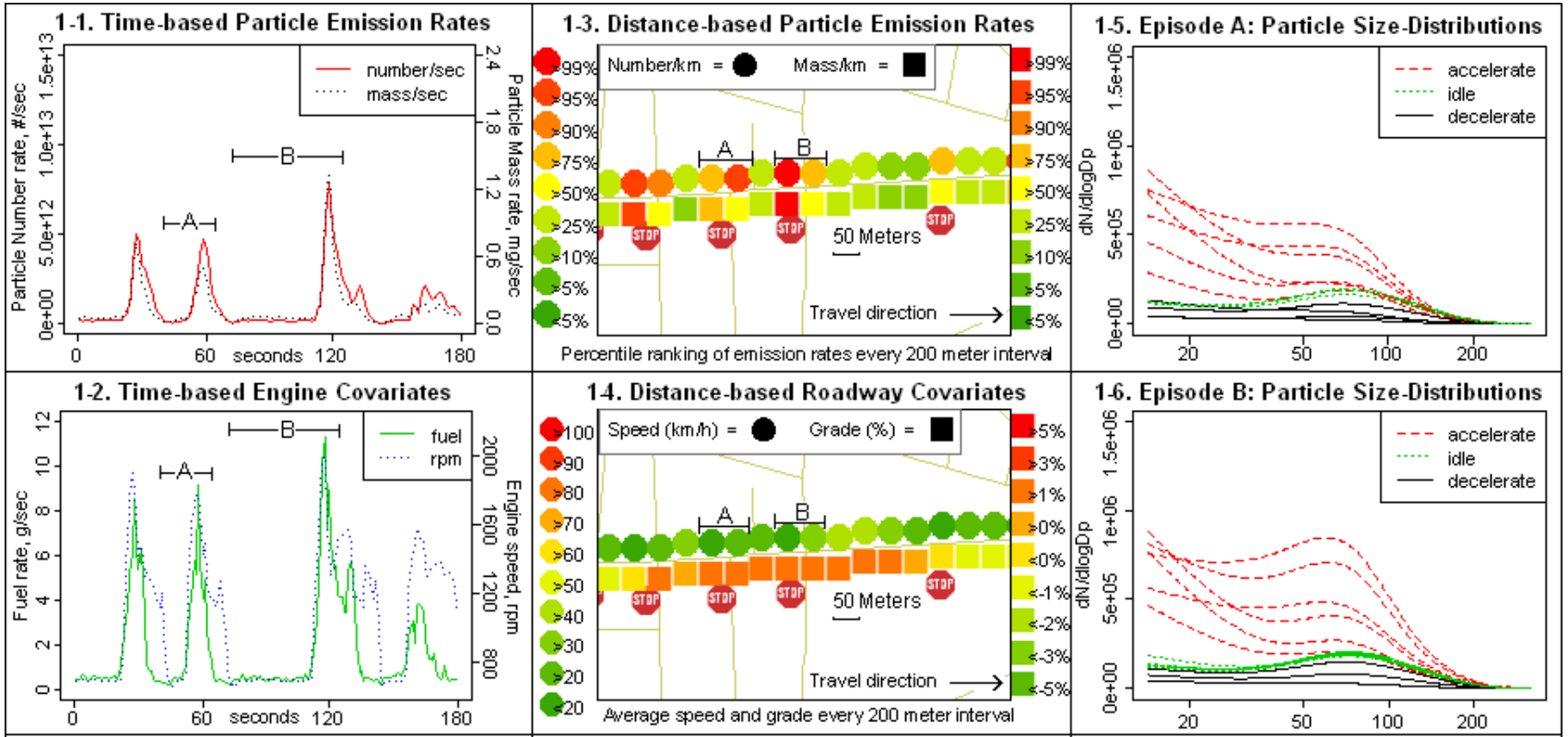

Time-based Particle Emissions

- Fuel rate and engine speed are higher at Episode B, which causes a higher peak in both particle metrics.
- Mass emission rates increase more at Episode B than number emission rates.

Distance-based Particle Emissions

- The grade during Episode A is 1.1% and at B is 1.5%, the slightly higher grade seems to result in higher emissions at B.
- Mass emission rates are more affected by the change in grade between Episodes A and B than number emission rates.

Particle Size-Distributions

- The majority of particles across all sizes occur during acceleration events, idle emission concentrations are higher than decelerating.
- The size-distribution shifts towards a larger accumulation mode in Episode B, which has a larger tail extending above 100 nm that contributes to the increase in mass emissions.

Figure 5.2. Detailed particle number and mass emission rates for a three-minute segment of the rural arterial. Figure 5.2-1: Time-series plots of particle number and mass emission rates. Figure 5.2-2: Time-series plots of fuel rate and engine speed. Figure 5.2-3: GIS plots of distance-based emission rates for every 100 meter segment. Figure 5.2-4: Average grade and speed over 100 meter segments. Figures 2-5 and Figure 5.2-6: Particle number size-distribution concentrations measured for two 200 meter segments (Episodes C and D).

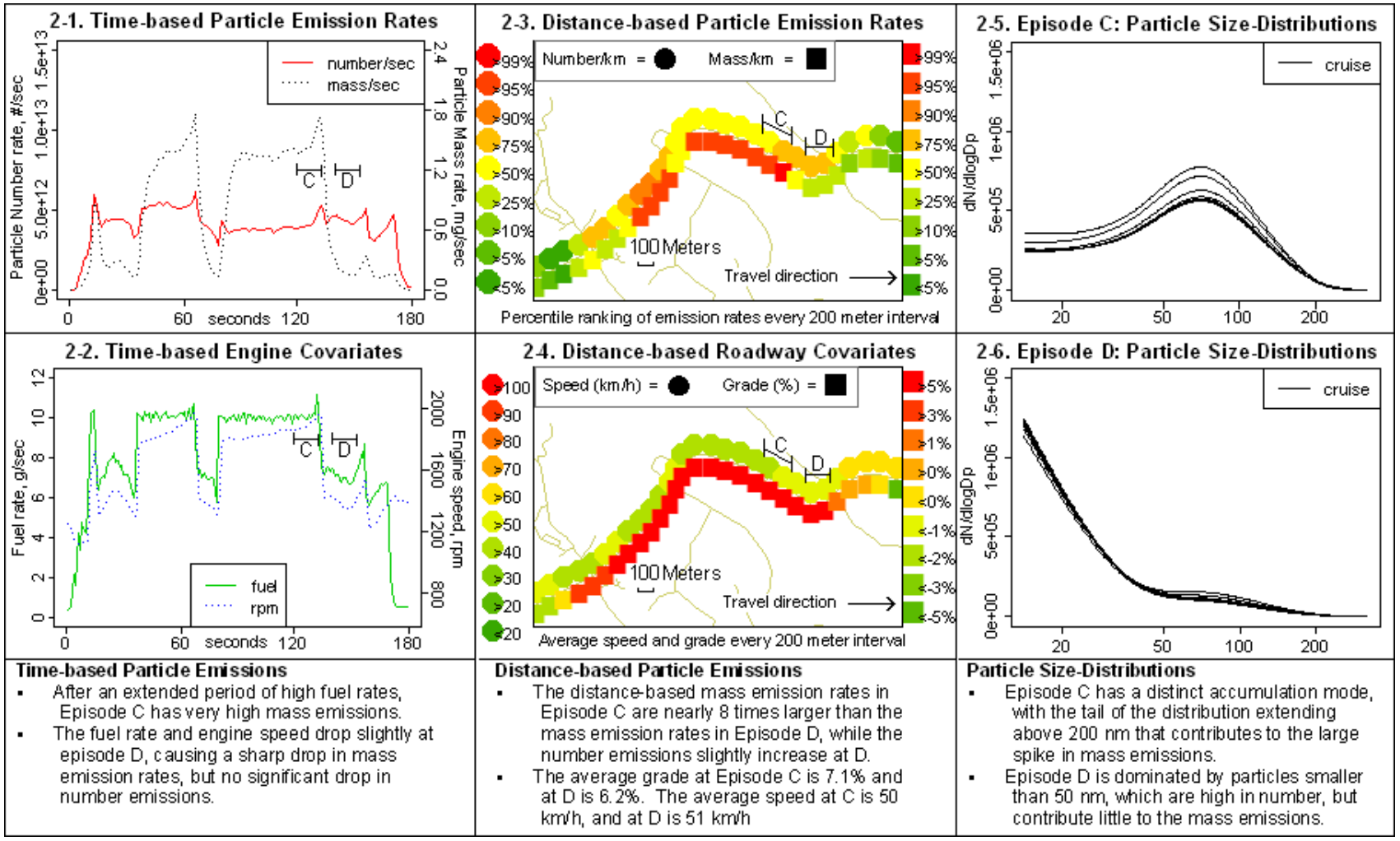

Time-based Particle Emissions

- After an extended period of high fuel rates, Episode C has very high mass emissions.
- The fuel rate and engine speed drop slightly at episode D, causing a sharp drop in mass emission rates, but no significant drop in number emissions.

Distance-based Particle Emissions

- The distance-based mass emission rates in Episode C are nearly 8 times larger than the mass emission rates in Episode D, while the number emissions slightly increase at D.
- The average grade at Episode C is 7.1% and at D is 6.2%. The average speed at C is 50 km/h, and at D is 51 km/h

Particle Size-Distributions

- Episode C has a distinct accumulation mode, with the tail of the distribution extending above 200 nm that contributes to the large spike in mass emissions.
- Episode D is dominated by particles smaller than 50 nm, which are high in number, but contribute little to the mass emissions.

Figure 5.3. Detailed particle number and mass emission rates for a three-minute segment of divided freeway. Figure 5.3-1: Time-series plots of particle number and mass emission rates. Figure 5.3-2: Time-series plots of fuel rate and engine speed. Figure 5.3-3: GIS plots of distance-based emission rates for every 200 meter segment. Figure 5.3-4: Average grade and speed over 200 meter segments. Figures 3-5 and Figure 5.3-6: Particle number size-distribution concentrations measured for two 400 meter segments (Episodes E and F).

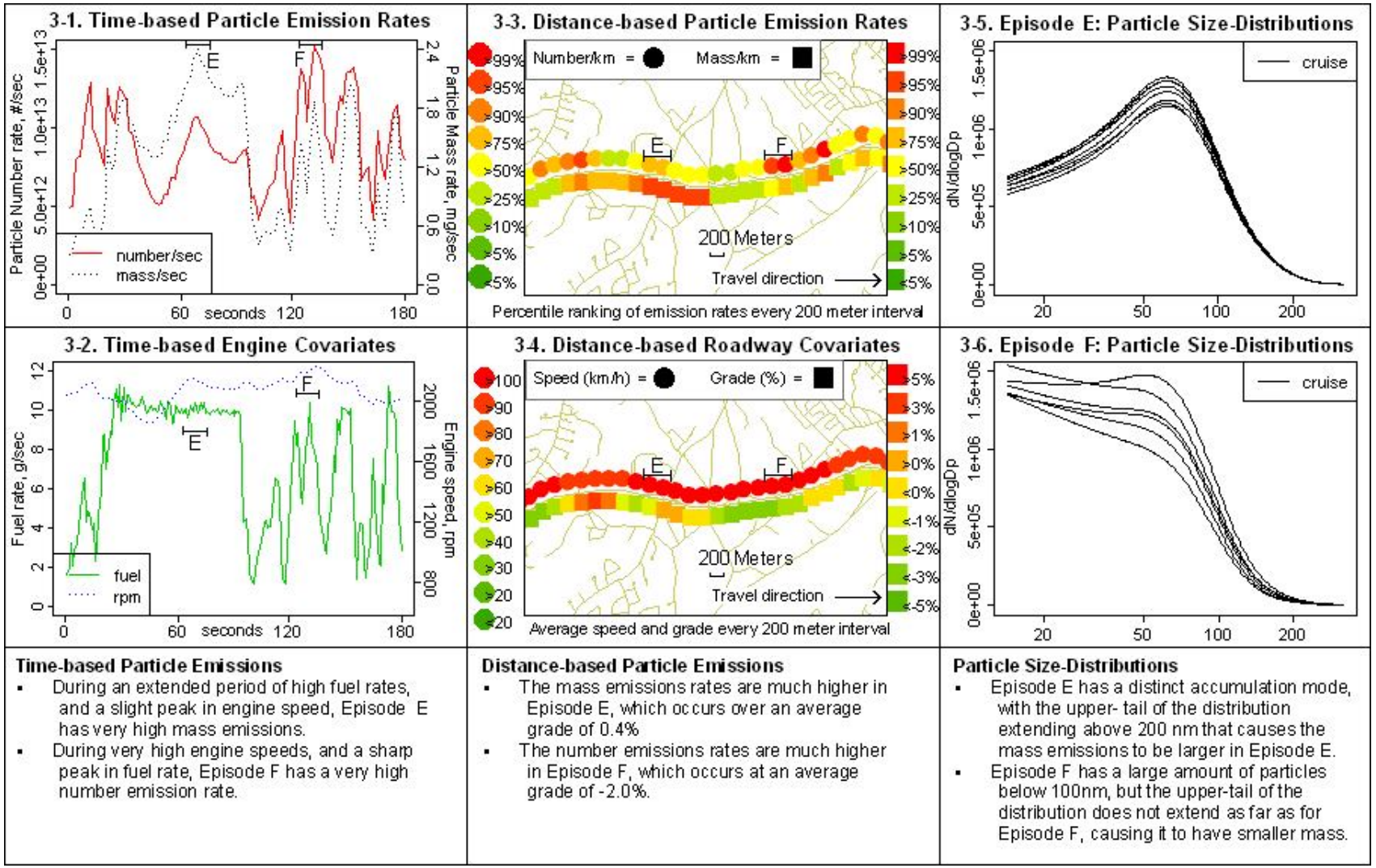

Time-based Particle Emissions

- During an extended period of high fuel rates, and a slight peak in engine speed, Episode E has very high mass emissions.
- During very high engine speeds, and a sharp peak in fuel rate, Episode F has a very high number emission rate.

Distance-based Particle Emissions

- The mass emissions rates are much higher in Episode E, which occurs over an average grade of 0.4%
- The number emissions rates are much higher in Episode F, which occurs at an average grade of -2.0%.

Particle Size-Distributions

- Episode E has a distinct accumulation mode, with the upper- tail of the distribution extending above 200 nm that causes the mass emissions to be larger in Episode E.
- Episode F has a large amount of particles below 100nm, but the upper-tail of the distribution does not extend as far as for Episode F, causing it to have smaller mass.

arterial, the distance-based mass emission rates were among the highest on the entire route, while the number emissions were only moderately elevated (Table 5.1).

Divided Freeway. The time-based particle number and mass emission rates reach their maximum values across the entire bus route on the segment of divided freeway in Figure 5.3. Both the particle number and mass emissions are highly variable, as the bus sustains high engine speeds and a large range of engine loads. Number and mass emissions were positively correlated (R^2=0.54), but also behave remarkably different as evidenced by the dynamic behavior of the particle size-distribution. Particle number emissions appear to be more influenced by short spikes in fuel rate, rather than long-sustained segments of high fuel rate.

Although the bus is cruising within a narrow speed window, the distance-based particle emissions do have considerable spatial variation. The high-emitting episodes for particle mass and number appear to occur at or slightly before positive changes in grade. The rural and urban arterials have short segments where the distance-based emission rates are larger than the freeway. However, due to constant high load conditions on the freeway, the average emission rates are highest on the divided freeway for both particle metrics (Table 5.1).

Modeling Section

The observations made from the exploratory analysis were statistically evaluated by modeling the relationship between particle emissions and engine parameters. Individual statistical models were estimated for particle number and mass emissions for three sections of the bus route. The urban section was 23 minutes in length and captured stop-and-go conditions, the rural hill section captured uphill and down hill sections of the rural arterial (6 minutes) and the freeway section captured the entire trip on the freeway including the on-ramp and off-ramp (16 minutes). The time-based emission rates were aggregated every 3-seconds for analysis because the ELPI

only recorded particle concentrations every 1-2 seconds, and the standard deviation of the time lag between the engine and the ELPI was estimated to be 2.01 seconds (Holmen et al., 2005).

Linear regression models were estimated with normalized emission rates and engine parameters, $(y-\bar{y})/\sigma_y$, so that the parameters could be more easily compared between the number and mass models, and between different engine parameters. Although non-linear relationships are likely to exist between the particle emissions and engine covariates, by estimating separate models for each roadway condition, linear models were anticipated to be able to approximate this relationship while maintaining interpretability. The linear models were estimated in the following form: $\textit{Particle emission rate}(\textit{per second}) = \beta_o + \sum_{i=1}^{k}(\beta_i \cdot \textit{engine parameter}_i) + \varepsilon$, for both the particle number and mass emission rates. Three engine parameters were evaluated for inclusion in each model: fuel rate, engine speed, and exhaust temperature. Previous analysis found that these parameters explained the majority of the engine parameter variation of the dataset (Sonntag, 2009). In addition, transformations and lags of the covariates were also considered to capture the temporal-dependence of the emission rates and approximate non-linear relationships. For example, the marginal effect of fuel rate on particle emissions appears to depend on the level of fuel rate. This non-linear relationship was approximated in the linear model by raising fuel rate to the second power. Each term was included in the model if it was significant at the 5% level on both the September 20th and 21st datasets. If one of the three original engine parameters was not significant but its transformation or lag was significant (i.e. Fuel^2) then both terms were included in the model. The estimated model parameters from September 20th are displayed in Table 5.2, and September 21st in Table 5.A7.

Table 5.2. Model Coefficients

	1. Urban Model		2. Rural Hill Model		3. Freeway Model	
Parameter	Number	Mass	Number	Mass	Number	Mass
Intercept	-0.34	-0.44	-0.13	-0.71	-0.04	-0.53
Fuel	0.22	0.22	0.40	0.01	0.32	0.10
$Fuel^2$	0.18	0.32	-0.14	0.21		0.28
$Fuel_{t-1}$	0.26	0.19	0.28	0.25	0.23	0.43
Engine Speed	0.30	0.24		0.48	-0.33	-0.96
$Engine\ Speed^2$	0.12	0.10		0.63	1.19	0.91
$Engine\ Speed_{t-1}$	-0.03	-0.10				
Exhaust Temperature	-0.08			-0.05	-0.70	0.12
Fit Statistics						
Adjusted R^2	0.95	0.93	0.91	0.97	0.86	0.89

Results

Urban Model. As expected, number and mass emissions are both well predicted using fuel and engine speed. The coefficients for the $Fuel^2$ and $EngineSpeed^2$ terms are both positive, meaning their marginal effect on both particle mass and number emissions increases at higher levels. The $Fuel^2$ coefficient is larger for mass emissions, while the $EngineSpeed^2$ coefficient is larger for number emissions. The negative effect of the lagged engine speed (the engine speed 3-seconds prior) likely captured the effect that, during deceleration engine speed can still be high, while emissions are low.

Rural Hill Model. On the rural hill section, particle mass is a stronger function of the operating conditions (R^2=0.97) than particle number emissions (R^2=0.91). Fuel rate and engine speed are significant predictors for mass emissions, but only fuel rate is a significant predictor for number emissions. Mass emissions are increasingly affected by fuel rate and engine speed at higher levels, as evidenced from the positive $Fuel^2$ and $EngineSpeed^2$ coefficients. Interestingly, the $Fuel^2$ coefficient is negative in the number model. As fuel rate increases, the marginal fuel effect on number decreases as it approaches the maximum fuel rate. Exhaust temperature was not significant in the

number emission models, but it did have a significant negative effect on the particle mass emissions.

Freeway Model. As was evident from the exploratory analysis, fuel rate has a larger effect on mass emissions, while engine speed has a larger effect on number emissions. Number emissions were not significantly effected by large spikes in fuel rate ($Fuel^2$ coefficient is insignificant); however, the $EngineSpeed^2$ has a large positive effect. Mass emissions are positively influenced by spikes in both fuel and engine speed. Exhaust temperature had a different relationship on particle number and mass emissions. For particle number it was strongly negative, and was moderately positive for particle mass.

Model Verification. The same models were fit for the same sections of roadway tested on September 21, 2004. The models had similar fits to the data both in terms of R^2 values and model coefficients. The model coefficients for all significant variables were of similar magnitude and had the same positive/negative signs (Table 5.A7). Even though the statistical models did not pass all diagnostic tests for normal independently distributed residuals, confirming the results on separate data sets provides robust evidence that the models estimated true relationships between particle emissions and the evaluated engine parameters.

Discussion

The statistical models are useful for comparing the engine factors influencing particle number and mass emissions, rather than quantifying an absolute relationship between particle emissions and engine operation. The model intercepts and coefficients change significantly across facility types, due to the effect of approximating highly non-linear and complex data with simple linear relationships. From these models, conclusions need to be made within "context" or the "facility effect" of each model in consideration. For the estimation of more general relationships between particle

number and operating parameters across different driving conditions, see Sonntag and Gao (2009), which estimated particle number emission at the roadway link-level. However, several conclusions about the transient behavior of particle number and mass emissions can be drawn from the observed data and model results:

1. Mass emissions are a strong function of the fuel rate, and are especially sensitive to high fueling rates. All the fuel coefficients, including the $Fuel^2$ coefficient was positive and significant in all three mass emission models. Previous observations confirm that diesel transit bus particulate mass emissions are a strong function of fuel transients (Hofeldt and Chen, 1996). Peaks in mass emission rates occur at high fuel rates regardless of the duration of the engine load. In some instances, it appears the large mass emission rates are favored by sustained fueling events. For example, the largest mass emission rates on the rural and freeway route occur during sustained high-fueling events (Figure 5.2-1 and 3-1).

2. In contrast, particle number emission rates had more complex relationships with the engine parameters coefficient depending on the roadway type. The changing relationships with number emissions appear to be caused by the storage and release of particles from the engine and exhaust system. During the intermittent, hard accelerations on the urban arterial, the particle number emissions are positively associated with both $EngineSpeed^2$ and $Fuel^2$. However, on the rural hill route, which contains a long uphill section with sustained high loads, $Fuel^2$ has a negative effect on particle number emissions and engine speed was insignificant (Table 5.2). On the freeway route, particle number emissions were a strong function of engine speed. The particle number emissions are likely a stronger function of particle number emissions on the freeway due to the release of particles from the walls of the engine cylinders and exhaust system which occurred at high engine speeds and exhaust flows (Mathis et al., 2005).

3. In all three road types, exhaust temperature had a negative effect on number emissions, although it was not significant in the rural section. Low exhaust temperatures can encourage the formation of nucleation mode particles from gaseous hydrocarbons from DOC-equipped diesel buses (Rönkkö et al., 2006). The effect of exhaust temperature on mass emission rates is mixed, with high exhaust temperatures both favoring and discouraging particle mass emission rates.

4. Fuel rate is a more reliable predictor of both particle metrics than engine speed. The Fuel, $Fuel^2$ and $Fuel_{t-1}$ coefficients have more consistent values across facility types than engine speed and exhaust temperature. The other coefficients add significant predictor information, but are much more affected by different driving conditions on each facility type. Particles formed from hydrocarbons in the fuel and lubricating oil, are better linearly related to the fuel rate. Additionally, engine speed can remain high during deceleration events and does not linearly converge to zero at low loads. Using fuel-based emission factors (Zhang et al., 2005), which assume linear relationships between particles and fuel, (i.e. particles/kg fuel) is a reasonable method to estimate particle emissions, although the ratios will likely change between road types and operating modes.

Conclusions

For the bus studied, the particle number and mass emissions are positively correlated throughout a route, both temporally and spatially. However, statistical models confirmed several differences of behavior for particle number and mass emissions during real-world bus operation. Particle mass emissions were more sensitive to high fueling events that occurred at high grade segments and accelerations on the freeway. Particle number emissions were more influenced by high engine speed and short accelerating events, likely due to the storage and release of ultrafine particles. Both metrics were most consistently correlated to fuel rate.

To limit particle exposure, transit authorities could implement several practices. 1. By eliminating unnecessary accelerations (through priority intersections or exclusive bus lanes), DOC-equipped buses could significantly reduce particle exposure in terms of number and mass. 2. While acceleration events dominate emissions for typical bus stops, idling can be significant if the bus idles for several minutes. Enforcement of anti-idling policies can have a significant benefit on both particle number and mass emissions. 3. The cleanest buses should be used on the routes that have the highest population exposure and the highest distance-based emission rates. For the evaluated bus routes the selection would not be straightforward, as the freeway route had the highest average distance-based particle emission rate, but the intersections on the urban and rural arterial had the maximum distance-based emission rates. We would recommend using the cleanest buses on the urban arterials, because of the close proximity of pedestrians and urban residents to the roadway. The divided freeway has a larger shoulder, allowing more time and distance for high particle number concentrations to decay before reaching populated areas offset from the freeway.

Comparison of results to previous studies

The particle emission rates and particle size distributions were compared to other particle emission studies to verify their validity. In this work, the mean values for the dominant road types ranged from 1.2E+14 particles/km on the rural arterial to 2.7E+14 particles/km on the divided highway. These values are somewhat lower than the mean particles/km emission rate of 3.08E+14 reported in the review by Morawska et al. (2008) for diesel transit buses.

The particle mass emission rates in our study ranged between 19 mg/km on the rural arterial and 38 mg/km on the freeway, which are almost an order of magnitude lower than should be expected. Lanni (2003) reported mass emission rates for New York City transit buses tested on chassis dynameters between of 90 and 400 mg/km for

conventional buses with diesel oxidation catalysts, and between 5 and 25 mg/km for buses equipped with diesel particle filters (DPF). Thus, our measurements appear to be unrealistically low, and compare better with DPF-equipped buses. Comparison in absolute particle number and mass with other studies should always be seen as approximate due to different particle measurement instruments, dilution techniques, diesel buses, testing conditions, fuel types, and driving cycles/operating conditions. However, the Lanni (2003) measurements are typical of conventional diesel vehicles (Prucz et al., 2001, Robert et al., 2007) and diesel particle filter-equipped vehicles (Biswas et al., 2008).

The particle concentration measurements from the ELPI, SMPS and gravimetric filter are consistent with one another, and are deemed valid for comparing the relative variability of particle number and mass measurements. The unrealistically low emission rates could be due to measurement errors of the dilution ratio. Underestimating the dilution ratio would have caused the emission rates to be systematically lower, even if the particle concentrations measurements were correct (Equation 1). Other studies have reported difficulty in calculating accurate dilution ratios in both artificial dilution tunnels (Clark et al., 2007) and chase-plume studies (Kittelson et al., 2006a).

The particle size distributions measured in this work compare well with previous heavy-duty diesel emission studies that measure particles in artificial dilution tunnels. The particle number size distribution has both a variable nucleation mode, and a repeatable accumulation mode, with the peak of the accumulation mode occurring between 60 and 100 nm (Shi et al., 2000, Vaaraslahti et al., 2004, Liu et al., 2007, Ristovski et al., 2006). The particle mass distributions have a single peak in accumulation mode occurring between 100 and 180 nm (Robert et al., 2007).

The particle size distributions in our study frequently showed the presence of a nucleation mode. However, the artificial dilution conditions and sampling system may have underestimated the nucleation mode concentration. Recent vehicle chase studies of heavy-duty diesel exhaust revealed that a large nucleation mode is often present in the exhaust plume, below 10 or 20 nanometers. The nucleation mode concentration dominates the total number of particles, with a peak concentration of 1 to 2 orders of magnitude higher than the peak accumulation mode concentration (Kittelson et al., 2006a, Rönkkö et al., 2006). Figure 5.2-6, gives evidence that the nucleation mode is larger than is measured by the ELPI. The SMPS coincided with the ELPI measurements, and also may have missed a significant nucleation mode peak, because the SMPS only measured particles down to 10 nm (Vikara and Holmen, 2006). Rönkkö et al. (2006) concluded that instruments that only measure down to 10 nm would miss or seriously underestimate nucleation mode particles.

The nucleation mode may have been suppressed in our measurements by the mini-dilution system, because dilution conditions that favor large nucleation mode formation are difficult to replicate using an artificial dilution tunnels (Kittelson et al., 2006a, Rönkkö et al., 2006). Two emission processes were shown to contribute to the formation of a large nucleation mode from a DOC-equipped diesel transit bus (Rönkkö et al., 2006). At low engine loads and exhaust temperatures, the nucleation mode is comprised of unburned hydrocarbons from the fuel and lubricating oil. At high loads, the nucleation mode is comprised of sulfates that were oxidized at high exhaust temperatures in the diesel oxidation catalyst. The consistent negative effect of exhaust temperature on particle number emissions in our results (Table 5.2), suggests that a sulfate-based nucleation mode was suppressed or undetected by the measurement equipment. The mini-dilution used in our study was previously shown to suppress

nucleation mode formation for particles from a DPF-equipped and CNG vehicles (Holmen and Ayala, 2002).

Small particle losses may have contributed to an underestimation of the nucleation mode particles in the mini-dilution sampling system. Particle losses due to diffusion in the sampling line system and measurement equipment can dominate small particle measurements. Kittelson et al. (2006a) found that the measured particle number concentration were four times smaller than the actual concentration in the exhaust, due to small particle losses. The ELPI corrects for small particle losses, but no corrections were made for particle losses within the sampling lines and mini-dilution system (Holmen et al., 2005).

The formation of nucleation mode is complex, and the understanding of the underlying mechanisms of formations is rapidly changing. Even though the nucleation mode may have been suppressed from our data, the measurement methods and results are consistent with the current state of practice. For example, Ristovski et al. (2006) measured diesel transit bus emissions using a chassis dynamometer and artificial dilution tunnel, but rarely detected a significant nucleation mode when operating on ultralow sulfur diesel fuel. Additionally, no protocol has been established for measuring nucleation mode particles and measurements can be substantially different based on sampling conditions and the sampling equipment. The European Union has established a particle measurement procedure (PMP) used to establish a particle number based standard. The PMP removes the volatile fraction of the exhaust, which is responsible for the formation of the nucleation mode, in order to maintain repeatable results (Morawska et al., 2008). Ideally, sampling methods should repeatedly measure the true magnitude of nucleation mode particles that exist in the exhaust plume from vehicles driving in real-world measurements, however such measurement methods are still evolving for artificial dilution systems (Rönkkö et al., 2006, Kittelson et al., 2006a).

In summary, the particle size distribution measurements made in this study are consistent with the state of practice. However, the data should be used with the qualification that a large nucleation mode for particles smaller than 30 nm may have been suppressed by the artificial dilution and sampling system. The particle mass distributions are less sensitive to dilution conditions, and are consistent with other studies. The absolute concentration of particle number and mass concentration were lower than should be expected for a conventional diesel bus, which likely reflects an error in the dilution ratio measurements. The relative variation of particle number and mass instruments are valid for the qualifications given, however the absolute concentration of the particle number and mass emissions are likely invalid and should not be used to compare with other studies.

This is the first known study measuring particle number emissions with an on-board dilution system. Future work is needed to assure that particle number measurements made in artificial dilution tunnels compare well with real-world exhaust plumes. Additional research is needed to better quantify the contribution of particle number and mass emissions from a larger set of vehicles, including low-emission diesel vehicles in transient operating conditions. Even though the data from this study may have limited application, the presented analysis provides a useful framework for analysis of complex real-world emissions. In depth exploratory analysis, coupled with statistical analysis across two days of testing was a useful strategy to extract useful conclusions about the variation of particle number and mass emission rates.

Acknowledgment

We gratefully acknowledge Zhong Chen and Derek M. Vikara for conducting the field measurements, Eric D. Jackson for assistance with data processing and providing insights for analyzing the data, and Yiannis Kamarianakis for giving statistical methods advice. This research was sponsored by the New York Metropolitan Transportation Council and University Transportation Research Council through the September 11th Program Fellowship Program, the New York State Energy Research Development Authority through the Environmental Monitoring, Evaluation, and Protection PhD Fellowship Program, the Joint Highway Research Advisory Council of the University of Connecticut, and the Connecticut Department of Transportation through Projects 03-8 and 05-9.

APPENDIX

Table 5.A1. Summary Statistics of Each Road Type (September 20th)

Roadway type	Time, m:s	Distance, km	Mean speed , km/ hr (min/max)	Stops	Mean grade, % (min/max)
Divided Highway	15:32	24.5	95 (18/110)	0	-0.04 (-3.3/4.1)
Rural Arterial	12:16	10.1	19 (0/61)	3	-0.5 (-8.5/9.0)
Urban Arterial	39:22	12.7	49 (0/84)	38	-0.5 (-6.7/5.6)
Overall	67:10	47	42 (0/110)	41	-0.3 (-8.5/9.0)

Table 5.A2. Time-Based Emission Rates for September 20th

Road Type	Number (#/sec)		Mass (mg/sec)		Correlation R^2
	Mean	CV	Mean	CV	
Divided Freeway	7.0E+12	0.44	1.00	0.55	0.54
Rural Arterial	1.7E+12	1.11	0.26	1.7	0.62
Urban Arterial	9.2E+11	1.36	0.11	1.6	0.81
Overall	2.48E+12	1.29	0.34	1.49	0.80

Table 5.A3. Time-Based Emission Rates for September 21st

Road Type	Number (#/sec)		Mass (mg/sec)		Correlation R^2
	Mean	CV	Mean	CV	
Divided Freeway	6.63E+12	0.51	1.34	0.63	0.70
Rural Arterial	1.30E+12	1.17	0.24	1.75	0.71
Urban Arterial	6.92E+11	1.57	0.10	1.88	0.83
Overall	2.12E+12	1.45	0.40	1.70	0.86

Table 5.A4. Distanced-Based Emission Rates for each 50 meter Segment on September 20th

Road Type	Number (#/km)		Mass (mg/km)		Correlation R^2
	Mean	CV	Mean	CV	
Divided Freeway	2.6E+14	0.38	37.5	0.51	0.49
Rural Arterial	1.2E+14	1.20	18.5	1.8	0.65
Urban Arterial	1.7E+14	1.03	18.9	1.5	0.87
Overall	2.0E+14	0.86	28.0	0.82	0.70

Table 5.A5. Percentiles for Distance-based Particle Emission Rates for Sep. 20th

	Number/km			Micrograms/km		
Percentiles	**50m**	**100m**	**200m**	**50m**	**100m**	**200m**
5	4.7E+11	8.9E+11	8.9E+11	0.1	0.1	0.6
10	1.1E+13	2.2E+13	2.2E+13	1.0	1.5	3.0
25	8.1E+13	9.9E+13	9.9E+13	6.1	8.3	8.7
50	2.1E+14	2.2E+14	2.2E+14	19.4	22.2	24.3
75	2.9E+14	3.0E+14	3.0E+14	44.5	45.2	42.4
90	3.9E+14	3.9E+14	3.9E+14	61.4	60.7	57.5
95	4.3E+14	4.2E+14	4.2E+14	76.4	71.6	67.7
99	6.8E+14	5.5E+14	5.5E+14	107.6	105.7	102.7

Table 5.A6. Summary Statistics on all (42) of the 50-meter Episodes that included Bus Stops.

	Deceleration	Idle	Acceleration
Mean time, s	7.46	16.1	7.3
Median time ,s	7	9	8
Minimum time,s	2	1	0
Maximum time, s	15	81	13
Total time in all 50 meter segments, m:s	5:05	11:00	5:21
Mean particle number emission rate, #/s	1.4E+11	1.6E+11	2.1E+12
Sum, total number, #	4.4E+13	1.0E+14	6.8E+14
Percent contribution of particle number emissions	5.3%	12.7%	82.0%
Mean particle mass emission rate, ug/s	27.8	50.0	275.4
Sum, mass emissions, mg	8.49	33.0	88.4
Percent contribution of particle mass emissions	6.5%	25.4%	68.1%

Table 5.A7. Model Coefficients for September 21st

	1. Urban Model		**2. Rural Hill Model**		**3. Freeway Model**	
Parameter	Number	Mass	Number	Mass	Number	Mass
Intercept	-0.33	-0.43	-0.26	-0.52	-0.55	-0.84
Fuel	0.16	0.12	0.36	0.09	0.26	-0.08
$Fuel^2$	0.10	0.22	-0.08	0.09		0.28
$Fuel_{t-1}$	0.28	0.19	0.21	0.11	0.36	0.54
Engine Speed	0.30	0.15		-0.12	0.52	-0.09
Engine $Speed^2$	0.17	0.07		1.04	0.73	0.44
Engine $Speed_{t-1}$	-0.04	-0.07				
Exhaust Temperature	-0.04			-0.02	-0.70	0.18
Fit Statistics						
Adjusted R^2	0.96	0.93	0.95	0.99	0.85	0.84

Table 5.A8. Operation Mode Definitions for Table 5.1

Road type	Operating Mode	Acceleration, kmh/s	Vehicle Speed, kmh	Grade, %
Urban Arterial	Acceleration	>= 0	< 40	
	Acceleration	>= 1	>= 40	
	Deceleration	< 0	< 40	
	Deceleration	<-1	>= 40	
	Cruise	(-1,1)	>= 40	
	Idle		= 0	
Rural Arterial	Acceleration	>= 0	< 40	
	Deceleration	< 0	< 40	
	Uphill cruise		>= 40	>= 1
	Downhill cruise		>= 40	=< -1
	Level cruise			(-1,1)
	Idle		= 0	
Divided Freeway	Acceleration	>= 1	< 40	
	Deceleration	=< -1	< 40	
	Cruise	(-1,1)		

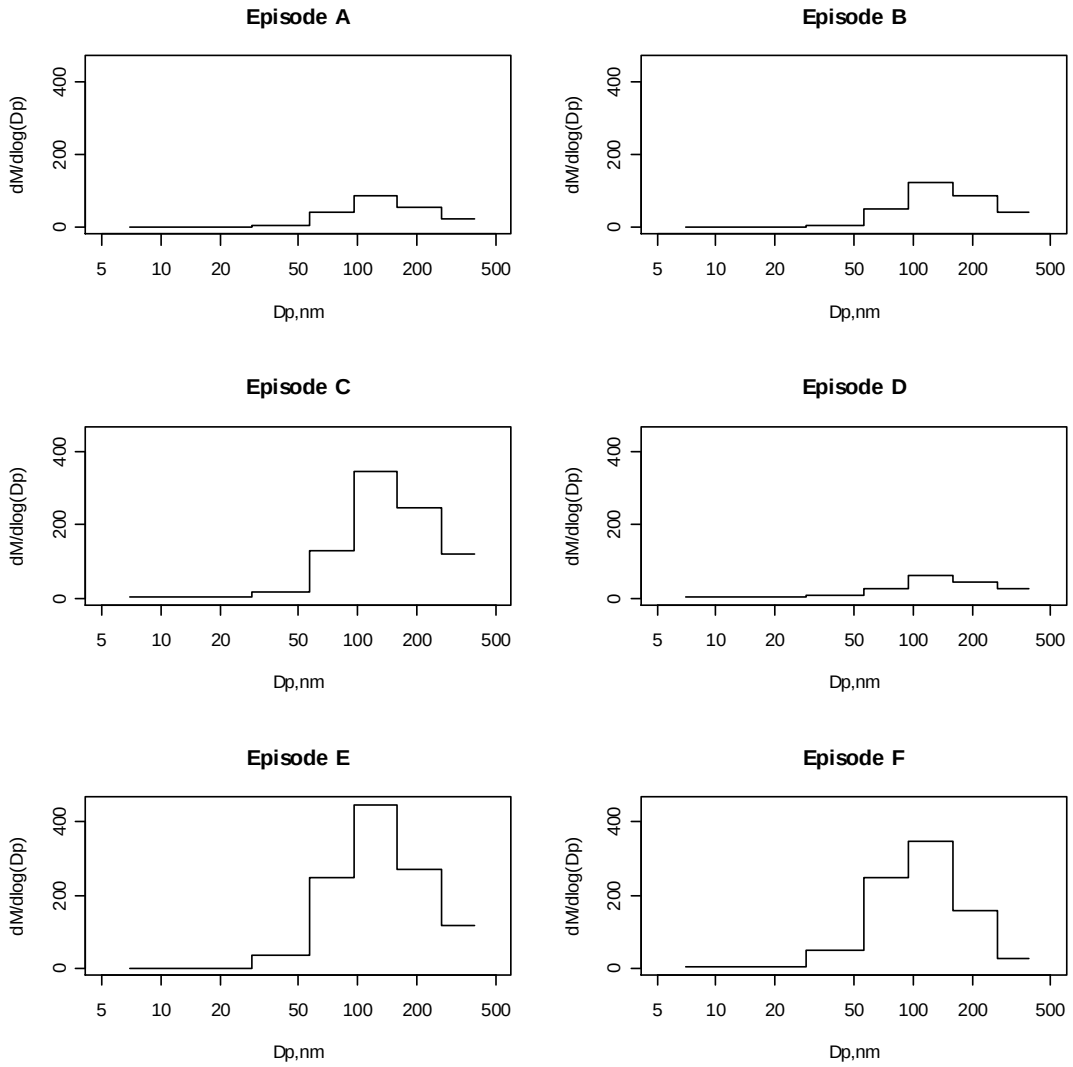

Figure 5.A1. Mean mass-distributions for selected episodes. Units for mass concentrations are in ug nm^{-1} m^{-3}. Only particles in the lower 6 stages (diameter < 387 nm) are used to compute mass concentrations.

ELPI-derived number emissions rate

To compute temporally resolved particle number emission rates, the particle concentration data and the exhaust flow rate was synchronized to the engine data. This was required because of the different clock-times on the instruments and to account for the time needed for the aerosol to travel from the engine through the exhaust and dilution systems to the ELPI. To align the data, the lag between the engine and ELPI was estimated by observing the initial engine start and initial spike in particle concentration. Then the lag that produced a maximum cross-correlation between the engine speed (RPM) and particle concentrations was calculated. The temporal shift that produced the best correlation between engine speed and particle concentrations and was consistent with the observed lag was used to synchronize the particle

concentration measurements to the engine data. Similarly, a temporal shift was applied to synchronize the exhaust flow rate to the engine data. Once all the data were temporally aligned to the engine data, the particle number emissions rate was calculated using equation 1.

ELPI-derived mass emissions rate

One of the key disadvantages of the filter measurements is aggregate time resolution. In this study, mass-weighted particle size distributions and concentrations were derived from ELPI particle measurements, as has been done in other studies (Kinsey et al. 2006; Maricq et al., 2006;; Shi et al., 2000). To illustrate the calculations, the particle mass distribution was calculated for a one minute period on the urban arterial section. The ELPI measured 31 observations during this one minute period. During the minute period, the bus was traveling between 20 and 37 mph, with engine load ranging between 0 and 100%. The number-weighted, average particle size distribution in terms of dN/dlogDp for the 31 observations is plotted in Figure 5.A2a., showing that the majority of particles are below 100 nm.

Initially, the mass-weighted size-distribution was calculated by using all 12 ELPI stages, using a straightforward approach assuming that all the particles were unit density spheres with diameters equal to the geometric mean of each stage. The particle mass density was computed in terms of dM/dlog(Dp) in Figure 5.2b. The average mass distribution is dominated by particles in the upper two stages (particles > 2.42 um) suggesting that the mass is dominated by coarse mode particles. However, the mass-weighted particle size distribution for diesel exhaust is typically dominated by the accumulation mode around 100 nm (Kittelson, 1998; Burtscher, 2005). In Figure 5.2c the observations that had readings in the upper two stages were removed, showing that most observations have a characteristic accumulation mode around 100 nm. For the entire data set, only 30% of the ELPI measurements recorded readings in the stages 11 and 12, yet these readings contribute to over 75% of the total mass.

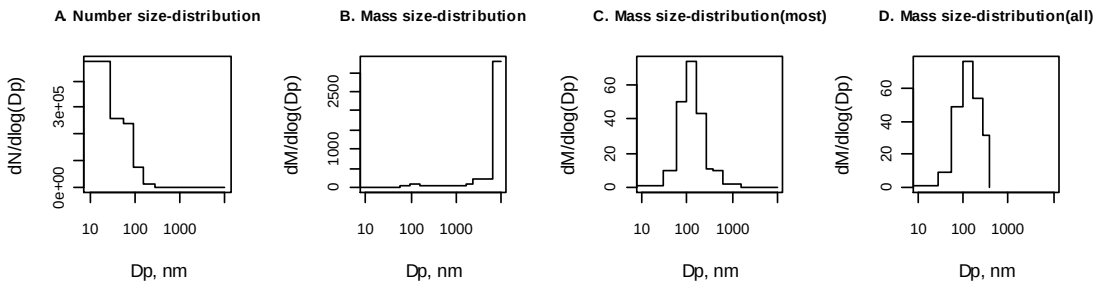

Figure 5.A2. Average particle size distributions for a one-minute period (31 observations) along the urban arterial. A. Number-weighted particle size distribution averaged for all 31 observations. B. Mass-weighted particle size distribution averaged for all 31 observations. C. Mass-weighted particle size-distribution for the 20 observations with no coarse mode particles. D. Mass-weighted particle size-distribution for all the observations, but excluding the all particles above 387 nm.

The large mass in the coarse mode is believed to be an erroneous measurement from the ELPI. Other researchers have observed similar phenomenon, concluding that summing over all 12 stages of the ELPI can lead to significant over estimation of the PM mass concentrations of diesel exhaust (Kinsey et al., 2006; Maricq et al., 2006; Shi et al., 2000). The overestimation occurs due to positive artifacts that occur on the upper stages of the ELPI (Maricq et al., 2006). More accurate mass concentrations have been obtained by only using the bottom 5 stages (Kinsey et al., 2006). Maricq et al. (2006) has proposed an iterative algorithm that uses the measurements from all 12 stages and assumed properties for diesel agglomerates (i.e. lognormal distribution, mobility densities) to estimate a particle mass distribution from ELPI data. The algorithm has yielded errors within 20% compared to gravimetric filter based measurements.

In this study we used the lower stage approximation for simplicity in calculating mass concentrations for a large amount of data. In Figure 5.2d, the mass distribution is plotted by only including the bottom 5 stages and the electrical filter stage. By so doing, the data has a characteristic accumulation mode similar to the observations without inflated coarse-mode readings.

The accuracy of computing the total mass concentration from using the lower stages of the ELPI was evaluated by comparing it to the filter measurements. The average mass concentration was computed by assuming the particles were unit density spheres, with diameter equal to the geometric mean of each stage, yielding the following summation across the 6 stages:

$$M\left(\frac{\mu g}{m^3}\right) = \sum_{i=1}^{6}\left(\frac{\pi}{6}\right)\cdot \rho_o \cdot \overline{D_i}^3 \cdot \Delta N_i \cdot DR_A$$

The average mass concentration over each route was compared to the average mass concentration derived from the gravimetric filter measurements. For the routes measured on September 20th and 21st, the ELPI and filter mass measurements correlated by an R^2 of 96% and the ELPI were 15% larger than the filter measurements (Figure 5.A3). Given that gravimetric mass filter measurements are also prone to error (e.g. hydrocarbon absorption on the filter, (Maricq et al., 2006). The strong correlation between the two measurements gives credence to the ELPI-derived mass concentrations.

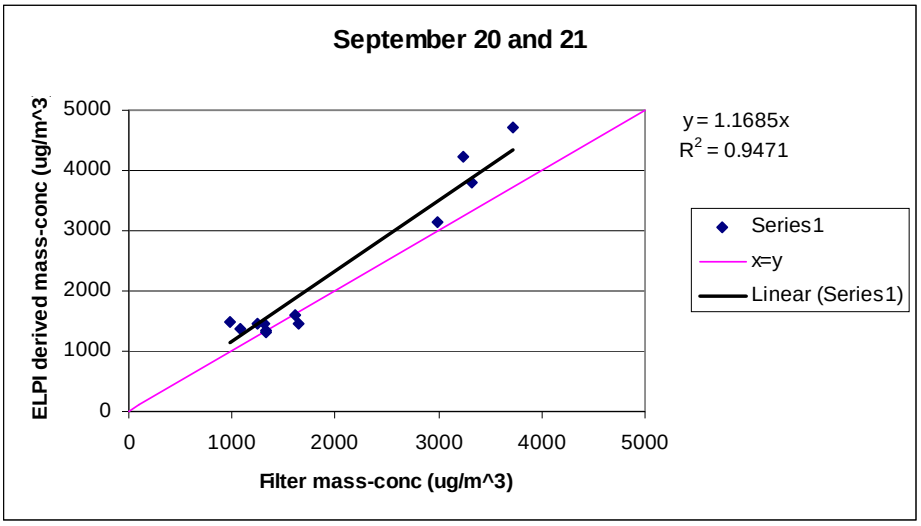

Figure 5.A3. Comparison of particle mass concentrations derived from the ELPI and gravimetric filter. The mass concentrations are the route-averages for 16 routes measured on September 20th and September 21st.

Comparisons of the two approaches for all the available conventional diesel bus tests from the Holmén et al. (2005) study are plotted in Figure 5.A4, which includes results from 62 test runs over 8 days on two conventional diesel buses. The ELPI–derived PM mass emissions are correlated with the filter-based PM mass concentrations with a R^2 coefficient of 76%. On average the ELPI derived-mass measurements are 16% larger than the filter mass concentrations. The higher PM mass results from ELPI-based calculation could be due to the unit density assumption which tends to be too high based on ELPI measurement (Shi et al., 2000).

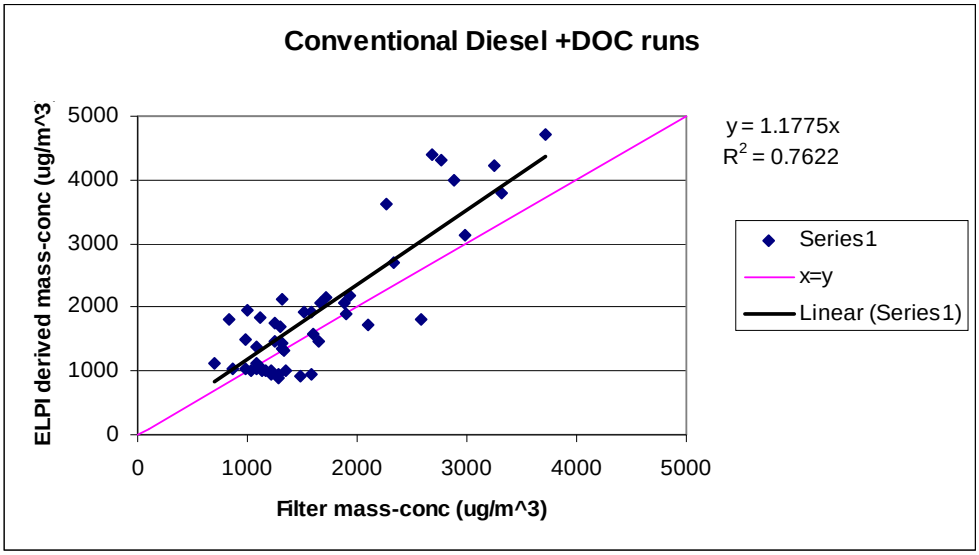

Figure 5.A4. Comparison of ELPI derived mass concentrations and gravimetric filter mass concentrations for the 62 bus routes tested with conventional diesels.

Negative and Low Exhaust Flow Rates

The emission rates depend on the accurate measurements of emissions concentrations and total exhaust flow rate. The exhaust flow rate was measured from a pitot tube assembly included in the Horiba gas analyzer. Obtaining reasonable exhaust flow rates was problematic, and during the first months of testing large amounts of negative exhaust flow rates were recorded. In an effort to solve the problem of low exhaust flow rates, an extension on the tail-pipe was built to prevent wind-backflow, and the pitot tube was re-zeroed after each testing route (Holmén et al. 2005). Even still, the Horiba frequently recorded unreasonably low and negative exhaust flow readings. For the 8 days of testing runs of the conventional diesel buses, more than 1 in 20 observations on the urban arterial had a negative exhaust flow rate recorded. Most of these observations (over 65%) occurred when the bus was idling.

To correct for the negative and unreasonably low exhaust flow values, a minimum exhaust value of 1300 L/min was set. 1300L/min was chosen because it was the median value for exhaust flow rate for the bus during idle during bus routes that did not have significant amounts of negative exhaust flow rates. Theoretically, the minimum exhaust flow rate at idle can be calculated from the engine speed, which is roughly 700 rpm for the analyzed transit bus. The diesel engine intakes and vents the cylinders once every two cycles, yielding the following equation:

$$Exhaust\ \ flow = Engine\ displacement \times Engine\ speed \times volumetric\ efficiency \times \left(\frac{1}{2}\right)$$

$$2100\ L/\mathrm{m} = 8.7 L \times 700\ rpm \times 0.7 \times \left(\frac{1}{2}\right)$$

This minimum exhaust flow rate should be seen as an approximate, "back of the envelope" estimate. The volumetric efficiency is assumed to be 0.7, no consideration is given to the fuel rate, which should be a minor contribution of exhaust flow at low fuel rate, and the exhaust gas is assumed to be at constant pressure and temperature between the cylinder and exhaust flow measurements. However, this is not the case due the turbocharged engine. Regardless, it appears that we are warranted in setting a minimum exhaust flow rate to correct for the low and negative exhaust flow rates. The 1300 L/min is smaller than 2100 L/min but will be retained for two reasons. Because it is derived from the Horiba values it is more consistent with the other exhaust flow measurements. Additionally, we do not have any data on the true volumetric efficiency constant for the bus at idle, and the exhaust flow calculation is only approximate.

For the September 20th runs evaluated in detail in the report, 10.7% of the exhaust flow values are under the minimum value of 1300 L/min. Of these 64.5% of these occur in the idling mode, which consists of 42% of all the idling values. Another 22% of the low exhaust values occurred during low speed decelerations, while another 12% occurred during low speed cruising modes. Because there is anticipated to be considerable variability in the exhaust flow rates within these operating modes, using a larger value than 1300 L/min value, would eliminate a larger portion of the emission rate variability.

The sensitivity of the results was examined by setting the somewhat arbitrary minimum exhaust flow rate of 1300 L/min. The overall mean of the September 20 emission rates for particle number and mass only increased slightly. For the divided

highway section, there was no change due to the high exhaust flow rates. On the urban arterial the number emission rates increased by 1.2% and the mass emission rates increased by 3.2%. The other routes had changes less than 1%. The overall share of idling emissions increased from 0.9% to 1.1% for number emissions and from 1.9% to 2.4% for mass emissions. The emission rates were not highly sensitive to the emission rate changes. Overall, we are interested in the high emission events which have exhaust flow rates far above 1300 L/min, so our results and conclusions will not be very sensitive to the selected minimum exhaust flow rate.

Cold Start

All data analyzed in the report were measured with the warmed up transit bus. To examine if cold-start idling had high emission rates, the cold-start recorded from September 21 was analyzed. The mass emission rate was 0.029 mg/sec and number emission rate was 1.29e+11 particles /sec. The mass emission rate was 42% smaller than the mean idle emission rate for the entire route on September 20th, and the number emission rate was 26% smaller than the mean idle emission rate. Mathis et al. (2005) examined cold start emissions from diesel and spark ignition vehicles. For the diesel engine (with oxidation catalyst) the cold start had almost no effect on the idling emission rates in terms of particle emissions. Even though only one cold start was analyzed, our data confirm previous results, that cold-start idling does not have a significant impact on particle number of mass emission rates for a conventional diesel bus.

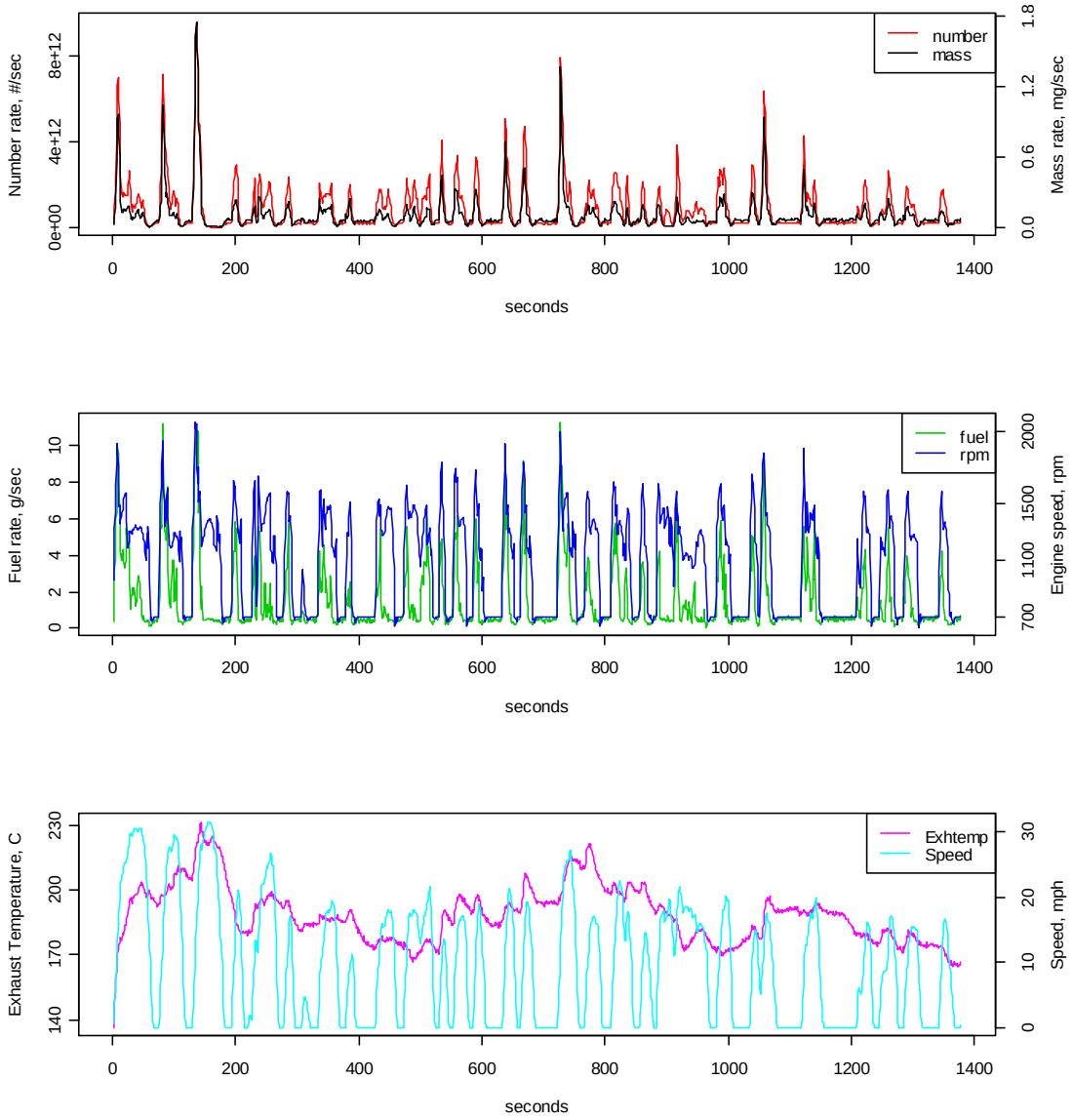

Figure 5.A6. Particle emissions and covariates for modeled urban arterial section.

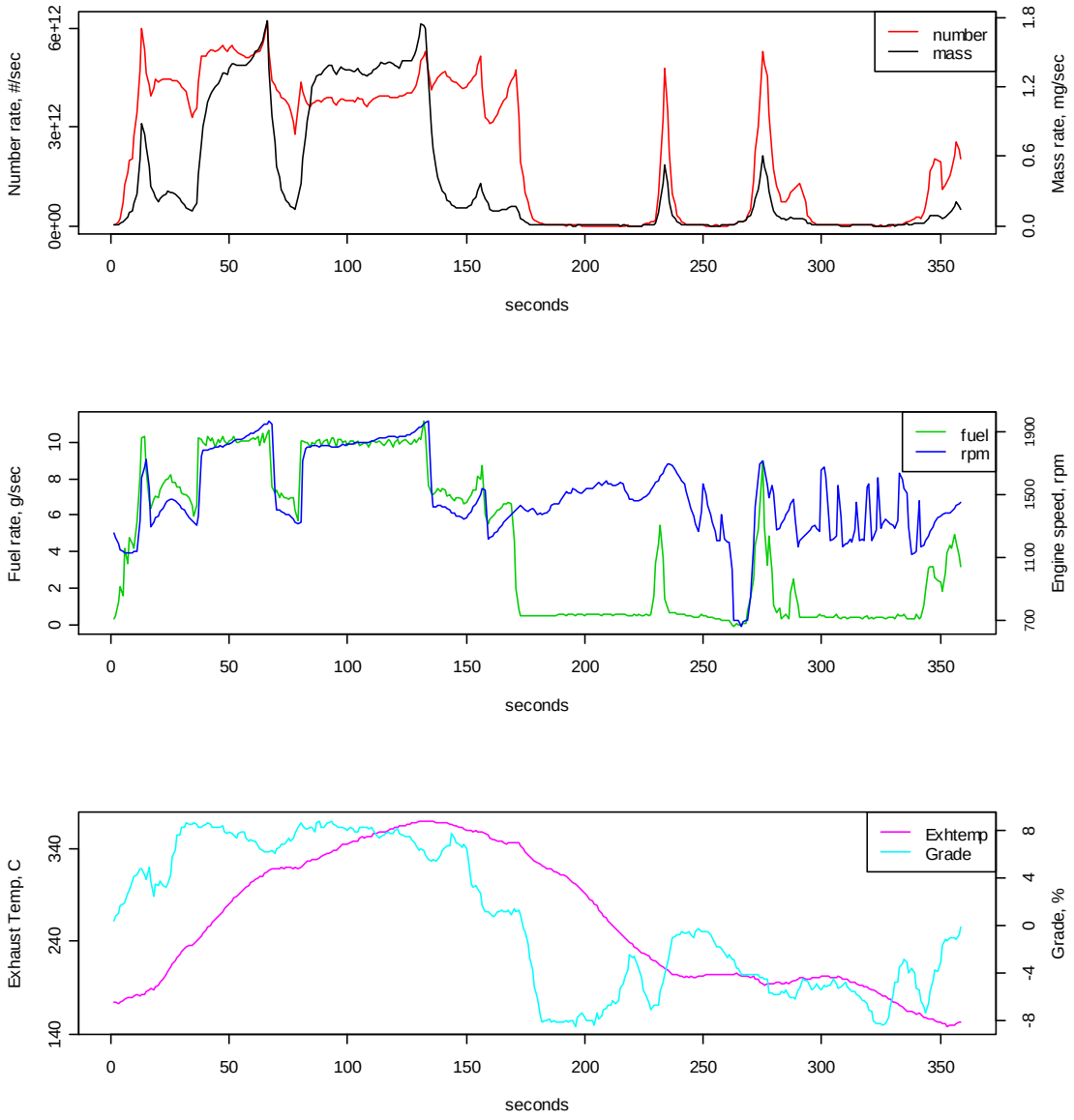

Figure 5.A7. Particle Emissions and covariates for modeled rural arterial section.

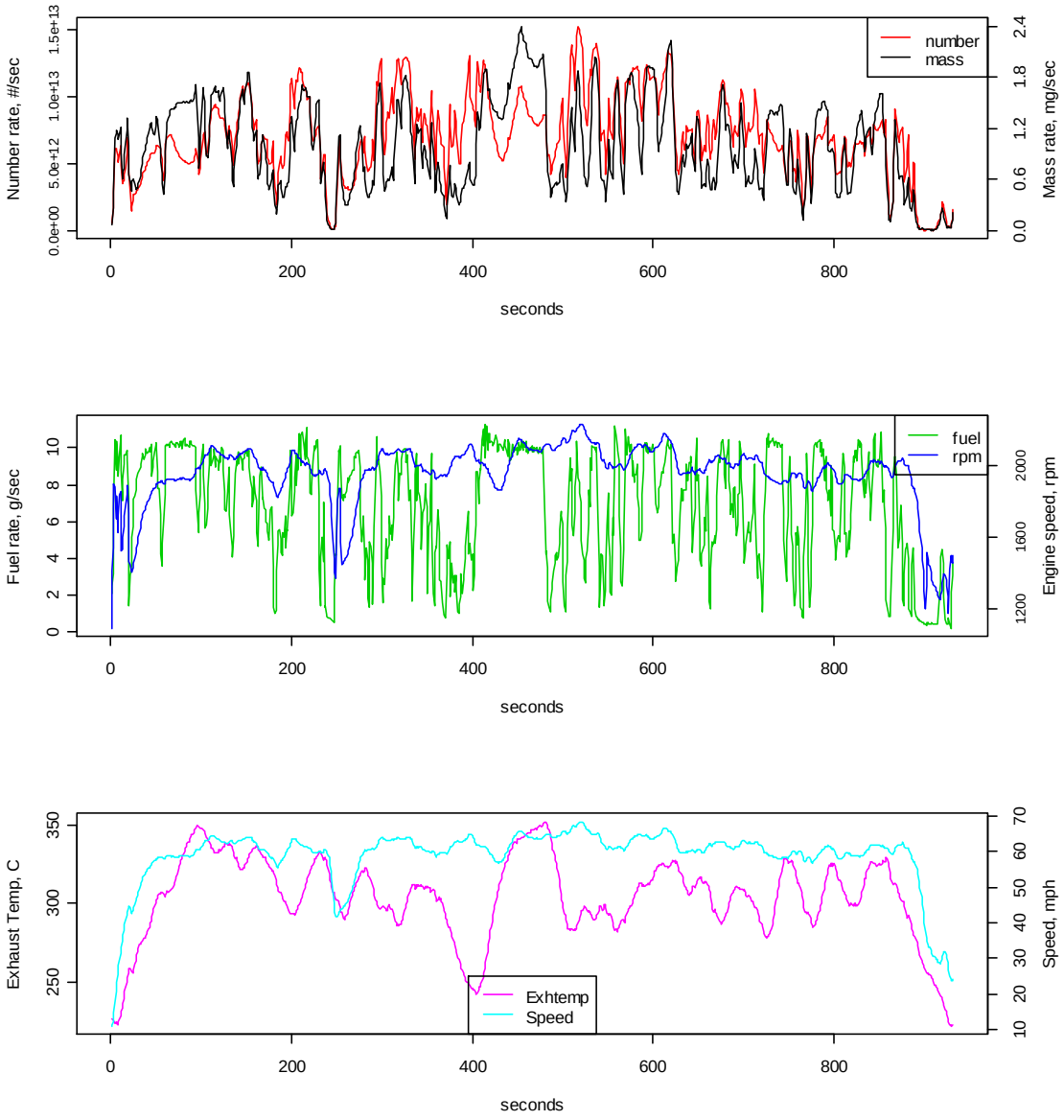

Figure 5.A8. Particle Emissions and covariates for modeled divided freeway Section.

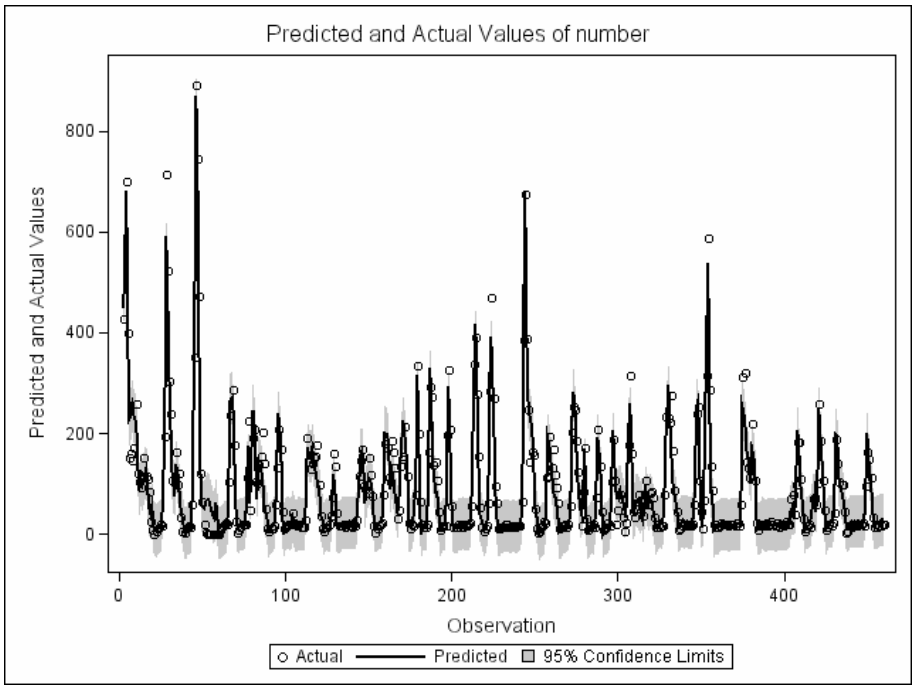

Figure 5.A9. Predicted and actual values for particle number emissions on urban arterial section.

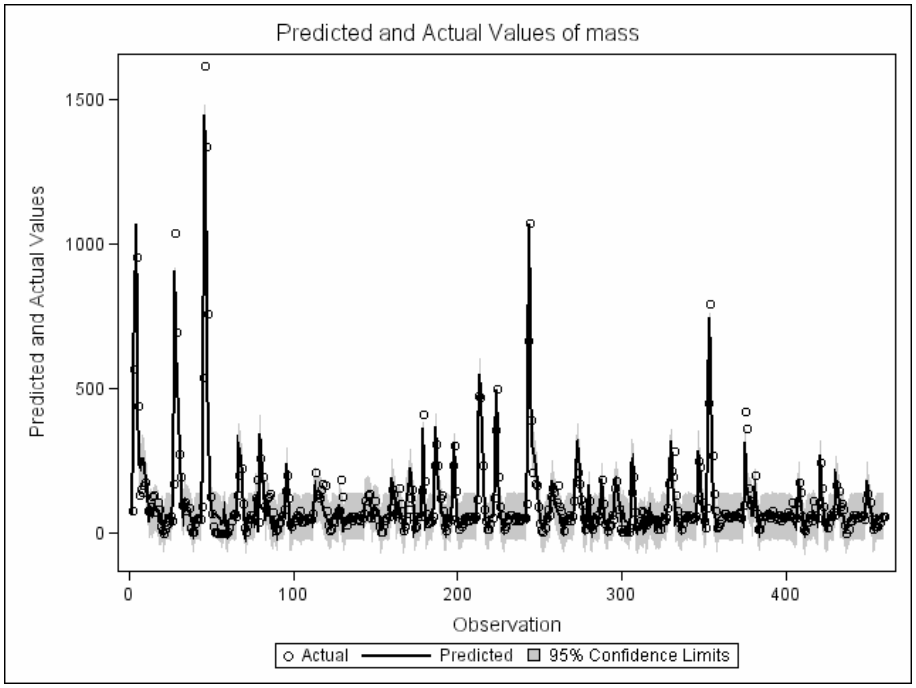

Figure 5.A10. Predicted and actual values for particle mass emissions on urban arterial section.

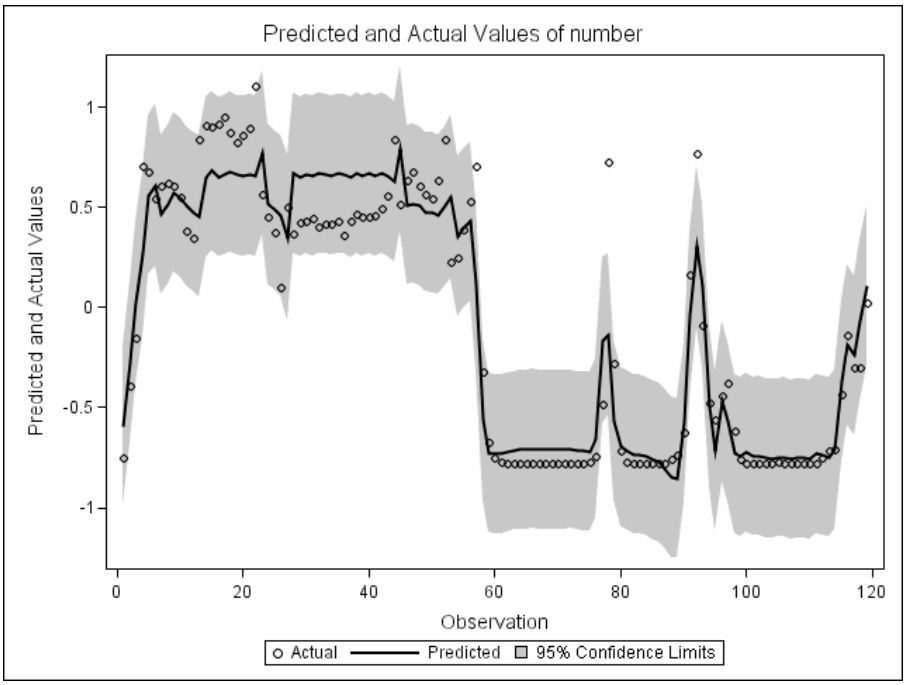

Figure 5.A11. Predicted and actual values for particle number emissions on rural arterial section.

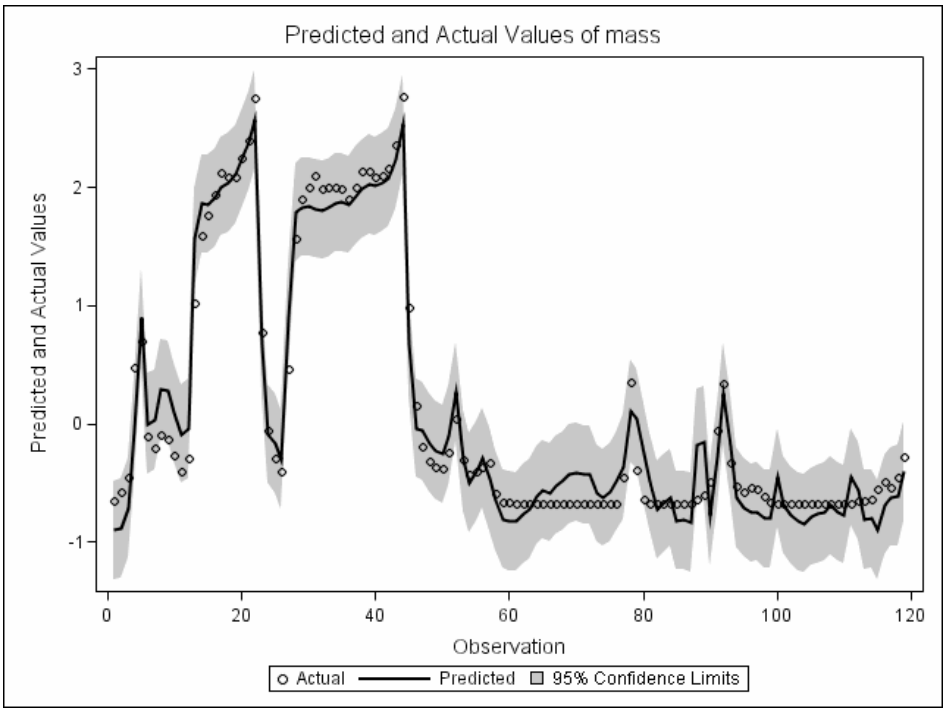

Figure 5.A12. Predicted and actual values for particle mass emissions on rural arterial section.

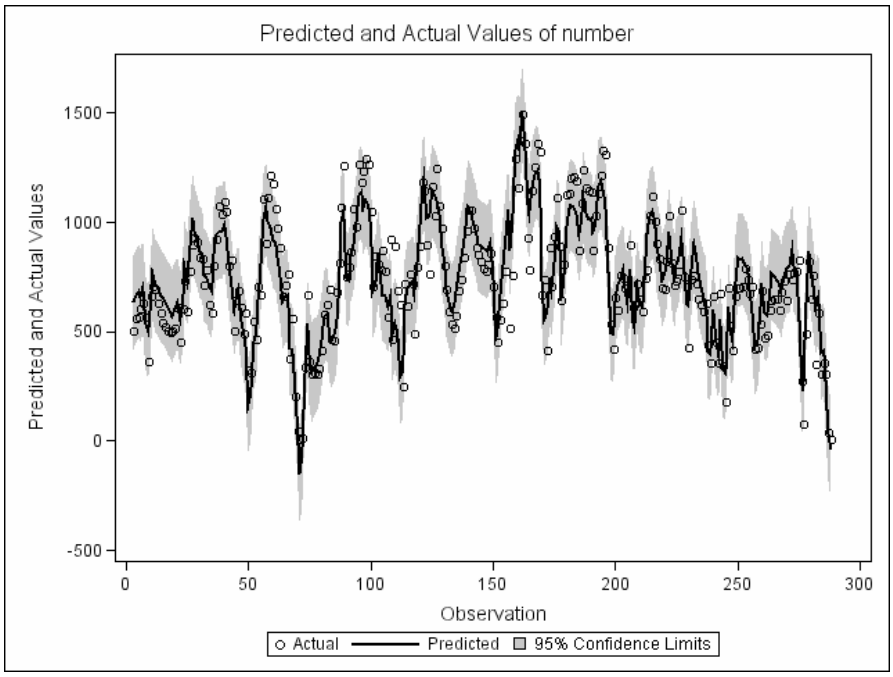

Figure 5.A13. Predicted and actual values for particle number emissions on divided freeway section.

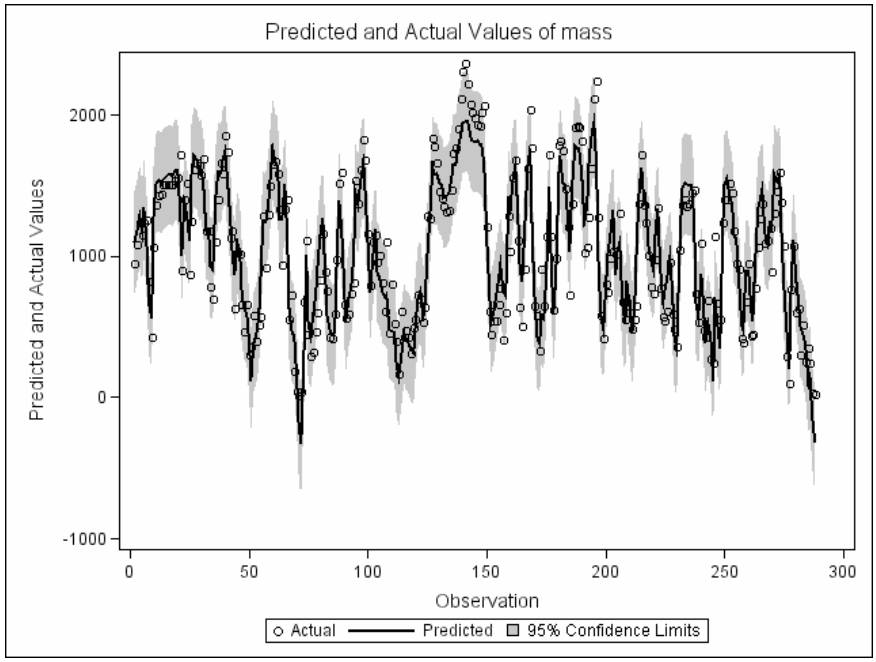

Figure 5.A14. Predicted and actual values for particle mass emissions on divided freeway section.

REFERENCES

American Lung Association (ALA): State of the Air 2007. Available at http://www.lungusa.org.

Baltensperger, U.; Weingartner, E.; Burtscher, H. Dynamic Mass and Surface Area Measurements. In *Aerosol Measurement - Principles, Techniques, and Applications (2nd Edition)*. Baron, P. A.; Willeke, K. John Wiley & Sons: New York, 2001.

Baron, P. A.; Willeke, K. Bridging Science and Application in Aerosol Measurement: Accessing Available Tools. In *Aerosol Measurement - Principles, Techniques, and Applications (2nd Edition)*. Baron, P. A.; Willeke, K. John Wiley & Sons: New York, 2001.

Biswas, S.; Hu, S.; Verma, V.; Herner, J. D.; Robertson, W. H.; Ayala, A; Sioutas, C. Physical properties of particulate matter (PM) from late model heavy-duty diesel vehicles operating with advanced PM and NOx emission control technologies. *Atmospheric Environment*. **2008**, *42* (22), 5622-5634.

Brunekreef, B.; Holgate, S. T. Air pollution and health. *Lancet*. **2002**, *360*, 233-42.

Clark, N. N.; Gautam, M.; Wayne, W. S.; Lyons, D. W.; Thompson, G., Zielinska, B. HEAVY-DUTY Vehicle Chassis Dynamometer Testing for Emissions Inventory, Air Quality Modeling, Source Apportionment and Air Toxics Emissions Inventory August 2007; CRC Report No. E55/59: Desert Research Institute (Subcontractor),: West

Virginia University Research Corporation, Department of Mechanical & Aerospace Engineering: Morgantown, WV, 2007.

Harrison, R. M.; Shi, J. P.; Xi, S.; Khan, A.; Mark, D.; Kinnersley, R.; Yin, J. Measurement of number mass and size distribution of particles in the atmosphere. In *Ultrafine Particles in the Atmosphere*; Brown, L. M., Collings, N., Harrison, R. M., Maynard, A.D., Maynard, R.L., Eds.; Imperial College Press: London, 2000.

Hofeldt, D. L.; Chen, G. *Transient particulate emissions from diesel buses during the central business district cycle*. SAE Technical Paper Series 960251; SAE International. International Congress and Exposition: Detroit, Michigan, 1996.

Holmén, B. A.; Chen, Z.; Davila, A. C.; Gao, O. H.; Vikara, D. M. *Particulate Matter Emissions from Hybrid Diesel-Electric and Conventional Diesel Transit Buses: Fuel and Aftertreatment Effects*. JHR 05-304, Project 03-8; Joint Highway Research Advisory Council: Hartford, CT, 2005.

Holmén, B. A.; Ayala, A.; Ultrafine PM emissions from natural gas, oxidation-catalyst diesel, and particle-trap diesel heavy-duty transit buses. *Environ. Sci. Technol*. **2002**, *36*, 5041-5050

Imhof, D.; Weingartner, E.; Ordóñez, C.; Gehrig, R.; Hill, M.; Buchmann, B.; Baltensperger, U. Real-world emission factors of fine and ultrafine aerosol particles for different traffic situations in Switzerland. *Environ. Sci. Technol*. **2005**, 39, 8341-8350.

Jackson, E. D., Holmen, B. A. Modal analysis of vehicle operation and particulate emissions from Connecticut Transit Buses; Transportation Research Board: Washington D.C. 2009.

Kinsey, J. S.; Mitchell W. A.; Squier W. C.; Linna, K.; King, F. G.; Logan, R.; Dong, Y.; Thompson G. J.; Clark, N. N. Evaluation of methods for the determination of diesel-generated fine particulate matter: Physical characterization results. *J. of Aerosol Science*. **2006**, *37*, 63-87.

Kittleson, D. B. Engines and nanoparticles: A review. *J. Aerosol Sci*. **1998**, *29*, 575-588.

Kittleson, D. B.; Watts, W. F.; Johnson, J. P. Nanoparticle emissions on Minnesota highways. *Atmos. Environ*. **2004**, *38*, 9-19.

Kittelson, D. B.; Watts, W.F.; Johnson, J. P. On-road and laboratory evaluation of combustion aerosols—Part1: Summary of diesel engine results. *Aerosol Science*. **2006a**, *37*, 913–930.

Kittelson, D. B.; Watts, W. F.; Johnson, J. P.; Schauer, J. J.; Lawson, D. R. On-road and laboratory evaluation of combustion aerosols—Part 2: Summary of spark ignition engine results. *Aerosol Science*. **2006b**, *37*, 931 – 949.

Lanni, T. Fine urban and precursor emissions control for diesel urban transit buses. *Environmental Pollution*. **2003**, *123*, 427-437.

Liu, Z. G.; Ford, D. C.; Vasys, V. N.; Chen, D.; Johnson, T. R. Influence of engine operating conditions on diesel particulate matter emissions in relation to transient and steady-state conditions. *Environ. Sci. Technol*. **2007**, *41* (13), 4593-4599.

Maricq, M. M.; Xu, N.; Chase, R. E. Measuring particulate mass emissions with the electrical low pressure impactor. *Aerosol Science and Technology*. **2006**, *40*, 85-96.

Mathis, U.; Mohr, M.; Forss, A. Comprehensive particle characterization of modern gasoline and diesel passenger cars at low ambient temperatures. *Atmos. Environ*. **2005**, *39*, 107–117.

McCarthy, M. C.; Eisinger, D. S.; Hafner, H. R.; Chinkin, L. R.; Roberts, P. T.; Black, K. N.; Clark, N. N.; McMurry, P. H.; Winer, A. M. Particulate matter: A strategic vision for transportation-related research. *Environ. Sci. Technol*. **2006**, *40*, 5593–5599.

Morawska, L.; Ristovski, Z.; Jayaratne, E. R.; Keogh, D. U.; Ling, X. Ambient nano and ultrafine particles from motor vehicle emissions: Characteristics, ambient processing and implications on human exposure. *Atmospheric Environment*. **2008**, *42*, 8113-8138.

Prucz, J. C.; Clark, N. N.; Gautam, M.; Lyons, D. W. Exhaust emissions from engines of the Detroit Diesel Corporation in transit buses: A decade of trends. *Environ. Sci. Technol*. **2001**, *35*, 1755-1764.

Ristovski, Z. D.; Jayaratne, E. R.; Lim, M.; Ayoko, G. A.; Morawska, L. Influence of diesel fuel sulfur on nanoparticle emissions from city buses. *Environ. Sci. Technol*. **2006**, *40*, 1314-1320.

Robert, M. A.; Kleeman, M. J.; Jakober, C. A. Size and composition distributions of particulate matter emissions: Part 2—Heavy-duty diesel vehicles. *J. Air & Waste Manage. Assoc.* **2007**, *57*, 1429-1438.

Rönkkö, T.; Virtanen, A.; Vaaraslahti, K.; Keskinen, J.; Pirjola, L.; Lappi, M. Effect of dilution conditions and driving parameters on nucleation mode particles in diesel exhaust: Laboratory and on-road study. *Atmospheric Environment*. **2006**, *40* (16), 2893-2901.

Shi, J. P.; Mark, D.; Harrison, R. M. Characterization of particles from a current technology heavy-duty diesel engine. *Environ. Sci. Technol*. **2000**, *34*, 748-755.

Sioutas, C.; Delfino, J.; Singh, M. Exposure assessment for atmospheric ultrafine particles and implications in epidemiologic research. *Environmental Health Perspectives.* **2005**, *113*, 947-955.

Vaaraslahti, K.; Virtanen, A.; Ristimäki, J.; Keskinen, J. Nucleation mode formation in heavy-duty diesel exhaust with and without a particulate filter. *Environ. Sci. Technol*. **2004**, *38* (18), 4884-4890.

Vikara, D.; Holmen, B. A. Ultrafine particle number concentrations from hybrid urban transit buses: Onboard single-diameter Scanning Mobility Particle Sizer Measurements. *Transportation Research Record*. **2006**, *1987*, 54 -61.

Wichmann, H. E.; Peters, A.; Epidemiological evidence of the effects of ultrafine particle exposure. In *Ultrafine Particles in the Atmosphere*; Brown, L. M., Collings, N., Harrison, R. M., Maynard, A.D., Maynard, R.L., Eds.; Imperial College Press: London, 2000.

Zhang K. M.; Wexler, A. S.; Niemeier, D. A.; Zhu Y. F.; Hinds, W. C.; Sioutas, C. Evolution of particle number distributions near roadways Part III: Traffic analysis and on-road size resolved particulate emission factors. *Atmospheric Environment*. **2005**, *39*(22), 4155-4166.

Zhu, Y.; Hinds, W.; Kim, S.; Sioutas, C. Concentration and size distribution of ultrafine particles near a major highway. *J. Air Waste Manage. Assoc*. **2002**, *52*, 1032–1042.

CHAPTER 6

MULTI-POLLUTANT EMISSION MODES FROM A DIESEL TRANSIT BUS UNDER REAL DRIVING CONDITIONS[1]

Abstract

Multiple components of diesel exhaust are known to cause adverse health and environmental effects. Better understanding of the relationship among diesel pollutants could assist multi-pollutant control techniques and strategies. This work introduces the concept of multi-pollutants emission modes to better understand the complex relationship among diesel pollutants. Cluster analysis revealed six emission modes from real-time emissions measurements from the exhaust of a diesel transit bus traveling under a wide variety of conditions on three bus routes in Hartford, CT. The emission modes captured repeatable convolutions among four gaseous emissions: carbon dioxide (CO_2), carbon monoxide (CO), hydrocarbons (HC) and nitrogen oxides (NO_x) and two measures of particulate matter: particle mass (PM) and number (PN). The emission modes were developed using testing data on one day, and were found to capture more than 75% of the total random variability of the emissions tested on the same routes the following day. Classification models were then developed to predict multi-pollutants emission modes based on bus operating parameters. The emission modes were generally well predicted by operating parameters, except for two of the emission modes which occurred at practically identical operating conditions, highlighting the potential limitations of using only operating modes (i.e., modal emission modeling approach) to evaluate transient emissions modes. For the diesel bus tested, CO and HC emissions were more independent of the other emissions and bus operating parameters. More repeatable relationships were found to exist among

[1] Darrell B. Sonntag, Eric Liu and H. Oliver Gao

the most important pollutants from diesel exhaust: CO_2, NOx, and particulate matter measurements.

Introduction

Under the Clean Air Act (CAA), the US Environmental Protection Agency (US EPA) regulates six criteria pollutants important for human health. Currently, three of these air pollutants are of primary concern for human health in both developed and developing nations: ambient ozone, nitrogen oxides (NO_x), and particulate matter (PM) (Brunerkreef and Holgate, 2002). The primary precursor pollutants of ozone are NOx and hydrocarbon (HC) emissions. As of 2006 more than 100 million US citizens lived in areas with ozone or $PM_{2.5}$ concentrations that exceed the national air quality standards (EPA, 2008). Heavy-duty diesel vehicles are major sources for NOx and PM emissions. The US fleet is dominated by light-duty gasoline vehicles; however, heavy-duty diesel vehicles contribute over 27% of mobile-source NO_x and 60% of mobile-source PM (Yanowitz et al., 2000). Though not of primary concern, carbon monoxide (CO) is another important criteria pollutant produced from transportation sources.

The US EPA previously set federal emission standards for PM, HC, CO, and NOx emissions from heavy-duty diesel vehicles (Yanowitz et al., 2000). To reach lower emission standards, engine designers cannot depend solely on adjusting engine parameters, such as lowering injection pressure, retarding the engine timing, or lowering the fuel to air ratio, due to the trade-off between emission standards (i.e. increasing one pollutant, will likely decrease another). There is a known tradeoff between vehicle emissions from diesel engines. Lower PM, HC, and CO emissions can generally be achieved by increasing the air to fuel ratio near stoichiometric conditions. However, NOx emissions are favored when combustion conditions are near stoichiometric that increase exhaust temperatures (Yanowitz et al., 2000; Clark et al., 2002).

The EPA's updated federal emission standards beginning in 2007 are more stringent for PM, HC, and NOx emission standards (US EPA, 2001). Continuous regenerating traps (CRTs) are composed of both a diesel oxidation catalyst and a particle filter that can effectively reduce CO, HC and PM emissions. Both oxidation catalysts and CRTs have observed slight reductions in NOx emissions as well (Clark et al., 2002). However, to reach the new NOx standards, diesel engines need to employ multi-pollutant aftertreatment systems. Multi-pollutant aftertreatment systems are composed of both a diesel oxidation catalyst and a particle filter to reduce CO, HC and PM emissions, as well as a NOx catalyst or selective catalytic reduction (SCR) system to reduce NOx (Maricq, 2007).

Recently, the US EPA made a momentous decision by including carbon dioxide (CO_2) as a regulated vehicle emission under the Clean Air Act (EPA, 2009). Lowering greenhouse gas emissions will be another important co-objective in reducing vehicle emissions. However, engine modifications used to lower NOx, such as retarding the injection timing or using cooled exhaust gas recirculation (EGR) systems, decrease fuel efficiency (Clark et al., 2002).

Besides the criteria pollutants, there are a host of other important emissions from diesel engines that can impact human health. These include air toxics such as benzene and formaldehyde (U.S. EPA, 2008) and ultrafine particles (particles with diameter < 100 nm). Formaldehyde emission rates are regulated on new heavy-duty diesel vehicles. Ultrafine particles are often quantified by the total number of particles, because the majority of particles emitted from diesel engines are smaller than 100 nm. Only focusing on criteria pollutants can have unintended consequences. For example, particle traps drastically reduce PM mass emissions, but can increase the number of ultrafine particles (Kittelson et al., 2008, Biswas et al., 2008). These examples stress the need to analyze vehicle emissions with a multi-pollutant perspective.

The tradeoffs and relationships among multiple pollutants from different engine configurations and aftertreatment devices are well-documented. However, the focus of this work is to improve the understanding of multi-pollutants behavior during real-world operation.

Additional research is needed to understand the relationship among vehicle emissions, and real-world driving conditions. Due to the large range of the operation of vehicles in real-world driving conditions and the inherent dependency of vehicle emissions on operating conditions, understanding the relationships among multi-pollutant emission data sets can be challenging. In order to better quantify and reduce diesel emissions, more understanding is needed on the relationship among multi-pollutants within diesel emissions.

Two recent analyses considered the relationship among particulate matter and gaseous emissions during the transient operation of light-duty vehicles. North et al. (2006) used regression analysis to model PM mass emissions based on gaseous pollutants measurements from a diesel passenger car tested on a chassis dynamometer. Their model was able to explain a large proportion of variation in PM mass emissions. The relationship between PM mass and gaseous "co-pollutants" was found to be stronger than that between PM and vehicle operating mode parameters such as velocity, acceleration and vehicle specific power. North et al. (2006) also brought forth the idea of "emission footprints," where certain engine operating states exhibit repeatable relationships with tailpipe emissions measurements. Qu et al. (2008) examined the relationship of particle number emission with other gaseous emissions from a gasoline spark-ignition mini-van. The mini-van was tested along a 17-mile route, with replicates across 22 drivers. Qu et al. (2008) modeled significant relationships between particle number and measurements of gaseous emission concentrations, relative humidity, and ambient and exhaust temperature. The data is

complex, and the model only explained a minor portion of the total variability in log-transformed particle number emissions (R^2 =25%). Both analyses estimated PM emissions, however many of the regression parameters were not interpretable and provided few clear insights into the complex relationships occurring among multiple pollutants.

In this work, discrete "emission modes" of multi-pollutants emissions are defined to capture and model the typical patterns of major vehicular pollutant emissions. Better understanding and characterization of the convolutions among vehicle emissions will assist in holistic multi-pollutants control designs and strategies. In many emission studies and emission models, discrete vehicle "operating modes", which are defined by operating parameters such as vehicle speed and vehicle specific power, have been used to model individual pollutants separately (Zhai et al., 2008; Frey and Kim, 2006; Frey et al., 2008). Operating modes are defined to maximize variation in emissions across real-world driving conditions, while retaining model simplicity and interpretability (Frey et al., 2002). Similarly, the emission modes introduced in this work are used to evaluate real-world emissions, except that emission modes are defined according to the joint convolution of emission pollutants. Repeatable "emission modes" (of a limited number) could be useful for understanding the interdependency among pollutants and for relating their joint behavior to vehicle operating modes. Cluster analysis was used to define discrete emission modes from the multi-pollutant emissions data, so the terms "clusters" and "emissions modes" are used interchangeably throughout the paper.

Experimental

The data used in this study was collected by Holmén et al. (2005) on a 2002 Connecticut Transit bus on September 20 and 21, 2004. The transit bus was equipped with a direct injection, turbocharged Detroit Diesel Series 40 Series engine, with a

diesel oxidation catalyst. The bus was tested on several routes representative of driving conditions in the Hartford CT area, including a high-speed freeway, stop-and-go urban arterial, and a rural arterial with sections of high-grade. Each test run was measured twice with one run in each direction. The testing route was 29 miles in length in one-direction, with nearly half of the distance traveled occurring on the freeway, but nearly 60% of the travel time occurring on the slower stop-and-go urban arterial. The number of second-by-second observations totaled more than 15,500 for the 2 days evaluated in this study. Further information on the transit bus, measurement equipment, and experimental design is detailed in the report by Holmén et al. (2005). The data on September 20th, were divided into training and validation data by including one directional run in each data set. Both directional runs made on September 21st were classified as the testing data set.

Particulate matter emissions were measured using an on-board dilution system and a Dekati, Ltd. Electrical Low Pressure Impactor (ELPI). The ELPI measured particle number distribution between 7 nm and 10,000 nm, from which both the particle number and particle mass measurements were computed. The ELPI has a time resolution of 1-2 seconds, and observations were interpolated to yield a complete second-by-second dataset. From the particle size distribution, two bulk measurements of the particulate matter emission rates were calculated: particle mass (PM) emission rate, and particle number (PN) emission rate. Over 93% of the particles are below 95 nm, so PN largely represents the ultrafine particle fraction. The PM mass was computed using the lower stages of the ELPI (diameters < 387 nm), comparisons with gravimetric measurements assured that the majority of the mass distribution occurred between 56.4 and 387 nm (Chapter 4).

A Horiba OBS-1000 gas emission analyzer measured gaseous emissions rates of nitrogen oxides (NO_x), carbon dioxide (CO_2), carbon monoxide (CO), and

hydrocarbons (HC) at 1 second resolution. Negative concentrations values of NO_x emissions were replaced with zero concentration values because they occurred at low engine loads and were small in absolute magnitude.

Exploratory Analysis

Exploratory analysis was conducted to examine potential relationships among the multi-pollutant emissions data for the gaseous pollutants measured by the Horiba Gas Analyzer (CO_2, CO, HC, and NO_x) and the two measurements of particulate matter from the ELPI (PM and PN). The relationships among the six pollutants for the north and east-directional runs conducted on September 20th are displayed in Figure 6.1.

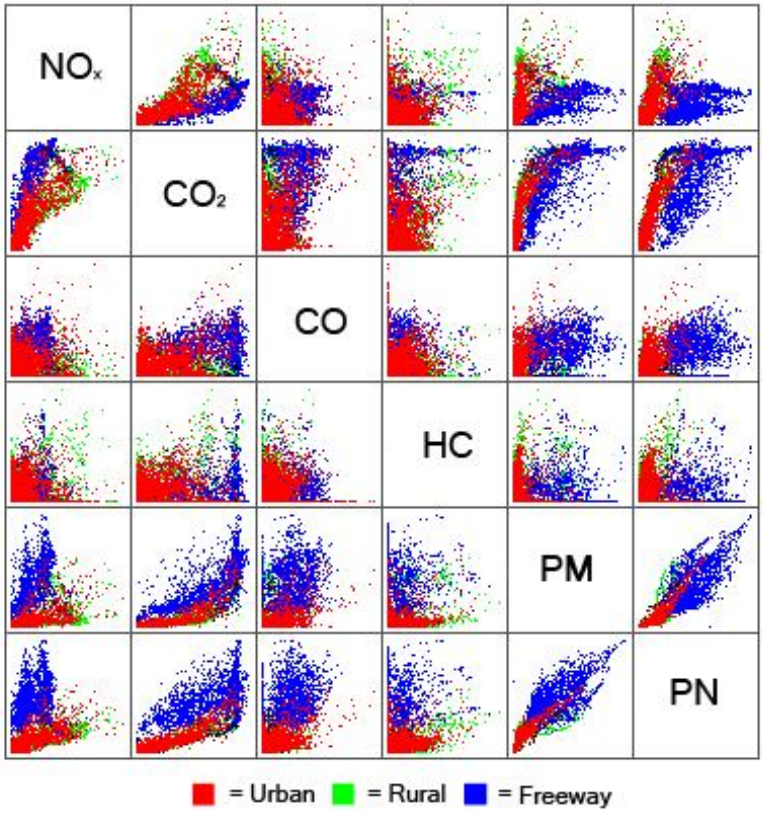

Figure 6.1. Bivariate scatter plot matrix of all six pollutants, color coded according to road type for the training data.

Positive correlations exist among CO_2, NO_x, PM and PN. In general, CO, PM, and HC formation is favored by fuel-rich conditions, where incomplete combustion occurs with strong linear correlations existing between CO and PM (Yanowitz et al., 2000). However, the CO and HC measurements in this study are more erratic with respect to other pollutants, and have a large percentage of zero values (17.1% and 31.4% for CO and HC respectively), which occur when the emissions fall below the sensitivity limits of the Horiba instrument.

The data suggests complex relationships among the emission rates. NOx appears to be highly correlated with CO_2 in a linear fashion, but appears to have different slopes according to facility type (e.g., urban arterial, rural road with high grades, and freeway). Different slopes between NOx and power have been observed due to different injection timing strategies (Clark et al., 2002), it appears that driving conditions may also be influential. PM and PN exponentially increase with CO_2 emissions, which may reflect the previous observations that fuel transients are good indicators of PM emissions (Hofeldt and Chen, 1996). Different emission modes or patterns appear to occur on different road types—in most of the bivariate scatter plots, the observations are well differentiated according to road type. The interrelationship among the multivariate emissions data suggests that clustering techniques may be an appropriate method to identify and understand the major modes of convolution among the pollutants.

Cluster Analysis

Cluster analysis was used to partition the multivariate emission rates data into a finite number of emission modes/clusters by minimizing variation within individual clusters and maximize variation between them. K-means clustering was used to identify the emission modes. K-means clustering is a non-hierarchical method that involves selecting k-number of seed points as centroids and redistributing/merging

clusters until each observation is assigned to the nearest cluster. K-means is a heuristic algorithm, in which the final clusters arrangement depends on the initial selection of centroids and the manner in which the centroid locations were updated at each iteration (Tan et al., 2006). The benefit of k-means is its relative simplicity and shorter computational time compared to other clustering methods (Tan et al., 2006). Beddows et al. (2009) applied k-means clustering analysis to interpret the variability in particle emissions data from ambient measurements made at different times of the day, different locations, and during different weather and emission source conditions. The objective of this analysis is to use clustering analysis to identify transient emission modes across multiple pollutants emitted from a transit bus in real world driving conditions.

The bus emissions data was split into subsets as training, validation, and testing data. The clustering analysis was conducted on the training data, using the information criteria computed from the validation data to prevent clusters from "overfitting" the random variation of the dataset. The testing data was used to test the performance of the resulting emission clusters. Specifically, measurements during the north/east bus runs on September 20th were used as the training data; the south/west runs on September 20th were used for validation; and all the test runs made on September 21st were retained for model performance testing.

SAS Enterprise Miner was used for clustering analysis, which used a standardized distance measure of the multi-pollutants emission rates, with equal weights for each of the emission variables regardless of its units or inherent variability. The furthest apart observations (in terms of the vector distance in the multi-pollutant emission space) were selected as initial seed points. Incremental training was used to update the centroid location after allocating each observation to a

cluster. The maximum number of iterations was set to the highest possible value to assure convergence of the algorithm.

Cluster Number Selection. Two information criteria were computed to guide the selection of clusters for defining emission modes: error sum of squares (SSE) and the silhouette coefficient. SSE quantifies the within-cluster variation, by $SSE = \sum_{i=1}^{k} \sum_{j=1}^{n_i} (y_{ij} - \bar{y}_i)^2$, *where* y_{ij} is the standardized emission rate for pollutant *y*, observation *j*, which is located in cluster *i*. $\bar{y}_i$ is the average standardized emission rate of cluster *i*. The total sum of squares was also calculated: $SST = \sum_{i=1}^{k} \sum_{j=1}^{n_i} (y_{ij} - \bar{\bar{y}})^2$, where $\bar{\bar{y}}$ is a grand mean across all clusters. Pollutant-specific R^2 values can then be calculated to quantify the amount of variation explained by the emission modes, using: $R^2 = 1 - SSE/SST$. The silhouette coefficient is a ratio that measures the cohesiveness of a cluster versus its separation from other clusters, computed as $s_i = (b_i - a_i)/\max(a_i, b_i)$, where a_i is the average distance of the ith point to all other points in its cluster, and bi is the minimum of the average distances between the ith point to all points contained in all other clusters. The silhouette coefficient takes values between -1 and 1, with values approaching 1 indicative of tightly grouped clusters and values closer to 0 and -1 indicative of widely dispersed observations within each cluster and poor separation between neighboring clusters. An overall silhouette coefficient is calculated for a particular clustering arrangement by taking the average value of the silhouette values across all observations (Tan et al., 2006).

Figure 6.2 displays the information criteria plotted for clusters analysis performed from k=2 to 30. As the SSE will generally decrease with increasing the number of cluster, the optimal number of clusters can be chosen where the SSE curve "elbows." Beyond the elbow, minimal reductions in SSE are gained for higher model complexity. On the other hand, the best cluster arrangement should ideally occur where the silhouette coefficient is maximized (Tan et al., 2006). As shown, the

silhouette coefficient generally decreases with the cluster number, and the maximum value occurs at k=2, which does not provide the resolution needed to provide meaningful results. At k=6 there is a local maximum in the silhouette coefficient, as well as a strong "elbow" in SSE. Six clusters were chosen to describe the multi-pollutant emissions mode from the dataset.

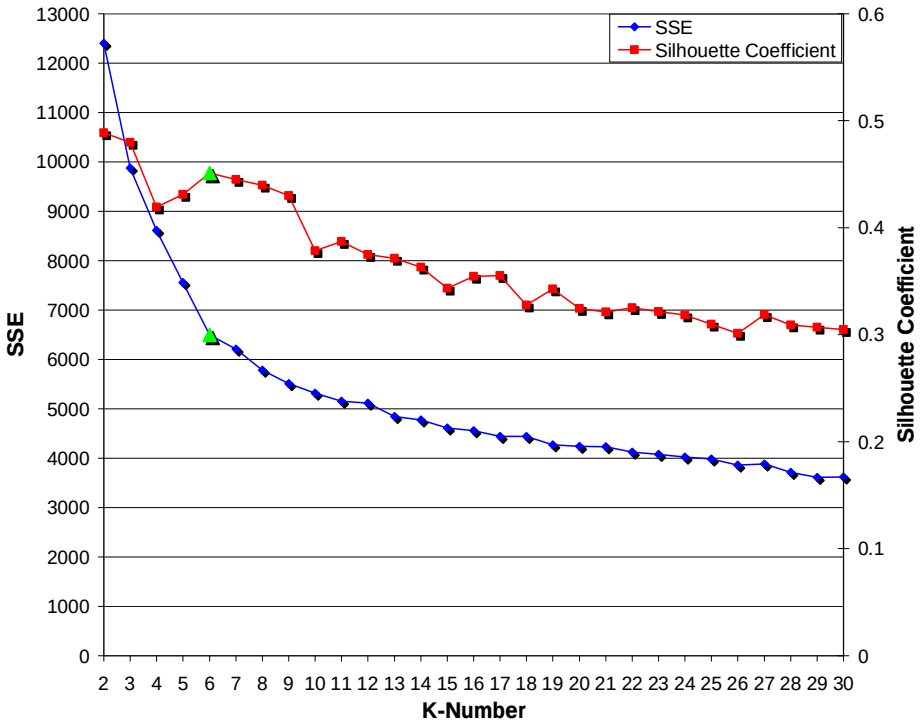

Figure 6.2. Information criteria for cluster number from k=2 to 30.

Cluster Analysis Results. Summary statistics for the 6 clusters are reported in Table 6.1. The clusters are ordered from 1 to 6 by the average speed. The average emission rates are reported for each cluster, which are ranked from the highest to the lowest. The clusters are quantified according to the percent of total observations in the data set, the total contribution of carbon emissions, engine and vehicle operating parameters, and the dominant road type of each cluster. In general the size of each cluster varied significantly, with cluster 1 containing almost 50% of the data, and cluster 3 containing only 4.1% of the data. However, in terms of total emissions

contribution, the clusters are more evenly split, with individual clusters contributing from 8.1 to 32.0% of total CO_2 emissions.

Table 6.1. Descriptive Statistics of 6 Clusters

Cluster	% of Data	CO_2 Contribution (%)	CO (mg/s)	Rank	CO_2 (g/s)	Rank	HC (mg/s)	Rank	NOx (g/s)	Rank	PM (mg/s)	Rank	PN	Rank
1	47.8	8.1	1.90	6	1.77	6	1.51	6	0.02	6	0.04	6	3.3E+11	6
2	20.9	15.4	6.35	3	7.69	5	6.74	2	0.07	5	0.13	5	1.4E+12	5
3	4.1	10.9	4.26	4	27.82	2	15.70	1	0.24	2	0.85	2	5.3E+12	3
4	7.5	18.3	4.23	5	25.50	3	3.00	4	0.27	1	0.63	3	3.7E+12	4
5	9.2	15.2	15.52	2	17.11	4	2.92	5	0.08	4	0.61	4	6.0E+12	2
6	10.5	32.0	19.10	1	31.84	1	3.35	3	0.17	3	1.46	1	9.2E+12	1

Cluster	Fuel Rate (g/s)	AFR	Engine Load (%)	RPM	Exhaust Temp (°C)	Speed (mph)	Acceleration (mph/s)	Grade (%)	Dominant Road Type
1	0.6	120	27.6	989	196	12.9	-0.50	-0.84	Urban
2	2.2	78	36.3	1382	192	23.7	0.57	-1.01	Urban/Rural
3	8.2	31	91.8	1690	245	30.9	0.85	2.81	Rural/Freeway/Urban
4	7.5	31	91.9	1570	267	33.5	0.65	2.48	Urban/Rural/Freeway
5	4.8	62	54.9	1953	291	54.7	0.21	-0.61	Freeway
6	9.1	35	94.9	2019	305	59.7	0.20	0.57	Freeway

The standardized emission rates for each cluster are plotted in Figure 6.3. The standardized emission rates have a mean and standard deviation of one. Side-by-side graphs are given for clusters 1& 2, 3 & 4, and 5 & 6 to assist in comparison. Clusters 1 and 2 occur primarily on the urban and rural arterial at relatively low engine loads and vehicle speeds. Cluster 1 had the lowest emission rates in all six evaluated pollutants. Cluster 2 has slightly higher engine loads and vehicle speeds than cluster 1. In Cluster 2, all emission rates increased, with HC having noticeably larger emission rates. High hydrocarbon emissions are frequently observed at low engine loads from heavy-duty diesel vehicles (Clark et al., 2002). PN emissions were more elevated in cluster 2 than PM emissions. This may be capturing the dependence of PN emissions and hydrocarbon emissions observed at low-loads of a DOC-equipped bus (Rönkkö et al., 2006).

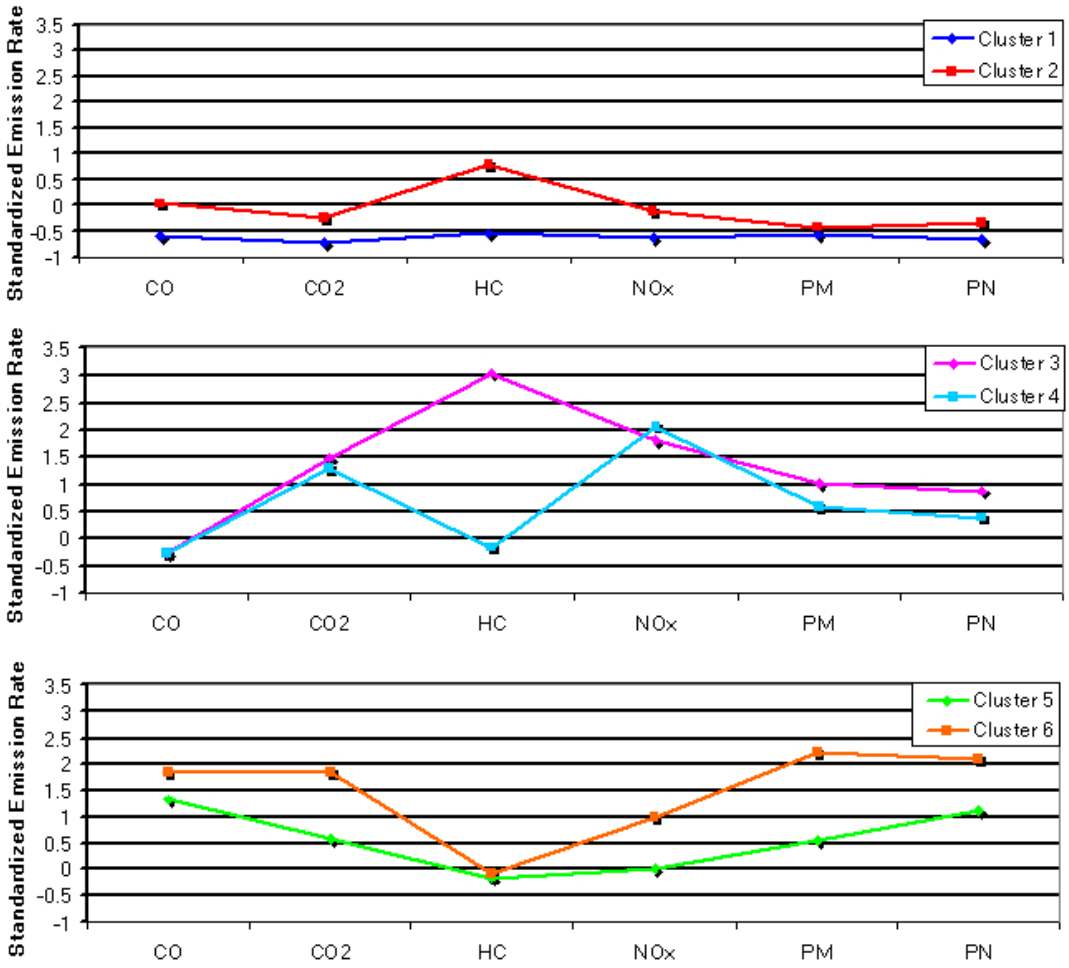

Figure 6.3. Standardized plot of the average emission rates in each cluster

Clusters 3 and 4 occur under similar driving conditions, with comparable average speed values (30.9 and 33.5 mph). In fact, Cluster 3 and Cluster 4 are practically indistinguishable in terms of operating conditions; both experience large engine loads, while the bus is accelerating at moderate speeds, or traveling on high grade sections of the urban and rural arterials. The two modes have significantly different emission patterns, with a large drop in HC emissions from Cluster 3 to Cluster 4, accompanied by a slight drop in CO, CO_2, PM and PN emissions, and a slight rise in NO_x emissions. The higher emissions of HC, CO, CO_2, PM and PN emissions in cluster 3 and higher NO_x emissions in cluster 4, indicate a shift from fuel rich to fuel lean conditions (Jarrett and Clark, 2001). The fuel rate in cluster 4 is lower

than in cluster 3, which supports our emission observations. However, the measured air fuel ratio (AFR) indicates few differences between the two clusters.

Cluster 5 and 6 both occur primarily on the freeway. Cluster 6 has a higher fuel rate, higher engine load, slightly higher average speed, and generally occurs on positive grades. Cluster 6 has the largest CO, CO_2, PM and PN emissions of all clusters, while Cluster 5 has the second highest CO and PN emissions. Although, PM and PN are highly linear correlated, the rank of PM better corresponds with the rank of fuel rate and CO_2 emissions while the rank of PN follows the rank of engine speed and exhaust flow (Table 6.1). The strong linear relationship of PM mass and fuel rate was observed previously (Chapter 4).

In order to better visualize the clustering arrangement, observations of the training data were plotted according to three directions on three emission rates in Figure 6.4: CO_2, NO_x, and PM. The clusters are fairly well differentiated, except for clusters 3 and 4, which appear to occur generally in the same location in the 3-dimentional space. This appears to be due to the fact that cluster 3 and 4 are mostly differentiated according to HC emissions.

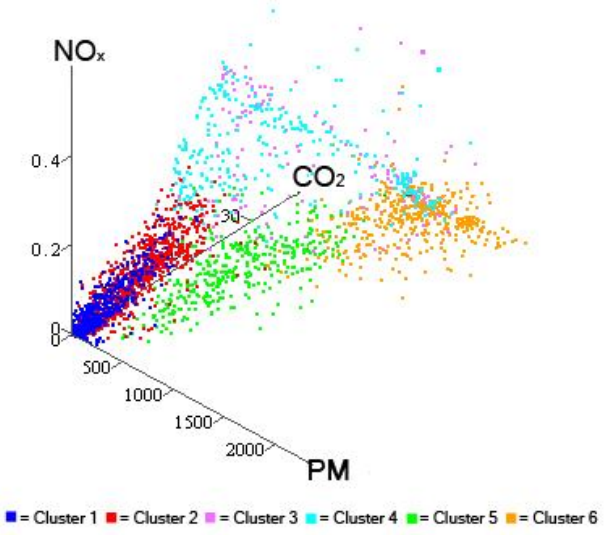

Figure 6.4. Observations on Sep. 20 plotted according to NO_x, PM, and CO_2 emissions, color coded to cluster.

The bivariate scatter matrix (Figure 6.5) was plotted with each observation color coded according to cluster ID. At least 5 of the clusters can be identified in each of the individual scatter plots; however, all six emission modes are not clearly distinguished using only direction. Cluster 3 (pink) and cluster 4 (light blue) are generally only well differentiated on the HC dimension, but are not well differentiated on other bivariate plots.

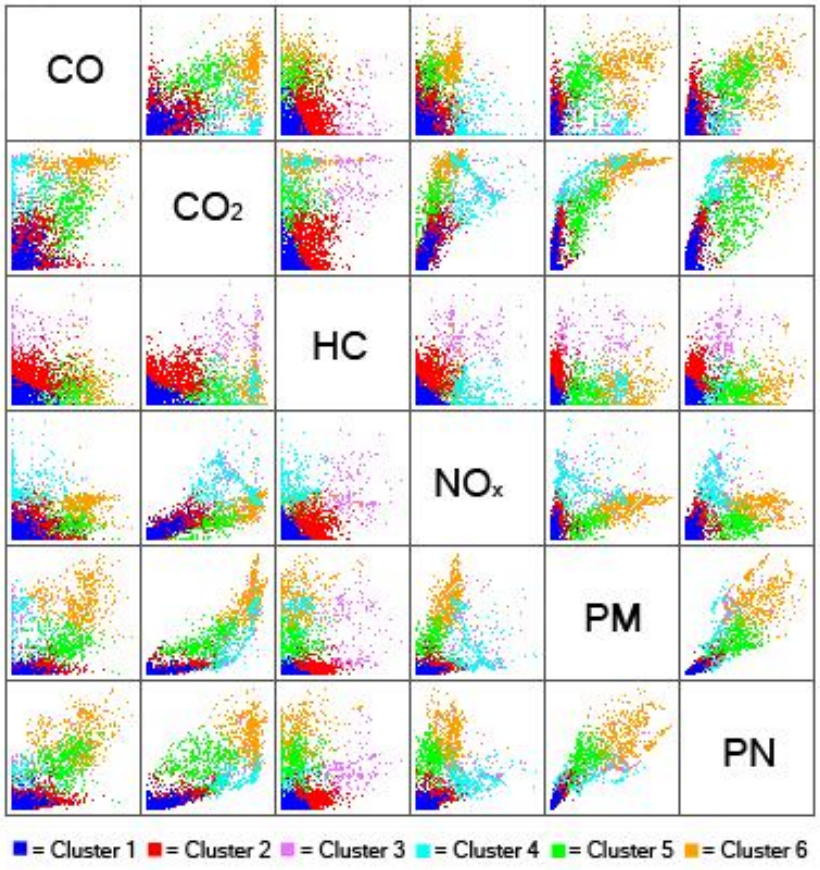

Figure 6.5. Bivariate scatter plot of training data color coded to cluster.

The six emission modes identified from the training data were used to evaluate the validation and testing data in Table 6.3. The clusters centroids identified from the training data, were used to cluster the observations in the validation and training data. R^2 values were computed for the validation and testing data, to compare the repeatability of the emission modes identified from the training data. The clustering

analysis had more explanatory power for CO_2, NO_x, PM and PN than for HC and CO. The R^2 values decreased on the validation and test data for HC and CO, while no substantial changes were observed for the other emission rates.

Table 6.2. Comparison of Predictive Power (R^2) for Training, Validation and Test Data Using 6 Pollutants on the Final Cluster Analysis

	Training	Validation	Test
CO	69.5%	46.3%	55.9%
CO_2	86.8%	86.1%	89.1%
HC	65.0%	49.2%	60.6%
NO_x	75.4%	77.1%	78.2%
PM Number	86.1%	83.0%	86.1%
PM Mass	81.3%	82.3%	84.3%
Total	77.4%	70.7%	75.7%

To evaluate the formation of spurious clusters in the training data, the clusters were evaluated to see if they were statistically significantly different from each other in the validation data set. Assuming the observations are independent observations, the t-tests detected that all the clusters were statistically different at the 5% level in at least five of the six pollutants in the validation data set. Clusters 3 and 4 were practically identical in terms of operating conditions, and significant differences between emissions were detected in the validation data. Cluster 3 had significantly larger HC, CO, PM and PN emissions, and cluster 4 had significantly higher NOx emissions. The training data appears to have captured complex, yet repeatable relationships among emission rates.

Classification Analysis

Classification regression models were used to quantify the extent to which emission modes can be predicted from operating parameters, including modes that did not have apparent differences in operating parameters. Multinomial logistic regression was chosen to classify the emission modes assigned from the cluster analysis using 1. engine operating parameters and 2. vehicle operating parameters. Multinomial

regression models predict the probability of selecting a discrete emission mode. The probability that observation *i* is in emission mode *j*, is modeled according to the operating parameters of observation *i*:

$$p_{ij} = \frac{\exp\left(\beta_{0j} + \beta_j \cdot operating\ \ parameters_i\right)}{\sum_{k=1}^{6} \exp\left(\beta_{0j} + \beta_j \cdot operating\ \ parameters_i\right)}$$

Because the probability of the six emission modes must sum to equal 1, we set the coefficients for the first emission mode equal to zero ($\beta_{0,1} = 0, \beta_1 = 0$). The parameters represent the effects of each operating parameter on the probability of choosing emission mode *j*, over the emission mode 1 (So and Kuhfeld, 1994).

The selection of variables for inclusion in each model was done using a stepwise selection method, which incrementally enters and removes variables from the model using a threshold significance level of 0.05. The stepwise regression was performed on the training data, and at each iteration the negative log likelihood value was calculated for the validation data. From the log likelihood value, the model error was calculated. The variables that minimized the validation error were selected as the final predictive variable set. Final results are reported using the test data, which was not used in the selection of the operating parameters.

Classification Results. The engine parameter model selected fuel rate, engine load, engine speed, and exhaust temperature from potential engine parameters. These are key emission parameters as identified from previous analysis of the dataset (Chapter 3). The vehicle parameter model selected all the available vehicles parameters: acceleration, grade, speed, and vehicle specific power. Interaction terms were not included, although they were evaluated in a few instances. In general the models with interaction terms overfit the training data, causing worse predictions on the validation and test data.

For the classification methods, the focus is on the predictive ability of the model, with limited emphasis on interpretation of the model's parameters. As noted earlier, multiple regression parameters in the context of vehicle emissions can be difficult to interpret (North et al., 2006; Qu et al., 2008). In general, increases in the operating parameters (except exhaust temperature), also increase the probability of the observation being classified in modes 2-6 instead of mode 1. However, because each is compared to emission mode 1, and due to the multiple predictive parameters, it is difficult to make conclusions about the importance of each operating parameter in relation to each emission mode. For reference, the parameters for both the engine and vehicle models are included in the appendix.

More emphasis was placed on the ability of the classification models to predict the interpretable emission modes. Summary results of the predictive power of the logistic models are reported in Table 6.3 according to misclassification rates. The misclassification rates report the percentage of observations that were assigned the wrong emissions mode from the classification analysis. As expected the engine parameters provide a more accurate prediction of the emission state than the vehicle parameters. Both models showed similar trends in classifying each cluster. The emissions mode from cluster 1 and 2 were correctly predicted very well (> 90% and 85% for engine and vehicle parameters, respectively). The other emission modes were correctly predicted for a majority of observations, except emission mode 3. The operating parameters in Cluster 3 were almost identical to those of cluster 4, which consequently absorbed many of the cluster 3 data points in the predicted model. This gives credence to the previous observation that different emission modes can occur at similar operating modes estimates from operating conditions.

Table 6.3. Misclassification Rates for the Classification Models on the Test Data (September 21st)

Cluster	Engine	Vehicle
1	0.10	0.15
2	0.38	0.43
3	0.80	0.86
4	0.19	0.31
5	0.23	0.40
6	0.09	0.14
Total	0.17	0.24

Despite the large misclassification rate, the emission mode of cluster 3 and 4 still appeared intact to some extent. The predicted emission mode 3 and 4 from the test data had a similar pattern as the cluster analysis: CO, HC, CO_2, PM, and PN emissions were larger in mode 3, and NOx emissions were larger in predicted mode 4. However, the magnitude difference between the average HC emissions between emission modes 3 and 4 is much smaller than for the emission modes identified by the cluster analysis

To understand the effect of misclassifications of emission modes on the prediction of the emission rates, predictive R^2 values were computed using the average value of each emission mode identified by the classification model and are shown in Table 6.4 Comparisons with Table 6.2 are useful to compare the information lost when predicting emission modes. Interestingly, the misclassification of the emission modes caused by the classification model, affected some pollutants much more than others. As shown, much of the predictive power of the classification model is retained for the CO_2, NOx, PM and PN emissions compared to the cluster analysis. But significant information is lost on the CO and especially the HC emissions rates. Because of the difficulty in distinguishing emission mode 3 from emission mode 4, significant predictive information was lost for HC emissions. Substantial information about emissions variability may be lost if emissions are only analyzed according to the mean values at discrete operating modes.

Table 6.4. Predictive R^2 for each Emission Rate for the Training, Validation, and Test Data from the Emission Modes Predicted from the Classification Analysis.

	Engine Parameters			Vehicle Parameters		
	Training	**Validation**	**Test**	**Training**	**Validation**	**Test**
CO	0.57	0.34	0.48	0.55	0.29	0.40
CO_2	0.89	0.89	0.89	0.84	0.83	0.82
HC	0.18	0.04	0.12	0.15	0.04	0.10
NO_x	0.77	0.82	0.78	0.66	0.71	0.66
PM	0.85	0.77	0.84	0.79	0.78	0.79
PN	0.87	0.86	0.86	0.83	0.85	0.83
Total	0.69	0.62	0.66	0.64	0.58	0.60

Discussion and Conclusions

For the evaluated on-board emission test of a diesel transit bus, 6 emission modes were found to explain more than 75% of the random variation of the data. Repeatable relationships were observed among CO_2, CO, HC, NO_x, PM mass and particle number (PN) emissions. For this data set, CO and HC emissions were more independent of the other emission rates, and were harder to predict on a consistent basis. However, the more important pollutants from diesel exhaust, CO_2, NO_x, PM and PN were found to be well predicted from cluster analysis and formed repeatable emission modes.

Operating parameters may not always detect a change in the emission mode for several reasons: 1. Limitations in the emission measurements. Many of the HC and CO measurements were below the sensitivity of the Horiba gas emission analyzer. This may have caused less repeatable relationships among HC and CO emissions. 2. Emissions are not only a function of the current driving conditions, but also the past operation of the vehicle. For example, the majority of cluster 3 occurs on the rural arterial, while the majority of cluster 4 occurred on the urban arterial. The two road types may be providing information about the "past" operation of the vehicle that influences "current" emission rates that are not reflected in the instantaneous engine and vehicle operating parameters. 3. There could be errors due to the dynamic

residence time of emissions in the exhaust and dilution system. In data preprocessing, the residence time was assumed constant over the entire route. This could distort the assignment of emission events with the appropriate operating events. 4. The relationship between emission modes and operating modes is approximated using a multinomial logit regression model. However, we anticipate that the complex relationships using this model form can only be roughly approximated.

By identifying six discrete emission modes from the data, much of the variability of the data was able to be quantified. Additionally, the emission modes identified important relationships that exist among the pollutants that would not have been detected using operating modes. Cluster analysis is referred to as a data mining method, because it can be efficiently applied to extract information from large datasets while using minimal prior information. Cluster analysis could be an effective method to analyze large emission datasets that contain emissions from many vehicles. Cluster methods could also be used impute missing emissions observations. Previous researchers have used a single pollutant, such as CO, to disaggregate PM filter data to the second-by-second level (Jarrett and Clark, 2001). Using cluster analysis, missing emission rates such as PM emission rates, could be apportioned according to the relationship among multiple pollutants: CO_2, CO, HC and NO_x. Because cluster analysis does not make distribution assumptions, this could be an appropriate method to for replacing missing values for large emissions data sets that have measurements from a wide variety of vehicles.

While using discrete emission modes assisted in interpretation of the data, a certain amount of predictive information was inherently sacrificed by disregarding the continuous nature of the data. Cluster analysis is an effective explorative technique that can be used to identify trends in the data, and as a starting point for more rigorous statistical analysis. Future work could apply multivariate regression models that

incorporate both the continuous nature of emissions and the covariance of pollutants to predict multiple emissions.

Acknowledgments

This research was sponsored by the New York Metropolitan Transportation Council and University Transportation Research Council through the September 11th Program Fellowship Program, the New York State Energy Research Development Authority through the Environmental Monitoring, Evaluation, and Protection PhD Fellowship Program, the Joint Highway Research Advisory Council of the University of Connecticut, and the Connecticut Department of Transportation through Projects 03-8 and 05-9.

APPENDIX

Table 6.A1. Classification Matrix for the Test Data for the Engine Parameter and Vehicle Parameter Models

Engine Parameters

		Actual Clusters						
	Cluster	**1**	**2**	**3**	**4**	**5**	**6**	**Total**
Predicted Clusters	**1**	3862	262	0	3	1	0	4128
	2	364	567	2	42	33	0	1008
	3	0	4	36	69	24	22	155
	4	0	34	91	619	27	21	792
	5	69	49	13	8	495	52	686
	6	0	2	35	27	64	937	1065
	Total	4295	918	177	768	644	1032	7834

Vehicle Parameters

		Actual Clusters						
	Cluster	**1**	**2**	**3**	**4**	**5**	**6**	**Total**
Predicted Clusters	**1**	3647	286	0	0	5	0	3938
	2	521	520	20	108	84	10	1263
	3	3	6	24	47	9	38	127
	4	45	63	90	527	18	10	753
	5	73	37	14	10	386	91	611
	6	6	6	29	69	142	883	1135
	Total	4295	918	177	761	644	1032	7827

Table 6.A2. Model Parameter Estimates for Engine Parameter Model

Parameter	Emission Mode	DF	Estimate	Standard Error	Wald Chi-Square	Pr > ChiSq	Standardized Estimate	Exp(Est)
Intercept	6	1	-67.66	3.80	317.16	<.0001	0	
Intercept	5	1	-31.52	1.91	271.32	<.0001	0	
Intercept	4	1	-17.90	1.89	89.43	<.0001	0	
Intercept	3	1	-26.21	2.13	151.24	<.0001	0	
Intercept	2	1	-3.62	0.48	57.54	<.0001	0.027	
Exhtemp	6	1	-0.05	0.01	89.24	<.0001	-1.55	0.95
Exhtemp	5	1	-0.03	0.00	41.01	<.0001	-0.90	0.97
Exhtemp	4	1	-0.03	0.00	32.10	<.0001	-0.82	0.97
Exhtemp	3	1	-0.05	0.00	84.00	<.0001	-1.42	0.96
Exhtemp	2	1	-0.03	0.00	156.95	<.0001	-0.94	0.97
Fuelsensor	6	1	1.81	0.15	150.96	<.0001	3.36	6.08
Fuelsensor	5	1	1.13	0.12	85.64	<.0001	2.09	3.08
Fuelsensor	4	1	2.40	0.15	255.19	<.0001	4.46	11.00
Fuelsensor	3	1	2.27	0.16	212.51	<.0001	4.22	9.67
Fuelsensor	2	1	0.72	0.08	84.50	<.0001	1.34	2.06
Percent_Load	6	1	0.23	0.02	210.19	<.0001	4.22	1.26
Percent_Load	5	1	0.08	0.01	87.54	<.0001	1.54	1.09
Percent_Load	4	1	0.10	0.01	89.41	<.0001	1.85	1.11
Percent_Load	3	1	0.15	0.01	121.69	<.0001	2.64	1.16
Percent_Load	2	1	0.02	0.00	32.77	<.0001	0.35	1.02
RPM	6	1	0.03	0.00	306.96	<.0001	8.20	1.03
RPM	5	1	0.02	0.00	243.01	<.0001	4.91	1.02
RPM	4	1	0.01	0.00	21.59	<.0001	1.41	1.01
RPM	3	1	0.01	0.00	79.70	<.0001	2.90	1.01
RPM	2	1	0.01	0.00	320.33	<.0001	1.53	1.01

Table 6.A3. Model Parameter Estimates for Vehicle Parameter Model

Parameter	Emission Mode	DF	Estimate	Standard Error	Wald Chi-Square	Pr > ChiSq	Standardized Estimate	Exp(Est)
Intercept	6	1	-41.1585	2.7515	223.76	<.0001	0	
Intercept	5	1	-13.9946	0.69	411.36	<.0001	0	
Intercept	4	1	-6.7577	0.5099	175.67	<.0001	0.001	
Intercept	3	1	-11.0068	0.7416	220.28	<.0001	0	
Intercept	2	1	-2.2366	0.0969	532.6	<.0001	0.107	
Speed	6	1	0.7578	0.0516	215.47	<.0001	9.1506	2.133
Speed	5	1	0.3166	0.0148	459.78	<.0001	3.8228	1.372
Speed	4	1	0.0492	0.0165	8.87	0.0029	0.5943	1.05
Speed	3	1	0.1557	0.0189	67.66	<.0001	1.8803	1.168
Speed	2	1	0.0726	0.00396	336.95	<.0001	0.877	1.075
Acceleration	6	1	11.8089	0.8865	177.44	<.0001	6.9353	999
Acceleration	5	1	4.5672	0.2903	247.56	<.0001	2.6823	96.274
Acceleration	4	1	0.3782	0.3232	1.37	0.242	0.2221	1.46
Acceleration	3	1	2.7322	0.3354	66.35	<.0001	1.6046	15.367
Acceleration	2	1	0.9931	0.1026	93.69	<.0001	0.5832	2.7
Grade	6	1	2.4666	0.2137	133.26	<.0001	3.4581	11.783
Grade	5	1	0.703	0.0809	75.52	<.0001	0.9856	2.02
Grade	4	1	-0.03	0.0898	0.11	0.7386	-0.042	0.97
Grade	3	1	0.5469	0.094	33.88	<.0001	0.7667	1.728
Grade	2	1	0.0035	0.0354	0.01	0.9212	0.00491	1.004
VSP	6	1	0.2475	0.0793	9.75	0.0018	0.7641	1.281
VSP	5	1	0.2211	0.0473	21.84	<.0001	0.6825	1.247
VSP	4	1	1.1456	0.0739	240.29	<.0001	3.5365	3.144
VSP	3	1	0.8131	0.069	138.69	<.0001	2.51	2.255
VSP	2	1	0.2509	0.0311	65.26	<.0001	0.7744	1.285

Table 6.A4. Summary Statistics of the Emission Modes Predicted using the Engine Parameter Classification Analysis on the Training Data

Cluster	% of Data	CO_2 Contribution (%)	CO (mg/s)	Rank	CO_2 (g/s)	Rank	HC (mg/s)	Rank	NO_x (g/s)	Rank	PM (mg/s)	Rank	PN	Rank
1	49.5	7.1	2.21	6	1.49	6	2.12	6	0.02	6	0.04	6	3.3E+11	6
2	19.6	17.5	6.09	4	9.27	5	5.45	3	0.08	4	0.13	5	1.5E+12	5
3	2.0	5.5	7.02	3	28.77	2	9.59	1	0.24	2	0.91	2	5.3E+12	3
4	9.4	14.9	15.08	2	16.55	4	3.52	5	0.08	5	0.63	4	6.2E+12	2
5	11.8	36.1	16.78	1	31.96	1	4.72	4	0.17	3	1.45	1	8.8E+12	1
6	7.8	18.9	4.35	5	25.31	3	5.46	2	0.27	1	0.56	3	3.7E+12	4

Cluster	Fuel Rate (g/s)	AFR	Engine Load (%)	RPM	Exhaust Temp (°C)	Speed (mph)	Acceleration (mph/s)	Grade (%)	Dominant Road Type
1	0.5	124	25.9	984	197	13.7	-0.53	-0.94	Urban
2	2.6	61	41.9	1417	188	21.7	0.77	-0.76	Urban/Rural
3	8.5	32	93.0	1707	212	23.3	1.46	2.53	Urban
4	4.8	66	53.0	1976	297	56.9	0.11	-0.62	Freeway
5	9.2	35	95.5	2014	305	58.1	0.22	0.75	Freeway
6	7.5	30	94.1	1526	266	32.7	0.62	2.88	Rural/Urban

Table 6.A5. Summary Statistics of the Emission Modes Predicted using the Vehicle Parameter Classification Analysis on the Training Data

Cluster	% of Data	CO_2 Contribution (%)	CO (mg/s)	Rank	CO_2 (g/s)	Rank	HC (mg/s)	Rank	NO_x (g/s)	Rank	PM (mg/s)	Rank	PN	Rank
1	49.1	7.6	2.76	6	1.61	6	2.25	6	0.02	6	0.04	6	3.3E+11	6
2	20.8	19.9	5.34	4	9.97	5	5.44	3	0.09	4	0.15	5	1.6E+12	5
3	1.0	2.4	11.08	3	25.47	3	6.10	2	0.23	2	0.84	2	5.5E+12	3
4	9.0	14.2	14.61	2	16.39	4	3.62	5	0.08	5	0.65	3	6.3E+12	2
5	12.0	35.9	17.03	1	31.24	1	3.87	4	0.16	3	1.39	1	8.6E+12	1
6	8.1	20.1	2.83	5	25.66	2	6.51	1	0.26	1	0.64	4	3.9E+12	4

Cluster	Fuel Rate (g/s)	AFR	Engine Load (%)	RPM	Exhaust Temp (°C)	Speed (mph)	Acceleration (mph/s)	Grade (%)	Dominant Road Type
1	0.6	124	25.5	991	193	12.1	-0.57	-0.85	Urban
2	2.8	61	44.5	1409	195	24.2	0.89	-0.98	Urban/Rural
3	7.2	33	89.2	1686	193	15.8	2.29	1.27	Urban
4	5.0	70	52.3	1979	298	58.4	0.06	-0.83	Freeway
5	8.7	36	93.6	1999	309	59.9	0.19	0.68	Freeway
6	7.4	30	96.5	1551	268	32.4	0.57	3.60	Rural/Urban

REFERENCES

Beddows, S. C. D.; Dall'osto, M.; Harrison, R. M. Cluster analysis of rural, urban, and curbside atmospheric particle size data. *Environ. Sci. Technol.* **2009**, *43* (13), 4694-4700.

Biswas, S.; Hu, S.; Verma, V.; Herner, J. D.; Robertson, W. H.; Ayala, A; Sioutas, C. Physical properties of particulate matter (PM) from late model heavy-duty diesel vehicles operating with advanced PM and NOx emission control technologies. *Atmospheric Environment*. **2008**, *42* (22), 5622-5634.

Brunerkreef, B.; Holgate, S. T. Air Pollution and Health, *Lancet*, **2002**, *360*, 1233-42.

Clark, N. N.; Kern, J. M.; Atkinson, C. M.; Nine, R.D. Factors affecting heavy-duty diesel vehicle emissions. *J. Air & Waste Manage. Assoc.* **2002**, *52*, 84-94.

EPA Office of Transportation and Air Quality: EPA Will Propose Historic Greenhouse Gas Emissions Standards for Light-Duty Vehicles. EPA-420-F-09-028. Available at http://epa.gov/otaq/climate/regulations/420f09028.htm. Accessed July 21, 2009.

Frey, H.C.; Kim, K. Comparison of real-world fuel use and emissions for dump trucks fueled with B20 biodiesel versus petroleum diesel. *Transportation Research Record*. **2006**, *1987*, 110-117.

Frey, H.C.; Rouphail, N. M.; Zhai, H. Speed- and facility-specific emission estimates for on-road light-duty vehicles based on real-world speed profiles. *Transportation Research Record*. **2006**, *1987*, 128-137.

Frey, H.C.; Unal, A.; Chen, J.; Li, S.; Xuan, C. *Methodology for Developing Modal Emission Rates for EPA's Multi-scale Motor Vehicle & Equipment Emission System*. Publication EPA420-R-02-027. US EPA. Prepared by North Carolina State University for Office of Transportation and Air Quality, 2002.

Hofeldt, D. L.; Chen, G. *Transient Particulate Emissions from Diesel Buses during the Central Business District Cycle*; SAE Technical Paper Series 960251; SAE International Congress and Exposition: Detroit, Michigan, 1996, 125-138.

Holmén, B.A.; Chen, Z.; Davila, A.C.; Gao, O. H.; Vikara, D.M. 2005. *Particulate Matter Emissions from Hybrid Diesel-Electric and Conventional Diesel Transit Buses: Fuel and Aftertreatment Effects*. JHR 05-304, Project 03-8. Joint Highway Research Advisory Council. Available at: http://www.ct.gov/dot/LIB/dot/documents/dresearch/CT_JHR_05-304_JH_03-8.pdf

Jarrett, R. P.; Clark, N. N. *Evaluation of Methods for Determining Continuous Particulate Matter from Transient Testing of Heavy-Duty Diesel Engines*; SAE Technical Paper Series 2001-01-3575, pp. 1- 10.

Kittelson, D. B.; Watts, W. F.; Johnson, J. P.; Thorne, C.; Higham, C.; Payne, M.; Goodier, S.; Warrens, C.; Preston, H.; Zink, U.; Pickles, D.; Goersmann, C.; Twigg, M. V.; Walker, A. P.; Boddy, R. Effect of fuel and lube oil sulfur on the performance

of a diesel exhaust gas Continuously Regenerating Trap. Environmental Science & Technology. 2008 42 (24), 9276-9282.

Maricq, M. M. Chemical characterization of particulate emissions from diesel engines: A review. *Aerosol Science*. **2007**, *38*, 1079 – 1118.

McCarthy, M. C.; Eisinger, D. S.; Hafner, H. R.; Chinkin, L. R.; Roberts, P. T.; Black, K. N.; Clark, N. N.; McMurry, P. H.; Winer, A. M. Particulate matter: A strategic vision for transportation-related research. *Environ. Sci. & Technol*. **2006**, *40*, 5593-5599.

North, R. J.; Noland, R. B.; Ochieng, W. Y.; Polak, J. W. Modeling of particulate matter mass emissions from a light-duty vehicle. *Transportation Research Part D: Transport and Environment*, **2006**, *11*(5), 344-357.

Qu, Y.; Holmén, B. A.; Ravishanker, N. Prediction on-road particle number concentrations of light-duty gasoline vehicles from gas concentrations with time-series cross-section regression. *Transportation Research Record: Journal of the Transportation Research Board*, **2008**, *2058*, 97-105.

Rönkkö, T.; Virtanen, A.; Vaaraslahti, K.; Keskinen, J.; Pirjola, L.; Lappi, M. Effect of dilution conditions and driving parameters on nucleation mode particles in diesel exhaust: Laboratory and on-road study. *Atmospheric Environment*. **2006**, *40* (16), 2893-2901.

So, Y.; Kuhfeld, W. F. Multinomial Logit Models. SAS Institute, Cary, NC, 1994. Available at: www.sas.com/techrep/download.

Tan, P.; Steinbach, M.; Kumar, V. *Introduction to Data Mining 5th Ed.*; Addison Wesley: Boston, 2006, 487-547.

U.S. Environmental Protection Agency. Control of air pollution from new motor vehicles: Heavy-duty engine and vehicle standards and highway diesel fuel sulfur control requirements; Final Rule. 40 CFR Parts 69, 80, and 86. *Fed. Regist.* **2001,** *66*, 5001–5193.

U.S. Environmental Protection Agency [US EPA] (2007e). *Nitrogen Dioxide Limits from Retrofit Technologies.* Available at http://www.epa.gov/otaq/retrofit/documents/420b08005.pdf

U.S. Environmental Protection Agency. *Latest Findings on National Air Quality-2006 Status and Trends*; EPA-454/R-07-007: U.S. EPA, 2008.

Yanowitz J.; McCormick, R.L. Effect of biodiesel blends on North American heavy-duty diesel engine emissions. *European Journal of Lipid Science and Technology*. **2009**, *111*(8), 763-772.

Yanowitz, J.; Mccormick, R. L.; Graboski, M. S. In-use emissions from heavy duty diesel vehicles. *Environ. Sci. & Technol.* **2000**, *34* (5), 729-740.

Zhai, H.; Frey, H. C.; Rouphail, N. M. A vehicle-specific power approach to speed- and facility-specific emissions estimates for diesel transit buses. *Environ. Sci. Technol*. **2008**, *42*(21), 7985-7991.

Zhu, Y.; Hinds, W.; Kim, S.; Sioutas, C. Concentration and size distribution of ultrafine particles near a major highway. *J. Air Waste Manage. Assoc*. **2002,** *52*, 1032–1042.

CHAPTER 7

FUNCTIONAL DATA ANALYSIS OF PARTICLE SIZE DISTRIBUTIONS: APPLIED TO HIGH-FREQUENCY EXHAUST MEASUREMENTS FROM A FLEX-FUEL VEHICLE[1]

Abstract

Functional data analysis (FDA) was used to analyze the particle size distribution measured from the exhaust of a flex-fuel passenger car with a Cambusion© DMS50 Fast Particulate Spectrometer. The DMS50 provides an estimate of the particle size distribution at 34-channel across a spectrum between 5 to 560 nm. Functional data analysis was used to smooth and analyze the particle size-distributions as continuous functions. We introduced a non-parametric technique to optimally smooth discrete particle spectrum concentrations, which uses no prior distributional assumptions.

Functional data analysis statistical tools were used to understand the behavior of the particle size distribution within and between testing runs. Functional principle component analysis identified major directions of variation for the accumulation mode particles and nucleation mode particles for two test runs. A functional linear model was used to quantify the relationship among particle size distributions, operating mode, and fuel type. The functional linear model was useful in comparing the particle size distributions between the gasoline and E85 runs at equal levels of engine speed. A time-series functional linear model was estimated to control for the autocorrelation in the second-by-second data. In both the concurrent and time-series models a significant relationship exists between accumulation mode particles and engine speed. The accumulation mode particles measured during the E85 run had significantly lower

[1] Darrell Sonntag, Giles Hooker and H. Oliver Gao

concentrations at low engine speeds, but were insignificantly different from the gasoline run at high engine speeds. Due to the variable nature of the nanoparticles mode particles (<50 nm), more data is needed to assess the effect of fuel and operating modes on these particles.

Functional data analysis was found to be a useful tool to analyze size-distributed particle emissions. Beyond laying a framework for analysis, the study also outlined several areas of research that will improve the interpretation and analysis of size-distributed particle emissions using functional data analysis.

Introduction

The formation of particulate matter emissions within the engine, the effectiveness of particle control devices, and subsequent evolution of aerosol in the atmosphere is a complex and much researched topic due to the known health effects from vehicle-source particles. Analyzing particle-size distributions adds a new dimension to vehicle emission studies, by analyzing not only the particle number or mass concentration, but also the shape of the particle size distribution

Importance of Particle Size Distribution for Health Effects. The size of particles is an important indicator for health effects of particulate pollution. Particles have been found to be increasingly toxic at smaller sizes, with ultrafine particles having a larger biological effect than the equal amount of mass distributed among larger particles (Lighty et al., 2000). Ultrafine particles can efficiently deposit toxic pollutants in the lungs due to their abundant number concentration, ability to penetrate deep within the lung, large surface area to mass ratio, and high deposition fraction (Brunerkreef and Holgate, 2002; Chalupa et al., 2004).

While useful information about the exhaust aerosol can be quantified through a distinct metric such as the ultrafine number concentration, a more complete picture of the potential health effects and emission characteristics can be understood by

measuring the entire particle-size distribution. Indeed, additional ambient data on the size distribution of particulate matter is needed to better distinguish health effects due to each size fraction (Wichmann and Peters, 2000). Particle size distributions can be weighted according to the total particle number, total surface area, volume or mass. Because ultrafine fractions represent a large number or the numbers of particles, the particle number size distribution is examined in this study.

Particle size-distribution measurement. Vehicle exhaust is composed of millions of individual particles that have a continuum of diameters. Because the diameter of each individual particle cannot be measured, the particle size distribution is approximated by measuring particles within discrete size range bins. Improved aerosol measurements have facilitated the measurement of size-resolved particle concentrations, including the SMPS, ELPI, and DMS500 (see introduction). These instruments measure the particle size distributions at a number of finite size fractions. Examples of the range and resolution of the measurements include: 7 to 8,100 nm at 12 size fractions for the ELPI (Holmen et al., 2005), 12 to 661 nm at 106 size fractions for the SMPS (Beddows et al., 2009) and 5 to 500 nm at 34 size fractions for the DMS500 (Liu et al., 2007).

Although particle size distributions are measured at a finite number of bins across the particle spectrum, the particle size distribution is best represented by a smooth continuous function. The particle number size-distribution is mathematically represented as $n_N(\log D_p) = dN/d\log Dp$, where N represents the cumulative particle concentration measured in particles/cm^3, and D_p is the particle diameter, typically measured by the aerodynamic or electric mobility diameter. When plotting the diameter on the log-scale, $dN/d\log Dp$ is used to represent the particle size distribution, so that the area under the particle size distribution is the total number of particles, represented as the integral:

$$N(\log D_p) = \int_{1}^{\log(D_p)} n_N(\log D_p) d \log D_p \quad .$$

(Sienfield and Pandis, 2007). In practice we are unable to approximate the limit $\Delta \log D_p = 1$, by measuring particles at infinitely fine size bin resolutions. (Sienfield and Pandis, 2007). We can analyze the discrete values of $n_N(\log D_p)$ to represent the particle size distribution. To approximate the smooth function $n_N(\log D_p)$, we can plot the values of $\Delta N / \Delta \log D_p$ at the midpoints of each measured size bin and then interpolate or a fit a probability density function, such as the lognormal distribution through the data points.

Factors that influence particle size-distributions from vehicle exhaust. Analyzing particle-size distributions adds a new dimension to particulate matter emission studies. Not only is the magnitude of particle-size distribution important, but the shape, or relative proportion of different sized particles is of interest. Particle size distributions of vehicle emissions are influenced by many factors including: engine type, engine design, engine operation, fuel and oil parameters, exhaust aftertreatment, sampling system and sampling conditions (Kittelson et al., 2006a, Rönkkö et al., 2006). A more extensive discussion of the factors that influence vehicle exhaust particle size distributions is given in the Introduction Chapter. In this paper, the important factors influencing particle size distributions from light-duty gasoline exhaust are briefly reviewed.

Gasoline vehicles tend to have smaller particle modes (40-80 nm), and have more asymmetric distributions than diesel exhaust. (Harris and Maricq, 2001; Maricq et al., 1999). The particle number and mass emission rates of the accumulation mode are much smaller compared to conventional diesel for accumulation mode particles (Maricq et al., 1999). Mass emission rates can be 10-100 times smaller than diesel engines, while number emission rates for accumulation range particles can be 10^4-10^5

times smaller (Harris and Maricq, 2001). While gasoline vehicles have smaller particle emission rates, their large proportion to the on-road fleet make them important contributors to on-road particle concentrations (Kittelson et al., 2004). The particle size distributions of individual vehicles can differ substantially, with some particle size distributions dominated by a nucleation mode, while in other cases the nucleation mode is absent (Kittelson et al., 2006b).

Gasoline particle emissions are more responsive to operating conditions than diesel engines. At full-throttle accelerations, particle emissions from gasoline vehicle can be similar to those of diesel vehicles under the same conditions. (Kittelson et al., 2006b). Particle concentrations across the entire measured spectrum (8-283 nm) are shown to be affected by large acceleration events. However, the effect of operating mode on particle concentrations is a function of particle size, and operating conditions will affect the shape of the particle size distribution.

The effect of operating conditions on nucleation mode particles for both diesel and gasoline vehicles is complicated by the storage and release of particles. During transient conditions, nucleation mode particles can deposit in the engine and exhaust system and be subsequently released during high exhaust temperatures and exhaust flow achieved at high loads (Kittelson et al., 2006b; Mathis et al., 2005).

Ethanol blends have been shown to reduce PM mass (Mulawa et al., 1997) and number (Lee et al., 2009) in light-duty gasoline vehicles. In laboratory testing of a spark ignition flex-fuel vehicle, Lee et al. (2009) showed that an E10 ethanol blend impacted the particle size distribution, with an observed decrease in accumulation mode particles (50-150 nanometers), while only a slight decrease for particles < 50 nanometers. However the effect across the entire particle-size range was not fully quantified and results will likely differ in real-driving conditions.

Particle size distribution analysis methods. Mathematical functions improve the interpretability of size-resolved particle measurements through smoothing methods, while also eliminating noise in the discrete particle concentration measurements. While, interpolation maintains the actual measurements of the particle instrument, the particle size distribution is measured with some error and the particle size distribution measurements can be noisy, especially at low particle concentrations. Simply interpolating the data can yield noisy and jagged particle size distribution measurements.

Smoothing the particle concentration data is commonly performed by fitting the discrete particle spectrum with a parametric distribution, nearly always with the lognormal distribution. The accumulation mode of diesel particle emissions has been consistently shown to be well parameterized with a lognormal distribution among different studies (Burtscher, 2005). To estimate multi-modal distribution of both vehicle exhaust (Kittelson et al., 2006b) and ambient particle concentrations, several individual lognormal distributions are fit to the particle size distribution, (Sienfield and Pandis, 2006). The lognormal distribution is especially appealing for estimating mass distribution estimates, because the lognormal converges to zero asymptotically, thus reducing the noise or artifact readings on the large particles, which can significantly bias particle mass rates. (Symonds et al., 2007; ELPI).

As to date, most analysis of the particle size distribution of vehicle exhaust is conducted under steady state conditions, due to the long-scan times of particle measurement systems such as the SMPS. Additionally, by sampling the exhaust plume behind a vehicle, chase-studies collect intermittent data and must collect samples under average driving conditions. Conclusions are made from plotting the average particle size distribution from testing different vehicles, operating conditions, or fuel

types ((Kittelson et al., 2006a; Kittelson et al., 2006b; Rönkkö et al., 2006; Giechaskiel et al., 2005).

With the introduction of two fast particle size measurement systems, the TSI EEPS and the Cambustion DMS50/500 the particle size distributions can be measured up to 10 samples/second, permitting analysis of transient vehicle behavior on particle size distributions (Liu et al., 2007). While the capability to analyze such time-resolved behavior will improve the understanding of particle emission processes, the size and complexity of the data can be overwhelming to analyze. For example, at a one second/sample rate, 1,400 particle size distributions are measured for an urban driving cycle (UDC) (Kittelson et al., 2006b; Liu et al., 2007). At the 10 sample/second rate, 14,000 particle size distributions will be measured, yielding nearly half a million data points measured across the 34-channel particle spectrum (DMS specs). Effective data reduction and statistical analysis techniques are needed to data screen, analyze, and understand the results from transient particle size distribution data sets.

Vehicle exhaust studies have used the means or graphical "snapshots" of the transient particle size distribution in analysis (Maricq et al., 1999; Liu et al., 2007; Lee et al., 2009). These studies provide useful and accessible data to assess the influence of transient behavior on particle distributions. However, more quantitative analysis that incorporates all of the measured data, while also expressing the variability of the data is desirable.

Multivariate Data Analysis. Multivariate methods add quantitative insight into the dynamic behavior of particle size distributions. Multivariate statistical methods have been employed by ambient aerosol studies, but not by vehicle exhaust studies. Multivariate statistical methods are useful methods for analyzing stationary ambient aerosol measurements that can collect large amounts of data due to long sampling periods. These methods are useful for understanding the variability of

particle size distributions as a function of ambient conditions and other factors. Beddows et al. (2009) applied cluster analysis to 5000 hourly measurements of ambient particle size distribution data. The clusters of particle size distribution corresponded to different times of day and measurement location, and were useful in understanding atmospheric events and emission sources. Charron and Harrison, (2003) used principle component analysis to analyze the effects of vehicle traffic on road-side particle size distributions. This method was useful for identifying the particle sizes that were influenced by truck traffic, light-duty traffic, and traffic jams. Multivariate methods have extracted useful data from ambient particle size distribution measurements.

Application of functional data analysis in particle emission studies. In this chapter, we introduce functional data analysis (FDA) to smooth and analyze particle size distribution measurements of exhaust emitted from an on-road vehicle.

In many cases, the particle size distribution measurements are not well approximated by lognormal distributions. Harris and Marcq (2001) found that gasoline vehicles had an asymmetric, positively skewed particle size distribution. Particle size distributions can have asymmetric modes in ranges that are difficult to classify as either nucleation or accumulation mode (Shi et al., 2000), especially during transient operation (Liu et al., 2007). A bi- or even a tri-modal lognormal distribution can ignore important features of real particle measurements.

Non-parametric smoothing methods can be used to obtain smooth particle size distribution without applying any prior distributional assumptions. Accounting for the inherent “smoothness” of the data is an effective tool for correcting for measurement error that is frequently observed in particle measurements, especially at low concentrations (Harris and Marcq, 2001; Kittelson et al., 2006b). Non-parametric smoothing methods can be used to estimate the degree of smoothness, directly from

the data, facilitating smoothing analysis that does not require any prior assumptions about the data.

Functional data analysis is a natural extension of multivariate data analysis that takes into account the inherent "smoothness" of the data. Instead of analyzing discrete points, FDA is used to analyze smooth curves. Functional data analysis of particle size distributions can yield results that are both more interpretable and theoretically pleasing by accounting for the smoothness of particle size distributions. Many standard multivariate statistical methods have been extended into functional data analysis (Ramsay et al., 2009), including functional principle component analysis and functional linear models.

Functional principle component analysis (fPCA) could assist analysis of the variability among particle size distributions, by extending the principle component analysis done by Charron and Harrison (2003), by accounting for the smoothness of the data. For example, under certain conditions a high accumulation mode will suppress the nucleation mode by providing a large surface area that adsorbs semi-volatile gases. fPCA could be used to examine under what conditions there exists a negative covariance between nucleation and accumulation mode particles. Additionally, functional principle component analysis could be used to cluster data. Functional data analysis will likely confirm earlier results obtained through multivariate analysis, but may do so in a more interpretable and theoretically robust manner.

Functional linear models could be used to model relationships between the important covariates and the entire particle size distribution. Functional linear models would estimate effects that are continuous functions of the particle size. This could add important dimensions in identifying the range of particles that are influenced by

covariates, rather than using single metrics used in previous models (Kittelson et al., 2008; Qu et al., 2008; North et al., 2006).

In this study, functional data analysis was used to analyze size-distributed particulate emissions from a flex-fuel light-duty passenger car. The scope of this paper is focused on the application of FDA to analyze particle-size distributions, rather than making general conclusions about the effects of ethanol blends on vehicle emissions.

Experimental Data

The data was collected as part of a pilot study assessing the effects of alternative fuels on ultrafine particle emissions. The data was collected on November 17-18, 2008 in Ithaca, NY on a 2008 Chevrolet Impala flex-fuel passenger sedan. On November 17th the vehicle was tested on conventional gasoline, and on November 18th the vehicle was tested on an E85 ethanol-gasoline blend. The vehicle test route began at Cornell University and ran on a testing route x miles long on local streets, freeway conditions, and rural highways.

The particle emissions were tested using a Cambusion© DMS50 Fast Particulate Spectrometer with the DLC50 Dilution Line Controller. The DLC50 controls a heated line and primary dilution ratio that allows the DMS50 to directly sample tail-pipe emissions on-board vehicles in real-driving conditions. Figure 7.A1 shows the DMS50 and DLC50 during installation before the testing on the Chevy Impala on November 18, 2008.

The DMS50 has 22 electrometers that detect the impaction of charged particles within a classification column. An inversion method computes the 22 raw electrometer inputs into particle concentrations in terms of dN/dlogDp at 34 diameters between 4.87 and 560.34 nm (Symonds et al., 2007). The particle number size distribution, as estimated from the 34-channels output, will be referred to as the discrete particle size

spectrum or 34-channel particle size spectrum in this report. The DMS50 measured at a sampling rate of 1 sample/second.

Being a short pilot study, limited emissions data was collected that yielded good data with a strong signal to noise ratio. The overall dilution ratio was set to 90:1 to avoid condensation of the exhaust vapors in the sampling line and DMS50. However, the particle concentration was frequently below the sensitivity limits of the instrument during the testing route. The DMS50 is designed for sampling diluted engine exhaust, however the low emissions from the vehicle coupled with an excessively large dilution rate, may have contributed to a poor signal to occur on much of the route. The freeway segment had the highest particle emissions along the testing route, and thus the best signal to noise ratio. The freeway segment was deemed of sufficient quality to merit further analysis.

The analyzed runs included four successful test runs, two conducted on gasoline on November 17th and two runs on an E85 ethanol-gasoline blend on November 18th. Each segment of data was between 2:20 and 3 minutes in duration. The freeway segment begins with an on-ramp with a positive grade, and ends at an intersection after an off-ramp. The end of the segment was chosen when the vehicle decelerated to 20 mph. An on-board diagnostic scan tool recorded operating parameters every 2-3 seconds during the route including engine speed (rpm), engine load (%), vehicle speed (mph), and engine air flow rate. The average speed for each run ranges between 49 and 57 mph, and the average engine load ranges between 64 and 67%. Summary data of the four test runs are shown in Table 7.A1.

The average 34-channel particle concentrations for each run are plotted in Figure 7.1. The most obvious difference between the runs is the large nucleation mode centered around 15 nm for run 2. Figure 7.1b focuses on the smaller range of particle concentrations to emphasize the differences among the other three runs. For the

particle diameters > 50 nm, the runs within each fuel type are fairly consistent, while for the particles < 50 nm, the average particle concentrations vary considerably. Nucleation mode particles typically dominate the particles below 50 nanometers. Nucleation mode particles are formed from volatile compounds which make them notoriously sensitive to operating, atmospheric, dilution and measurement conditions. The accumulation mode of particles observed in our test between 30 and 200 nm are typically comprised of solid carbonaceous material, and are a more repeatable observation between vehicle emission tests (Morawska et al., 2008).

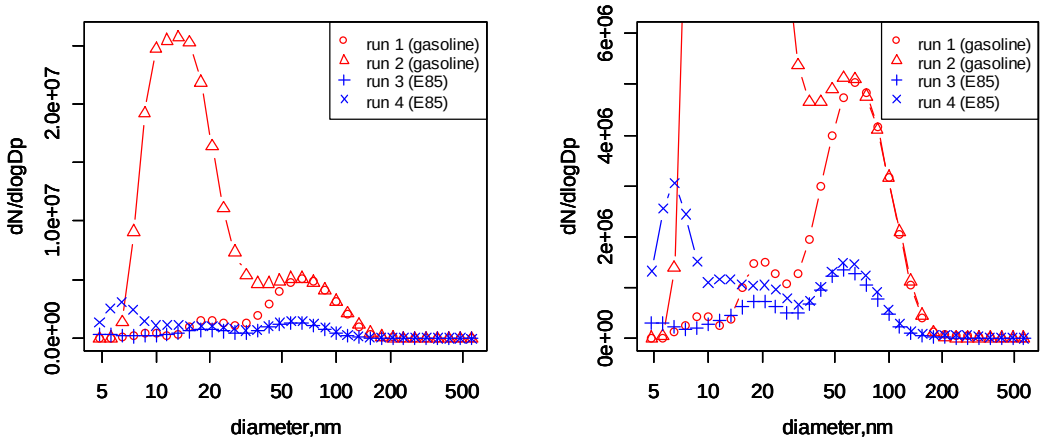

Figure 7.1. Average 34-particle spectrum concentration data for the four test runs (a) large-view to contain all data (b) close-up view.

Smoothing

The large nucleation mode observed in run 2 is more than an order of magnitude larger than the comparable particle concentrations on the other runs. The large variation in particle concentrations made it difficult to concisely demonstrate the application of functional data analysis to the data. Because the purpose of the paper is focused primarily on demonstrating the methodology, for now, the analysis will focus on run 1 and run 4, one run from each fuel type. We will return to discuss how the large peak in particle concentration can be addressed using functional data analysis at the end of the paper.

Smooth functions extract useful data from noisy and discrete data. The substantial variability, especially in the small particle ranges below 50 nm make the data set well-suited for smoothing techniques. Smoothing basis splines were used to estimate a smooth function (a continuous particle-size distribution) for each 34-channel particle spectrum observation. In our case, knots were placed at each of the 34 sample points, with 4th order basis function which required 36 basis functions (Ramsay et al., 2009). A linear combination of the scaled basis splines were used to used to smooth the 34-channel particle spectrum observations into continuous functions, expressed as: $\hat{p}(s) = \sum_{i=1}^{36} c_i \cdot \phi_i(s)$, where $\hat{p}(s)$ = the smooth particle-size distribution concentration measured by dN/dlogDp cm^{-3}, s = size of particles (measured by diameter in nanometers), c_i = coefficient assigned to each of the 36 basis splines, and $\phi_i(s)$ = basis spline i. Figure 7.2 illustrates a set of scaled smoothing splines, $\left(c_1\phi_1(s), c_2\phi_2(s), ..., c_{36}\phi_{36}(s)\right)$, whose sum yields the illustrated smooth particle size distribution for one of the observations from run 1.

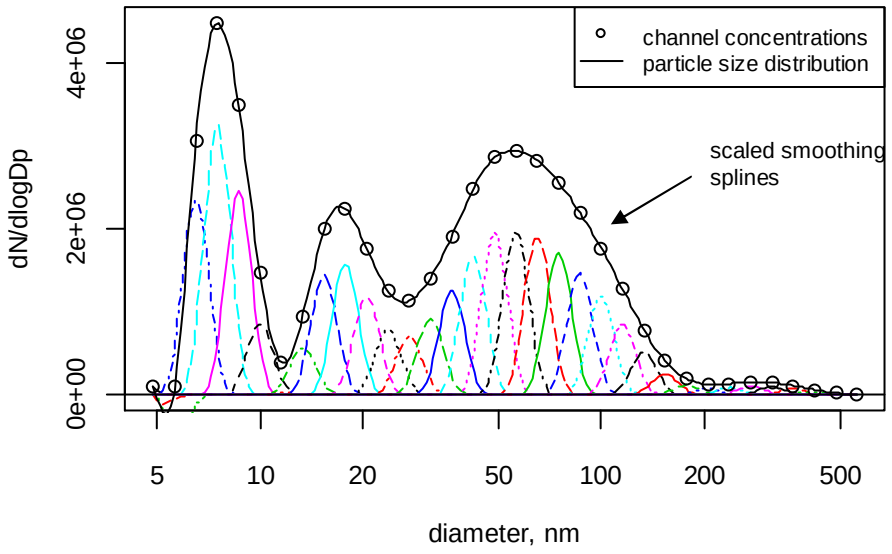

Figure 7.2. Scaled basis splines used to smooth the 34-channel particle concentrations into a continuous particle size distribution.

The coefficients $c_1, c_2, \ldots, c_{36}$ are typically determined by the set of values that minimizes the sum of square errors between the discrete values and predicted smooth values, expressed as: $SSE(\hat{p}) = \sum_{j=1}^{34} \left(p_j - \hat{p}(s) \right)^2$. However, with knots placed at each of the 34 observed diameters, the number of coefficients (36) exceeds the number of data points (34), meaning an infinite number of basis coefficients could be used to pass exactly through the 34-channel spectrum. A smoothing penalty, λ, was imposed using the integral of the second derivative to penalize curvature of the particle-size distribution. Minimizing the penalized squared error yields a unique solution for a given value of λ. The formulation of the penalized sum of squared error is represented by: $PENSSE_{\lambda}(\hat{p}) = \sum_{j=1}^{34} \left(p_j - \hat{p}(s) \right)^2 + \lambda \int [D^2 \hat{y}(s)]^2 ds$.

The smoothing parameter λ is often selected experimentally by visually evaluating the fit obtained by using different values of λ. While visually evaluating the effect of smoothing penalties should be conducted, it is appealing to select λ in a more quantitative way. Generalized cross-validation (GCV) can be used to optimally select λ from the data, defined as:

$$GCV(\lambda) = \left(\frac{n}{n - df(\lambda)} \right) \left(\frac{SSE}{n - df(\lambda)} \right)$$

(Ramsay, et al. 2009). For the 34-particle spectrum measured on the each run runs, the GCV was calculated for a range of lambda values on a logarithmic scale. For run 1 and 4, $\lambda = 10^{-10}$ yielded the smallest average GCV.

The particle-size distributions estimated from the penalized smooth closely fit the discrete particle size spectrum observations. However, many functions estimated negative concentration values for a portion of the spectrum (i.e. Figure 7.2 at 5 nm). A large range of lambda values (imposing a strong and weak smoothing penalty) were estimated, but none were able to yield strictly positive functions for all the observations on runs 1 and 4.

Constrained Smoothing

To prevent the smoothing splines from predicting negative concentration values, positive constrained smoothing was performed. We transformed our smoothing predictor by estimating particle concentrations using an exponential function: $\hat{p}(s) = e^{W(s)}$, where $W(s) = \sum_{i=1}^{36} c_i \cdot \phi_i(s)$, and c is again determined by minimizing the penalized squared error: $PENSSE_\lambda = \sum_{j=1}^{34} \left(p_j - e^{W(s)} \right)^2 + \lambda \int \left[D^3 W(s) \right]^2 ds$. 5th order b-splines were used so that the third derivative could be used as the linear smoothing operator[2]. If we assume that the particle size-distribution has similar curvature to the lognormal distribution [3], then by penalizing the third derivative, we are penalizing for departures of curvature from a lognormal-type distribution[4].

In the normal case, the minimum PENSSE can be solved linearly and computationally efficiently, however solving for the minimum $PENSSE_\lambda$ with our positively constrained basis function poses a non-linear problem that requires a search algorithm to solve. To seed the search algorithm, first the $PENSSE_\lambda$ was solved using a linear case with ln-transformed particle concentrations,

$$\ln\left[\frac{dN}{d \log(Dp)} \right].$$

The basis coefficients, *c*, from the ln-transformed smooth were then used as initial starting points for the positive constrained smooth algorithm. The algorithm had difficulty converging due to the frequent zero concentration values on some channels of the discrete particle spectrum, so a minimum concentration was set (see supporting

[2] The derivatives are continuous up to the order of smoothing splines minus two.

[3] $y(x) = \frac{1}{\sqrt{2\pi\sigma}} e^{-(x-\mu)^2/\sigma^2}$, In our case, the log was taken of the particle diameter (x) before smoothing.

[4] If we assume that $W(s) = x^2$ is smooth, then we should penalize the third derivative because the third derivative of x^2 is zero, while the second derivative of x^2 is a constant.

documents). Additionally, the data was reduced in magnitude by 10^6 before smoothing, and then rescaled after the smoothing was performed to avoid numerical errors. These steps proved necessary for the constrained smooth algorithm to converge or avoid spurious convergences.

The optimal smoothing penalty, λ, could not be determined using $GCV(\lambda)$ because the degrees of freedom, *df(λ)* cannot be directly calculated using the positive constrained smooth. Using a Taylor's series expansion, a linear approximation was derived of degrees of freedom when positive constrained basis smoothing splines are used. The derivation of the approximate *df(λ)* and R code developed for computing the approximate GCV are included in the supplemental information.

Due to the long computation time introduced the non-linear search procedure to solve for the smooth for each function, the approximate GCV was calculated on a subsample of 12 observations (6 each from test run 1 and 2). The smoothing parameter that yielded the minimum average GCV for the 12 observations occurred at: $\lambda = 10^{-9}$. The rest of the 284 samples from both runs were smoothed using the constrained smoothing with a $\lambda = 10^{-9}$. By so doing, all of the particle-size distributions yielded satisfactory fits to the 34-channel spectrum. The constrained positive fit is displayed in Figure 7.3 for the same sample observation previously evaluated in Figure 7.1. In addition to being strictly positive, the constrained fit is slightly smoother than the unconstrained fit. Figure 7.A3 displays the positive constrained smooth on additional observations from runs 1 and 4. Figure 7.A4 displays the mean particle size distribution computed from the 34-channel spectrum, the normal smooth, and the positive constrained smooth. While the effect is visually significant for many observations, for the entire mean values the effect is barely detectable.

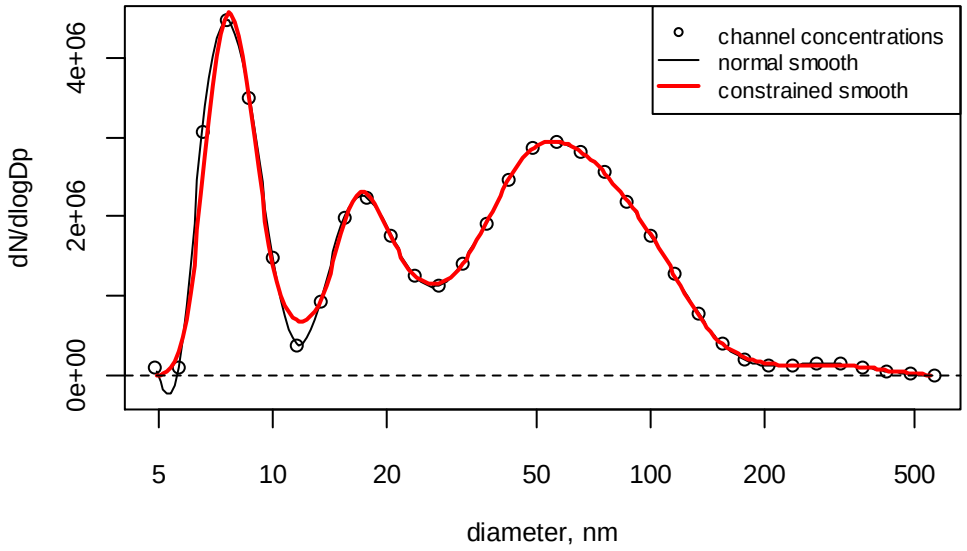

Figure 7.3. Constrained-positive smooth for the observation #13.

Functional Data Analysis

The standard functional data analysis requires a linear basis expansion so a finely resolved linear basis expansion was to trace the shape of the positive constrained smooth functions. First, the positive constrained smooths were discretized into the 206 points along the particle size spectrum, then they were smoothed using 40 linear basis function (as compared to 34), with 4^{th} order polynomials and no smoothing penalty. The means of the smoothed functions for the run 1 (gasoline) and run 4 (ethanol) are plotted in Figure 7.4, with accompanying confidence intervals.

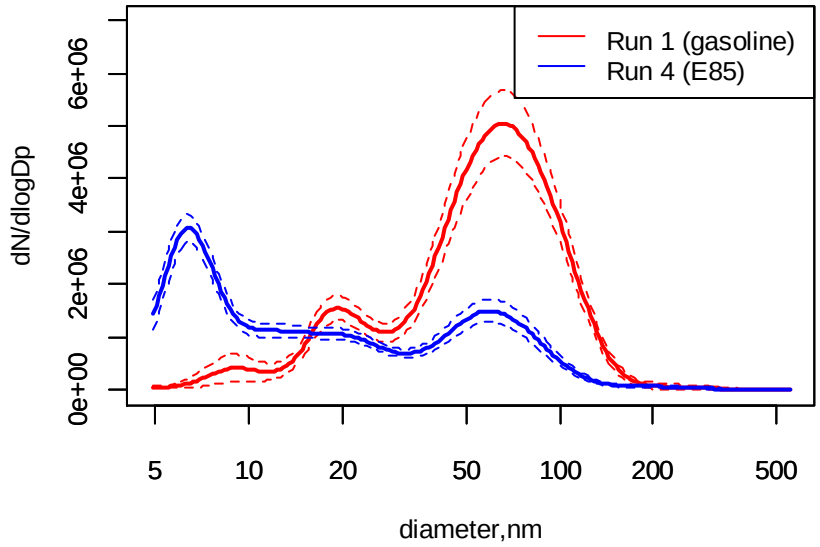

Figure 7.4. Mean particle size-distributions from the positive constrained smooth for the gasoline and ethanol test runs.

Functional Principle Components Analysis. Functional principle components analysis (fPCA) was used to explore the variability in the particle-size distributions. Principle components analysis is a dimension reduction strategy to better interpret the underlying modes of variation within multivariate datasets. Instead of analyzing the variability of data according to one covariate (x or y-direction), principle components identifies new directions that are a transformation of 2 or more variables. Principle component analysis has been used to understand the variation in discrete particle size spectrum data (Charron and Harrison, 2003). In the discrete case, the directions are identified by a vector containing values for each of the channels from the discrete particle spectrum. In the functional data analysis setting, a small number of smooth functions (called functional principle components) are used to identify the major directions of variation. The mechanics of functional principle components analysis is well presented in Ramsay et al. (2009) and is not presented here.

Functional principle components was applied to runs 1 and 4. The two functional principle components are well interpreted by adding and subtracting each

principle component from the mean curve by a fixed value as shown in Figure 7.5. Figure 7.5 plots the mean particle distributions with a solid line, and the addition of the principle component displayed with a positive symbols and the subtraction of a principle component given with negative symbols. Each particle size distribution within the two runs, can be approximated by the mean and multiplying the two principle components by a score, such that 93% of the variability of the original data set is retained.

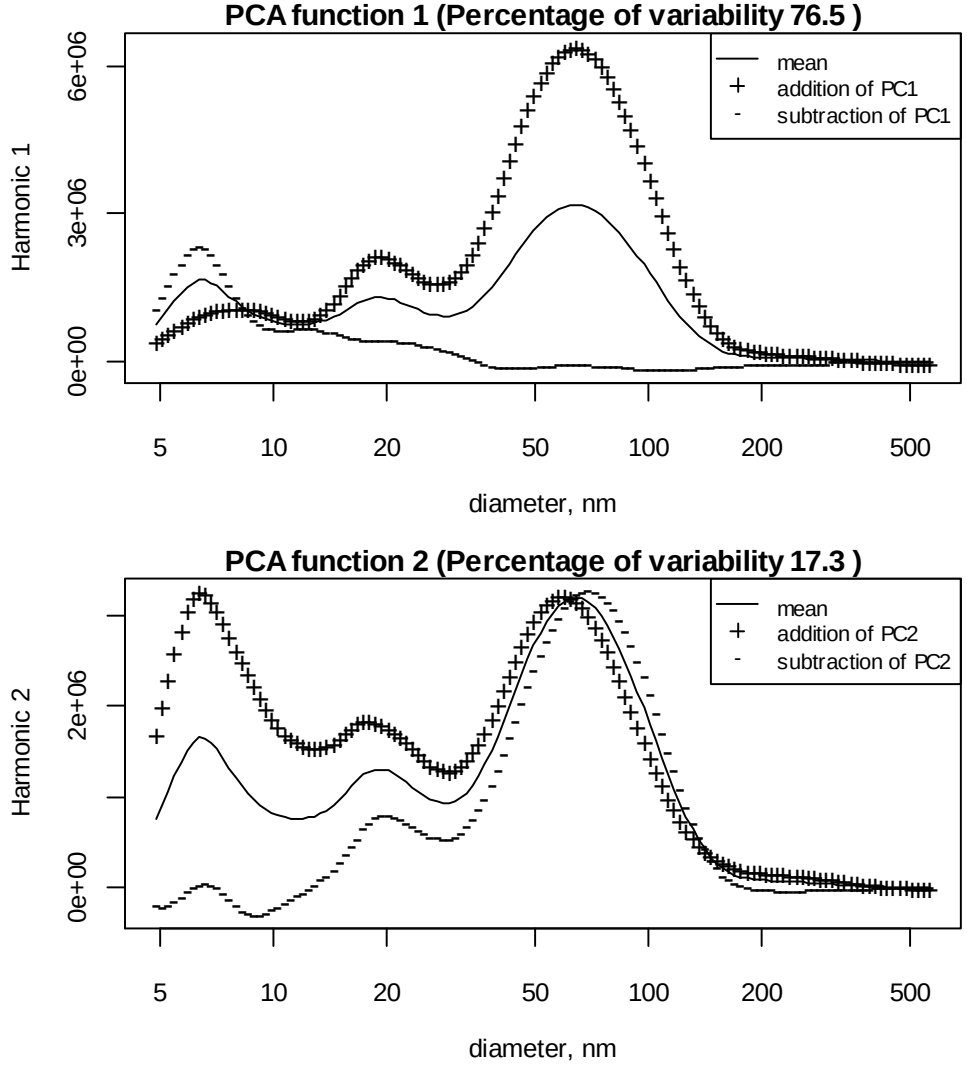

Figure 7.5. Functional principle components plotted relative to the mean.

The first principle component largely captures the variation in the accumulation mode particles (between 35 and 100 nm). A slight drop in particle concentration for the smallest particles (<10 nm), accompanies large positive increases in accumulation mode particles. This is partly due to the differences in the datasets, with run 1 having a larger accumulation mode, and smaller nucleation mode. The second component emphasizes large variation in the nucleation mode particles. As the nucleation mode particle increases, the accumulation mean diameter slightly decreases. This behavior is evident in the second test run with a larger nucleation mode, and the smaller mean diameter for the accumulation mode.

The scores of the principle components are plotted for each of the observations for both test runs in Figure 7.6. The two different test runs are clearly distinguished by the principle components. The gasoline run has larger score 1 (larger accumulation mode) and smaller score 2 (larger nucleation mode). Functional principle components may be an effective method to perform cluster analysis for particle size distribution data to distinguish differences in particle-size distribution in large datasets, as compared to using the discrete particle spectrum (Beddows et al. 2009).

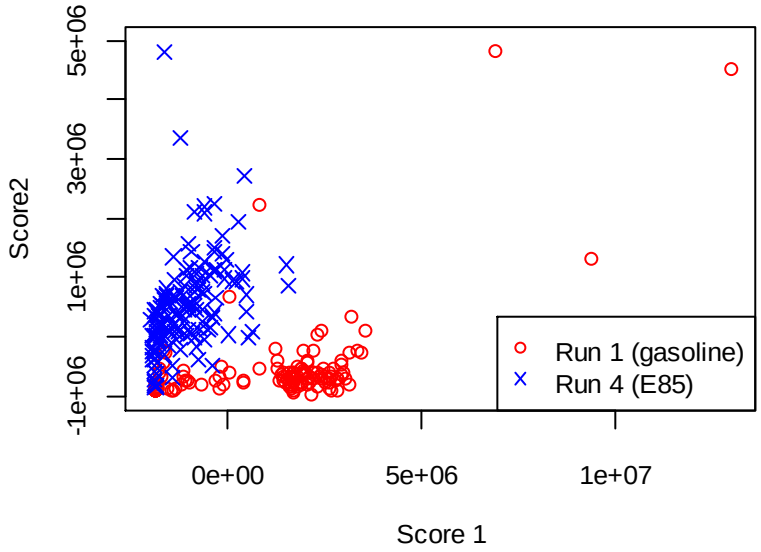

Figure 7.6. Comparison of functional principle component scores between Run 1 (gasoline) and Run 2 (ethanol).

To examine the variability of particle-size distributions occurring within each run, the fPCA scores were plotted against covariates such as percent engine load, engine speed, manifold engine pressure and engine air intake. Figure 7.7 shows the relationship between the two fPCA scores and engine speed. Score 1, which emphasizes accumulation mode particles, appears to be more strongly correlated to engine speed than score 2. In run 4, score 2 appears to be a random process with no relationship with engine speed.

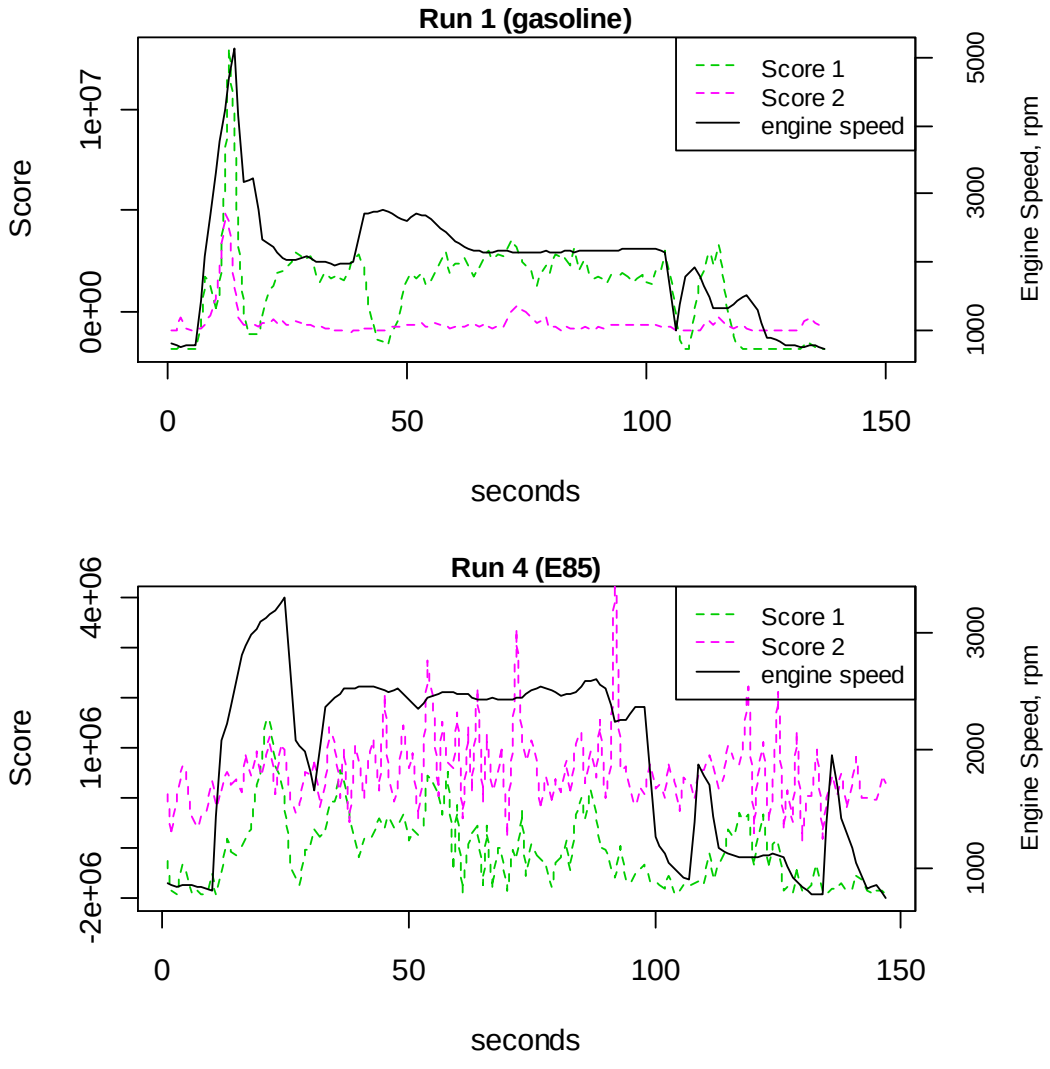

Figure 7.7. Principle component scores of each observation plotted in time for each run.

Functional Linear Model. The confidence intervals displayed in Figure 7.4 were computing by:

$$\bar{p}(s) \pm 2 \cdot \frac{std(s)}{\sqrt{n}}.$$

The confidence intervals represent the distance wherein a t-test would show an insignificant difference between the two samples. Figure 7.4 suggests that the run 1 has significantly larger concentration of particles between 20 and 200 nm, while the ethanol run has significantly higher concentration of particles smaller than 15 nm. The confidence intervals rely on the assumption of independent, approximately normally distributed variables. However, as confirmed in Figure 7.7, the particle-size distributions are influenced by engine conditions. The two runs are not exact replicates of driving conditions, for example the maximum engine speed and engine load are higher on run 1. By using a functional linear model, we can control for the effect of varying driving conditions. The fact that the observations are time-series was be addressed later.

The functional linear model is based on similar assumptions made for the simple linear model:

1. The conditional distribution of particle size distribution at each particle size, s, are normally distributed.
2. The conditional mean is a linear function of x.
3. The constant distributions have a fixed variation across x.
4. Each observation is an independent random variable. (Larsen and Marx),

The assumptions are represented by $p_i(s)\big|x \sim N\left[\beta_0(s) + \beta_1(s)x, \sigma^2(s)\right]$, with independent and identically distributed $p_i(s)\big|x$. Details on functional linear regression are given in Ramsay et al. (2009). We will model the effect of driving conditions by using engine speed raised to the second power. Engine speed raised the second power,

was found to best approximate a linear relationship with the fPCA scores as shown in Figure 7.8. The relationship with engine load is plotted in Figure 7.A5.

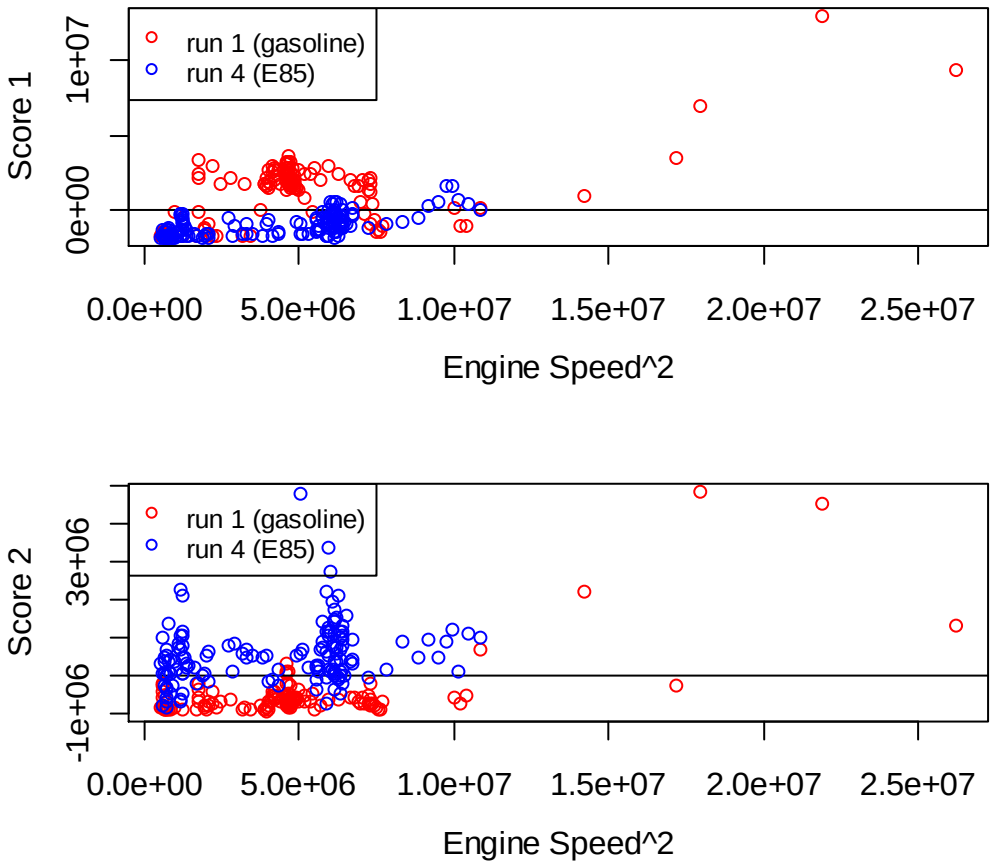

Figure 7.8. PCA scores plotted against engine speed^2

Based on these observations, the following functional linear model was estimated: $p_i(s) = \beta_o(s) + \beta_1(s)(engine\,speed_i - 7.5)^2 + \varepsilon_i(s)$, where $p_i(s)$ is the particle size distribution at time *i* and the engine speed is measured 1000 rpm units. $\beta_o(s)$ and $\beta_1(s)$ estimated for run 1 and 4 are displayed in Figure 7.9, with accompanying confidence intervals. The intercept, $\beta_o(s)$ is quite different between the two runs. The effect of engine speed, $\beta_1(s)$, has a similar shape for both runs, with the strongest effect occurring for particles between 30 and 200 nm. Variation in particle size-distribution attributable to engine speed appears to vary in the same direction,

while the intercept appears to capture the between-run variation that is not attributable to engine speed.

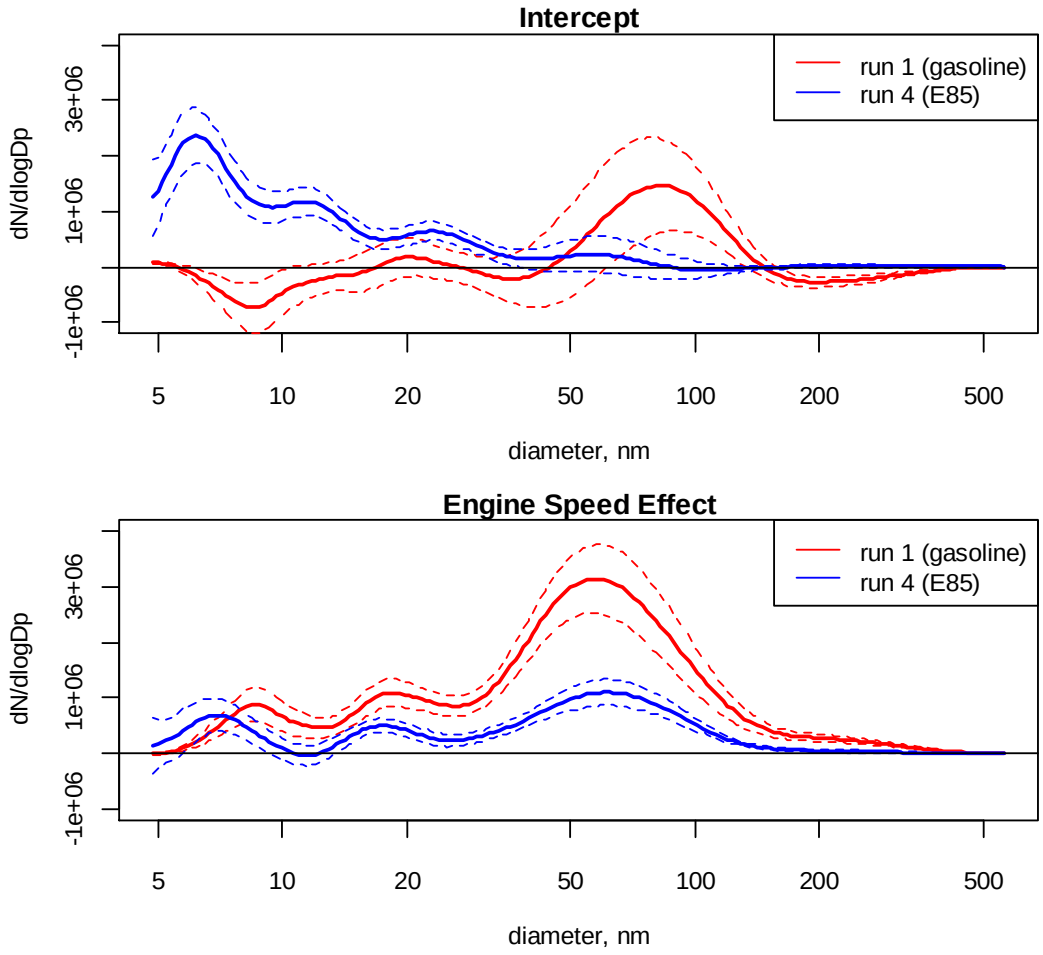

Figure 7.9. Functional beta coefficient estimates with 95% confidence intervals. Figure 7.9a. is the intercept, $\beta_o(s)$ and Figur 9b, is the effect of engine speed, $\beta_1(s)$ measured in Δ[dN/dlogDp]/Δ 1000 rpm

The linear model is a useful tool to control for driving mode variability that occurred between tests, by comparing the particle-size distributions at the same levels of engine speed. The expected value for the model estimates is expressed as $E\left[\, p(s)\middle| x\,\right] = E\left[\,\hat{p}(s)\right] = \beta_0(s) + \beta_1(s)\cdot x$, and using the assumptions of a simple functional linear model, the variance of the model estimate is given as:

$$Var\left[\,\hat{p}(s)\right] = Var\left[\,\beta_0(s) + \beta_1(s)\cdot x\right] = Var\left[\,\overline{p}(s) - \beta_1(s)\cdot\overline{x} + \beta_1(s)\cdot x\right] = Var\left[\,\overline{p}(s)\right] + \left(x - x\right)^2 Var\left[\,\beta_1(s)\right]$$

From these values we can estimate the confidence intervals, using:

$$E\left[\hat{p}(s)\right] \pm 2 \cdot \sqrt{Var\left[\hat{p}(s)\right]}.$$

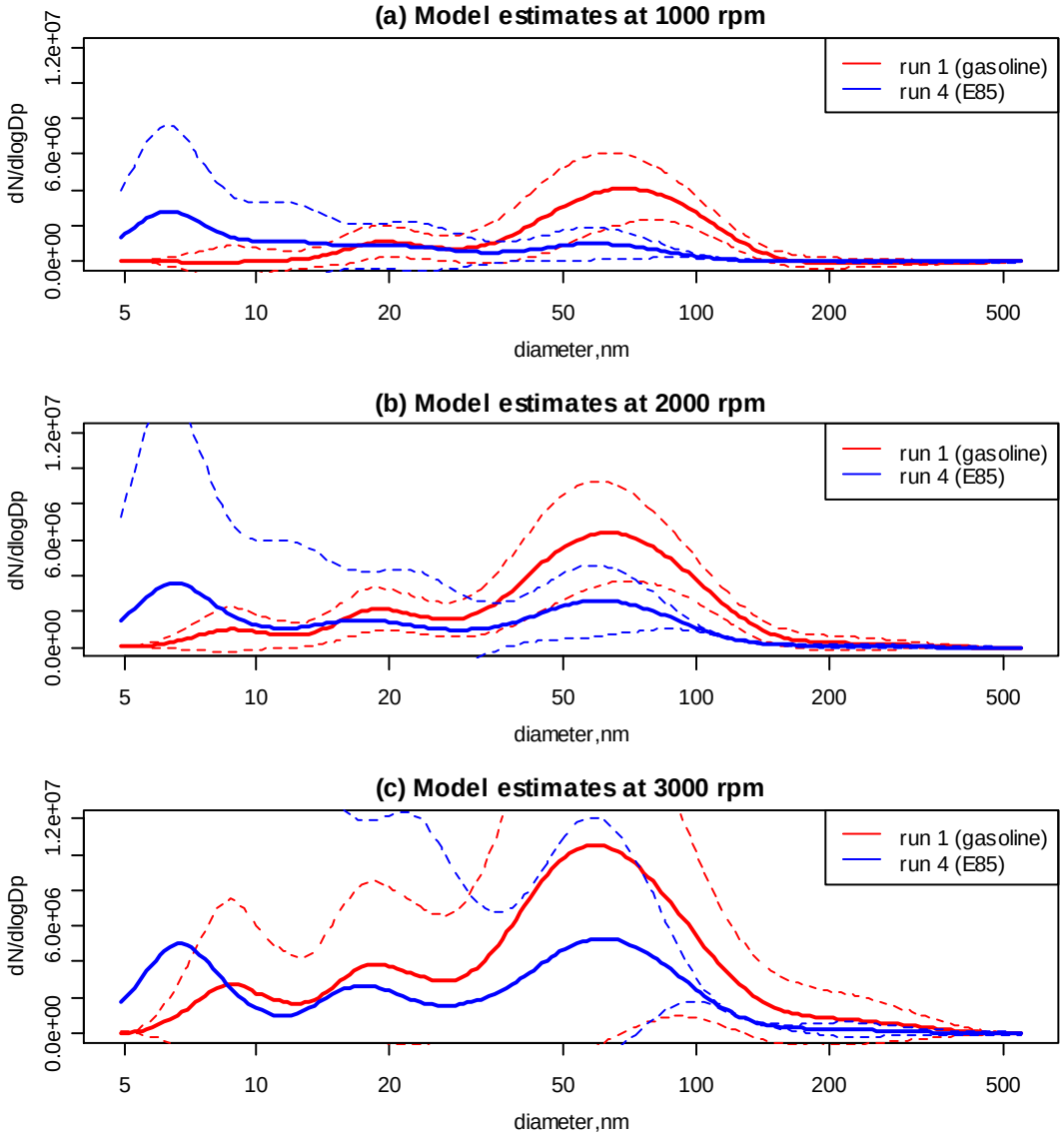

Figure 7.10. Model estimates at 1000, 2000, and 3000 engine speed rpm.

Figure 7.10 contains the model estimates for three engine speed levels that were obtained in both runs: 1000, 2000, and 3000 rpm. In all cases the gasoline run has a mean concentration larger in the accumulation mode, and the E85 has a higher nucleation mode. However, the variation changes considerably at different engine speed levels. At 1000 rpm, the two runs are significantly different for particles

between 70 and 120 rpm. At 2000 rpm, the range of particles that are significantly decreases is shortened, and at 3000 rpm, the particle-size distributions are not significantly different from one another.

Model Diagnostics. The functional linear model assumptions were evaluated through the use of several diagnostic graphs, statistics, and tests. In Figure 7.11, the residuals are color coded according to engine speed level (rpm), to view how the residuals change with respect to engine speed. The normal distribution assumption of $p_i(s)|x$ may be more difficult to accept for the smaller particle sizes, where the large variation and positive constraint yields positively skewed data for run 2. For run 1, between 50 and 100 nm, the residual distribution appears to be bimodally distributed. However given the difficulty of determining the normal distribution for continuous curves, the curves generally appear to by symmetrically distributed around zero, and the normal assumption is reasonable.

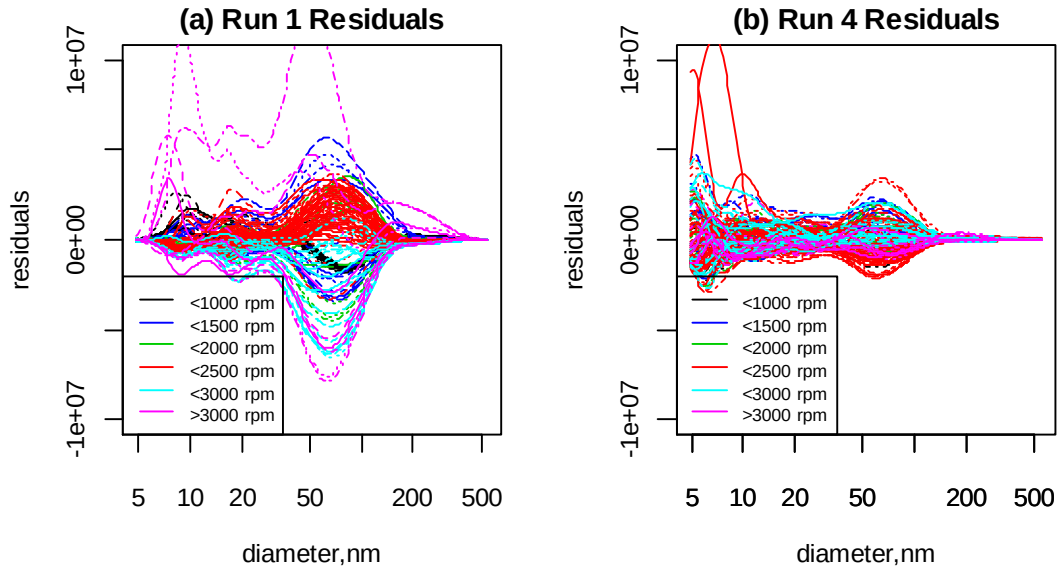

Figure 7.11. Residuals from runs 1 and 4 according to particle size, color coded according to engine speed level.

The constant variance assumption across engine speeds was also evaluated from Figure 7.11. For run 1 the variation increases with engine speed, with the

residual recorded above 3000 rpm having the largest variation. In Figure 7.11b, the variance appears to greatest between 2000-2500 rpm, rather than the largest rpm levels. Weighted least squares could be used to capture the non-constant variance effect, however it was not used, because there does not appear to be a simple linear relationship that could be used to approximate the changing variance.

The linearity assumption of the model was also valuated from Figure 7.11. For run 1, engine speeds between 2000-2500 have a mean above zero for the accumulation mode. However, in general, the means of the residuals appear to be around zero regardless of engine speed. Functional R^2 values were calculated to assess linear relationship explained by the model, and shown in Figure 7.12. For run 1, the R^2 varies around 0.40, with the best explanation occurring for large particles between 150 and 500nm. For run 2, the model best explains the variation in the accumulation mode between 50 and 100 nm.

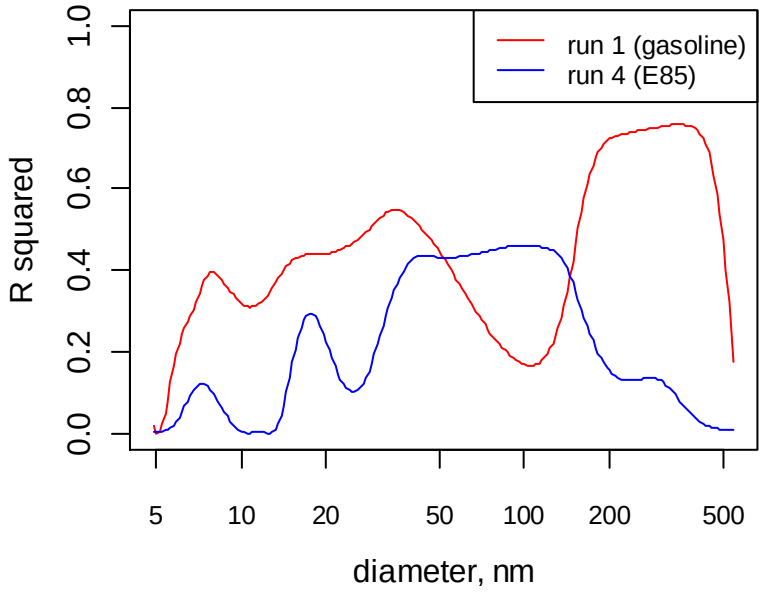

Figure 7.12. R-squared from the functional linear model

A permutation F-test was performed to assess the significance of the estimated model. The F-statistic is calculated by:

$$F(t) = \frac{Var\left[\hat{p}(t)\right]}{\frac{1}{n_1}\sum\left(p_i(t) - \hat{p}(t)\right)^2}$$

(Ramsay et al. 2009). The critical value is determined by permutating or randomly shuffling the response curves with respect to the respective engine speed values. The maximum *F(t)* values from the permutation is used to develop a null-distribution. The critical value is determined by the upper 95th percentile of permutated F(t) values, both the maximum across the entire curves, and point-wise at each particle size. The F-values are plotted Figure 7.13, with the accompanying critical values. As shown, the model for run 1 is significant for nearly all the particle sizes spectrum. The run 2 model is statistically significant for the values between 20 and 200 nm.

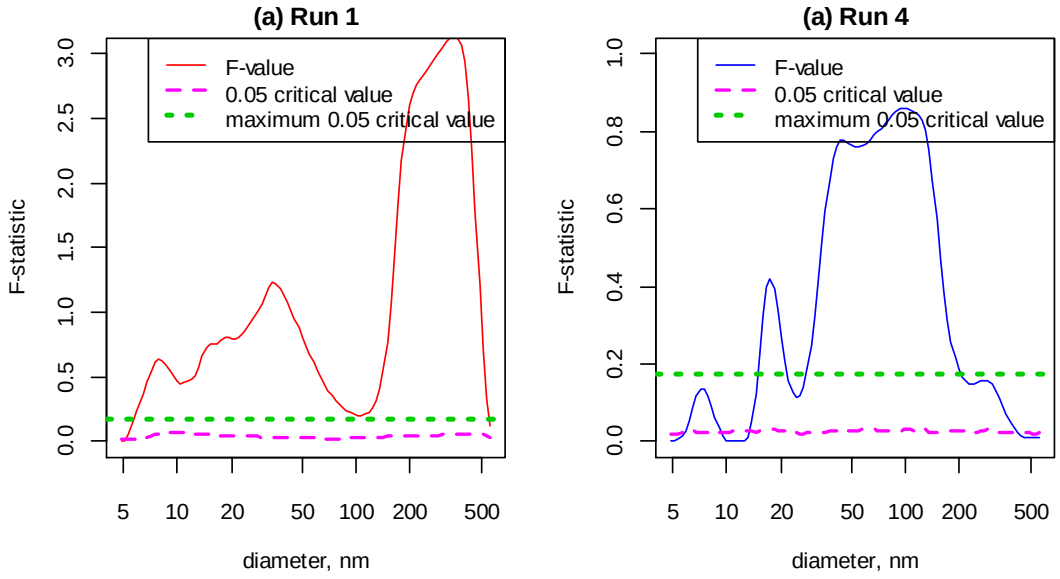

Figure 7.13. Permutation F-Test of engine speed functional linear model

Assumption 4, independent residuals, was believed to be violated because the data are second by second observations and should be strongly correlated through time. The functional correlation among neighboring observations was evaluated by

plotting the functional principle component scores against their lagged values in Figure 7.14. As observed, score 1 (representing the accumulation mode particles) are highly correlated with previous observations. Score 2 is also highly correlated to its lagged values for the gasoline run, while Score 2 appears to be uncorrelated temporally for the E85 run .

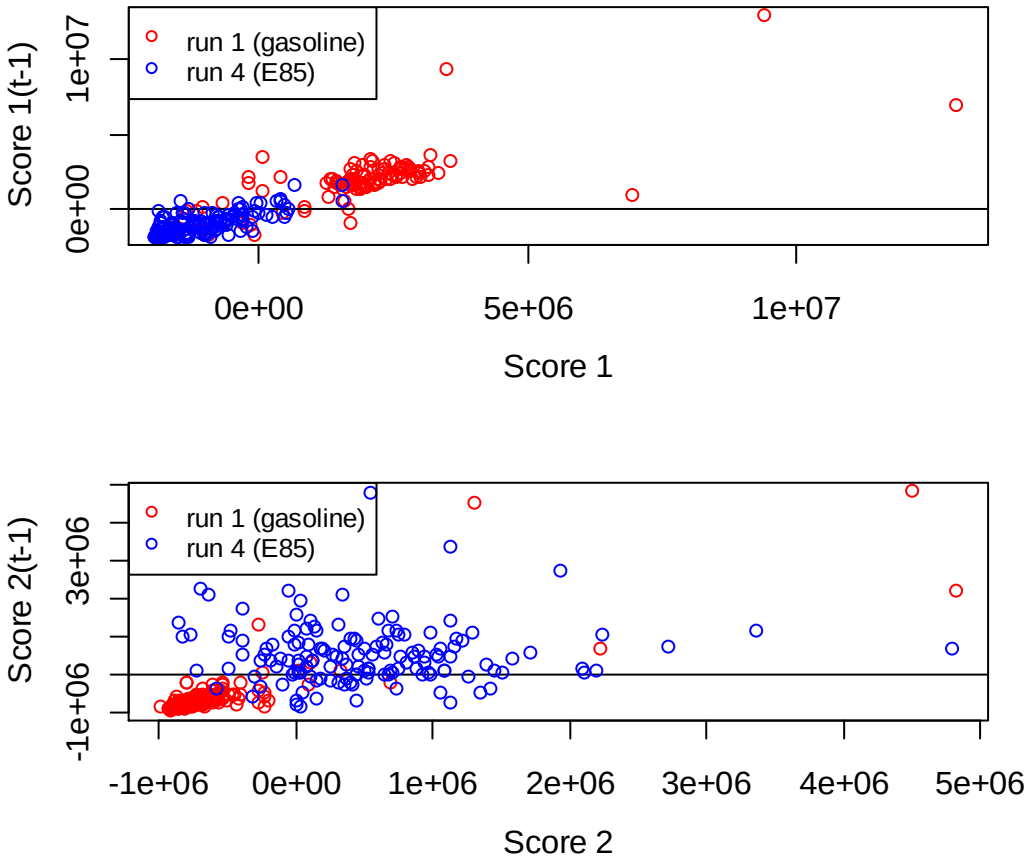

Figure 7.14. PCA scores plotted lagged values.

Functional Time-Series Model. The presence of autocorrelation casts doubt upon our previous observations. By not accounting for the autocorrelation, we likely have inflated the significance of the coefficients in our model. To control for autocorrelation, functional time-series model was estimated by including the lagged particle-size distribution as a covariate: $p_i(s) = \beta_o(s) + \beta_1(s)x_i + \rho(s)p_{i-1}(s) + \varepsilon_i(s)$.

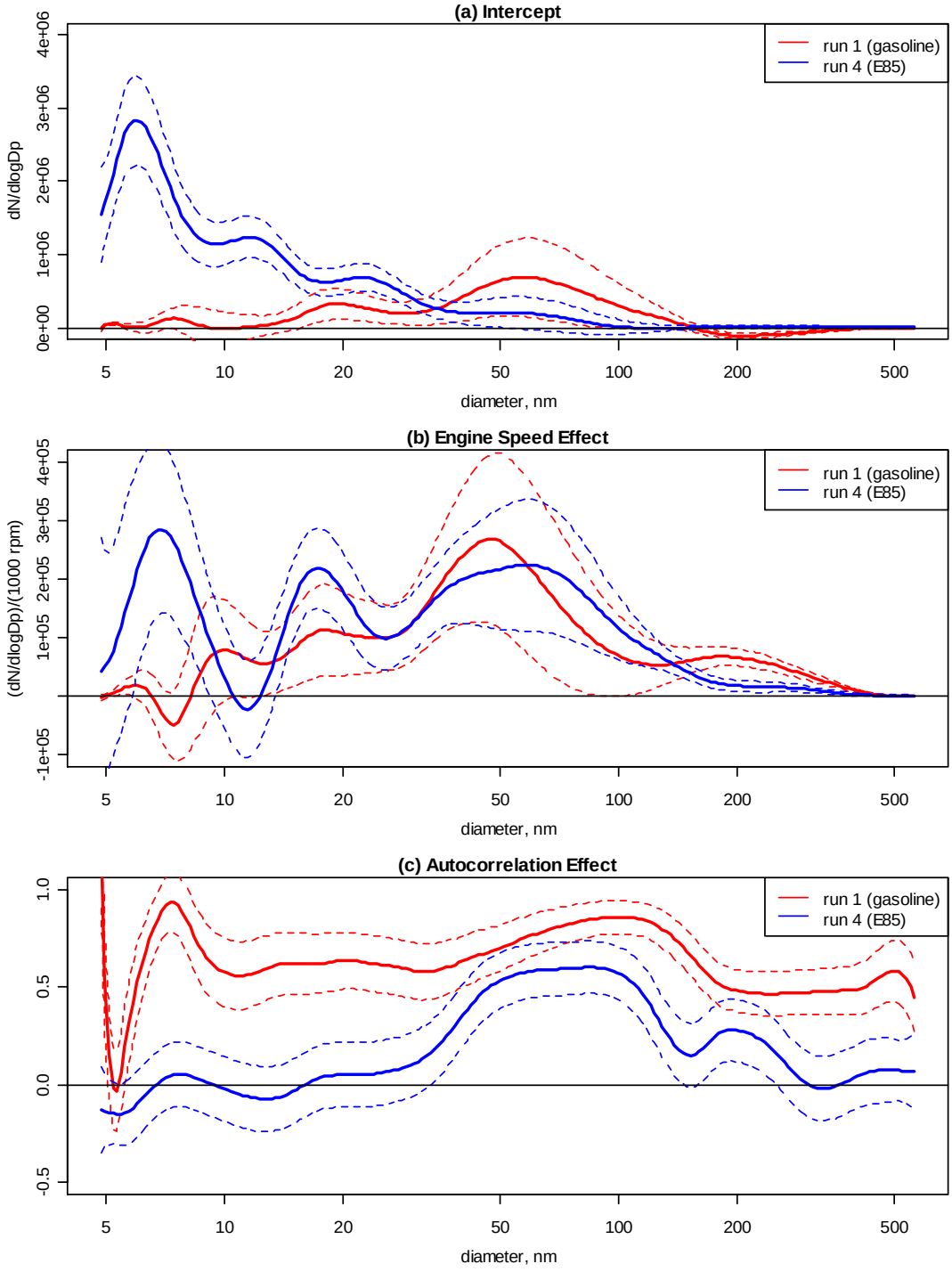

Figure 7.15. Comparison of time-series models for run 1 and run 4.

Figure 7.15 displays the estimated coefficients for run 1 and 4. The intercept $\beta_o(s)$ for run 3 is very similar to the concurrent linear model, while

the $\beta_o(s)$ for run 1 is significantly smaller in magnitude. As expected $\rho(s)$ accounts for the positive autocorrelation in the time-series data. In run 1, $\rho(s)$ is above 0.5 for almost the entire particle spectrum. In run 4, $\rho(s)$ is significantly greater than zero for particles in the accumulation mode, and is near zero for particles less than 30 nm.

By controlling for autocorrelation, the effect of engine speed is significantly reduced for both runs, as shown in Figure 7.A6 which compares the $\beta_1(s)$ from both the concurrent and time-series models. The effect of engine speed $\beta_1(s)$ in the time-series models for both run1 and 4 are now similar in magnitude to each other. In the concurrent linear models, $\beta_1(s)$ was significantly larger for the gasoline run for most of the particle spectrum, while in the time-series models $\beta_1(s)$ is only significantly larger on the gasoline run for particles greater than 160 nanometers. The functional R^2 of the time-series model is displayed in Figure 7.A7 and is significantly larger than the concurrent linear model.

Discussion of Results

Results about the effect of E85 on size-distributed particles are preliminary and are based on the limited data. However, two general patterns have emerged from the analysis. These patterns can be used as starting points for further analysis.

1. The effect of engine speed and load has a similar relationship on the gasoline and E85 runs. From the concurrent linear model, it appears to have the a stronger effect on the gasoline run. The estimated particle size distribution from the concurrent linear model showed that the concentration of particles between 70 and 120 nm were significantly larger than the E85 run for operating conditions where the engine speed was < 2000 rpm. The time-series model lessened the effect of engine speed on emissions. However, the time-series model is likely accounting for the non-constant exhaust lag between engine events and recorded measurements (see discussion below). Even with

the time-series model, the effect of engine speed was greater on the particles from 160-400 nm for the gasoline run. This data are consistent with the observations in Figure 7.1, in that the particle concentrations above 50 nanometers are quite consistent between runs of the same fuel type, and for large particles the gasoline run has consistently higher particle concentrations. Further analysis and more data at a larger variation of driving conditions would be needed to validate this preliminary evidence.

2. The nanoparticles (<50 nm) are highly variable and no conclusions about the effect of fuel type on these particles can be made. The concurrent linear model showed a slight difference in these particles, but model estimates at 1000, 2000, 3000 rpm showed no differences. The time-series model showed no significance difference in the effect of engine speed for small particles except for a very small range (7 and 8 nm). The large confidence intervals from the functional linear model for nanoparticle estimates is consistent with the observations made for the other two runs in Figure 7.1. At this level of variability much more data would be necessary to make statistically robust conclusions about the effect of fuel type on particles smaller than 50 nm.

Conclusions

The main contribution of this paper was to lay the groundwork for the application of functional data analysis in aerosol research. We were successfully able to address several challenges of using functional data analysis on size-resolved particle emissions, including:

Positive Constrained Smoothing. Positive constrained smoothing was an effective method to estimate particle size-distributions from discrete particle spectrum data. It is a useful alternative to smooth particle size distributions data that does not require any distributional assumptions. To estimate an optimal smoothing penalty for

positive constrained smoothing, we introduced a method (with provided code) to minimize generalized cross-validation error for particle size distributions.

Under the current algorithm in FDA library in R, we found that several steps were also needed to conduct positive smoothing for particle-size distributions. 1. Seed the algorithm with basis coefficients from a smooth conducted using ln(dn/dlogDp). 2. Provide reasonable minimum positive values. 3. Lower the magnitude of the data for smoothing then rescale after smoothing.

Functional Principle Component Analysis. Functional principle components was a useful method to assess the variability between and within test runs. It could be an effective method to conduct clustering analysis to distinguish particle emissions to different events, source types, or other behavior. Additionally, it was a useful tool to explore the effect of covariates, such as engine speed, on the entire particle size distribution, which assisted the formulation of a functional linear model.

Functional Linear Model. The functional linear model was a useful tool to control for differences between operating conditions that existed for the on-road test. By approximating a linear relationship with engine speed raised to the second power, the functional linear model was able to provide estimates of particle-size concentrations at equal engine speed levels. The functional linear model was a useful tool to quantify effect of operating modes on the particle concentrations across the entire spectrum. Functional R^2 values and functional F-tests were able to assess the goodness of fit and significance of the models across all particle sizes. A functional time-series model was also conducted that accounted for the temporal correlation exhibited in high-frequency aerosol measurements.

Future Work

In our formal functional data analysis we only focused on two of the four tests made on the flex-fuel vehicle. This was done to place emphasis on the methods rather

than the conclusions of the data. The nature of the data, particularly run 2, made it difficult to apply the functional data analysis tools. Future work is needed to address issues related to problematic data properties and address unresolved issues from the initial analysis. These include:

Positive Constrained Smoothing. As shown in Figure 7.1, run 2 has an incredibly large nucleation mode that dominates the particle-size distribution. This nucleation mode is not present throughout the entire run, but emerges mid-way through the run (Figure 7.A8). Constrained positive smoothing was attempted for run 2, however the curve is extremely difficult to fit, with concentrations falling from 1e8 to 0 in neighboring points. With the previous steps, good fits were not always able to be attained with the current algorithm in FDA library in R within reasonable computation time limits (Figure 7.A9). We made initiated some changes within the FDA library to improve convergence; however more work could be done to improve the convergence to larger sets of data.

Functional Principle Component Analysis. fPCA was conducted on all four runs using the data smoothed without the positive constraint (Figure 7.A10 and A11). Only two functional principle components capture nearly 98% of the variability. However, the components only explained variation in the nucleation mode for run 2, with little variation explained in the other runs (Figure 7.A11). Because the magnitude of the nucleation mode is so great, it dominates the fPCA analysis, and ignores important variability in the accumulation mode that we are also interested in. However, the large nucleation mode posed difficulty in analysis in other methods as well as a function linear model applied to the data failed to yield interpretable results besides the dominating effect of the nucleation mode. A time-series model ran into numerical errors in trying to account for the large variation in concentration. As shown in Figure 7.A8, the particle concentration jumps orders of magnitude at the beginning

of the nucleation mode. The functional linear model assumptions are very difficult to satisfy with such variable data.

One method to address these issue is to analyze the log-transformed particle size distribution, or the

$$\log\left[\frac{dN}{d\log(Dp)}\right].$$

By assuming minimum positive values given in the supporting documents we obtain the following curves for

$$\frac{dN}{d\log(Dp)}$$

plotted on the log scale in Figure 7.16. Here the large nucleation mode of run 2 around 20 nanometers is very subdued. Additionally, the data is necessarily positively constrained and other elements of the distribution curve can be analyzed in more detail.

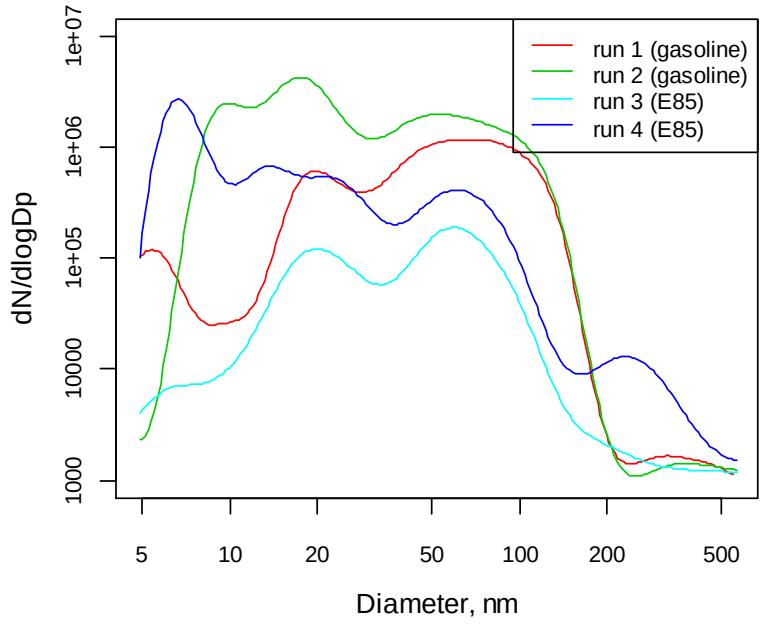

Figure 7.16. Mean particle smooths where dN/dlogDp is smoothed and plotted using the log scale.

The smoothing parameter, λ, that minimizes the generalized cross-validation error can be efficiently calculated using the log-transformed values. However a small degree of smoothing in log space will have an enormous smoothing effect as well as bias on the untransformed data. In generally, it was found that using the λ smaller than the GCV was better when transforming the curves back to

$$\frac{dN}{d\log(Dp)}.$$

Despite its disadvantages, using

$$\log\left[\frac{dN}{d\log(Dp)}\right]$$

can be very informative in analyzing the variance of curves that may otherwise be dominated by a single feature of the data (i.e. the nucleation mode in run 2). fPCA was conducted on the data from all four runs. Five principle components were required to explain 90% of the data, compared to only one component when using untransformed data, illustrating the richness in variation added by using the lognormal transformation. Figure 7.17 displays the scores for the first two principle components using the log-transformed curves. The data better is much better adapted for fPCA. The scores are within a much smaller range and appear to be more normally distributed. In the previous case, Figure 7.A11, the scores were positively skewed with a few observations having large influences. By taking the log-transformation, we should able to achieve more repeatable results between tests.

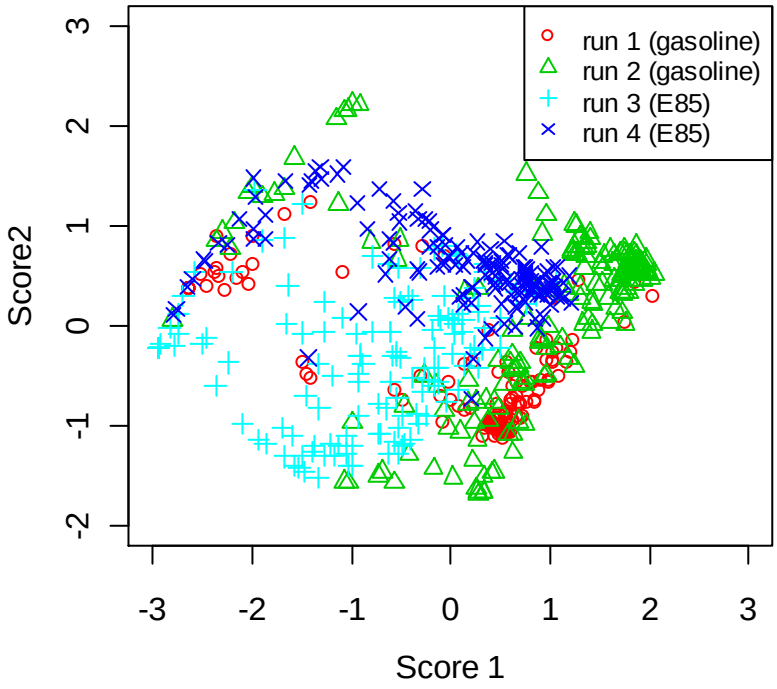

Figure 7.17. Functional Principle Component Analysis from log-transformed particle-size distribution functions.

Despite these advantages, there are also several key disadvantages to using the log-tranformation data. These include:

1. Determining the minimum positive values to impute for zero values. In our case 1000 dN/dlogDp was chosen as the minimum value. However, if a lower value was chosen such as 100 or 10, it would have an enormous effect on the shape of the curves. Selecting the minimum positive value is very subjective and is quite sensitive on the results.

2. The log-transformed data emphasizes differences magnitude so difference in small concentrations, i.e. 10,000 to 1,000, is just as important as differences between very large particle concentrations, i.e. 1e8 to 1e7. However we have more confidence in the data measured at high concentrations as opposed to small concentrations, and are often most interested in the large concentration differences.

3. Interpretation is much more difficult. The data can be transformed back to dN/dlogDp space, however, it will then be biased on overly smooth. Selecting a suitable smoothing parameter in

$$\log\left[\frac{dN}{d\log(Dp)}\right]$$

for all curves can be difficult. Examples are given in Figure 7.A13 and 7.A14. However, the approximate GCV we developed could be used to calculate optimal lambda.

Functional Linear Model. Several issues identified related to our functional linear model are worthy of further investigation.

1. We approximated a linear relationship between engine speed and particle concentration in the linear model. By only including one covariate, it facilitated a rather simple calculation of confidence intervals at estimated levels of engine speed. However, by examining the Figure 7.8 (or Figure 7.A5) a better model fit could be obtained by including several terms of an polynomial function, such as the simple case $p_i(s) = \beta_o(s) + \beta_1(s)x_i + \beta_2(s)x^2{}_i + \varepsilon_i(s)$. However determining the standard deviations for the point estimates from multiple linear regressions is not trivial (Devore, 2004). Additional work could calculate confidence intervals for estimates from functional multiple linear models.

2. We implemented a functional time-series model which added another variable to the functional linear model. In future work, we may want to add additional covariates to predict particle emissions. To assess the significance of more variables, we can evaluate the point-wise confidence intervals, as given in Figure 7.15. However, we would also like to have a single statistic to evaluate the significance of adding variables to the functional linear model. Future work could develop bootstrap techniques to test variable significance within the functional linear model.

Bootstrapping could to be used to develop a distribution of F-statistics for the null-model, against which the alternative model could be tested.

3. The concurrent linear model assumes a constant lag between engine events and the particle measurements. The emission lag is due to the time it takes for the exhaust to travel from the engine to the DMS50. The engine data and particle measurements were time-aligned such that the cross-correlation between engine speed and accumulation mode concentration was maximized. By examining Figure 7.7, it is evident that non-constant exhaust lag is probably for our data. Previous researchers have determined that the exhaust transport time for gasoline vehicles can vary between 0.1 and 7 seconds (Ajtay, and Weilenmann, 2004).

The dynamic lag literally muffles the relationship between engine parameters and particle concentrations in our linear model. By incorporating this effect, we anticipate the engine speed coefficient would be stronger. In the time-series model, the autoregressive term $\rho(s)$ likely captured much of the relationship between engine speed and emissions, but was not attributed to the engine speed coefficient because of the misalignment of the data. Curve registration would be a useful extension to better estimate the effect of operating conditions on particle emissions. Additionally, the registration curve would have a useful interpretation, by capturing the dynamic transport time of the exhaust.

Acknowledgments

This research was sponsored by the New York Metropolitan Transportation Council and University Transportation Research Council through the September 11th Program Fellowship Program, and the New York State Energy Research Development Authority through the Environmental Monitoring, Evaluation, and Protection PhD Fellowship Program

APPENDIX

Derivation of approximate GCV

Using matrix algebra, where **c** and ϕ**(s)** are both 36 by 1 vectors, and $\hat{\mathbf{p}}$**(s)** is a 34 by 1 vector. In the linear case (no positive constraint) we can solve for the predicted values $\hat{\mathbf{p}}$**(s)** explicitly by $\hat{p}(s) = S_\lambda p$, where $S_\lambda = \phi(\phi'\phi + \lambda R')\phi'$. (Giles book). Where R incorporates the degree of roughness, with $R_{i,j} = \int D^3\phi_i(t) D^3\phi_j(t)$ A useful result for the degrees of freedom, *df*, from the penalized smooth can be calculated by $df(\lambda) = trace(S_\lambda)$. The *df(λ)* can then be input into

$GCV(\lambda) = \left(\frac{n}{n - df(\lambda)}\right)\left(\frac{SSE}{n - df(\lambda)}\right)$, to compute the generalized cross-validation error.

However when we conducting a constrained smooth via: $\hat{p}(s) = e^{W(s)}$, where $W(s) = \phi(s)c$, then S_λ cannot be calculated explicitly. However, S_λ can be approximated by conducting a Taylor's series expansion. In our case, $\hat{p}(s) \approx \exp[W_0(s)] + [W(s) - W_0(s)]\exp[W_0(s)]$, where $\exp[W_0(s)]$ is obtained from the positive smooth algorithm (smooth.pos in the FDA library) at the current λ. These can be used to approximate $S_\lambda \approx G\phi(\phi'G^2\phi + \lambda R')\phi'G$, where *G* is an 36 by 36 matrix with $\exp[W_0(s)]$ on the diagonal. By using a linear approximation, we can compute the approximate degrees of freedom, and compute the generalized cross-validation error.

R Code for Computing Approximate GCV

The R code we used to compute the constrained smooth df, and GCV is included below:

```
##### perform for loop to compute mean gcv at three different lambda's #####

for (i in 1:3){
        lambda=10^{i-11}
        log_D3fdPar = fdPar(log_bbasis,3,lambda=lambda)
        log_D3fdPar$fd = fd(c_all[,c],log_bbasis)
        con_smoothD3 =smooth.pos(log_diameter,runs_14_example,log_D3fdPar,iterlim=30000, conv=5e-7)
        xval = eval.posfd(log_diameter,con_smoothD3$Wfdobj)

        # this outputs yhat= exp(W(s)) at each point, log_diameter

        xval=as.array(xval)
        Phi = eval.basis(log_diameter,log_bbasis)
        R = eval.penalty(log_bbasis, 3)

# create place holders matrices #
        G=array(data=rep(0,34*34*12),dim=c(34,34,12))
        S=array(data=rep(0,34*34*12),dim=c(34,34,12))
        SSE=matrix(rep(0,12),12,1)
        SSE=as.vector(SSE)
        trace_S=matrix(rep(0,12),12,1)
```

```
trace_S=as.vector(trace_S)

for(j in 1:12){

# place exp(w(s) on the diagonal of G

        diag(G[,,j]) = xval[,j]
        S[,,j] = G[,,j]%*%Phi%*%solve(t(Phi)%*%G[,,j]^2%*%Phi+lambda*R,t(Phi)%*%G[,,j])
        SSE[j] = sum((runs_14_example[,j] - xval[,j])^2)
        trace_S[j] =sum(diag(S[,,j]))
        gcv[i,j] = SSE[j]/(length(runs_14_example[,j]) - trace_S[j])^2*length(runs_14_example)
}

gcv_mean[i]=mean(gcv[i,])}
```

Notes on smoothing

To assure convergence of the positive smooth algorithm, it was necessary to replace the zero values of the discrete particle spectrum. The largest particle concentrations generally are at smaller particles, and a step-down minimum value was set. The zero values were roughly replaced with half of the minimum value for the given particle range.

The minimum dN/dlogDp concentration values were set for three sets of particle ranges. For particles between 4.87 and 6.49 nm, the minimum value = 1e5, for 7.50 to 13.34 nm, the minimum value = 1e4, and for 15.40 to 562.34 nm, the minimum value = 1e3.

However, in a few (6) observations from runs 1 and 4, the search algorithm failed to converge and yielded spurious fits to the data. For these problematic curves, lower minimum values were used to impute the zero particle concentrations for the upper channels (421.70 to 562.34 nm), with the minimum particles descending from 700 to 500 to 300.

Table.A1. Summary Results of the Four Test Runs.

	Test Run 1 (gasoline)			Test Run 2 (gasoline)			Test Run 3 (E85)			Test Run 4 (E85)		
Variable	Mean	Min	Max	Mean	Min	Max	Mean	Min	Max	Mean	Min	Max
Duration	2:20			2:57			2:29			2:27		
Engine speed ,rpm	2048	735	5124	2223	752	4010	1980	762	2962	1921	745	3293
Percent Engine Load, %	64	16	99	66	16	96	65	18	98	64	15	96
Speed, mph	51	17	60	57	18	69	49	20	59	49	18	62
Acceleration, mph/sec	-0.1	-3.7	5.0	-0.1	-4.7	2.8	0.0	-3.1	4.0	-0.1	-2.8	2.8
Number con-centration, (#/cc)	2.8E+06	0.0E+00	1.7E+07	1.5E+07	6.1E+04	8.8E+07	8.9E+05	0.0E+00	4.1E+06	1.8E+06	3.6E+04	5.0E+06

Figure 7.A1. Installation of DMS50 on the Chevrolet Impala, November 18, 2008.

Figure 7.A2. Aerial view of test section in Ithaca, NY.

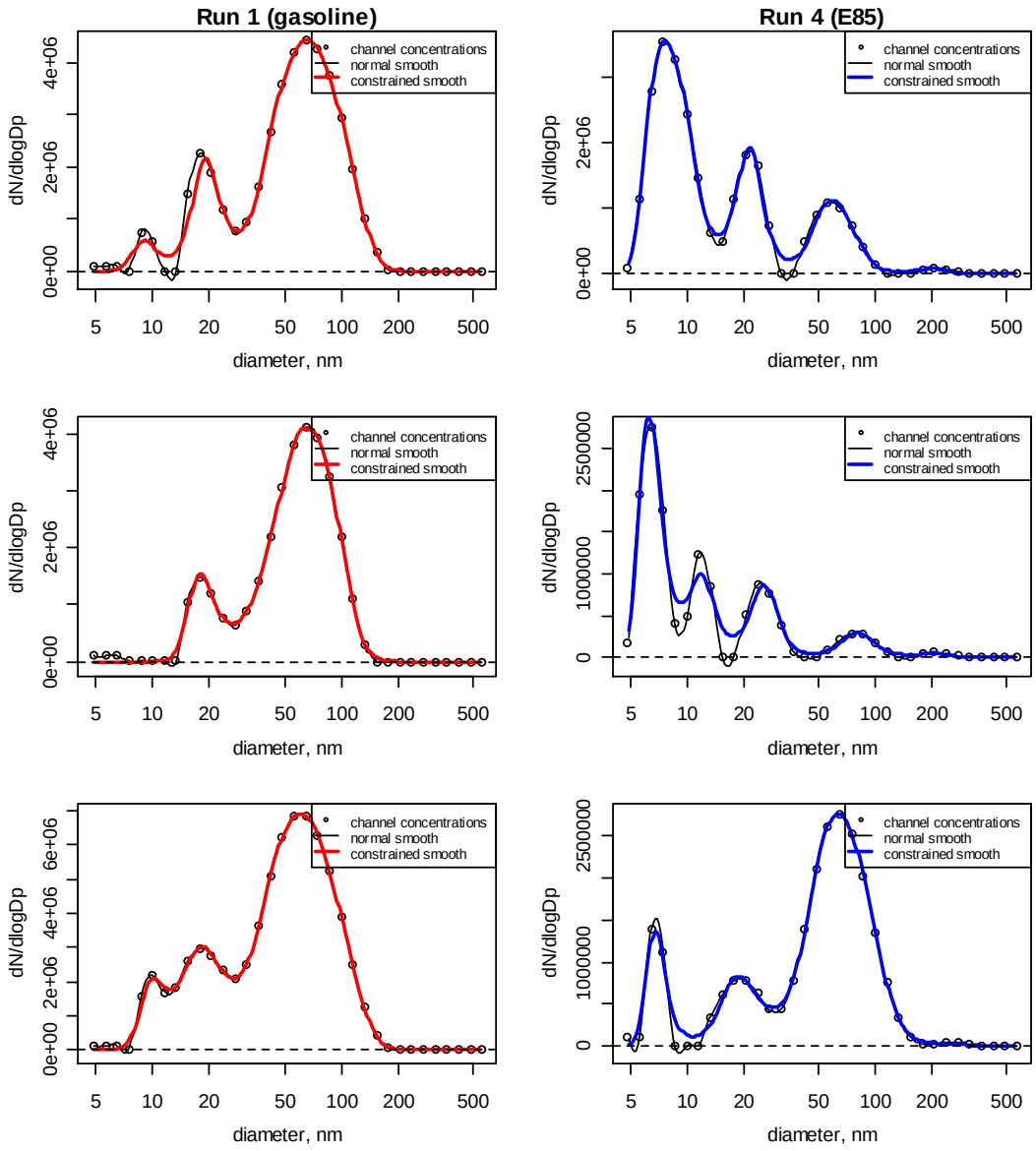

Figure 7.A3. Example observations from Runs 1 and 2, with the particle size-distribution smoothed using the linear basis expansion (normal), and the positive constrained basis expansion.

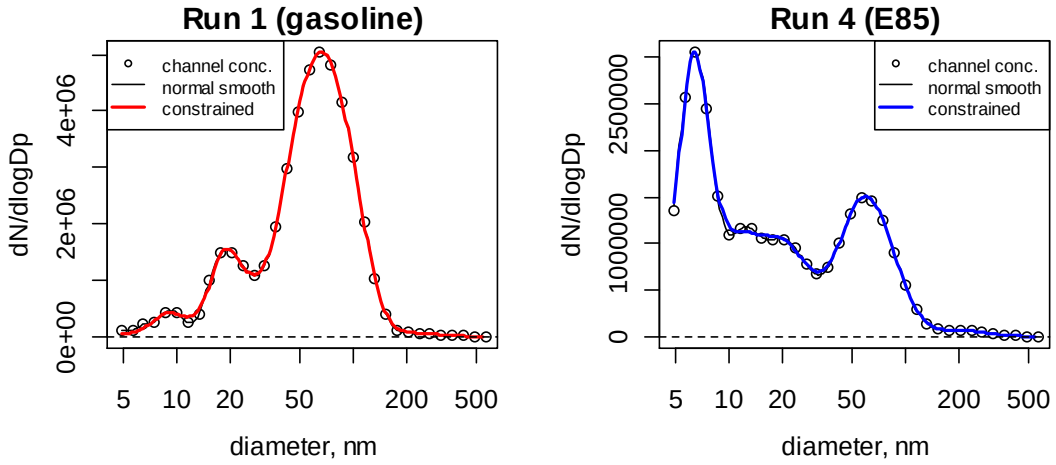

Figure 7.A4. Mean particle size-distribution for Runs 1 and 2, compared to the mean of the normal smooth function and the mean of the positive constrained basis expansion.

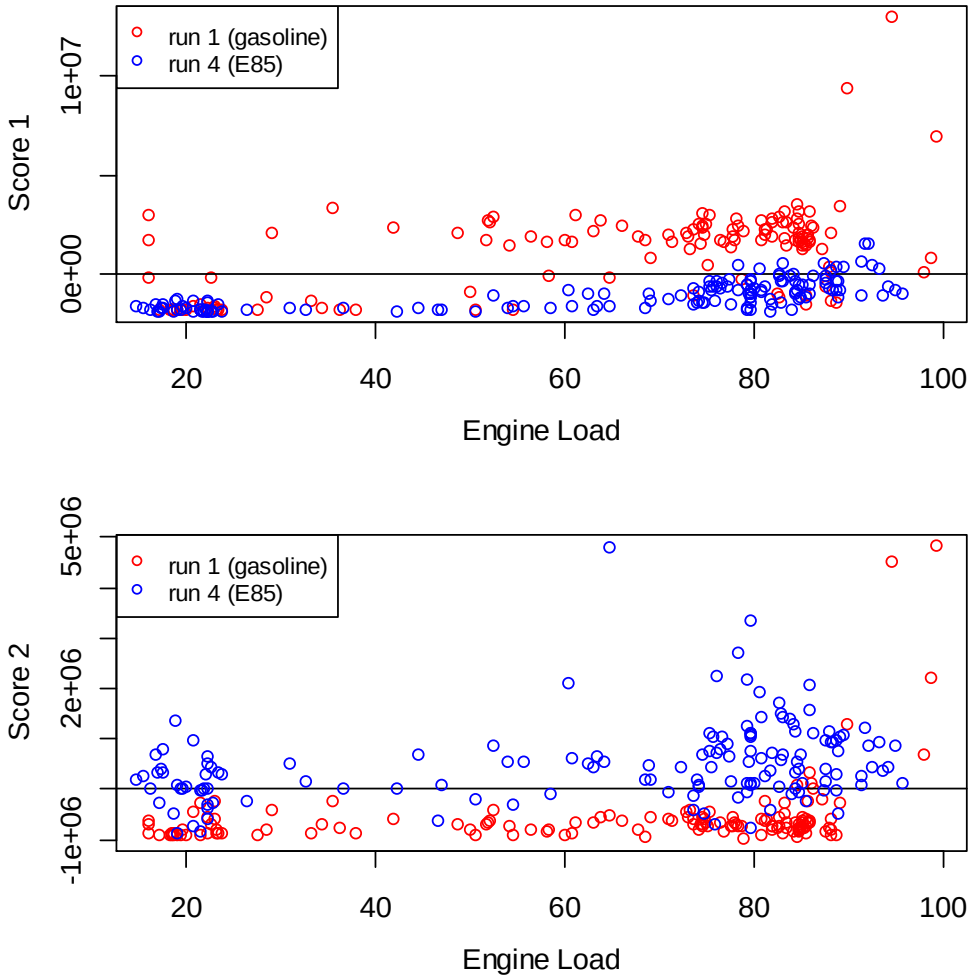

Figure 7.A5. fPCA scores plotted against engine load.

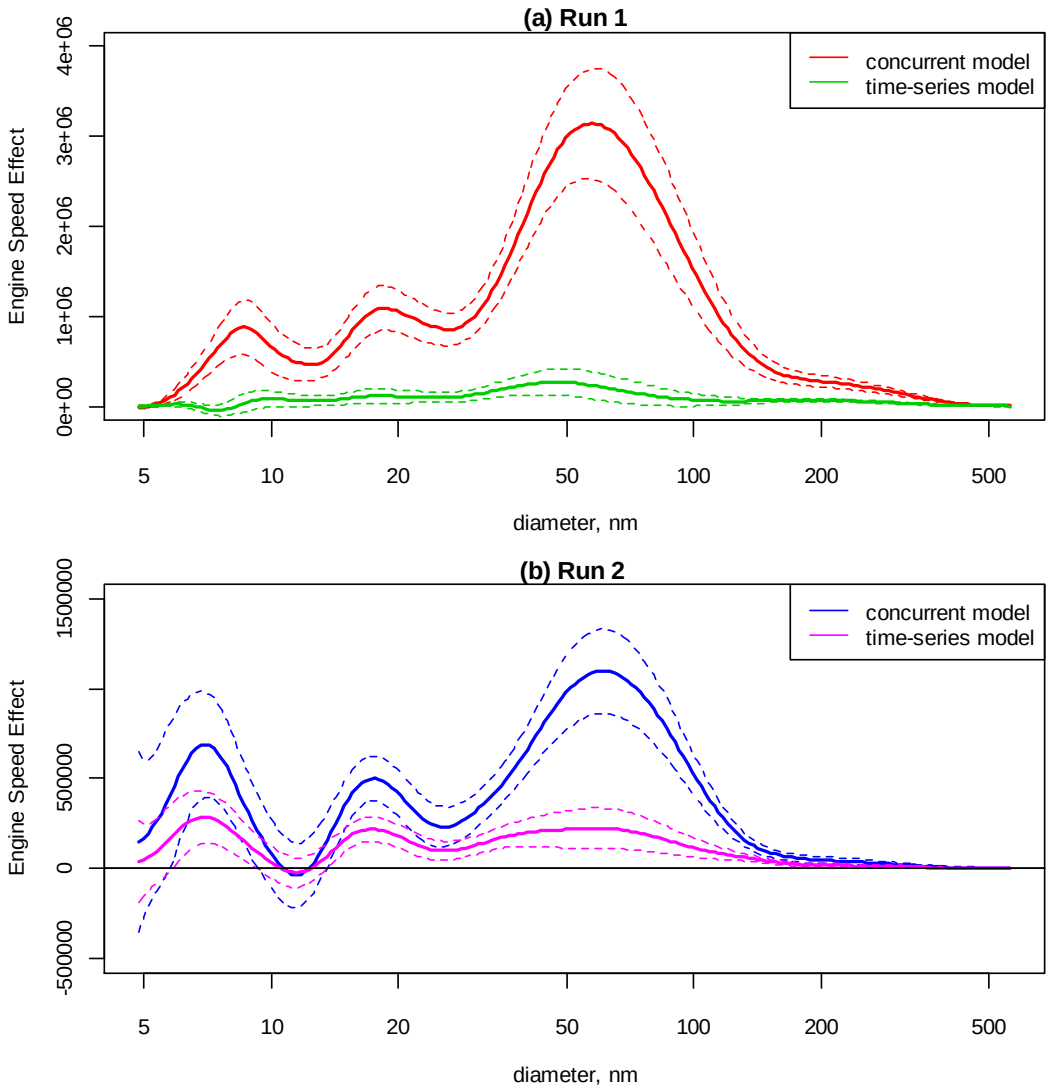

Figure 7.A6. Comparison of engine speed effect for run 1 (a) and run 4 (b) using both a concurrent and time-series model.

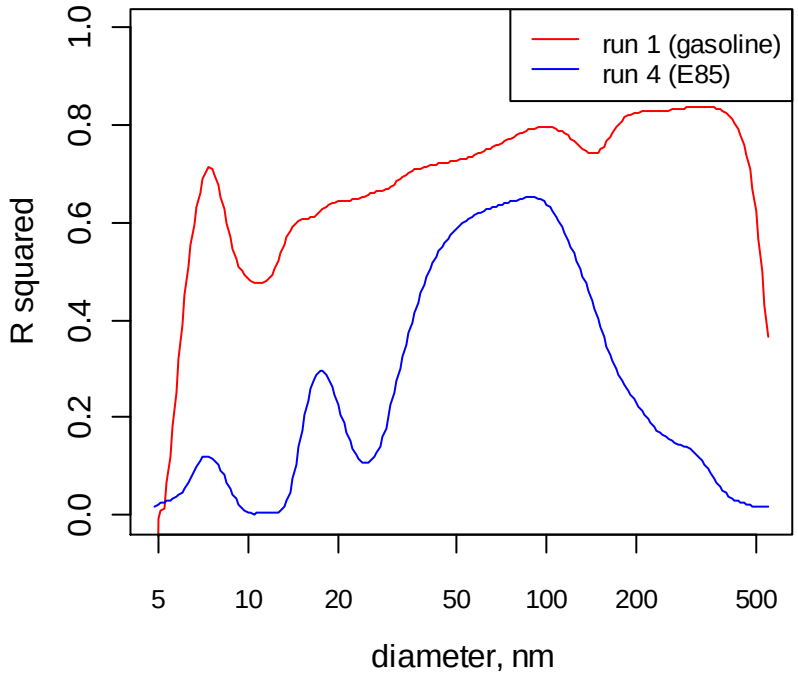

Figure 7.A7. R^2 from time-series model.

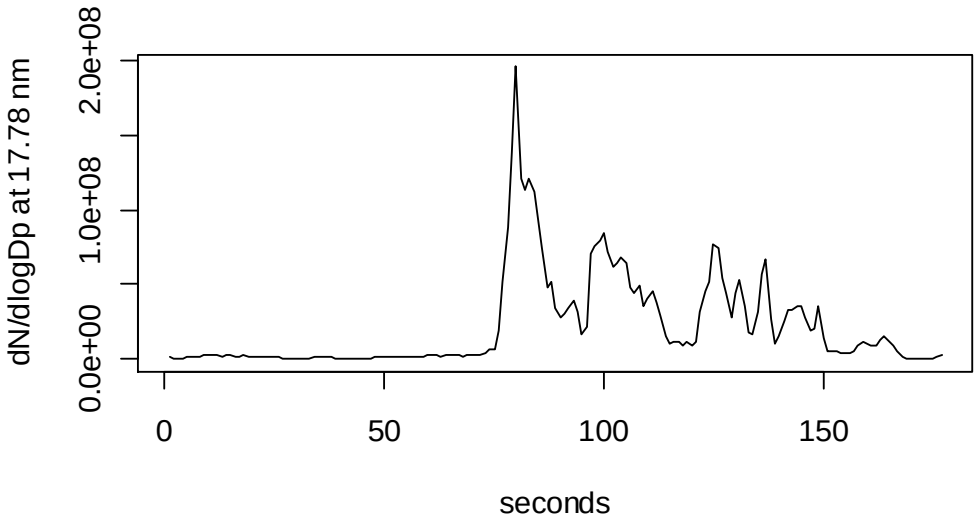

Figure 7.A8. Difficulty of using a linear model to analyze run 2

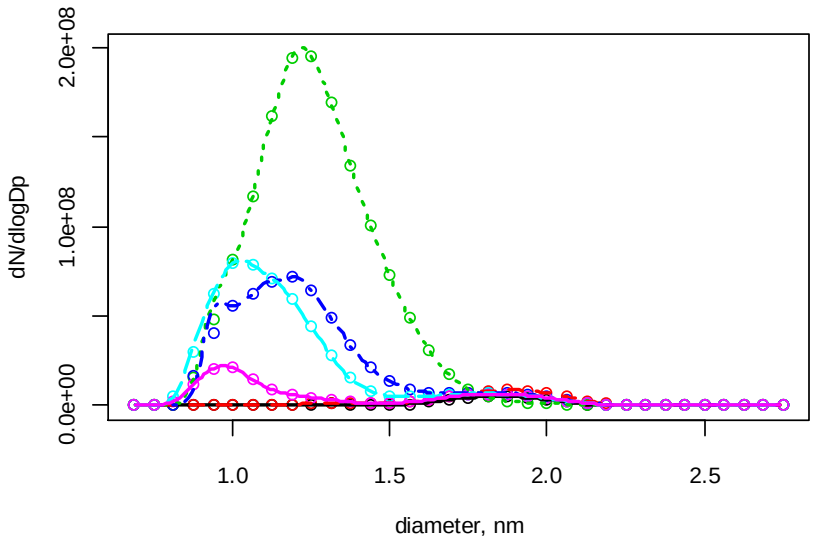

Figure 7.A9. Positive Smooth fits for Run 2

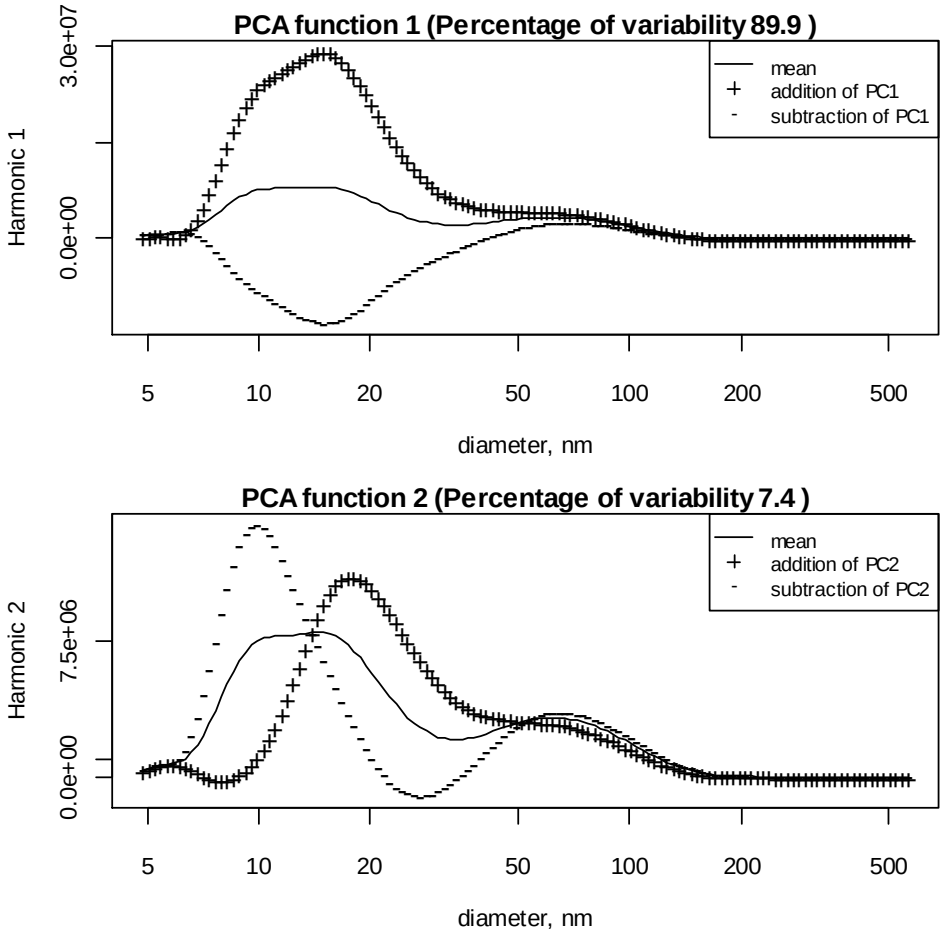

Figure 7.A10. Two fPCA components used to analyze all four runs.

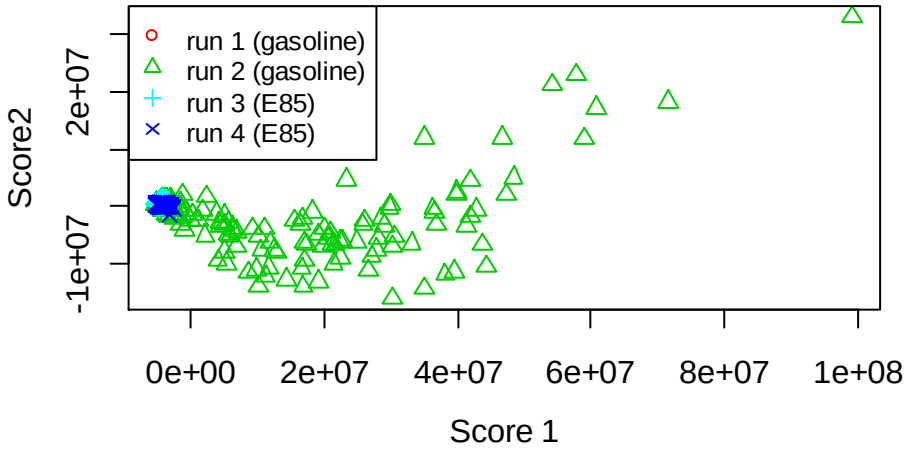

Figure 7.A11. fPCA scores from using all four runs.

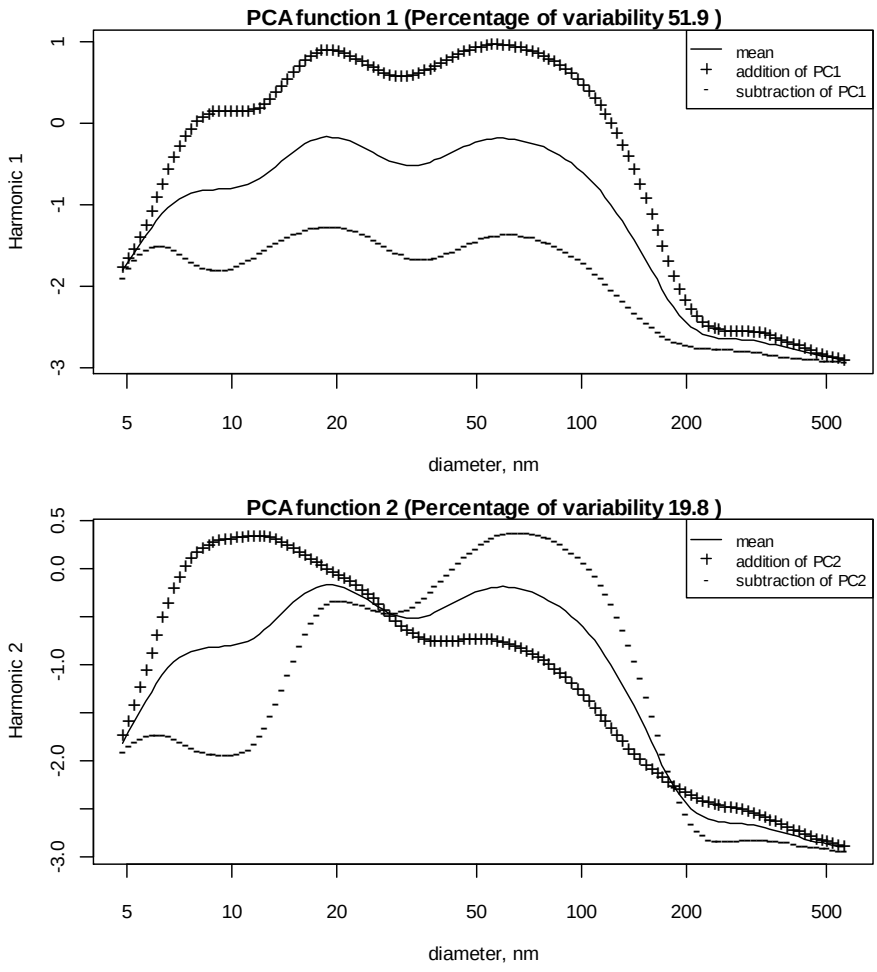

Figure 7.A12. Two fPCA components used to analyze all four runs from log-transformed data.

REFERENCES

Ajtay, D.; Weilenmann, M. Compensation of the exhaust gas transport dynamics for accurate instantaneous emission measurements. *Environ. Sci. Technol*. **2004**, *38*, 5141–5148.

Beddows, S. C. D.; Dall'osto, M.; Harrison, R. M. Cluster analysis of rural, urban, and curbside atmospheric particle size data. *Environ. Sci. Technol.*. **2009**, *43* (13), 4694-4700.

Brunerkreef, B.; Holgate, S. T. Air pollution and health. *Lancet.* **2002**, *360*, 1233-42.

Burtscher H. Physical characterization of particulate emissions from diesel engines: A review. *Aerosol Science* **2005**, 36, 896-932.

Charron, A.; Harrison, R. M. Primary particle formation from vehicle emissions during exhaust dilution in the roadside atmosphere. *Atmospheric Environment*, **2003**, 37, 4109-4119.

Chalupa, D. C.; Morrow, P. E.; Oberdörster, G.; Utell, M. J.; Frampton, M. W. (2004). Ultrafine particle deposition in subjects with asthma. *Environmental Health Perspectives*. **2004**, *112*(8), 879–882.

Devore, J. L. Probability and Statistics for Engineering and the Sciences; Brooks/Cole: Belmont, CA, 2004.

Giechaskiel, B.; Ntziachristos, L.; Samaras, Z.; Scheer, V.; Casati, R.; Vogt, R. Formation potential of vehicle exhaust nucleation mode particles on-road and in the laboratory. *Atmospheric Environment*. **2005**, *39* (18), 3191-3198.

Harris, S. J.; Maricq, M. M. Signature size distributions for diesel and gasoline engine exhaust particulate matter. *Journal of Aerosol Science*. **2001**, *32*, 749–764.

Holmén, B. A.; Chen, Z.; Davila, A. C.; Gao, O. H.; Vikara, D. M. *Particulate Matter Emissions from Hybrid Diesel-Electric and Conventional Diesel Transit Buses: Fuel and Aftertreatment Effects*. JHR 05-304, Project 03-8; Joint Highway Research Advisory Council: Hartford, CT, 2005.

Kittleson, D. B.; Watts, W. F.; Johnson, J. P. Nanoparticle emissions on Minnesota highways. *Atmos. Environ*. **2004**, *38*, 9-19.

Kittelson, D. B.; Watts, W.F.; Johnson, J. P. On-road and laboratory evaluation of combustion aerosols—Part1: Summary of diesel engine results. *Aerosol Science*. **2006a**, *37*, 913–930.

Kittelson, D. B.; Watts, W. F.; Johnson, J. P.; Schauer, J. J.; Lawson, D. R. On-road and laboratory evaluation of combustion aerosols—Part 2: Summary of spark ignition engine results. *Aerosol Science*. **2006b**, *37*, 931 – 949.

Kittelson, D. B.; Watts, W. F.; Johnson, J. P.; Thorne, C.; Higham, C.; Payne, M.; Goodier, S.; Warrens, C.; Preston, H.; Zink, U.; Pickles, D.; Goersmann, C.; Twigg, M. V.; Walker, A. P.; Boddy, R. Effect of fuel and lube oil sulfur on the performance

of a diesel exhaust gas Continuously Regenerating Trap. *Environmental Science & Technology*. **2008** *42* (24), 9276-9282.

Larsen, R. J.; Marx, M. L. *An Introduction to Mathematical Statistics and Its Applications*. (Fourth Edition). Pearson Education, Inc. 2006. Upper Saddle River, NJ.

Lee, H.; Myung, C.; Park, S. Time-resolved particle emission and size distribution characteristics during dynamic engine operation conditions with ethanol-blended fuels. *Fuel*. In Press, Corrected Proof, Available online 27 March 2009.

Lighty, J. S.; Veranth, J. M.; Sarofim, A. F. Combustion aerosols: factors governing their size and compositions and implications to human health. *J. Air & Waste Manage. Assoc*. **2000**, *50*, 1565-1618.

Liu, Z. G.; Ford, D. C.; Vasys, V. N.; Chen, D.; Johnson, T. R. Influence of engine operating conditions on diesel particulate matter emissions in relation to transient and steady-state conditions. *Environ. Sci. Technol*. **2007**, *41* (13), 4593-4599.

Maricq, M. M.; Podsiadlik, D. H.; Chase, R. E. Examination of the size-resolved and transient nature of motor vehicle particle emissions. *Environ. Sci. Technol*. **1999**, *33* (10), 1618-1626.

Mathis, U.; Mohr, M.; Forss, A. Comprehensive particle characterization of modern gasoline and diesel passenger cars at low ambient temperatures. *Atmos. Environ*. **2005**, *39*, 107–117.

Morawska, L.; Ristovski, Z.; Jayaratne, E. R.; Keogh, D. U.; Ling, X. Ambient nano and ultrafine particles from motor vehicle emissions: Characteristics, ambient processing and implications on human exposure. *Atmospheric Environment*, **2008**, *42*, 8113-8138.

Mulawa, P. A.; Cadle, S. H.; Knapp, K.; Zweidinger, R.; Snow, R.; Lucas, R.; Goldbach, J. Effect of ambient temperature and E-10 fuel on primary exhaust particulate matter emissions from light duty vehicles. *Environ. Sci. Technol*. **1997**, *31*(5), 1302-1307.

North, R. J.; Noland, R. B.; Ochieng, W. Y.; Polak, J. W. Modeling of particulate matter mass emissions from a light-duty vehicle. *Transportation Research Part D: Transport and Environment*, **2006**, *11*(5), 344-357.

Qu, Y.; Holmén, B. A.; Ravishanker, N. Prediction on-road particle number concentrations of light-duty gasoline vehicles from gas concentrations with time-series cross-section regression. *Transportation Research Record: Journal of the Transportation Research Board*, **2008**, *2058*, 97-105.

Ramsay, J.O.; Hooker, G.; Graves, S. Functional Data Analysis with R and MATLAB; Springer: New York, 2009.

Rönkkö, T.; Virtanen, A.; Vaaraslahti, K.; Keskinen, J.; Pirjola, L.; Lappi, M. Effect of dilution conditions and driving parameters on nucleation mode particles in diesel exhaust: Laboratory and on-road study. *Atmospheric Environment*. **2006**, *40* (16), 2893-2901.

Shi, J. P.; Mark, D.; Harrison, R. M. Characterization of particles from a current technology heavy-duty diesel engine. *Environ. Sci. Technol*. **2000**, *34*, 748-755.

Sienfield, J. H.; Pandis S. N.; Atmospheric Chemistry and Physics: From Air Pollution to Climate Change; John Wiley & Sons, Inc.: Hoboken, New Jersey, 2006.

Symonds, J. P. R.; Reavell, K S. J.; Olfert, J. S.; Campbell, B. W.; Swift, S. J. Diesel soot mass calculation in real-time with a differential mobility spectrometer. *Aerosol Science* **2007**, *38*, 52-68.

Wichmann, H. E.; Peters, A.; Epidemiological evidence of the effects of ultrafine particle exposure. In *Ultrafine Particles in the Atmosphere*; Brown, L. M., Collings, N., Harrison, R. M., Maynard, A.D., Maynard, R.L., Eds.; Imperial College Press: London, 2000.

CHAPTER 8

CONCLUSIONS

1. Particle emissions data was collected and processed from two unique measurement studies.

- The first study measured particle number emissions from four Connecticut Transit buses. This was the first known data collection of size-resolved particle number emissions collected on-board a transit bus in real-world operating conditions. Temporally resolved particle mass emission rates were successfully computed from the size-distributed measurements from the Electrical Low Pressure Impactor (ELPI) in transient driving conditions.
- The second study was a pilot study assessing the effects of alternative fuel on particle emissions. Data was successfully collecting by the authors on a light-duty flex-fuel vehicle for four runs on conventional gasoline and an E85 ethanol blend. The particle number concentrations and size distributions were measured from the tail-pipe exhaust as the vehicles were operating in real-world conditions.

2. The analysis of the collected data advanced the knowledge of factors that influence particle number emissions.

Connecticut Transit Buses

- The evaluated hybrid diesel-electric transit buses did not have improved particle emissions compared to the conventional diesel transit buses.
- Diesel particle filters substantially reduce particle number emissions, although the sampling conditions may have suppressed a volatile nucleation mode.

- Engine load, engine speed, and exhaust temperature are able to explain most of the linear variation in engine parameters, and can be effectively used to model particle number emissions.
- Particle number emissions are generally well correlated with particle mass emission in real-world driving of a diesel transit bus. However, distinct differences in behavior of particle number and mass emissions do occur.
- Particle mass emissions are more favored by fuel rates, while particle number emission rates are more influenced by spikes in exhaust flow.
- The majority of variation of four gaseous and two particulate matter emission rates can be explained by six discrete emission modes.

Light-Duty Flex-Fuel Vehicle

- Particle emissions are quite low, and can be difficult to measure under low load conditions
- Significant variation in nucleation mode particles are observed. Nucleation modes were observed that much higher (orders of magnitude) number concentrations than the accumulation mode particles, while other instances, under the same driving conditions, the nucleation mode was hardly detected.
- Measurements of accumulation mode particles were more repeatable, and ethanol had lower concentrations of accumulation mode particles at low and moderate engine speeds. At high engine speeds, the differences in particle size distributions were indistinguishable due to variability of the data.

3. The dissertation introduced new concepts for analyzing vehicle emissions, including:

- The use of statistical models to control for several sources of random variability in emissions testing.

- The important vehicle operating parameters were identified to explain particle emissions from the underlying relationships between engine operating parameters and vehicle emissions
- The particle number and mass emissions were contrasted in transient vehicle behavior to identify changes in particle-size distributions of emissions
- The particle emissions were analyzed over temporal and spatial scales, to understand the connection between vehicle operation exposure and exposure rates of particle emissions.
- The concept of emission modes was developed, which are repeatable convolutions of multiple emission rates, to understand the relationship among multi-pollutant exhaust and transient operating conditions.
- Smooth particle size distributions were estimated from exhaust measurements without imposing distributional assumptions, by applying non-parametric smoothing.
- The covariance of particle concentrations was evaluated across the measured particle spectrum.
- The relationships, as a function of particle size, were quantified among particle concentrations and important factors such as operating condition and fuel type.

The analysis concepts were facilitated by novel applications of statistical models:

- Linear mixed models analyzed vehicle emissions and control for multiple sources of variability.
- Principle component analysis was used to determine relative factors to include in predictive emissions models.
- Linear time-series models were applied to sections of common driving conditions to identify important factors of variation in otherwise complex and non-linear data.

- Cluster analysis was used understand relationships among multiple pollutants.
- Multi-nominal regression classified discrete emission modes from operating parameters.
- Basis splines smoothing was conducted on strictly positive particle size distributions from discrete data without imposing distributional assumptions.
- Functional principle components analysis was applied to analyze variability of particle size distributions.
- Functional linear modeling of particle size distribution studies was conducted as a function of operating mode and fuel type. Functional time-series models were also estimated.